



THE EFFECT OF INORGANIC NITRATE AND NITRITE
ON THE PRODUCTION AND FUNCTION OF
EXTRACELLULAR VESICLES

BY

NICHOLAS BURNLEY-HALL

A THESIS SUBMITTED FOR THE DEGREE

DOCTOR OF PHILOSOPHY

INSTITUTE OF MOLECULAR AND EXPERIMENTAL MEDICINE

WALES HEART RESEARCH INSTITUTE

SCHOOL OF MEDICINE, CARDIFF UNIVERSITY

2017

DECLARATION

This work has not been submitted in substance for any other degree or award at this or any other university or place of learning, nor is being submitted concurrently in candidature for any degree or other award.

Signed (candidate) Date.....

Statement 1

This thesis is being submitted in partial fulfilment of the requirements for the degree of PhD.

Signed (candidate) Date

Statement 2

This thesis is the result of my own independent work/investigation, except where otherwise stated, and the thesis has not been edited by a third party beyond what is permitted by Cardiff University's Policy on the Use of Third Party Editors by Research Degree Students. Other sources are acknowledged by explicit references. The views expressed are my own.

Signed (candidate) Date

Statement 3

I hereby give consent for my thesis, if accepted, to be available online in the University's Open Access repository and for inter-library loan, and for the title and summary to be made available to outside organisations.

Signed (candidate) Date

*To my mother,
Thank you for supporting me,
&
To Grace,
For always believing in me.*

ACKNOWLEDGEMENTS

First and foremost, my sincerest thanks go to Professor Philip James and Dr Aled Rees. I count myself extremely fortunate to have had two supervisors I get on with so well. Not only have you made my PhD experience so enjoyable, but your help and advice throughout my PhD has been invaluable, and has made me the scientist I am today.

A further thank-you to my colleagues and friends who have helped me along the way: Dr Gareth Willis, Dr Katherine Diana Connolly, Dr Rebecca Wadey, Dr Fairoz Abdul, Dr Justyna Witzcak, Dr Vitaliy Androshchuk, Dr Lee Butcher, Miss Donna Mathew, Miss Rhiannon Roberts, and Miss Sami Jennings. I also owe a large amount of thanks to Professor Keith Morris, not only for his statistical expertise but also for laughing at every single joke I ever told him. I would also like to take this opportunity to apologise to all of the above for inflicting them with some truly awful jokes on an almost daily basis.

I would like to thank Dr Aled Clayton, Dr Chris von Ruhland, Professor Adrian Evans, and Dr Matthew Lawrence for their help and support with the work within this thesis. I would also like to thank Dr Derek Lang, Dr Kirsten Pugh, Dr Marcus Coffey, Dr Lisa Wallace and the rest of the Pharmacology department at Cardiff University for making me a credible PhD candidate in the first place!

A special thank-you to the friends I have made over the last 6 years, especially Dr Hugo Trevelyan-Thomas, Dr Oliver Post, Dr Nicholas Hargreaves and Mr Nicholas Bennion. I couldn't have chosen a better group of boys to share 6 years of university with.

To my mother and sister, thank you for your unwavering support over the years, even through the toughest periods. To my girlfriend Grace, I don't know where I would be without your constant belief and encouragement.

Finally, I would like to thank Rafael Benítez, for restoring hope and pride in my beloved Newcastle United Football Club. Your hard work and dedication continues to inspire me.

Figures within this thesis were created using Servier Medical Art, licensed under a Creative Commons Attribution 3.0 Unported License.

This PhD was funded by a grant from Health and Care Research Wales.

TABLE OF CONTENTS

1	Introduction.....	1
1.1	Cardiovascular Disease.....	2
1.1.1	Epidemiology.....	2
1.1.2	Risk Factors	3
1.1.2.1	Hypertension.....	3
1.1.2.2	Tobacco use	3
1.1.2.3	Dyslipidaemia.....	3
1.1.2.4	Physical inactivity & obesity	3
1.2	Vascular endothelium	4
1.2.1	Overview	4
1.2.2	Structure of the vascular wall.....	4
1.2.3	Effect on vascular tone	6
1.2.3.1	Nitric Oxide	6
1.2.3.2	Prostacyclin (PGI ₂).....	7
1.2.3.3	Endothelium-derived hyperpolarising factor (EDHF).....	8
1.2.3.4	Endothelin-1.....	9
1.2.3.5	Thromboxane A ₂	10
1.2.4	Effect on haemostasis	10
1.2.5	Effect on inflammation	13
1.3	Atherosclerosis.....	15
1.3.1	Endothelial dysfunction.....	15
1.3.2	Fatty streak formation.....	16
1.3.3	Intermediate lesion & atheroma formation	16
1.3.4	Fibroatheroma	17
1.3.5	Complicated lesion	17
1.4	Oxygen and hypoxia in cardiovascular disease	19

1.4.1	Oxygen levels <i>in vitro</i> and <i>in vivo</i>	19
1.4.2	Consequences of hypoxia on the vasculature.....	20
1.4.2.1	Vascular tone.....	20
1.4.2.2	Inflammation.....	20
1.4.2.3	Coagulation.....	20
1.4.2.4	Oxidative stress.....	21
1.4.2.5	eNOS function.....	21
1.5	Nitric Oxide.....	23
1.5.1	Nitric Oxide Synthase.....	23
1.5.1.1	Uncoupling of eNOS.....	25
1.5.2	Function of Nitric Oxide.....	26
1.5.2.1	Function in the cardiovascular system.....	26
1.5.2.2	Function in the nervous system.....	26
1.5.2.3	Function in the immune system.....	27
1.5.3	NO metabolism.....	28
1.5.3.1	Within the blood.....	28
1.5.3.2	Within erythrocytes.....	29
1.5.4	NO metabolites.....	30
1.5.5	Nitrate-nitrite-nitric oxide pathway.....	31
1.5.5.1	Haem proteins.....	33
1.5.5.2	Molybdopterin containing enzymes.....	33
1.5.5.3	Other mechanisms of NO ₂ ⁻ reduction.....	34
1.5.6	Nitrate and nitrite in therapeutics.....	35
1.5.6.1	History.....	35
1.5.6.2	Physiological effects of NO ₃ ⁻ and NO ₂ ⁻	36
1.5.7	Detrimental effects of NO ₃ ⁻	39
1.6	Extracellular vesicles.....	40
1.6.1	History.....	40

1.6.2	Nomenclature	41
1.6.3	The mechanism of EV biogenesis	42
1.6.3.1	The classical “exosome” pathway	42
1.6.3.2	The direct pathway.....	45
1.6.4	Composition	48
1.6.5	EV internalisation.....	49
1.6.6	EV Processing.....	53
1.6.6.1	Sample collection.....	53
1.6.6.2	EV isolation.....	54
1.6.6.3	Measurement of EVs.....	55
1.6.6.4	Storage of EVs.....	55
1.6.7	Function of EVs	56
1.6.7.1	EVs in angiogenesis.....	56
1.6.7.2	EVs in the immune system.....	56
1.6.7.3	EVs in cancer.....	57
1.6.8	EVs in the cardiovascular system	58
1.6.8.1	Coagulation.....	58
1.6.8.2	Endothelial dysfunction	59
1.6.8.3	Inflammation	60
1.6.8.4	Arterial stiffness	61
1.6.9	Emerging therapeutic opportunities	62
1.6.9.1	Biomarkers.....	62
1.6.9.2	Delivery vectors	63
1.6.9.3	Vaccination	63
1.7	Thesis hypothesis and aims.....	65
1.7.1	Hypothesis.....	65
1.7.2	Aims	65
2	General Methods	66

2.1	Cell Culture.....	67
2.1.1	Human Vascular Endothelial Cell (HECV) Culture	67
2.1.2	Human Umbilical Vein Endothelial Cell (HUVEC) Isolation & Culture	67
2.1.3	Cellular treatments	69
2.1.4	Hypoxia exposure.....	70
2.1.5	Cell Counting & Viability	70
2.1.5.1	Trypan blue exclusion	70
2.1.5.2	Haemocytometer.....	71
2.1.5.3	MTS assay.....	71
2.1.5.4	Caspase-Glo® 3/7 assay	71
2.1.6	Silencing RNA	72
2.2	Electron Microscopy	73
2.2.1	Scanning electron microscopy	73
2.2.2	Transmission electron microscopy.....	73
2.3	Nanoparticle tracking analysis	74
2.3.1	Background	74
2.3.2	Experimental methodology	76
2.4	EV Isolation & Storage.....	77
2.4.1	Isolation of cell-derived EVs.....	77
2.4.2	Isolation of plasma-derived EVs	77
2.4.3	Storage of EVs	77
2.5	Time resolved fluorescence	79
2.5.1	Background	79
2.5.2	Experimental method.....	80
2.6	Plasma NO metabolites: Ozone Based Chemiluminescence	82
2.6.1	Background	82
2.6.2	Plasma NO ₂ ⁻	83
2.6.2.1	NO ₂ ⁻ standard curve	85

2.6.3	Plasma RSNO	85
2.6.4	Plasma NO ₃ ⁻	86
2.6.4.1	NO ₃ ⁻ standard curve	88
2.7	<i>Ex vivo</i> platelet EV production	89
2.7.1.1	RSNO measurement.....	89
2.8	Leukocyte Adhesion Assay.....	91
2.8.1	Leukocyte Isolation.....	91
2.8.2	Leukocyte Adhesion Assay.....	92
2.9	Platelet Function.....	94
2.9.1	Background	94
2.9.2	Experimental methodology	94
2.10	Rheology.....	95
2.10.1	Background	95
2.10.2	Experimental methodology	96
2.11	Thrombin activity assay.....	96
2.12	ROS detection.....	97
2.13	Calpain activity assay.....	97
2.14	Protein Assay.....	98
2.14.1	Bicinchoninic acid (BCA) assay	98
2.14.1.1	Background	98
2.14.1.2	Procedure.....	98
2.14.2	NanoDrop Spectrophotometer	99
2.15	Western Blotting.....	100
2.15.1	Background	100
2.15.2	Cell Lysis	100
2.15.3	Sodium Dodecyl Sulfate-Polyacrylamide Gel Electrophoresis (SDS-PAGE) ..	101
2.15.4	Electroblotting.....	102
2.15.5	Incubation of antibodies.....	104

2.15.6	Developing	106
2.15.7	Densitometry	106
2.16	Statistical analysis.....	106
3	Results I: Production of extracellular vesicles by endothelial cells: the effect of hypoxia and nitrite.....	107
3.1	Perspective	108
3.2	Introduction.....	109
3.3	Aims	111
3.4	Methods.....	112
3.4.1	Cell culture	112
3.4.2	Hypoxia exposure.....	112
3.4.3	Cell viability and apoptosis	112
3.4.4	Cellular treatments	112
3.4.5	EV Isolation	112
3.4.6	EV size, concentration and distribution	112
3.4.7	Electron microscopy	113
3.4.8	Time resolved fluorescence	113
3.4.9	siRNA transfection.....	113
3.4.10	Calpain activity assay	113
3.4.11	Western blotting.....	113
3.4.12	Statistics.....	114
3.5	Results	115
3.5.1	Electron microscopy	115
3.5.2	The effect of hypoxia on EV size, concentration and distribution	116
3.5.3	Viability and apoptosis.....	120
3.5.4	Characterisation of EV.....	121
3.5.5	HIF-1 α expression	122
3.5.6	Silencing RNA	122

3.5.7	Desferrioxamine mesylate (DFO) addition	124
3.5.8	Rab22a expression in hypoxia	126
3.5.9	Sodium nitrate (NaNO ₃) and sodium nitrite (NaNO ₂) addition	127
3.5.9.1	NaNO ₃	127
3.5.9.2	NaNO ₂	127
3.5.10	Sodium nitrite & xanthine oxidoreductase inhibition	129
3.5.11	S-Nitrosoglutathione addition	135
3.5.12	Hypoxia exposure and NaNO ₂ addition in HUVECs	136
3.5.13	TNF- α addition	139
3.5.14	Calpain inhibition	140
3.5.15	Calpain activity	144
3.6	Discussion	145
3.6.1	Key findings	145
3.6.2	Main discussion	145
3.6.3	Limitations	148
3.6.4	Conclusions	149
4	Results II: The influence of hypoxia and nitrite on the function of endothelial-derived extracellular vesicles	150
4.1	Perspective	151
4.2	Introduction	152
4.3	Aims	154
4.4	Methods	155
4.4.1	Cell culture	155
4.4.2	Cellular treatments	155
4.4.3	EV Isolation	155
4.4.4	EV concentration	155
4.4.5	Cell viability and apoptosis	155
4.4.6	Electron microscopy	156

4.4.7	Reactive oxygen species detection.....	156
4.4.8	Leukocyte adhesion assay	156
4.4.9	Western blot	156
4.4.10	Rheology	156
4.4.11	Platelet aggregation.....	157
4.4.12	Thrombin activity	157
4.4.13	Time resolved fluorescence	157
4.4.14	Statistics.....	157
4.5	Results	158
4.5.1	Platelet aggregation.....	158
4.5.2	Thrombin activity	160
4.5.3	Fractal dimension (d_f) and clot formation time (T_{GP}).....	161
4.5.4	Electron microscopy	162
4.5.5	Leukocyte Adhesion	164
4.5.5.1	Adhesion molecule expression.....	166
4.5.6	Viability and apoptosis.....	168
4.5.7	Oxidative stress.....	169
4.5.8	eNOS function	170
4.5.9	Characterisation of EV.....	172
4.6	Discussion	174
4.6.1	Key Findings.....	174
4.6.2	Main discussion.....	174
4.6.3	Limitations	178
4.6.4	Conclusions.....	179
5	Results III: The effect of chronic dietary nitrate supplementation on extracellular vesicles in healthy volunteers.....	180
5.1	Perspective.....	181
5.2	Introduction.....	182

5.3	Aims	184
5.4	Methods.....	185
5.4.1	Subjects and protocol	185
5.4.2	Plasma NO metabolites	185
5.4.3	EV isolation	185
5.4.4	EV size and concentration	186
5.4.5	Time resolved fluorescence	186
5.4.6	Statistics.....	186
5.5	Results	187
5.5.1	Patient Characteristics.....	187
5.5.2	Plasma NO metabolites	187
5.5.2.1	Plasma NO ₃ ⁻	187
5.5.2.2	Plasma NO ₂ ⁻	188
5.5.2.3	Plasma Nitrosothiol (RSNO).....	188
5.5.3	EV size and concentration	190
5.5.4	EV immunophenotyping.....	193
5.6	Discussion	194
5.6.1	Key Findings.....	194
5.6.2	Main discussion.....	194
5.6.3	Limitations	196
5.6.4	Conclusions.....	197
6	Results IV: The effect of acute dietary nitrate supplementation on extracellular vesicles in coronary artery disease patients	198
6.1	Perspective.....	199
6.2	Introduction.....	200
6.3	Aims	202
6.4	Methods.....	203
6.4.1	Subjects and protocol	203

6.4.2	Biochemical measurements.....	205
6.4.3	Plasma NO metabolites.....	205
6.4.4	Platelet aggregation.....	205
6.4.5	EV isolation.....	205
6.4.6	EV size and concentration.....	205
6.4.7	Time-resolved fluorescence.....	205
6.4.8	<i>Ex vivo</i> platelet EV production.....	206
6.4.9	Statistics.....	206
6.5	Results.....	207
6.5.1	Patient characteristics.....	207
6.5.2	Plasma NO metabolites.....	209
6.5.3	Platelet Aggregation.....	211
6.5.4	EV size and concentration.....	213
6.5.5	EV size distribution profile.....	214
6.5.6	EV immunophenotyping.....	217
6.5.7	<i>Ex vivo</i> platelet EV generation.....	219
6.6	Discussion.....	221
6.6.1	Key Findings.....	221
6.6.2	Main discussion.....	221
6.6.3	Limitations.....	224
6.6.4	Conclusions.....	225
7	General Discussion.....	226
7.1	Overview and conclusions.....	227
7.2	Future directions.....	231
	References.....	226
	Appendices.....	270

SUMMARY

Extracellular vesicles (EVs) are spherical, submicron particles enclosed in a phospholipid bilayer, shown to have pathophysiological roles in a plethora of disease states, including cardiovascular disease (CVD). The development of an atherosclerotic plaque can lead to downstream hypoxia, which is known to stimulate the production of EVs. Nitric oxide (NO) plays a pivotal role in vascular homeostasis, highlighted by the deficiency of NO in CVD states. The inorganic anions nitrate (NO_3^-) and nitrite (NO_2^-) represent bioactive reservoirs of NO, particularly under hypoxic conditions. Therefore, the aim of this thesis was to explore the effect of inorganic NO_3^- / NO_2^- on the production and function of EVs in CVD.

In vitro, hypoxia-inducible factor-1 α (HIF-1 α) was shown to mediate hypoxic EV release in endothelial cells. Furthermore, NO_2^- derived NO increased HIF-1 α degradation, and subsequently reduced EV production. This effect was attenuated by inhibition of xanthine oxidoreductase, preventing NO_2^- conversion to NO.

Following this, hypoxic endothelial-derived EVs were shown to enhance pro-coagulant and pro-inflammatory responses in comparison to EVs derived from normoxia. Treatment of hypoxic cells with NO_2^- reversed the pro-coagulant effects of the EVs produced, but did not alter their effect on inflammation.

In order to determine whether modulation of EV production was also possible *in vivo*, healthy volunteers were given a dietary NO_3^- supplement daily for 6 days. However, there was no change in circulating EVs over the course of this treatment. Finally, a NO_3^- supplement was given to CVD patients, which significantly reduced circulating EVs only in patients on clopidogrel, suggesting the formation of a thienopyridine-nitrosothiol derivative.

In conclusion, the NO metabolites NO_3^- and NO_2^- appear capable of reducing the production of pathogenic EVs, representing a novel therapeutic approach which may be of interest in the future treatment of CVD.

ABBREVIATIONS

AA	Arachidonic acid
ABC	ATP-binding cassette
AC	Adenylate cyclase
ACE	Angiotensin-converting enzyme
ACS	Acute coronary syndrome
ADP	Adenosine diphosphate
ALDH-2	Aldehyde dehydrogenase-2
APC	Activated protein C
APC	Antigen-presenting cell
APS	Ammonium persulphate
ATP	Adenosine triphosphate
AUC	Area under curve
BCA	Bicinchoninic-acid assay
BH ₄	Tetrahydrobiopterin
BMI	Body mass index
BR juice	Beetroot juice
BSA	Bovine serum albumin
BSS	Balanced salt solution
CABG	Coronary artery bypass graft
CAD	Coronary artery disease
CAM	Cell adhesion molecule
cAMP	Cyclic adenosine monophosphate

CCB	Calcium channel blockers
CcO	Cytochrome c oxidase
CFP	Culture filtrate proteins
cGMP	Cyclic guanosine monophosphate
CNS	Central nervous system
COPD	Chronic obstructive pulmonary disease
COX	Cyclooxygenase
COX-2	Cyclooxygenase-2
CSH	Cysteine
CuCl	Cuprous (I) chloride
CVD	Cardiovascular disease
DAG	Diacylglycerol
DCF	Dichlorofluorescein
DC-SIGN	Dendritic cell-specific intercellular adhesion molecule-3 grabbing non-integrin
d_f	Fractal dimension
DFCDA	2'7'-Dichlorofluorescein diacetate
DFO	Desferrioxamine mesylate
DISC	Death-inducing signalling complex
DII4	Delta-like 4
DMEM	Dulbecco's Modified Eagle Medium
DVT	Deep vein thrombosis
ECE	Endothelin converting enzyme
ECM	Extracellular matrix
EDHF	Endothelium-derived hyperpolarising factor

EDTA	Ethylenediaminetetraacetic acid
EGFR	Epidermal growth factor receptor
EM	Electron microscopy
EMCCD	Electron multiplying charge coupled device
eNOS	Endothelial nitric oxide synthase
EPAS-1	Endothelial PAS domain-containing protein 1
ESCRT	Endosomal sorting complex required for transport
ET-1	Endothelin-1
EV	Extracellular vesicle
FAD	Flavin adenine dinucleotide
FasL	Fas ligand
FasR	Fas receptor
FH	Familial hypercholesterolemia
FMD	Flow mediated dilation
FMN	Flavin mononucleotide
<i>g</i>	Centrifugal force
GLA	γ -carboxyglutamic acid
GP	Gel point
GPCR	G protein coupled receptor
GSNO	S-Nitrosoglutathione
GTN	Glyceryl trinitrate
GTP	Guanosine triphosphate
H ₂ O	Water
H ₂ O ₂	Hydrogen peroxide

HbFe ²⁺	Ferrous deoxyhaemoglobin
HbNO	Nitrosylated haemoglobin
HbSNO	S-nitrosylated haemoglobin
HCl	Hydrochloric acid
HDL	High density lipoprotein
HECV	Human vascular endothelial cells
HIF	Hypoxia inducible factor
HIF-1 α	Hypoxia inducible factor-1 α
HIF-2 α	Hypoxia inducible factor-2 α
HMDS	Hexamethyldisilazane
HRE	Hormone response element
HRS	Hepatocyte growth factor-regulated tyrosine kinase substrate
HUVEC	Human umbilical vein endothelial cells
ICAM-1	Intercellular adhesion molecule 1
IFN- γ	Interferon- γ
IHD	Ischemic heart disease
IL-1	Interleukin-1
ILVs	Intraluminal vesicles
iNOS	Inducible nitric oxide synthase
IP ₃	Inositol triphosphate
IP ₃ R	Inositol triphosphate receptor
IPA	Isopropanol
ISEV	International Society for Extracellular Vesicles
I κ B	Inhibitor of κ B

K _{IR}	Inward rectifying potassium channel
LAD	Leukocyte adhesion deficiency
LAMP	Lysosome-associated membrane glycoprotein
LDL	Low-density lipoprotein
LFA-1	Lymphocyte function-associated antigen 1
LPS	Lipopolysaccharide
MAPK	Mitogen activated protein kinase
MCP-1	Monocyte chemoattractant protein-1
MEA	Multiple electrode aggregometry
MHC	Major histocompatibility complex
MI	Myocardial infarction
MLCK	Myosin light chain kinase
MSC	Mesenchymal stem cells
mTOR	Mammalian target of rapamycin
MUC1	Mucin 1
MVBs	Multivesicular bodies
N ₂ O ₃	Nitrous anhydride
N ₂ O ₄	Dinitrogen tetroxide
NAC	N-acetyl-cysteine
NACSNO	Acetyl-cysteine-SNO
NADPH	Nicotinamide adenine dinucleotide phosphate
NaNO ₂	Sodium nitrite
NaOH	Sodium hydroxide
NK	Natural killer

NKG2D	Natural killer group 2D
nNOS	Neuronal nitric oxide synthase
NO	Nitric oxide
NO ⁺	Nitrosonium
NO ₂ ⁻	Nitrite
NO ₃ ⁻	Nitrate
NOA	Nitric oxide analyser
NOD1	Nucleotide-binding oligomerisation domain-containing protein 1
NOS	Nitric oxide synthase
NSF	N-ethylmaleimide-sensitive fusion
NTA	Nanoparticle tracking analysis
O ₂ ⁻	Superoxide
O ₃	Ozone
OBC	Ozone based chemiluminescence
OH [•]	Hydroxyl radical
PAD	Peripheral arterial disease
PAF	Platelet activating factor
PAI-1	plasminogen activator inhibitor-1
PAMPS	Pathogen associated molecular patterns
PBS	Phosphate buffered saline
PC	Phosphatidylcholine
PCI	Percutaneous coronary intervention
PDGF	Platelet derived growth factor
PE	Phosphatidylethanolamine

PECAM-1	Platelet endothelial cell adhesion molecule-1
PFP	Platelet free plasma
PG	Prostaglandin
PGH ₂	Prostaglandin H ₂
PGI ₂	Prostacyclin
PIP ₂	Phosphatidylinositol bisphosphate
PKA	Protein kinase A
PKC	Protein kinase C
PKG	Protein kinase G
PLA ₂	Phospholipase A ₂
PLC	Phospholipase C
PMCA	Plasma membrane calcium ATPase
PPP	Platelet poor plasma
PS	Phosphatidylserine
PSGL-1	P-selectin glycoprotein ligand-1
REC	Research Ethics Committee
R _i	Refractive index
ROCK	Rho-associated protein kinase
ROS	Reactive oxygen species
RSNO	S-Nitrosothiol
SEC	Size exclusion chromatography
SEM	Standard error of the mean
SERCA	Sarcoplasmic reticulum calcium ATPase
SFM	Serum free medium

siRNA	Silencing RNA
SNARE	Soluble NSF attachment protein receptor
SOD	Superoxide dismutase
TBS	Tris-buffered saline
TF	Tissue factor
TFPI	Tissue factor pathway inhibitor
TGF- β	Transforming growth factor- β
T _{GP}	Clot formation time
TIA	Transient ischemic attack
TNF- α	Tumour necrosis factor- α
tPA	Tissue plasminogen activator
TRAP	Thrombin receptor activating peptide
TRPS	Tuneable resistive pulse sensing
TSG101	Tumour susceptibility gene-101
TxA ₂	Thromboxane A ₂
VAMP	Vesicle-associated membrane protein
VASP	Vasodilator-stimulated phosphoprotein
VCAM-1	Vascular cell adhesion molecule-1
VCl ₃	Vanadium III Chloride
VEGF	Vascular endothelial growth factor
VSMC	Vascular smooth muscle cell
vWF	von Willebrand factor
XOR	Xanthine oxidoreductase

PRESENTATIONS

ORAL PRESENTATIONS

Welsh Cardiovascular Society Annual Meeting (Park Plaza Hotel, Cardiff, April 2017) – **FIRST PRIZE**

Postgraduate Research Day (Cardiff University, Cardiff, January 2017) – **FIRST PRIZE**

Induction for New Researchers (Cardiff University, January 2016-January 2017) – **INVITED SPEAKER**

Extracellular Vesicle Interest Group Seminar (Cardiff Metropolitan University, Cardiff, October 2016)

3 Minute Thesis® Cardiff University Heat (Cardiff University, Cardiff, June 2016) – **FOURTH PLACE**

The International Conference of Nitric Oxide (Sendai, Japan, May 2016)

Postgraduate Research Day (Cardiff University, Cardiff, December 2015)

University Graduate College “Speaking of Science” (Cardiff University, May 2015) – **FIRST PRIZE**

Cardiovascular Biology and Metabolism seminar (Cardiff University, Cardiff, November 2014)

POSTER PRESENTATIONS

Welsh Cardiovascular Society Annual Meeting (Park Plaza Hotel, Cardiff, UK, April 2017) - **FIRST PRIZE**

United Kingdom Extracellular Vesicle Forum (Cardiff University, Cardiff, UK, December 2015)

Cardiff University Postgraduate Research Day (Cardiff, UK, December 2014)

PUBLICATIONS

Burnley-Hall N, Lawrence M, Morris K, Evans A, Rees DA, James PE. Inorganic nitrite plays a protective role in the production of pro-coagulant hypoxic endothelial-derived extracellular vesicles. *Thrombosis & Haemostasis*. Submitted.

Burnley-Hall N, Abdul F, Androshchuk V, Morris K, Ossei-Gerning N, Anderson R, Rees DA, James PE (2017) Dietary nitrate supplementation reduces circulating platelet-derived extracellular vesicles vascular disease patients on clopidogrel therapy: a randomised, double-blind, placebo-controlled study. *Thrombosis & Haemostasis*. doi: 10.1160/TH17-06-0394

Burnley-Hall N, Willis G, Davis J, Rees DA, James PE (2016). Nitrite-derived nitric oxide reduces hypoxia-inducible factor 1 α -mediated extracellular vesicle production by endothelial cells. *Nitric Oxide*. 28(63):1-12. doi: 10.1016/j.niox.2016.12.005

Witczak JK, Burnley-Hall N, Abdul F, Androshchuk V, Ossei-Gerning N, Anderson R, Rees DA, James PE (2016). The 2nd United Kingdom Extracellular Vesicle Forum Meeting Abstracts: Differences in circulating extracellular vesicles between healthy volunteers and patients with established erectile dysfunction – do endothelial microvesicles play an ambivalent role? *Journal of Extracellular Vesicles*. 5: 10.3402/jev.v5.30924. doi: 10.3402/jev.v5.30924

1 INTRODUCTION

1.1 Cardiovascular Disease

1.1.1 Epidemiology

Cardiovascular disease (CVD) is an umbrella term encompassing numerous conditions affecting the heart and/or blood vessels. The main forms of CVD are coronary artery disease (CAD), cerebrovascular disease (stroke), peripheral arterial disease (PAD) and aortic disease, but can also include pulmonary embolism, rheumatic heart disease, congenital heart disease and heart failure (1). Despite the large range of conditions that the term CVD encompasses, within this thesis the focus will be primarily on CVD conditions that are due to endothelial dysfunction, and the subsequent development of atherosclerosis.

CVD is the leading cause of mortality across the globe, responsible for approximately 17.5 million deaths each year, an estimated 31% of total deaths worldwide (1). More than 3 million of these deaths occurred in individuals < 60 years of age, and were largely preventable (2). Based on projections of socioeconomic development, the number of global deaths caused by CVD is expected to increase to over 23 million by the year 2030 (3).

The range in premature deaths from CVDs between economically developed countries is startling, ranging from 4% in high-income countries to 42% in low-income countries. Furthermore, over the last 20 years, deaths from CVD have been declining in high-income countries, but continue to rise alarmingly in low- and middle- income countries (2). These large discrepancies in CVD mortality rates between populations are predominately due to both CVD risk factors and available healthcare and treatment. Closer to home, CVD has dropped to the second most common cause of mortality in the UK, causing 180,000 deaths in 2010 but only 155,000 in 2014 (4). Of these, 80,000 were from CAD, and around 49,000 from cerebrovascular disease. However, CVD still accounts for over a quarter of all deaths within the UK. There are approximately 7 million people living with CVD in the UK, and with an ageing and growing population, coupled with improving survival rates from cardiovascular events, this number is set to increase (5). CVD is estimated to cost the UK economy £15 billion annually, £11 billion of which is attributable to direct costs to the National Health Service (5). Thus, CVD represents a major public health issue, both nationally and internationally, and research within this field is therefore imperative to allow greater understanding of the pathophysiology, and subsequently establish potential interventions to aid the treatment and/or prevention.

1.1.2 Risk Factors

There are numerous risk factors associated with CVD – some, such as family history/genetic susceptibility, ethnicity, and age, cannot be altered. However, the majority of risk factors are behavioural in nature and can be altered to reduce the risk of CVD.

1.1.2.1 Hypertension

Hypertension is defined as a systolic blood pressure above 140 mmHg and a diastolic blood pressure above 90 mmHg (6). Hypertension increases the stress on the vasculature, increasing the likelihood of damage to the blood vessel wall. Hypertension represents the single largest risk factor for developing cerebrovascular disease, also playing a significant role in myocardial infarctions (MIs) (7). In some cases, hypertension may be inherited; however, more commonly hypertension develops as a result of other behavioural risk factors listed below.

1.1.2.2 Tobacco use

Tobacco use, both smoking and chewing tobacco, raises the risk of CVD. The risk is particularly high if individuals began smoking from a young age, smoke heavily, or are female. Cigarette smoking introduces a large amount of free radicals to the vasculature, impacting all stages of the pathophysiology of atherosclerosis (8). Smoking increases inflammation, thrombosis, and oxidation of low-density lipoprotein (LDL) cholesterol (9). Cessation of smoking has the greatest effect on CVD risk of any modifiable risk factor, reducing significantly soon after stopping.

1.1.2.3 Dyslipidaemia

Elevated LDL cholesterol and high density lipoprotein (HDL) cholesterol can lead to an accumulation of fatty material in the artery wall; the hallmark of atherosclerosis. LDL cholesterol is atherogenic, whereas HDL cholesterol is anti-atherogenic. Dyslipidaemia is often a result of other risk factors such as smoking, physical inactivity, and a poor diet high in saturated fat. However, it may also be due to an inherited condition known as familial hypercholesterolemia (FH).

1.1.2.4 Physical inactivity & obesity

Physical activity has a positive effect on many of the risk factors for CVD, such as reducing the weight and blood pressure of an individual. Additionally, exercise can reduce LDL, increase HDL, and elevate insulin sensitivity, thus improving glucose regulation (10). Obesity can increase CVD risk through other known risk factors such as dyslipidaemia, hypertension, glucose intolerance, in addition to other as yet unrecognized mechanisms (11).

1.2 Vascular endothelium

1.2.1 Overview

The vascular endothelium was once described by Nobel Laureate Lord Adrian Florey as a “cellophane wrapper” of the vasculature, acting solely as a selective barrier between the blood and the extravascular tissues (12). He did, however, predict that the following decade would yield a far greater understanding of the function of these cells. Today, not only is the endothelium well established as a semipermeable barrier, regulating the transfer of substances between the blood and the tissues, but can also be considered the largest endocrine organ in the human body (13). The endothelium plays a central role in the modulation of vascular tone, platelet activation, immune modulation, and vascular smooth muscle cell (VSMC) proliferation. Endothelial cells line the entire vasculature, forming the single cell layer of a capillary. The integrity of these cells is paramount for vascular homeostasis. Structurally, these endothelial cells link together typically via one of three junctions; tight, gap, or adherens junctions. Tight junctions serve the main functional “barrier”, regulating permeability and cell polarity. Gap junctions are communication structures allowing small molecular weight solutes between neighbouring cells. Adherens junctions, formed by cadherins, play a central role in contact inhibition of endothelial cell growth (14).

1.2.2 Structure of the vascular wall

The vascular wall can be broken down into three concentric layers: the tunica intima, tunica media, and tunica adventitia. The tunica adventitia consists of the extracellular matrix; predominantly collagen and elastin fibres. It functions to anchor vessels with surrounding tissues. Often, this layer is thicker in veins compared to arteries to prevent the collapse of the blood vessel, and provide additional protection due to their superficial location.

The tunica media consists predominantly of VSMCs and the external elastic lamina. This layer is far thicker in arteries than veins, allowing the arteries to adjust the volume of blood delivered to the tissues that they supply. VSMC layers tend to be highly organised in larger arteries, due to their participation in moving large volumes of blood. The VSMCs can respond to factors released from the tunica intima to adjust vascular tone, known as vasoconstriction (narrowing of the vessel) or vasodilation (widening of the vessel). A layer of elastic connective tissue lies immediately outside the VSMC layer of the tunica media, providing structural support (15).

The intima consists of a single layer of endothelial cells, mounted on an internal elastic lamina. (Figure 1.1). Endothelial cells as previously mentioned, act as a selective barrier but also regulate vascular tone through secretion of numerous vasoactive molecules. They can respond to various hormones, neurotransmitters, and other vasoactive factors to alter vascular tone. The internal elastic lamina separates the endothelial cells from VSMCs, and acts to provide flexibility and stability for endothelial cells, accommodating volume fluctuation in the arteries (16). Figure 1.1 summarises the structure of a blood vessel wall.

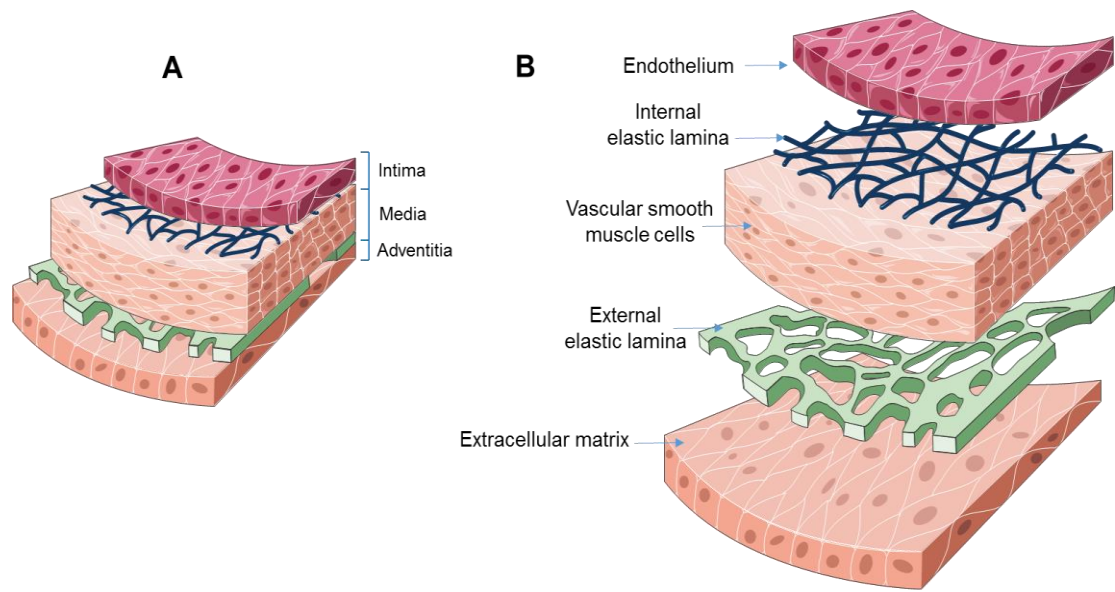


Figure 1.1 The layers of a blood vessel. A. The vessel consists of three layers or “tunics” – the intima, media, and adventitia. B. The intima consists of endothelium and an internal elastic lamina. The media consists of vascular smooth muscle cells and an external elastic lamina. The adventitia is composed of a series of collagen and elastin fibres making up the extracellular matrix.

There are 3 main types of artery: elastic arteries, muscular arteries, and arterioles. Elastic arteries receive blood directly from the heart (the aorta and the pulmonary artery). These vessels contain a “vasa vasorum” – as these arteries are so large that simple diffusion of oxygen and carbon dioxide across the vessel wall is not adequate. Thus, a network of smaller thin-walled vessels supply the large vascular wall with nutrients and oxygen (17). Elastic arteries facilitate the stretching of the wall to accommodate the blood surge following contraction of the heart. Between contractions the walls recoil in order to maintain blood pressure, allowing the movement of blood even after the ventricles of the heart have relaxed (18). Muscular arteries

distribute blood to various parts of the body; such as the coronary and femoral arteries. Muscular artery walls contain high amounts of smooth muscle, allowing them to alter the amount of blood delivered to the target organ as required. Muscular arteries have considerably less elastin than elastic arteries, and considerably more layers of VSMCs, as their name indicates (18). Finally, arterioles are small arteries that deliver blood to capillaries. They control the blood flow through capillary beds, contracting or dilating hence altering the diameter of the lumen.

1.2.3 Effect on vascular tone

As previously eluded to, the endothelium is integral in maintaining vascular homeostasis by releasing a plethora of vasoactive molecules, both vasodilatory; such as nitric oxide (NO), prostacyclin (PGI₂), and endothelium derived hyperpolarising factor (EDHF) and vasoconstrictive, such as thromboxane (TXA₂) and endothelin-1 (ET-1). These substances are released in response to both physical stimuli, such as shear stress, or neurohumoural substances, such as bradykinin or acetylcholine. These vasoactive substances are discussed in more detail below.

1.2.3.1 Nitric Oxide

Furchgott and Zawadzki first identified an endothelium-derived relaxing factor in 1980, demonstrating the endothelium-dependent nature of acetylcholine on VSMC relaxation (19). This factor was later identified as NO in 1987 (20,21). NO is a colourless gaseous free radical with numerous functions involving not only the cardiovascular system, but also the nervous and immune system. The production of NO is discussed in detail later in section 1.5.

Primarily, NO acts as an endogenous vasodilator. NO diffuses across the endothelial cell and into the adjacent VSMCs. Here, it binds to soluble guanylyl cyclase (sGC), which can be considered a NO receptor. Now activated, sGC increases the conversion of guanosine triphosphate (GTP) to cyclic guanosine monophosphate (cGMP). cGMP reduces calcium release within VSMCs via activation of protein-dependent kinases, such as protein kinase G (PKG). PKG phosphorylate a number of key target proteins, such as potassium channels, IP₃R (inositol triphosphate (IP₃) receptor), the plasma membrane calcium ATPase (PMCA), and the sarcoplasmic reticulum calcium ATPase (SERCA). All of these phosphorylations act to increase calcium extrusion and/or sequestration, reducing the formation of the calcium-calmodulin-myosin light chain kinase (MLCK) complex, thus decreasing phosphorylation of serine residues within the myosin light chain, and preventing vasoconstriction (Figure 1.2) (22).

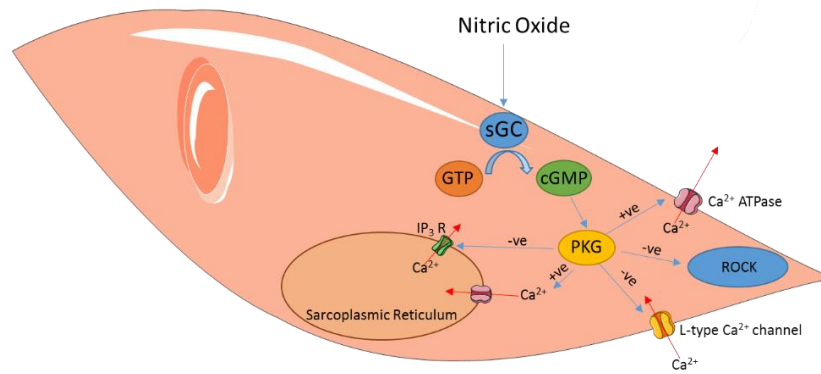


Figure 1.2 NO-mediated vascular smooth muscle cell relaxation. cGMP production and the subsequent activation of PKG, leading to phosphorylation of multiple proteins inducing relaxation. Many targets of PKG lead to a reduction in intracellular calcium, either by increasing calcium efflux from the cell, reducing calcium influx into the cell, or increasing calcium return to the sarcoplasmic reticulum. Additionally, PKG can phosphorylate ROCK, preventing the phosphorylation of myosin light chains and subsequent contraction of muscle fibres. GTP – guanosine triphosphate, cGMP – cyclic guanosine monophosphate, sGC – soluble guanylate cyclase, PKG – protein kinase G, ROCK – rho-associated protein kinase, IP₃R – Inositol triphosphate receptor.

1.2.3.2 Prostacyclin (PGI₂)

The discovery of prostaglandins (PG) predates NO, first identified in 1976 (23). Prostanoids (PGs and TXA₂) represent a group of molecules derived from arachidonic acid (AA) that can modulate vascular homeostasis under physiological conditions and promote thrombosis and inflammation in pathophysiological conditions. AA is a polyunsaturated fatty acid present within the phospholipids of cellular membranes. Phospholipase A₂ catalyses the hydrolysis of the sn-2 ester bond, generating a free fatty acid and a lysophospholipid (24). AA is converted to prostaglandin H₂ via cyclooxygenase (COX), before PGI₂ is produced following the action of PGI₂ synthase on PGH₂. PGI₂ acts as a paracrine signalling molecule, eliciting its effects via a PGI₂ receptor on neighbouring endothelial cells and platelets. The PGI₂ receptor is a G protein coupled receptor (GPCR) that contains the G_s α subunit, which following activation stimulates adenylyl cyclase to increase intracellular cyclic adenosine monophosphate (cAMP), subsequently activating protein kinase A (PKA) (25). In platelets, PKA increases phosphorylation of vasodilator-stimulated phosphoprotein (VASP), inhibiting the calcium-dependent association of glycoprotein IIb and IIIa, forming a receptor for both fibrinogen and Von Willebrand factor (vWF). In VSMCs, amongst other mechanisms, PKA increases the phosphorylation of myosin light chain kinase (MLCK), which inhibits the enzyme, reducing its activity, leading to vasodilation (Figure 1.3). Although primarily a platelet inhibitor, PGI₂ is also a very effective vasodilator, and has been shown to play a compensatory role when NO bioavailability is reduced, as seen in patients with endothelial dysfunction (26).

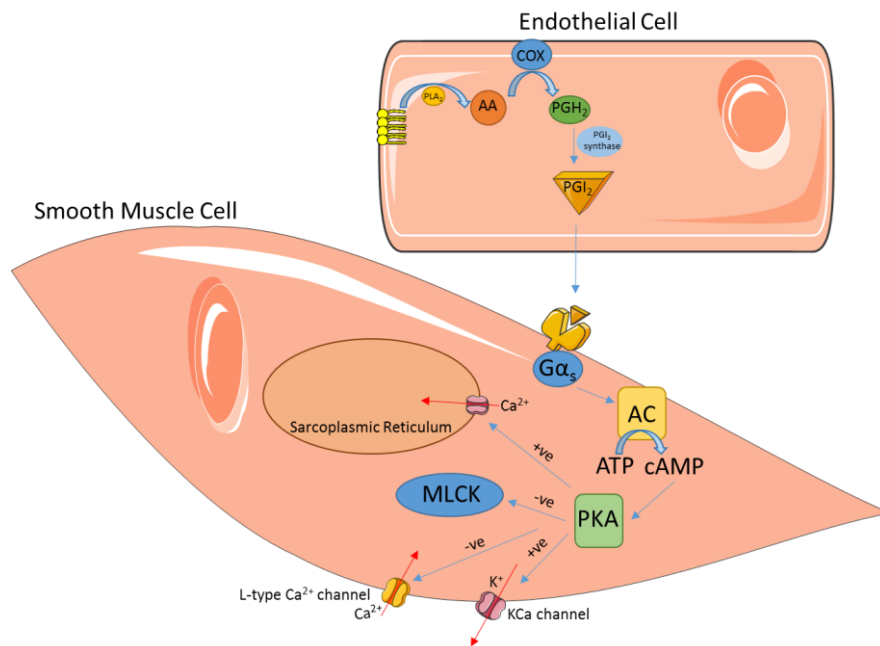


Figure 1.3 Prostacyclin mediated vasodilation. PGI₂, derived from AA, activates GPCR on the surface of the VSMC. Increases in intracellular cAMP and subsequent activation of PKA leads to phosphorylation of various proteins that act to increase relaxation, primarily via hyperpolarisation of the VSMC and inhibition of MLCK. COX – cyclooxygenase, PLA₂ – phospholipase A₂, AA – arachidonic acid, PGH₂ – prostaglandin H₂, AC – adenylate cyclase, PKA – protein kinase A, MLCK – Myosin light chain kinase.

1.2.3.3 Endothelium-derived hyperpolarising factor (EDHF)

Inhibition of both NO and PGI₂ synthesis has been shown to only partially attenuate the endothelium-dependent relaxation of VSMCs. This relaxation was shown to occur independently of increases in intracellular cyclic nucleotides, suggesting an additional pathway that involved smooth muscle cell hyperpolarisation, which was subsequently coined endothelium-dependent hyperpolarising factor (EDHF) (27). Hyperpolarisation of VSMCs occurs by reducing the open probability of voltage-gated calcium channels, and thus reducing the intracellular calcium concentration (28).

EDHF mediated responses are associated with an increase in intracellular calcium within the endothelial cell, in response to agonists that stimulate GPCR. Additionally, a reduction in extracellular calcium concentration attenuates EDHF responses, suggesting that the increase in endothelial [Ca²⁺] is a pivotal step (28). Subsequently, calcium activated potassium channels within the endothelial cell allow the release of potassium ions into the sub-endothelial space. This increase in extracellular potassium ions lead to activation of both the sodium/potassium pump, and inward rectifying (K_{IR}) potassium channels, resulting in hyperpolarisation of the VSMC (29).

Additionally, endothelial cells and VSMCs are connected via myo-endothelial gap junctions, capable of propagating the hyperpolarisation. Indeed, it has been shown previously that blockage of these junctions can attenuate EDHF-mediated relaxation in the rabbit mesenteric artery (30). However, the term endothelium derived hyperpolarising factor is ambiguous, as both NO and PGI₂ are derived from endothelial cells and can lead to VSMC hyperpolarisation via potassium channel activation.

1.2.3.4 Endothelin-1

Endothelin-1 (ET-1) is the predominant isoform of endothelin, a 21 amino acid peptide produced from endothelial cells. Each isoform is produced from big endothelin-1 (big ET-1), via endothelin converting enzyme (ECE) present on the surface of the endothelial cell membrane (31). ET-1 is released following endothelial cell stimulation by external stimuli, and binds to GPCR's present on VSMC membranes. There are two sub-types of ET-1 receptors; ET_A and ET_B. Both are coupled to a G_q α protein, leading to the formation of IP₃ and intracellular calcium accumulation, leading to contraction of VSMCs and vasoconstriction (Figure 1.4).

Interestingly, ET_B receptors are also present on the surface of endothelial cells. Activation of these receptors leads to the formation of both NO and PGI₂ within the endothelial cells. Thus, ET_B receptors play a crucial role in the control of vascular tone, protecting the vasculature against the potent vasoconstrictor effects of endogenous endothelins acting on VSMCs (32).

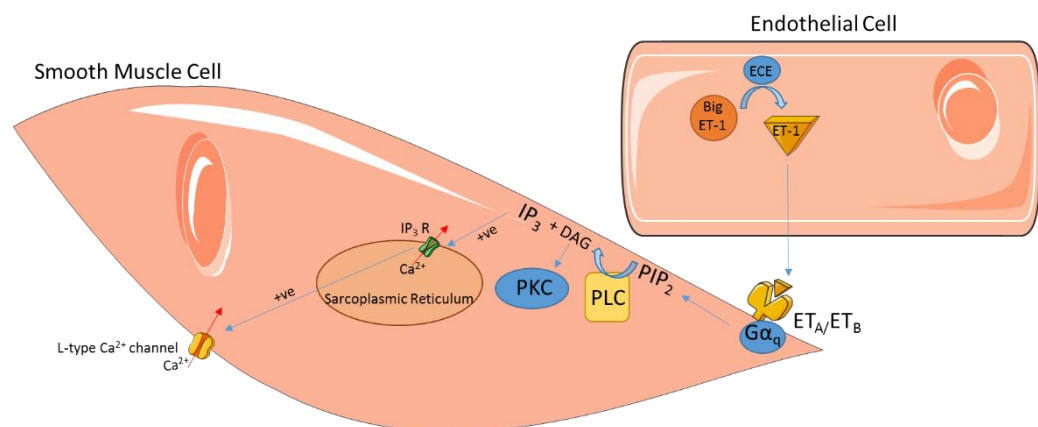


Figure 1.4 Endothelin-1 mediated vasoconstriction. ET-1 produced from endothelial cells binds to G_q coupled receptors leading to increases in intracellular calcium, primarily via IP₃ and activation of PKC. ET-1 - endothelin-1, ECE – Endothelin converting enzyme, IP₃ – inositol triphosphate, DAG – diacyl glycerol, PIP₂ - Phosphatidylinositol bisphosphate, PLC – phospholipase C, PKC – protein kinase C.

1.2.3.5 Thromboxane A₂

TXA₂ and PGI₂ are physiological antagonists, thus the balance between them is critical to maintaining vascular tone. In contrast to PGI₂, TXA₂ is both a potent vasoconstrictor and platelet activator. Although predominantly produced in platelets, endothelial cells are also capable of producing TXA₂ in small amounts (33,34). Similarly to PGI₂ it is produced following synthetase conversion of the PGH₂ intermediate. TXA₂ acts via the thromboxane receptor, a GPCR capable of coupling to at least four separate G protein families (35). Thus, TXA₂ is capable of eliciting a range of cellular responses. Its effects on vasoconstriction are thought to be primarily via the G_q protein pathway, leading to increases in intracellular calcium in VSMCs, similar to ET-1 (36).

1.2.4 Effect on haemostasis

In addition to its effect on vascular tone, the endothelium also plays a pivotal role in maintaining haemostatic balance. A healthy, functional endothelium provides a non-thrombogenic lining to the vessel, allowing platelets to flow without initiating adhesion and aggregation. In addition to their effect on vascular tone, NO and PGI₂ also act to reduce platelet aggregation. These molecules can prevent accumulation of intracellular calcium, preventing shape change, fibrinogen receptor activation and release of granules leading to further platelet activation.

In addition to these molecules, the endothelium utilises a range of anti-coagulant mechanisms to promote haemostasis. Endothelial cells express thrombomodulin, an integral membrane protein capable of binding thrombin, preventing its ability to activate platelets and promote fibrin clot formation. Furthermore, this thrombin-thrombomodulin complex, together with protein S, activates protein C (APC) a serine protease zymogen. APC proteolyzes peptide bonds in factor Va and factor VIIIa of the coagulation cascade (37). Furthermore, the endothelium produces antithrombin, a serine protease inhibitor that targets factors within the contact activation pathway; primarily factor Xa and factor IIa (thrombin) (38). Tissue factor pathway inhibitor (TFPI) is a single chain polypeptide which can reversibly inhibit factor Xa. This TFPI-Xa complex can then consequently further inhibit the FVIIa-TF complex (39). Additionally, the endothelium produces tissue plasminogen activator (tPA), which converts plasminogen to plasmin, a key enzyme in the degradation of fibrin clots (39). Figure 1.5 highlights these mechanisms within the coagulation cascade.

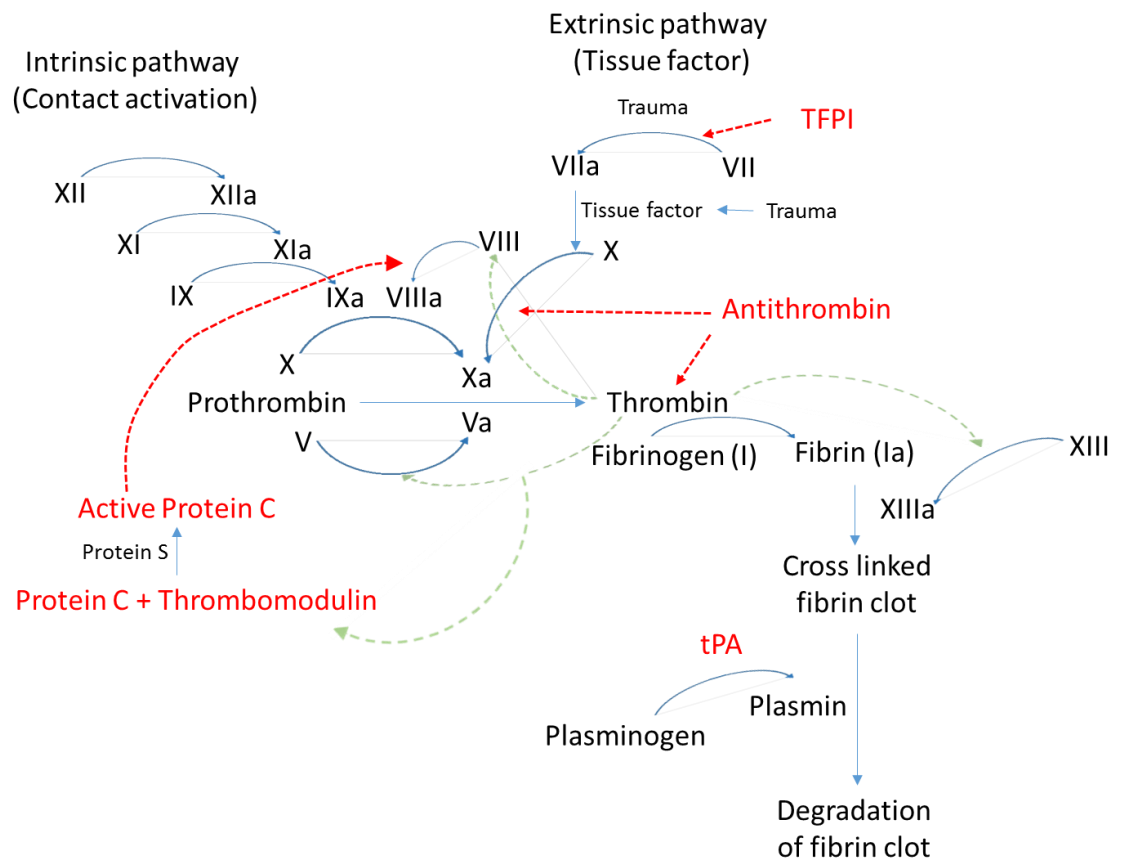


Figure 1.5 Regulation of the coagulation cascade by endothelium derived substances. Green arrows indicate positive feedback, red arrows indicate inhibition. The endothelium ensures coagulation is tightly regulated, producing various molecules that act to reduce thrombin generation and increase fibrinolysis. TFPI – tissue factor pathway inhibitor, tPA – tissue plasminogen activator.

Following injury or damage to the vascular wall, the endothelium can shift to promote a pro-coagulant state. Damage to the endothelium exposes tissue factor (TF), leading to activation of the extrinsic pathway of the coagulation cascade, enhancing factor VII activity. The endothelium can release vWF stored in Weibel-Palade bodies. vWF itself has no catalytic activity, and elicits its effects by binding to other proteins and molecules, such as factor VIII, allowing stabilisation of the protein (40). Additionally, its ability to bind to both collagen (type I and III) and platelet glycoprotein Ib ensures that platelets adhere to damaged vascular subendothelium. Upon activation, Factor VIII dissociates from vWF, and interacts with factor IXa, eventually leading to the production of thrombin from prothrombin (40). Activated endothelial cells release platelet activating factor (PAF) which can bind directly to its GPCR receptor on platelets leading to increases in intracellular calcium. Finally, plasminogen activator inhibitor-1 (PAI-1) is a serine protease inhibitor which inhibits tPA, preventing the breakdown of fibrin clots (41). Table 1.1 summarises these pro- and anti-thrombotic factors.

Table 1.1 Pro-thrombotic and anti-thrombotic factors and their mechanisms.

Molecule	Effect	Mechanism
Nitric oxide / Prostacyclin	Anti-thrombotic	Suppress platelet activation and adhesion
Thrombomodulin	Anti-thrombotic	Binds to thrombin, cofactor in thrombin-induced activation of Protein C
Protein S	Anti-thrombotic	Cofactor in thrombin-induced activation of Protein C
Protein C	Anti-thrombotic	Inactivates factor Va and VIIIa
Antithrombin	Anti-thrombotic	Serine protease inhibitor, targeting thrombin, and activated factors within the intrinsic pathway (Xa, IXa, XIa, XIIa).
Tissue factor pathway inhibitor	Anti-thrombotic	Inhibits factor Xa. Xa-TFPI complex can further inhibit FVIIa-TF complex
Tissue plasminogen activator	Anti-thrombotic	Converts plasminogen to plasmin, increasing fibrinolytic activity, degrades fibrin clots.
Urokinase	Anti-thrombotic	Converts plasminogen to plasmin, increasing fibrinolytic activity, degrades fibrin clots.
Platelet activating factor	Pro-thrombotic	Activates PAF receptor on platelets, increasing intracellular calcium accumulation leading to activation
von Willebrand factor	Pro-thrombotic	Binds to and stabilises factor VIII Binds to exposed collagen Binds to platelet glycoprotein Ib
Tissue factor	Pro-thrombotic	Combines with factor VIIa to form a tenase complex

1.2.5 Effect on inflammation

The endothelium can also control inflammation and the immune response, primarily via regulation of leukocyte recruitment from the blood into the sub-endothelial space. Upon activation by pro-inflammatory cytokines, such as interleukin-1 (IL-1) or tumour necrosis factor (TNF- α), endothelial cells express various cell adhesion molecules (CAMs), which allow for interaction with their respective counter-receptors on leukocytes (42). Selectins, such as P-selectin and E-selectin mediate the initial stage in leukocyte transmigration, allowing the rolling of leukocytes along the endothelium. P-selectin is expressed by both endothelial cells and platelets, whereas E-selectin is expressed only by endothelial cells. P-selectin is stored in Weibel-Palade bodies and can be rapidly mobilised to the cell surface upon activation of endothelial cells (43). E-selectin does not exist in a preformed pool, but is reliant entirely on transcriptional regulation and requires up to 3 hours to achieve peak expression. L-selectin present on leukocytes acts as a homing receptor, binding to both P- and E-selectin, slowing the velocity of leukocyte movement. P-selectin glycoprotein ligand-1 (PSGL-1) can bind to L- E- and P-selectin, but has the highest affinity for P-selectin (44).

The expression of the adhesion molecules intercellular adhesion molecule 1 (ICAM-1), vascular cell adhesion molecule-1 (VCAM-1) and platelet endothelial cell adhesion molecule (PECAM-1) are all increased following endothelial cell activation. They interact with their leukocyte counter-receptors, mediating firm adhesion of the leukocyte to the endothelium. ICAM-1 is constitutively expressed in most vascular beds; however, expression is increased following IL-1 or TNF α exposure (45). PECAM-1 is found largely in the intercellular junctions between endothelial cells (46).

Integrins present on the leukocyte surface are glycoprotein complexes consisting of α - and β -subunits. Lymphocyte function-associated antigen 1 (LFA-1) (CD11a/CD18, α L β 2) present on leukocytes bind to ICAM-1, playing a particularly important role in the firm adhesion of neutrophils. Macrophage-1 antigen (CD11b/CD18, α M β 2) utilises the same β -chain as LFA-1, and also binds to ICAM-1 (47). Integrin α 4 β 1 is present on leukocytes but does not interact with VCAM-1 until leukocytes are activated, undergoing the necessary conformational change allowing for interaction. Upregulation of these integrins, in combination with the shedding of L-selectin on leukocytes, allows for the transition between the "rolling" and "adhesion" states of transmigration (48).

Finally, once firmly attached, passage of the leukocytes across the endothelium is primarily regulated by PECAM-1. PECAM-1 is present on endothelial cells, platelets, and leukocytes, facilitating transmigration predominately via homophilic interactions (49).

Figure 1.6 summarises the process of leukocyte transmigration. Table 1.2 summarises the key interactions between endothelial adhesion molecules and leukocyte receptors.

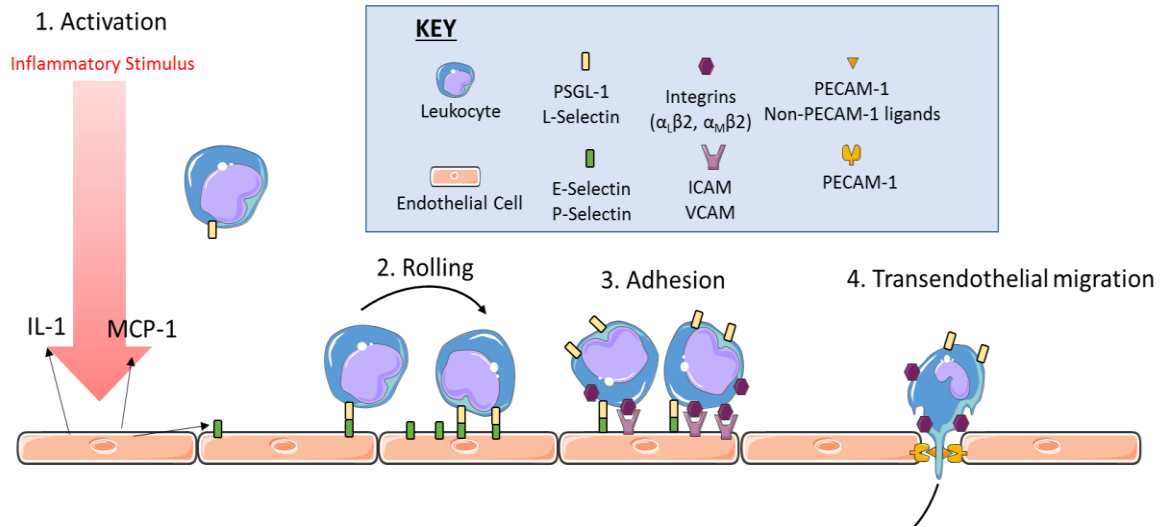


Figure 1.6 Illustration of leukocyte recruitment and transmigration through the endothelium. Endothelial cells are activated, and produce selectins, permitting leukocyte rolling. Firm adhesion is mediated by cell adhesion molecules. PECAM-1, situated between endothelial cells, facilitates transendothelial migration. IL-1 – Interleukin-1, MCP-1 – Monocyte chemoattractant protein-1, PSGL-1 – P-selectin glycoprotein ligand-1, ICAM – intercellular adhesion molecule, VCAM – vascular cell adhesion molecule, PECAM – platelet endothelial cell adhesion molecule-1.

Table 1.2 Summary of the key endothelial adhesion molecules complementary leukocyte receptor(s) and their role in leukocyte extravasation.

Adhesion molecule	Leukocyte receptor(s)	Function
P-Selectin	PSGL-1, L-Selectin, Sialyl-Lewis X	Capture
E-Selectin	L-Selectin, PSGL-1, Sialyl-Lewis X	Rolling
ICAM-1	LFA-1 (αLβ2), Mac-1 (αMβ2)	Firm adhesion, transmigration
VCAM-1	VLA-4	Firm adhesion
PECAM	PECAM-1	Transmigration

Adapted from (46). PSGL-1 – P-selectin glycoprotein ligand-1, ICAM – intercellular adhesion molecule, VCAM – vascular cell adhesion molecule, PECAM – platelet endothelial cell adhesion molecule-1, LFA – Lymphocyte function-associated antigen 1, Mac-1 – macrophage-1 antigen, VLA-4 – Very late antigen-4.

The importance of these interactions is highlighted by mutations within the genes encoding these adhesion molecule receptors, leading to leukocyte adhesion deficiency (LAD). LAD-1 is rare and often fatal, caused by mutations in the gene encoding CD18, present in the integrins LFA-1 and Mac-1. LAD-2 is caused by an absence of Sialyl-Lewis X, a ligand for P- and E-selectin (50).

1.3 Atherosclerosis

The development of atherosclerotic plaques is responsible for CAD, cerebrovascular disease and peripheral artery disease. Simply, atherosclerosis is characterised by the thickening of an arterial wall as a result of cholesterol deposition and subsequent leukocyte invasion and accumulation. Atherosclerosis develops over the course of decades, beginning in the early teenage years (51). The speed of progression and development can be accelerated by various risk factors mentioned in section 1.1.2. Large to medium size arteries are especially prone to developing atherosclerosis, such as the coronary, femoral, and cerebral arteries, whereas smaller coronary arteries are less susceptible to plaque formation.

1.3.1 Endothelial dysfunction

As previously mentioned, endothelial cells that line the blood vessels represent a dynamic interface between the blood stream and the arterial wall. The link between endothelial function and development of atherosclerosis was first established approximately 40 years ago (52), and has remained a key area of research within the cardiovascular field ever since. The response to injury hypothesis suggests that the initial step in atherogenesis is endothelial dysfunction, which may be triggered by a number of insults, such as reactive oxygen species (ROS), physical injury as a result of hypertension, turbulent blood flow, hyperlipidaemia, or chronically elevated blood glucose levels (9). Endothelial dysfunction can be defined as the impaired ability of the endothelium to regulate and maintain vascular homeostasis effectively (53). Under physiological conditions the endothelium maintains an anti-thrombotic surface, described in section 1.2.4. However, under pathophysiological conditions, the endothelium shifts towards a pro-thrombotic state, characterised by elevated levels of pro-thrombotic and pro-inflammatory molecules such as tissue factor (TF) and monocyte chemoattractant protein-1 (MCP-1) being released, and an increase in surface adhesion molecule expression (54). Indeed, a reduction in NO bioavailability is considered the hallmark of endothelial dysfunction. It is perhaps more appropriate to refer to this process not as endothelial dysfunction, but instead endothelial activation. This represents a switch from the quiescent phenotype, to one which involves the host defence response (53). Endothelial activation/dysfunction is often observed in the early stages of development of CVD, and is key to the initiation of atherosclerosis, often predating clinical symptoms of CVD (55).

1.3.2 Fatty streak formation

As a result of cellular activation, endothelial cells alter their morphology, and the tight junctions between them loosen, increasing permeability to lipids and leukocytes. LDL cholesterol enters the arterial wall and undergoes modification in the form of oxidation, typically from reactive oxygen species (ROS). Endothelial cells, now releasing chemokines (such as MCP-1) and expressing surface adhesion molecules (such as VCAM-1), recruit monocytes and T-lymphocytes to adhere and migrate through the endothelial cell layer (56). Once migrated into the intima, monocytes differentiate into macrophages, and begin to engulf the oxidised LDL that has deposited beneath the endothelial layer via scavenger receptors. Macrophages become lipid-laden, and are referred to as “foam cells”, a hallmark of early atherosclerosis. Fatty streaks are the first visible sign of atherosclerosis; they consist primarily of foam cells within the tunica intima. Although clinically insignificant, they are considered a precursor to more complex plaque formation.

1.3.3 Intermediate lesion & atheroma formation

Foam cells eventually undergo apoptosis; however the lipid remains within the intima, forming small extracellular lipid pools, characteristic of an intermediate lesion. At this stage, a large, confluent well-delineated accumulation of extracellular lipid, known as a lipid core, has not yet developed (56). This process of lipid accumulation and foam cell formation perpetuates the inflammatory response further. This inflammatory milieu includes cytokines such as interferon (IFN)- γ , platelet derived growth factor (PDGF) and transforming growth factor (TGF)- β , which induce a change in the phenotypic state of VSMCs, from a “contractile” state to an active “synthetic” state. In a contractile phenotype, VSMCs respond to agents that induce either vasoconstriction or vasodilation. Conversely, in a synthetic state, they are capable of expressing genes for a number of growth molecules and can synthesise extracellular matrix (ECM) components, namely collagen, elastin and proteoglycans (57). VSMCs in this state can migrate and proliferate from the tunica media to the tunica intima.

VSMCs within the tunica intima deposit these ECM components, producing a fibrous cap; a layer of fibrous connective tissue thicker and less cellular than the regular tunica intima. VSMCs continue to migrate and proliferate, which in combination with lipid accumulation, slowly expand the plaque and narrow the arterial lumen (58). A fibrous cap is formed of the ECM components, and separates the lipid core from arterial blood flow. These fibrous caps can be prone to rupture in response to a variety of triggers.

1.3.4 Fibroatheroma

A fibroatheroma typically consists of multiple lipid cores, with many fibrotic layers of VSMCs. As the plaque expands, the central region becomes hypoxic and thus necrotic (51). Over time, the plaque continues to occlude the arterial lumen. Typically, approximately 50-75% of the artery must be occluded before symptoms become apparent (51). VSMCs in their synthetic phenotype begin to deposit calcium, calcifying the plaque and leading to an increase in arterial stiffness.

1.3.5 Complicated lesion

Eventually, the fibrous cap may rupture, exposing thrombogenic material such as collagen to circulating platelets leading to the formation of a thrombus. Thrombus formation can either occlude arteries directly, or detach and occlude smaller downstream branches, causing a thromboembolism (59). Alternatively, expanding plaques can eventually completely occlude the lumen directly, which is often asymptomatic until stenosis reaches over 70%, leading to ischaemia. In severe cases, thrombus formation leads to an infarction; severe reduction or complete prevention of blood flow, leading to necrosis of the tissue supplied by this artery in approximately 5 minutes (60).

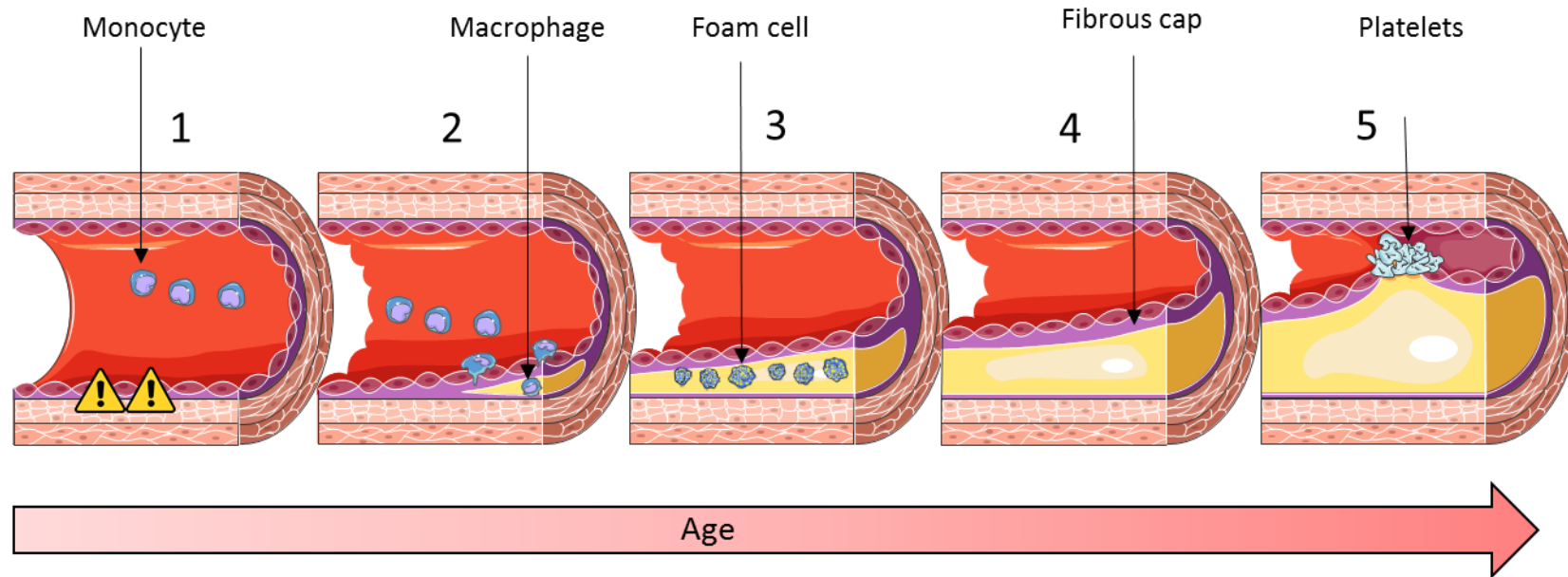


Figure 1.7 The progression of atherosclerosis over time. This diagram represents a blood vessel over decades of an individual's life, leading to occlusion of the vessel. 1. Endothelial dysfunction, leading to activation of endothelial cells. 2. LDL cholesterol accumulation, LDL is modified by ROS forming oxidised-LDL. Monocytes migrate through the endothelium and mature into macrophages. 3. Macrophages engulf oxidised-LDL, forming foam cells. Apoptosis of foam cells leads to extracellular lipid pools. 4. VSMC proliferation and fibrous cap formation to protect the plaque. 5. Plaque rupture and thrombosis, leading to occlusion of the vessel. LDL – low density lipoprotein, ROS – reactive oxygen species, VSMC – vascular smooth muscle cell.

1.4 Oxygen and hypoxia in cardiovascular disease

The presence of an atherosclerotic plaque in the wall of a coronary artery reduces the perfusion of downstream myocardial tissue. Ischemia is defined as the inability of the vasculature to supply adequate O₂ and nutrients to tissues. This, in turn, leads to tissue hypoxia (reduced oxygen), or in severe cases, anoxia (absence of oxygen). The physiological response to reduced tissue perfusion is that the resulting tissue hypoxia induces hypoxia inducible factor (HIF)-1 activity, leading to the transcription of genes involved in cell proliferation, angiogenesis and vascular remodelling.

1.4.1 Oxygen levels *in vitro* and *in vivo*

Precise measurement of *in vivo* oxygen concentration is a challenging task. However, available data suggests that oxygen concentrations vary between tissues significantly. One study in rats demonstrated that the partial pressure of O₂ ranges from 60 mmHg (7.5% O₂) in the bladder, to 40 mmHg (5% O₂) in muscle, and 20 mmHg (2.5% O₂) in the liver (61). Similarly, the pO₂ in human tissues varies between 2-20% O₂ (62). Typically, the pO₂ of human blood is between 75-100 mmHg, equivalent to 10-13% O₂ (63). *In vivo*, under physiological conditions, most human cells experience approximately 40 mmHg (5%) oxygen. Below this partial pressure of oxygen can be considered “hypoxic” (64). When the intracellular oxygen concentration in tissues is reduced from normoxia to “moderate hypoxia” (8 - 0.8 mmHg (1 - 0.1% O₂)), mitochondrial respiration is unaffected (65). Oxygen concentrations lower than 0.1% O₂ can be considered severe hypoxia, and can affect cell viability and survival (66). Most *in vitro* studies use 1-2% O₂ (8-16 mmHg), as an established model of hypoxia (64). HIF-1 is detected in many cell culture systems at a cut off around 5% O₂ (40 mmHg) and below (67). HIF consists of an oxygen sensitive HIF- α domain, and a constitutively expressed HIF- β domain. HIF- α consists of 2 isoforms, HIF-1 α and HIF-2 α . HIF-1 α is primarily involved in the acute response to hypoxia, and expression is reduced following prolonged hypoxia. HIF-2 α levels continue to increase in hypoxia over time, and are important for more chronic changes in hypoxia (68). Interestingly, the pO₂ in human tissues (3-10% O₂ (23-70 mmHg)) is close to those used in *in vitro* studies to mimic hypoxia. Thus HIF-2 α may be responsible for the transcription of genes involved in “physioxia” (62).

1.4.2 Consequences of hypoxia on the vasculature

Oxygen availability is a major determinant of cell metabolism and gene expression. Thus, as cellular O₂ levels decrease, these parameters are drastically altered. Upon exposure to hypoxia, both endothelial and VSMCs respond rapidly, utilising both acute and chronic changes to adapt. These changes are summarised in figure 1.8.

1.4.2.1 Vascular tone

Within pulmonary arteries, the response to hypoxia in terms of vascular tone can be considered in phases. First, an initial contraction phase, followed by a transient relaxation phase, then finally a sustained contraction (69). This appears to be mediated by both endothelium-dependent and endothelium-independent mechanisms (70). The molecular mechanism responsible for this involves hypoxia-sensitive voltage-gated potassium channels in pulmonary artery smooth muscle cells, which leads to depolarisation and activation of voltage-dependent calcium channels (71). The physiological role of this is to divert blood away from poorly ventilated regions of the lung, and towards regions with adequate oxygen supply, thus matching ventilation to perfusion (72). This is the opposite of the systemic circulation, where hypoxia leads to vasodilation (73). This effect may be direct, via an inadequate oxygen supply to sustain VSMC contraction, or indirect, via the production of vasodilator metabolites (74).

1.4.2.2 Inflammation

Hypoxia increases the expression of numerous adhesion molecules on the surface of the endothelium, including P-selectin, E-selectin, ICAM-1, and VCAM-1, thus augmenting its permeability to leukocytes (75). Endothelial cells also increase expression of numerous pro-inflammatory cytokines including IL-6, IL-1 α , IL-8 and MCP-1 under hypoxic conditions (76). These adaptations are largely driven by HIFs ability to bind to hypoxia-response promotor elements, inducing transcription of numerous genes involved in inflammation, such as nuclear factor- κ B (NF- κ B) (77).

1.4.2.3 Coagulation

Hypoxia exposure results in reduced production of thrombomodulin, leading to accelerated thrombin activity (78). Similarly, hypoxia has been shown to downregulate the expression of the TFPI gene, which is reversed following inhibition of HIF-1 α (79). Recently, in rat glioma cell lines, TF itself has shown to be upregulated following exposure to the hypoxia mimetic CoCl₂ (80). PAI-1 inhibits fibrinolysis, and is upregulated in hypoxia, promoting the stability of fibrin clots (81).

These observations are complemented by *in vivo* studies, which have demonstrated that a 2 hour hypoxic challenge in chronic obstructive pulmonary disease (COPD) results in an increase in coagulation activity (82).

1.4.2.4 Oxidative stress

Hypoxia leads to an increase in oxidative stress via numerous mechanisms. NADPH oxidase, an enzyme involved in transferring electrons across membranes, largely underlies this increase. Upregulation of NADPH oxidase in hypoxia has been shown to activate HIF-1 via an increase in ROS (83). Similarly, complex III in the mitochondrial electron transport chain also produces ROS under hypoxic conditions, leading to stabilisation of HIF- α , via an inhibition of prolyl hydroxylases (84). Many other oxygen-sensitive enzymes are capable of producing ROS, including xanthine oxidoreductase (85), cytochrome p-450 (86), and even nitric oxide synthase (NOS) (87).

1.4.2.5 eNOS function

The effect of hypoxia on eNOS function is complex. Firstly, hypoxia is capable of destabilising eNOS mRNA, an effect mediated by Rho-kinase (88). Interestingly, once eNOS has been transcribed, studies have shown that hypoxia leads to a reduction in eNOS phosphorylation at the activatory site Serine 1177, and increased phosphorylation at the inhibitory site Threonine 495 (89,90).

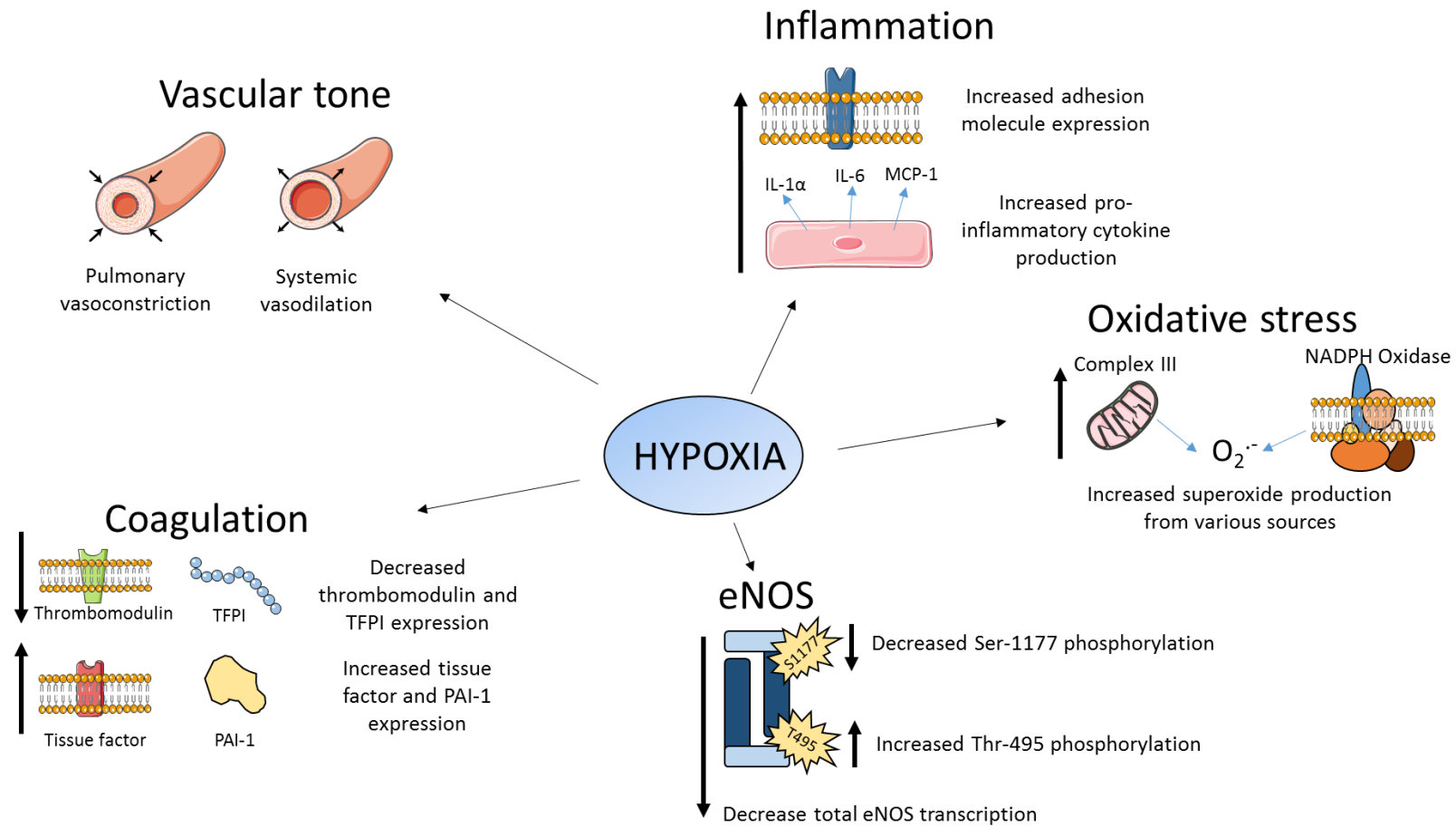


Figure 1.8 The effects of hypoxia on the vasculature. Hypoxia induces changes within cells in order for them to adapt to the reduced availability of oxygen. TFPI – tissue factor pathway inhibitor, PAI-1 - plasminogen activator inhibitor-1, eNOS – endothelial nitric oxide synthase, NADPH oxidase - nicotinamide adenine dinucleotide phosphate-oxidase. IL-1 α – interleukin 1 α , IL-6 – interleukin 6, MCP-1 – monocyte chemoattractant protein-1.

1.5 Nitric Oxide

1.5.1 Nitric Oxide Synthase

NO, or nitrogen monoxide, is a free radical signalling molecule, with a plethora of functions involved in regulating aspects of the cardiovascular, nervous and immune systems. NO is produced by one of three isoforms of NO synthase (NOS), catalysing the reaction between molecular oxygen and L-arginine. Two of these are constitutive forms, which are present under physiological conditions in both the endothelium (eNOS) and in neurones (nNOS). The third is an inducible form (iNOS), and expressed predominantly in macrophages, neutrophils, VSMCs and endothelial cells in response to pathological stimuli such as IL-1, TNF- α and IFN- γ (91).

The production of NO from all NOS isoforms is dependent on additional cofactors, including nicotinamide adenine dinucleotide phosphate (NADPH), and bound prosthetic groups including tetrahydrobiopterin (BH₄), flavin adenine dinucleotide (FAD), and flavin mononucleotide (FMN) (91). These cofactors control the assembly of the enzyme into its active dimer state. L-Arginine is typically present in excess within endothelial cell cytoplasm, therefore NO production is dependent on enzyme activity and/or O₂ availability. Calcium-activated calmodulin regulates electron transfer within the molecule. Interestingly, whilst iNOS and nNOS are located in the cytosol, eNOS is predominantly membrane-associated, due to post-translational modifications (N-myristoylation and cysteine palmitoylation) leading to association with caveolin (92). Caveolin is a membrane protein present within caveolae (invaginations in the plasma membrane containing high levels of cholesterol and sphingolipids). Following receptor-mediated agonist stimulation, the binding of calcium-activated calmodulin causes dissociation from caveolin, release of eNOS from caveolae and enzyme activation (92).

eNOS subunits are comprised of two domains; a reductase domain and an oxygen domain, connected by a central calcium-calmodulin binding region. Electrons are donated from NADPH, sequentially passed through FAD and FMN within the reductase domain, finally passing to an oxygenase domain that contains haem, BH₄, and the substrate. BH₄ stabilises the positively charged pterin ring of L-Arginine, thus increasing its binding to the enzyme, in addition to stabilising the dimeric form of the enzyme (93). The reduced haem can reduce O₂, simultaneously oxidising L-arginine, generating L-citrulline and NO. Calmodulin binding to eNOS increases electron transfer within the reductase domain (Figure 1.9).

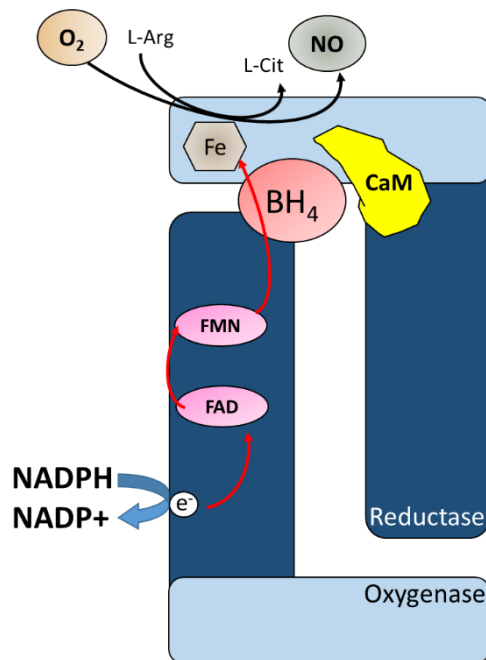


Figure 1.9 Structure of eNOS. eNOS consists of a dimer, each monomer comprised of an oxygenase domain and a reductase domain. Electrons are transferred through the reductase domain to the haem (Fe) containing oxygenase domain, facilitating the conversion of O₂ to NO. eNOS – endothelial nitric oxide synthase, L-Arg – L-Arginine, L-Cit – L-Citrulline, BH₄ – tetrahydrobiopterin, CaM – calmodulin, NADPH - nicotinamide adenine dinucleotide phosphate, NO – nitric oxide.

The production of NO is actually a two-step reaction; firstly, one molecule of NADPH (two electrons) is used with one molecule of oxygen to hydroxylate L-arginine to an enzyme bound intermediate (N ω -hydroxyl-L-arginine) (91). Secondly, eNOS utilises 0.5 molecules of NADPH (one electron) with one molecule of oxygen to oxidise this intermediate to L-citrulline and NO.

Stimulation of eNOS activity begins with agonist stimulation of receptors present on the endothelial cell membrane. Examples of such agonists include acetylcholine, substance-P and bradykinin. Receptors for these agonists are G_q coupled GPCR, leading to activation of PLC and intracellular calcium accumulation. Calcium can then bind to calmodulin facilitating enzyme activation. In addition, shear stress can initiate NO synthesis via mechanoreceptors, and subsequent signalling via Akt, phosphorylating eNOS (Ser 1177) and increasing eNOS sensitivity to calmodulin (94).

1.5.1.1 Uncoupling of eNOS

eNOS uncoupling is a mechanism that can lead to endothelial dysfunction, caused by increased monomerization of the enzyme. When the cofactor BH_4 is limited, due to oxidation or decreased synthesis, eNOS becomes uncoupled, and the damaging superoxide (O_2^-) radical is produced (93). In this scenario, electron transfer is “uncoupled” to L-arginine oxidation, leading to electrons being transferred to molecular oxygen, and the production of superoxide (Figure 1.10). This represents a vicious cycle of reduced NO bioavailability, as not only is NO production reduced, but superoxide production is increased. This leads to further reductions in NO bioavailability by scavenging NO, leading to peroxynitrite formation (ONOO^-), a potent inducer of cell death.

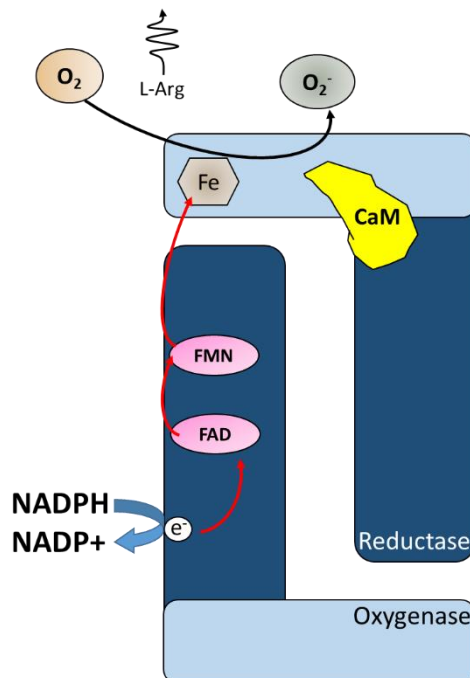


Figure 1.10 eNOS uncoupling. The lack of the cofactor BH_4 lessens L-Arginine binding to the enzyme, leading to electron transfer to oxygen, producing the damaging radical superoxide (O_2^-). eNOS – endothelial nitric oxide synthase, L-Arg – L-Arginine, CaM – calmodulin, NADPH - nicotinamide adenine dinucleotide phosphate.

1.5.2 Function of Nitric Oxide

1.5.2.1 Function in the cardiovascular system

The role of NO in maintaining vascular tone has already been discussed (section 1.2.3.1).

However, NO also elicits other beneficial effects within the cardiovascular system. NO has been shown to prevent aggregation and adhesion of platelets. Despite the importance of coagulation in the prevention of bleeding, over-stimulation of this process can lead to thrombosis. As in smooth muscle cells, the anti-platelet effect of NO is mediated via cGMP-dependent PKG, subsequently preventing intracellular calcium accumulation. This reduction in intracellular calcium reduces the formation of glycoprotein IIb/IIIa, a receptor for fibrinogen and vWF (95,96).

NO also modulates the adhesion of leukocytes to the endothelium following injury (97). Although many other effects of NO are cGMP dependent, the ability of NO to prevent leukocyte attachment to the endothelium is not. Several of the genes encoding pro-inflammatory cytokines and adhesion molecules, such as IL-8, MCP-1, E-selectin and VCAM-1, all share specific DNA binding motifs within their promoters, which interact with the transcription factor NF- κ B (98). NO affects the ability of NF- κ B to bind to these promoter regions, by modification of the conserved redox sensitive C62 residue (99). Secondly, NO induces and stabilises the NF- κ B inhibitor I κ B α (100). Thus, NO can reduce the expression of these molecules, and hence modulate leukocyte recruitment and adhesion via two distinct NF- κ B mechanisms.

NO can also reduce VSMC proliferation, through both cGMP dependent and independent mechanisms. NO can increase levels of PKA via cGMP. PKA can subsequently reduce intracellular calcium levels, counteracting the high calcium levels required for proliferation (101,102). Independently of cGMP, NO can inhibit the production of polyamines required for DNA synthesis, by inhibition of the enzymes arginase and ornithine decarboxylase (103).

1.5.2.2 Function in the nervous system

NO also acts as a neurotransmitter between neuronal cells in both the central and peripheral nervous system. It is a non-conventional neurotransmitter as it is a gas, and thus not stored in synaptic vesicles. Instead, it is synthesised on demand by neurones (104). In the central nervous system (CNS), NO is associated with cognitive function, synaptic plasticity, and control of sleep, appetite, and body temperature (104). Within the peripheral nervous system, NO regulates the non-adrenergic, non-cholinergic relaxation of smooth muscle cells. This can affect a number of tissues; it allows the stomach to accommodate large volumes of food without any significant

increases in intraluminal pressure. It also regulates muscle tone of internal sphincters and regulates peristalsis within the gastrointestinal tract (105).

1.5.2.3 Function in the immune system

The generation of NO is a key feature of many phagocytic cells of the immune system. NO can be produced via iNOS following pro-inflammatory stimuli. Prior to stimulation, the transcription factor NF- κ B is present within the cytosol in an inactive form, as a complex with I κ B (inhibitor of κ B). Once stimulated, by lipopolysaccharide (LPS) for example, the I κ B-NF- κ B complex is phosphorylated, allowing translocation of the transcription factor to the nucleus and induction of iNOS gene expression (106). This leads to production of micromolar levels of NO, far greater than the nanomolar levels produced by constitutively expressed eNOS and nNOS (93). The high level of NO is cytotoxic to pathogens such as viruses, bacteria, fungi and parasites. The NO produced reacts with superoxide generated from NADPH oxidase, producing peroxynitrite. This leads to peroxidation of proteins and lipids, including enzymes involved in cellular respiration, leading to destruction of the pathogen (107).

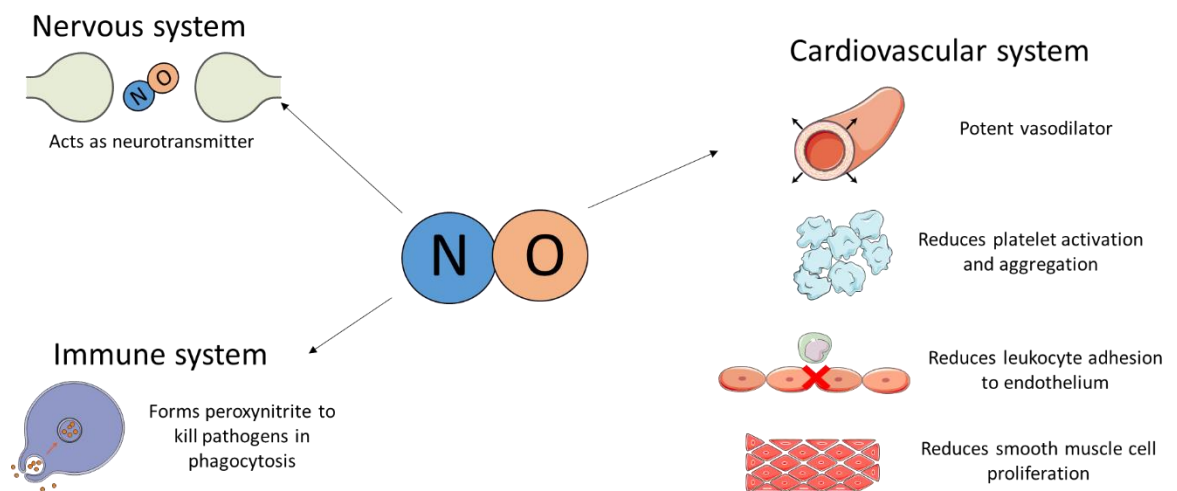


Figure 1.11 The varying functions of NO. NO has many functions throughout the human body, including roles in the nervous and immune systems. It is most studied in relation to its effects within the cardiovascular system, however, where it acts as a potent vasodilator, in addition to reducing platelet aggregation, inflammation, and smooth muscle cell proliferation.

1.5.3 NO metabolism

1.5.3.1 Within the blood

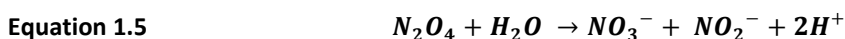
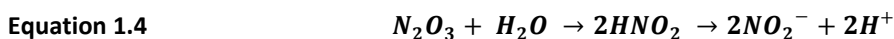
Once NO has been produced by eNOS within the endothelium, a proportion of it moves into the blood. NO acts mainly in an autocrine or paracrine fashion, as signalling is limited due to its rapid auto-oxidation, resulting in the formation of nitrite (NO_2^-) (equation 1.1) (108).



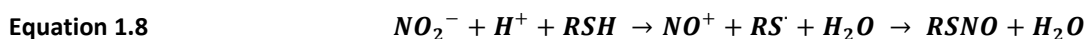
Following this, NO_2^- can undergo further reaction with NO to nitrous anhydride (N_2O_3) (equation 1.2) or it can dimerise, forming dinitrogen tetroxide (N_2O_4) (equation 1.3) (109).



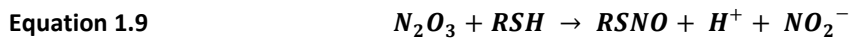
These products can be hydrolysed to yield NO_2^- and nitrate (NO_3^-) respectively, as shown in equations 1.4 and 1.5 (109).



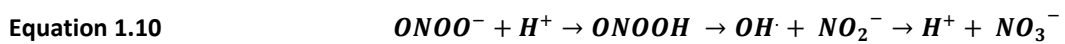
Both NO and its derivatives are capable of interacting with nucleophilic centres, such as thiol groups (R-S) on plasma proteins to generate a number of species. Thiol groups are readily nitrosylated, generating nitrosothiols (RSNOs). Often, RSNO formation first requires the formation of the nitrosonium ion (NO^+), formed via metals (such as iron) found in haem proteins (equation 1.6/1.7) (110). In areas of low pH, NO_2^- is also capable of generating NO^+ and thus RSNO (equation 1.8) (111).



In addition, RSNO can also be formed via N_2O_3 and a thiol group reacting, also producing NO_2^- and a hydrogen ion (equation 1.9) (110).



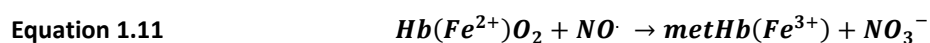
NO can also react with oxygen derived free radicals, such as superoxide (O_2^-), hydrogen peroxide (H_2O_2), and the hydroxyl radical (OH^\cdot). Superoxide is produced from various oxidase enzymes, including nicotinamide adenine dinucleotide phosphate-oxidase (NADPH oxidase), xanthine oxidase, as well as uncoupled eNOS. Notably, superoxide reacts with NO to yield peroxynitrite. Peroxynitrite can subsequently be protonated, leading to its decomposition to NO_3^- (equation 1.10) (112). Peroxynitrite is capable of eliciting a range of harmful effects, including modification of lipids, proteins and nucleic acids.



ROS play a central role in modulating endothelial function. Oxidative stress can be defined as an imbalance between the production of ROS and their removal by antioxidant defence systems, such as superoxide dismutase (SOD), which converts superoxide to hydrogen peroxide. Subsequently, hydrogen peroxide is converted to water (H_2O) and oxygen (O_2). Other antioxidants include glutathione, vitamin E and ascorbate (113). The damaging effects of ROS are well documented. Indeed, cardiovascular risk factors, such as smoking, have been shown to increase ROS levels within the vasculature (114). ROS can lead to DNA damage, lipid peroxidation and protein oxidation, often leading to apoptosis (115). ROS are implicated within the pathophysiology of CVD, as outlined in section 1.3.

1.5.3.2 Within erythrocytes

Haem has an affinity for NO approximately 10,000 times greater than for oxygen. Thus, NO can react with oxygenated haemoglobin, producing met-haemoglobin and NO_3^- (equation 1.11) (116). In this reaction, the oxidation state of the iron within haem is in the ferric state (Fe^{3+}), not the ferrous state (Fe^{2+}) present in regular haemoglobin. Met-haemoglobin cannot bind oxygen in this state.



Met-haemoglobin levels in healthy individuals are typically between 1-3% (117). They are kept at this low level by cytochrome b5 reductase (an NADH-dependent enzyme), and cytochrome b5 (a soluble electron carrier), which are capable of converting met-haemoglobin back to deoxyhaemoglobin (116).

NO utilises the same binding pocket of haemoglobin as oxygen, and can also bind to deoxygenated haemoglobin, forming nitrosylated haemoglobin (HbNO) (equation 1.12) (117).



HbNO can release NO following oxygenation, due to haemoglobin conformational changes allowing NO to bind to cysteine residues within the β -chain of haemoglobin, forming S-nitrosylated Hb (HbSNO) (equation 1.13) (118).



NO can thus be transported by red blood cells to microvascular sites of action in a protected S-nitrosothiol form. HbSNO can dispense NO bioactivity following the release of oxygen from this molecule, physiologically coupling oxygen delivery with vasodilation (119).

1.5.4 NO metabolites

Previously, NO metabolites NO_2^- and NO_3^- were considered physiologically inert, inactive oxidative end products of NO metabolism. Today, they are widely accepted as bioactive “storage pools” for NO bioactivity, capable of being recycled in blood and tissues to form NO and other bioactive nitrogen oxides under certain conditions. Indeed, their concentration is reduced following eNOS knockout in mice (120), and increased following exercise, which stimulates NO generation via eNOS due to circulatory shear stress (121). This pathway has been dubbed the “Nitrate-nitrite-nitric oxide pathway”, complementing the “traditional” L-arginine-eNOS pathway of NO formation.

NO_3^- is typically the dominant final oxidation product of NO, with concentrations at least 2 orders of magnitude higher than NO_2^- (micromolar vs nanomolar) (22). The half-lives of NO_3^- and NO_2^- are approximately 5-6 hours and 20 minutes, respectively (122). Indeed, lower levels of plasma NO_3^- and NO_2^- are detected in CVD patients in comparison to healthy controls, reflecting the degree of endothelial dysfunction and thus reduced NO bioavailability in this cohort (123). In healthy individuals, typical NO_3^- and NO_2^- levels are between 20-40 μM and 150-300 nM, respectively (124).

In addition to oxidation of NO, the second major source of NO_3^- , and to a lesser degree NO_2^- , is dietary intake. Vegetables such as beetroot, spinach, and rocket represent the most dominant dietary source of NO_3^- (125). Ingestion has been shown to increase plasma concentrations of NO_3^- and NO_2^- significantly. Per 80g serving, spinach contains approximately 2.76 mmol of NO_3^- , with beetroot containing approximately 1.88 mmol (125). Interestingly, diets traditionally high in these vegetables, such as the Mediterranean and Japanese diets, are associated with a low incidence of CVD (126–129).

1.5.5 Nitrate-nitrite-nitric oxide pathway

Dietary NO_3^- is absorbed in the upper gastrointestinal tract, and despite large amounts of circulating NO_3^- being excreted in the urine, approximately 25% is actively extracted by the salivary glands via entero-salivary circulation (130). This is subsequently concentrated in saliva, reaching millimolar concentrations (131). In the oral mucosa, commensal, facultative anaerobic bacteria are located within the deep crypts of the posterior and middle parts of the tongue (132). The most common anaerobes are thought to be of the *Veillonella* and *Actinomyces* species (132,133). These bacteria are capable of reducing NO_3^- to NO_2^- by NO_3^- reductase enzymes. They utilise NO_3^- as a final electron acceptor during respiration, gaining adenosine triphosphate (ATP) in the absence of oxygen (134). Humans are reliant on these bacteria for NO_2^- production, as human cells do not possess NO_3^- reductase activity. The importance of this bacteria is highlighted in studies demonstrating the use of antibacterial mouthwash preventing NO_2^- accumulation following dietary NO_3^- intake (135). A small amount of salivary NO_2^- meets the acidic gastric milieu, where it is protonated, forming nitrous acid. Here, it can subsequently decompose to NO and other nitrogen oxides, such as nitrous anhydride (N_2O_3), a potent nitrosating species capable of forming RSNO (equation 1.9) (136). This reaction is enhanced by the low pH and reducing compounds such as ascorbic acid (137). The high concentrations of NO produced in the gastric lumen may be of physiological relevance. NO is known to be bactericidal, and therefore may offer a first line of defence against ingested pathogens (138). In fact, it has been shown that gastric juice in combination with NO_2^- demonstrates significantly higher antimicrobial effects on known enteropathogens, compared to gastric juice alone (134,139).

Salivary NO_2^- that has escaped gastric conversion can enter the general circulation, along with newly formed RSNO molecules (140). There are multiple enzymes that possess NO_2^- reductase activity. Haemoglobin, myoglobin, xanthine oxidoreductase, aldehyde oxidase, mitochondrial enzymes and NOS have all been reported to elicit NO_2^- reductase activity (141). The contribution of NO_2^- reduction from each of these is dependent on pH, oxygen tension, and redox status. Figure 1.12 summarises the nitrate-nitrite-nitric oxide pathway.

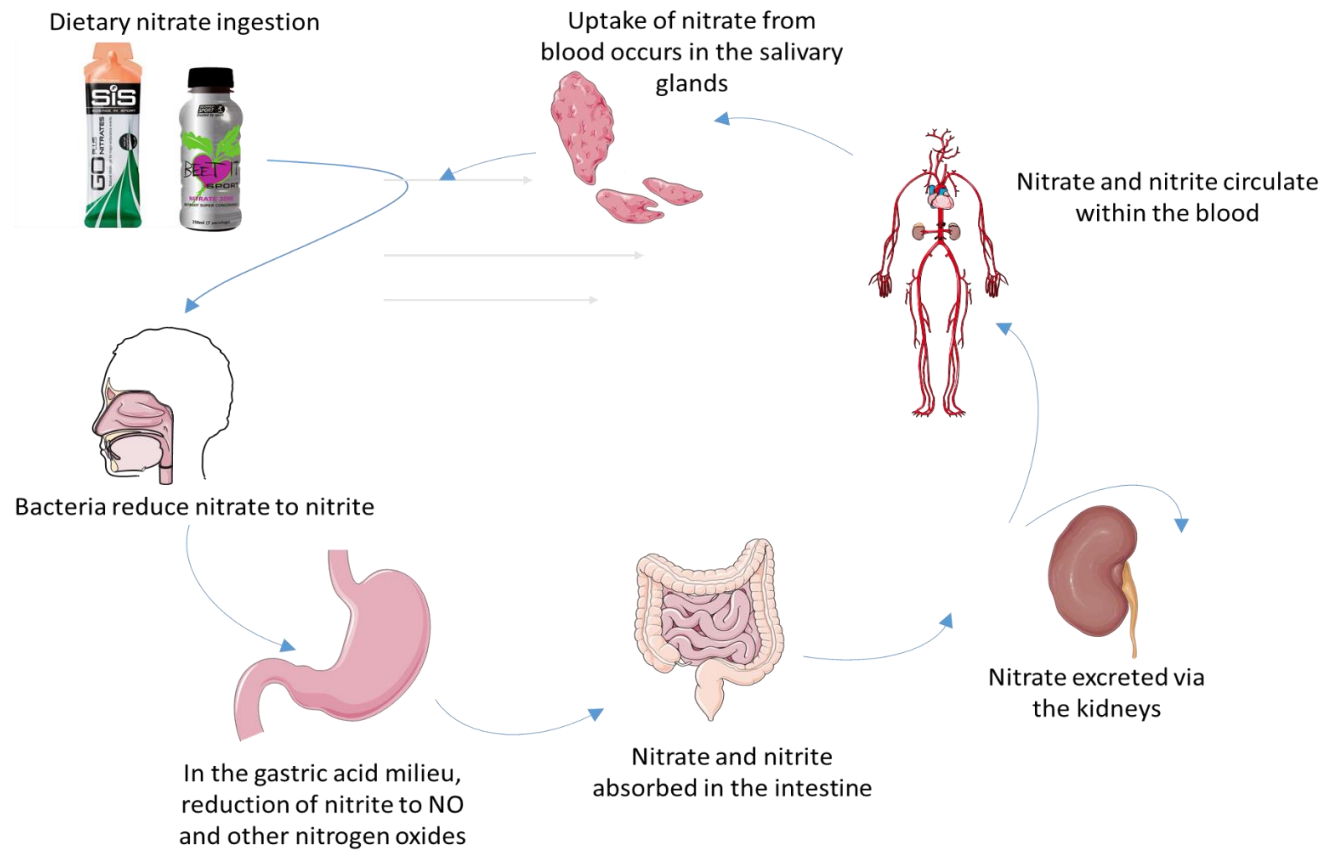
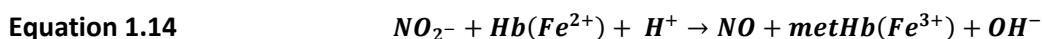


Figure 1.12. The nitrate-nitrite-nitric oxide pathway. Ingested dietary NO_3^- can be rapidly absorbed via the small intestine. Although a large amount of NO_3^- is excreted in the urine, up to 25% can be extracted by the salivary glands, and subsequently concentrated within the saliva. Commensal facultative anaerobic bacteria can reduce this NO_3^- to NO_2^- . Within the acidic gastric milieu, NO_2^- can then subsequently be reduced to NO, or other nitrogen oxides. NO_3^- and remaining NO_2^- are absorbed into the circulation and can be converted to bioactive NO within the blood. Adapted from (130).

1.5.5.1 Haem proteins

In addition to the reactions outlined in section 1.5.3.2, NO_2^- is capable of reacting with ferrous deoxyhaemoglobin (HbFe^{2+}), producing NO and methaemoglobin (metHbFe^{3+}) (equation 1.14) (142). This NO produced can then bind to a second deoxyhaemoglobin, as shown in equation 1.12.



This reaction allows NO delivery to be mediated by both pH and oxygen, as it requires deoxygenation of haemoglobin and proton availability. The haemoglobin conformation and oxygen binding status affects the ability of haemoglobin to reduce NO_2^- , with reduction most prevalent at approximately 50% oxygen bound haemoglobin (143). Thus, this allosteric regulation allows for targeted NO delivery to areas of poor oxygenation, and may partially explain hypoxic vasodilation (144). Myoglobin is capable of reducing NO_2^- in a similar way to haemoglobin (145). When it becomes deoxygenated, such as in exercising skeletal muscle, it will rapidly convert NO_2^- to NO.

1.5.5.2 Molybdopterin containing enzymes

Xanthine oxidoreductase (XOR) also possesses NO_2^- reductase activity in hypoxic conditions. Under physiological conditions, XOR is involved in purine catabolism, and reduces O_2 to superoxide (O_2^-). XOR consists of a FAD binding site, iron-sulfur centres and a molybdenum centre.

Typically, under physiological conditions, electrons flow from the molybdenum site, through the iron-sulfur centres to the FAD binding site, where oxygen rapidly removes electrons, leaving the molybdenum site in an oxidised state. As oxygen decreases, additional factors such as an acidic pH and elevated NADH levels allow for molybdenum to assume a reduced state. NADH occupies the FAD site, preventing oxygen binding. Following this, sequential reduction of FAD, iron-sulphur clusters and eventually the molybdenum site, allows for the reduction of NO_2^- to NO. NO_2^- can thus competitively reduce superoxide formation, preventing the reduction of molecular oxygen (142). This indirectly increases NO bioavailability further, preventing the formation of peroxynitrite from superoxide and NO. Figure 1.13 summarises xanthine oxidoreductase mediated NO_2^- reduction. Aldehyde oxidase also possesses NO_2^- reductase activity, through a mechanism similar to that of XOR, utilising the molybdenum-site of the enzyme (146).

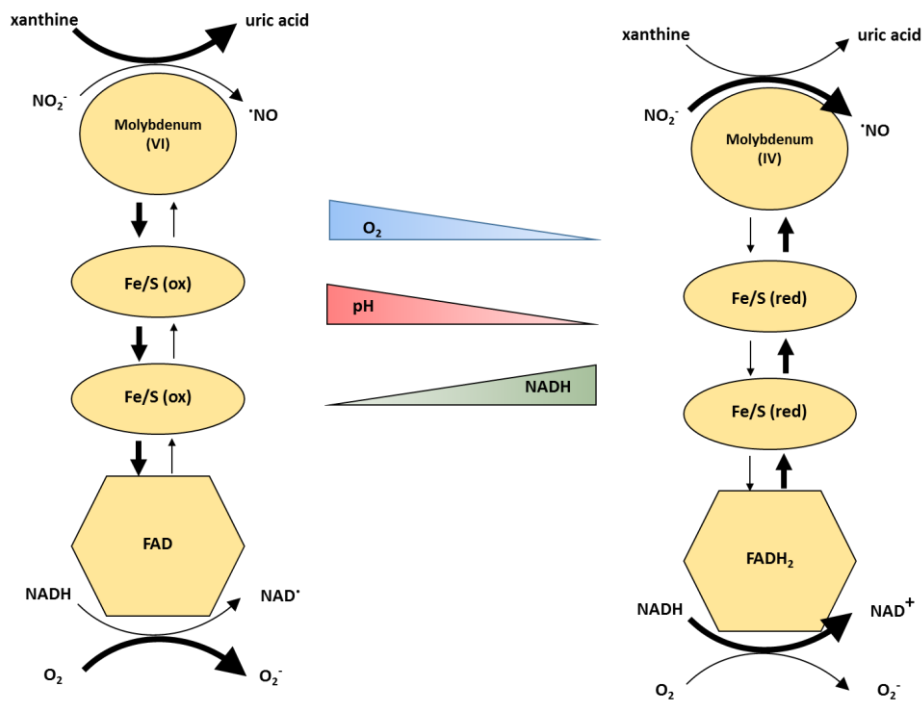


Figure 1.13. Xanthine oxidoreductase (XOR) mediated NO_2^- reduction. Typically, O_2 rapidly removes electrons from XOR, and thus the molybdenum site, resulting in its oxidation state of VI. These circumstances favour the formation of uric acid and superoxide (O_2^-). As O_2 and pH decrease, the molybdenum site assumes a more reduced state (IV), with electrons now flowing from the FAD site, via the iron-sulphur (Fe/S) clusters to the molybdenum site. Under these conditions, the production of NO is favoured.

1.5.5.3 Other mechanisms of NO_2^- reduction

Cytochrome c oxidase has been proposed to reduce NO_2^- utilising a similar mechanism to Hb, as the enzyme contains two haem groups (147). eNOS can also reduce NO_2^- to NO. It has been demonstrated that eNOS is the only isoform of NOS capable of this reduction, and thought to involve an additional active site aside from haem (148).

These pathways are all greatly enhanced under hypoxic conditions, offering an alternative electron acceptor to molecular oxygen. Thus, this pathway provides vasodilation in areas of ischaemia.

1.5.6 Nitrate and nitrite in therapeutics

1.5.6.1 History

Nitrates have been used as a pharmacological treatment for many years. Nitroglycerine was first discovered in 1847 by the Italian chemist Ascanio Sobrero, noting the “violent headache” produced by minute quantities of nitroglycerine on the tongue, which he quickly attributed to cerebral vasodilation. In 1867, British pharmacologists and physicians Brunton and Murrell used nitroglycerine and related compounds to treat patients with angina, with the use of these drugs becoming widespread. It was not until over a century later, in 1977, that Ferid Murad discovered that these nitrate compounds were in fact pro-drugs, and the biologically active molecule released was capable of acting on vascular smooth muscle. (149). Furchgott and Zawadski then recognised the importance of the endothelium in acetylcholine-mediated vasorelaxation in 1980. Furchgott observed that the endothelium produced an unknown substance that induced relaxation of the underlying smooth muscle, which he termed EDRF (19). Ignarro and Moncada eventually identified EDRF as NO in 1987 (20). Today, glycerol trinitrate remains a treatment of choice for relieving angina pectoris, myocardial infarction, and heart failure, along with other nitrates such as isosorbide dinitrate, and isosorbide-5-mononitrate (150). There is a wealth of evidence demonstrating that nitrates are effective at increasing coronary blood flow via a variety of mechanisms, including vasodilation and improvement of endothelial dysfunction(151). Tolerance to organic nitrates often occurs following frequent dosing, decreasing their efficacy. This may occur through a number of mechanisms, including increases in oxidative stress, impaired nitroglycerin bioconversion, desensitisation of soluble guanylate cyclase, increased sensitivity to vasoconstrictors and epigenetic mechanisms (152).

More recently, both our research group and others have shown that low-dose sodium nitrite (NaNO_2) can induce vasodilation in humans, an effect which is greatly enhanced in hypoxia (153,154). The potency of this inorganic NO_2^- is far lower than the organic nitrates used in the clinical settings described (155). This selective vasodilation in areas of hypoxia and/or acidosis could be of significant benefit in a clinical setting, and explain the benefits of NO_2^- observed in ischaemia reperfusion studies (156).

1.5.6.2 Physiological effects of NO_3^- and NO_2^-

The nitrate, nitrite, nitric oxide pathway can be further boosted by dietary intake of NO_3^- . As previously mentioned, a diet rich in fruit and vegetables, such as the Mediterranean diet, contains high levels of NO_3^- and is protective against CVD (157–160). Typically, an 80 gram serving of vegetables such as rocket, spinach, radish or beetroot contains approximately 2–4 mmol of NO_3^- (125). As NO_3^- and NO_2^- represent bioactive storage pools for NO, many of the effects of this compound have been shown to be mirrored following exogenous administration of NO_3^- and/or NO_2^- . The most established physiological effect of dietary NO_3^- ingestion is a reduction in blood pressure. This was first demonstrated in 2006 by Larsen *et al*, who showed that a sodium nitrate (NaNO_3) salt solution, at a dose similar to that of a NO_3^- rich meal, significantly reduced diastolic blood pressure by 3.5 mm Hg (161). In 2008, a reduction in both systolic (10 mm Hg) and diastolic (8 mm Hg) blood pressure was observed following ingestion of NO_3^- rich beetroot juice in healthy volunteers (162). Following these observations, numerous other studies have reported this effect using a range of dietary NO_3^- sources (163,164).

Dietary supplementation with NO_2^- has been shown to inhibit platelet activity, and subsequently increase bleeding time (165). Similarly, dietary NO_3^- administration, in the form of both beetroot juice, and potassium nitrate capsules, was capable of reducing *ex vivo* platelet aggregation, in response to ADP and collagen in male, but not female volunteers. (166). This group had also shown that the effects of NO_3^- on both blood pressure and platelet aggregation were abolished following interruption of the enterosalivary conversion of NO_3^- to NO_2^- , confirming the role of the nitrate, nitrite, nitric oxide pathway (162). Both NO_2^- and NO_3^- supplementation were reliant on erythrocyte-mediated reduction of NO_2^- to NO to elicit an effect.

Endothelial dysfunction and subsequent decreased NO bioavailability is central to the pathogenesis of CVD. Dietary NO_3^- supplementation has been shown to improve endothelial function in hypercholesterolemia patients, as measured by flow mediated dilation (FMD) (167). Indeed, FMD has been shown to improve following ingestion of 200 g spinach (≈ 6.9 mmol NO_3^-), in addition to augmenting NO status (168). There is also evidence that dietary NO_3^- intake can alleviate arterial stiffness in healthy volunteers, due to the influence of NO on vascular tone (169,170).

Ischemia reperfusion injury is defined as tissue damage that occurs as a result of restoration of the circulation after a period of lack of oxygen, or ischemia. Within the heart and brain, ischemia reperfusion injury is a major cause of death and morbidity (171). Dietary NO_3^- and NO_2^- are well documented to protect against ischemia reperfusion injury in both animal and human models. Generation of NO from NO_2^- by XOR protects the myocardium from ischemia reperfusion injury in

rat hearts (156,172). NaNO_2 can protect against ischemia reperfusion injury in patients with myocardial ischemia, but only when given before the onset of ischemia (173).

Aside from a disease setting, dietary NO_3^- has generated a large amount of interest from the sports and exercise field, due to its vasodilatory capacity, and consequent potential to increase delivery of oxygen and nutrients to exercising skeletal muscle. Administration of beetroot juice for four to six days reduced the oxygen cost of low and moderate intensity exercise, whilst also significantly increasing the time to exhaustion during high intensity exercise (174). It has also been shown to enhance time-trial performance in cycling (175). Whilst beetroot juice is high in NO_3^- , it also contains other bioactive compounds such as betaine and polyphenols, which may be responsible for the beneficial cardiovascular effects observed. Studies by Lansley *et al* using a NO_3^- depleted placebo version of beetroot juice failed to produce the same effects as the NO_3^- rich beetroot juice however, allowing the effects observed to be attributed to NO_3^- (175,176).

Table 1.3 summarises several key studies investigating the effect of NO_3^- supplementation in a range of cohorts.

Table 1.3 Current NO₃⁻ supplementation studies and their findings

Nitrate source	Dose	Cohort	Effect	Reference
Sodium nitrate	0.1 mmol kg ⁻¹ day ⁻¹ (3 days)	Healthy volunteers	<ul style="list-style-type: none"> • Reduction in blood pressure 	Larsen <i>et al.</i> 2006 (161)
Beetroot juice	500 mL (1 day) ≈ 11.2 mmol	Healthy volunteers	<ul style="list-style-type: none"> • Reduction in blood pressure • Prevention of endothelial dysfunction • Reduced platelet activation 	Webb <i>et al.</i> 2008 (162)
Beetroot juice	250 mL day ⁻¹ (6 weeks) ≈ 5.6 mmol	Hypercholesterolemia patients	<ul style="list-style-type: none"> • Improved vascular function 	Velmurugan <i>et al.</i> 2016 (177)
High nitrate soup	13.6 mmol day ⁻¹ (7 days)	Healthy volunteers	<ul style="list-style-type: none"> • Reduced arterial stiffness 	Jovanovski <i>et al.</i> 2015 (178)
Sodium nitrate	0.15 mmol kg ⁻¹ day ⁻¹ (4 weeks)	Elderly volunteers	<ul style="list-style-type: none"> • Reversed vascular dysfunction 	Rammos <i>et al.</i> 2014 (179)
Beetroot juice	250 mL (1 day) ≈ 5.6 mmol	Hypertensive patients	<ul style="list-style-type: none"> • Reduction in blood pressure 	Kapil <i>et al.</i> 2015 (180)
Beetroot juice	500 mL (1 day) ≈ 9.1 mmol	Peripheral artery disease patients	<ul style="list-style-type: none"> • Enhances exercise performance 	Kenjale <i>et al.</i> 2011. (181)
Sodium nitrate	0.1 mmol kg ⁻¹ day ⁻¹ (3 days)	Healthy young well-trained men	<ul style="list-style-type: none"> • Reduced oxygen cost of exercise 	Larsen <i>et al.</i> 2007. (182)
Beetroot juice	500 mL (1 day) ≈ 6.2 mmol	Male cyclists	<ul style="list-style-type: none"> • Improved cycling time trial performance 	Lansley <i>et al.</i> 2011 (175)

A plethora of studies have investigated the effect of NO₃⁻ supplementation in the cardiovascular system, both in a disease setting and in terms of exercise performance. This table highlights some of the effects observed thus far within the field.

1.5.7 Detrimental effects of NO₃⁻

It is noteworthy that there has been great concern over the potential detrimental effects of NO₃⁻ and NO₂⁻ in the past, specifically, their effects on cancer and methaemoglobinemia.

Both NO₃⁻ and NO₂⁻ are commonly used to cure and preserve meat, preventing bacterial growth. Concerns first arose when it was demonstrated that these NO metabolites were capable of producing carcinogenic N-nitrosamine compounds (183), which are capable of disrupting nucleic acids (184). However, ascorbic acid (vitamin C), also present in high amounts in green leafy vegetables, has been shown to be a potent inhibitor of nitrosamine formation (185). Indeed, the majority of the literature focusses on cured meat as the dietary source of NO₃⁻ and its potential carcinogenic effects, rather than vegetables. A meta-analysis performed in 2015 suggested high NO₃⁻ intake was associated with a statistically significant *reduced* risk of gastric cancer (186). Conversely, other studies have identified a link between dietary NO₃⁻ and both ovarian (187) and thyroid cancer (188). However, these associations are small, and further, larger cohort studies are required before causation can be concluded. Current data should thus be interpreted with caution.

Methaemoglobinemia, also referred to as blue baby syndrome, is caused by a high level of methaemoglobin, the production of which is highlighted in section 1.5.3.2. Levels greater than 10% can lead to asphyxia, which is fatal (189). Concerns about the effect of NO₃⁻ intake on methaemoglobinemia first arose in the 1940s, when it was noted that methaemoglobinemia and cyanosis were observed in infants ingesting well water with a high NO₃⁻ content (190). Since then, it has been shown that NO₃⁻ was not necessarily the cause of methaemoglobinemia, but rather faecal bacteria that was also present within the well water (191). Thus, NO₃⁻ may act as a marker of water contamination, rather than being toxic itself. Indeed, a review of NO₃⁻ in drinking water concluded that there is not sufficient evidence for a causal relationship between exposure to NO₃⁻ and methaemoglobinemia (192). It is important not to detract from the positives of a diet high in green leafy vegetables, having a various beneficial effects against CVD, in addition to protective anti-cancer effects (193).

1.6 Extracellular vesicles

1.6.1 History

Extracellular vesicles (EVs) are submicron, spherical particles enclosed in a phospholipid bilayer, typically between 30 nm to 1 μ m in diameter. EVs were initially regarded as inert, cellular debris, with no real biological function. The first suggestion that EVs were present in the blood was in 1946, following a study by Chargaff and West (194). They showed that plasma clotting time was increased if plasma underwent high speed centrifugation, which was subsequently shortened if the centrifugation pellet was added back to the plasma. However, it was not until 1967 when EVs were first visually identified by Peter Wolf (195). Wolf and his team identified a subcellular fraction using electron microscopy, visualising small spherical vesicles approximately 30-500 nm in diameter, describing his finding as “platelet dust”. Years later, in 1970, work by Webber and Johnson illustrated using electron microscopy that particles could “bleb” from activated platelets and be released into the circulation (196).

Simultaneously, work by the Nobel Prize winner Christian de Duve formed the basis for a new field of cell biology research, now known as membrane trafficking (197). Together with George Palade and Albert Claude, they were able to identify nearly every organelle in the eukaryotic cell, and their respective functions. This formed the basis for further understanding of the role of vesicles in endocytosis and intracellular protein transport (198,199). Two papers published in quick succession in 1983 first described exosomes and exosome secretion, detailing that shedding of the transferrin receptor was mediated by vesicles (200,201). In 1987, Rose Johnstone proposed the term “exosome” to refer to secreted membrane vesicles derived from multivesicular bodies (MVBs), a term which seems to have stood the test of time. This new field of research grew slowly following this work. A small number of papers were published over the next decade from a select few research groups. It was not until 1996 that a breakthrough paper was published that brought the EV field to the forefront of scientific research, where B-lymphocytes were shown to secrete antigen-presenting vesicles (202). This initiated the discussion that EVs could have a functional role in information transfer. In 2005, the first meeting that gathered scientists interested in exosomes was held in Montreal. A large increase in interest, and subsequently publications, occurred between 2006 – 2007, and in the last decade a sharp increase in EV research has been observed. In 2011, a large EV international workshop was held at the Institut Curie in Paris, and later that year the International Society for Extracellular Vesicles (ISEV) was formed. A year later, in 2012, ISEV launched the Journal of Extracellular Vesicles (JEV), specifically for EV related research (203).

1.6.2 Nomenclature

As research in EVs increased, with scientists from a variety of disciplines all interested in the role of EVs in their respective fields, it has been accompanied by a varied use of terminology. Frustratingly, this is often a source of much confusion within the literature as to the exact classification of the EVs being studied. Many of the terms used reflect the function of these secreted vesicles, such as “calcifying matrix vesicles” that initiate bone formation (204), and “tolerosomes” that induce immunological tolerance to antigens (205). Alternatively, vesicles cellular origin is often used when naming vesicles, such as “prostasomes” (206) and “oncosomes” (207). Although these terms are useful within a specific sub-speciality of EV research, broader terms are more helpful to the wider scientific community. “Exosomes”, “microvesicles”, “microparticles” and apoptotic bodies” were each used to describe differing sub-sets of EVs, however each with imperfect definitions and often substantial overlap. Indeed, these terms were often used interchangeably, or indeed incorrectly within the field. In the midst of these conflicting definitions, it was suggested that all EV research state their use of such terms explicitly, clearly state their methods of vesicle collection and isolation, and were encouraged to use the term “extracellular vesicle” as a generic term for all secreted vesicles (208). In 2014, ISEV produced a position paper to clarify terminology. Today, it is generally accepted that “extracellular vesicles” is an umbrella term encompassing exosomes, microvesicles and apoptotic bodies. Figure 1.14 summarises this nomenclature and differences between sub-types. It is important to note that as the name suggests, apoptotic bodies are released from cells undergoing apoptosis, and as such do not represent EVs from viable cells. The term EV henceforth in this thesis will refer to both exosomes and microvesicles, but not apoptotic bodies.

	Name	Size	Origin	Markers
Extracellular vesicles	Exosomes	30-100 nm	Intracellular endosomes and multivesicular bodies	Tetraspanins (CD9/CD63/CD81) TSG 101 ALIX
	Microvesicles	100-1000 nm	Plasma membrane	PS binding (Annexin V) Integrins Selectins
	Apoptotic bodies	1000-5000 nm	Plasma membrane	PS binding (Annexin V) C3b TSP

Figure 1.14. Classification of EV sub-types. The term “EV” encompasses all cell-derived secretory vesicles. These differ primarily by their size and mechanism of formation. TSG 101 – Tumour susceptibility gene 101. PS – Phosphatidylserine.

1.6.3 The mechanism of EV biogenesis

The generation of EVs can be attributed to one of two main pathways; the classical pathway for exosome secretion, and the direct pathway for microvesicle budding. However, “exosome-like vesicles”, within the defined size range and expressing exosome markers, have been shown to be released via the direct pathway (209).

1.6.3.1 The classical “exosome” pathway

Principally, exosomes are derived from endosomal origin. Their formation utilises the endocytic pathway, which is involved in regulating the composition of the plasma membrane and expression of cell surface receptors, which can be internalised and subsequently either degraded, or recycled back to the cell surface, depending on cellular requirements (210).

The first stage in exosome formation is invagination of the plasma membrane. Specifically, membrane proteins and surrounding material are endocytosed, and transported via small transport vesicles into early endosomes, which then matures into a late endosome (211). These transport vesicles are produced as a result of both clathrin- and non-clathrin (caveolae) mediated pathways of endocytosis (211,212). During the formation of late endosomes, intraluminal vesicles (ILVs) are formed within the lumen via an inward budding of the membrane of the endosome. At

this stage, they are referred to as either multivesicular bodies (MVBs) or multivesicular endosomes. ILVs contain proteins, lipids and other biogenic cargo that requires sorting.

Typically, MVBs experience one of two fates, either they fuse with lysosomes for subsequent degradation, or they fuse with the plasma membrane, releasing their content into the extracellular milieu as exosomes (213).

The best described mechanism for the formation of MVBs and ILVs from endosomes involves the endosomal sorting complex required for transport (ESCRT). This complex is composed of approximately 30 proteins, which assemble into 4 main complexes; ESCRT-0, -I, -II, and -III, which associate with VPS4, VTA1 and Alix (214). ESCRT-0 contains proteins that recognise and sequester ubiquitinated transmembrane proteins within the endosomal membrane, ESCRT-I and -II are responsible for membrane deformation into buds with sequestered cargo (215), and the ESCRT-III complex, drives the inward budding and scission to form ILVs within a MVB (216). Silencing of various components of the ESCRT-0 and -I all reduced the secretion of exosomes, highlighting their importance in this pathway (217). However, exosome formation is still apparent even in the absence of ESCRTs, suggesting that there may be ESCRT-dependent and ESCRT-independent mechanisms of MVBs (218).

One pathway possibly responsible for ESCRT-independent exosome formation involves the lipid metabolism enzyme sphingomyelinase, which is capable of hydrolysing sphingomyelin to ceramide. Blockade of sphingomyelinase using the inhibitor GW4869 has been shown to decrease exosome release (219). Furthermore, addition of exogenous sphingomyelinase to cells led to inward budding of endosomes, producing ILVs (220). However, this mechanism may not apply to all cell types, as depletion of the sphingomyelinase enzyme in melanoma cells did not impair either MVB biogenesis or exosome secretion (221). Instead, a CD63-dependent mechanism is required. Indeed, the tetraspanin proteins, in particular CD63 are also thought to be ESCRT-independent stimulators of exosome secretion (218). CD63 accumulates in ILVs even in the absence of ESCRT function, and is essential in the formation of ILVs within MVBs in HeLa cells (222). Tetraspanin enriched microdomains have been proposed to function as sorting machinery, facilitating exosome formation and release (223). Additionally, the enzyme phospholipase D₂ which hydrolyses phosphatidylcholine within the plasma membrane into phosphatidic acid is highly enriched in exosomes, and has been shown to be required for the formation of CD63-containing ILVs (224).

Despite the vast amount of research undertaken regarding the classical pathway of exosome formation, the exact mechanism is still not fully elucidated. Advances within this area have shown that formation appears to be mediated by an array of different proteins, some of which may be

shared between differing cell types, whilst some may be cell-specific. Research in this area is ongoing in order to clarify the mechanisms in play, and how different mechanisms of ILV and MVB formation may alter exosome fate. Interestingly, ILVs were shown to differ in size dependent on whether their formation was ESCRT-dependent or –independent, potentially representing a simple approach to distinguish between differing ILV sub-populations (222).

Once a MVB has been formed, they fuse with the plasma membrane to secrete their exosomes to the extracellular space. The intracellular trafficking required for this process is mediated by small GTPases of the Rab family. Numerous members of this family have been implicated in exosome secretion: Rab11 has been shown to be implicated in Ca²⁺ induced exosome secretion in erythroleukemia cell lines (225,226) and Rab35 inhibition impairs exosome secretion in oligodendrocytes (227). Furthermore, Rab27a and Rab27b have been shown to play a pivotal role in directing MVBs to the plasma membrane and assisting their docking for fusion and subsequent exocytosis (228). It is noteworthy that inhibition of Rab27a in cancer cells prevented exosome secretion *in vitro* (229), and reduced tumour metastasis *in vivo* (230). Interestingly, hypoxia has been shown to increase Rab22a expression, and thus microvesicle generation in breast cancer cells in a HIF-dependent manner, an effect which was eliminated following knockdown of Rab22a (231).

The final stage of exosome release involves fusion of MVBs with the plasma membrane, and exocytosis of exosomes. This process is thought to involve the SNARE (soluble NSF (N-ethylmaleimide-sensitive fusion) attachment protein receptor) proteins. The SNARE hypothesis states that a complex is formed between syntaxin and SNAP, between the cytosolic plasma membrane and the vesicle-associated membrane protein (VAMP) within the membrane of the MVB (232). The folding of these SNARE proteins facilitates the fusion of the membrane, providing the thermodynamic energy required to pull apart the membrane and create an opening for exosome secretion (233). The exact SNAREs involved in the fusion of MVBs with the PM to release exosomes have been poorly studied to date (234). Future research within this field will likely uncover further details regarding the exact proteins involved in exosome generation and secretion.

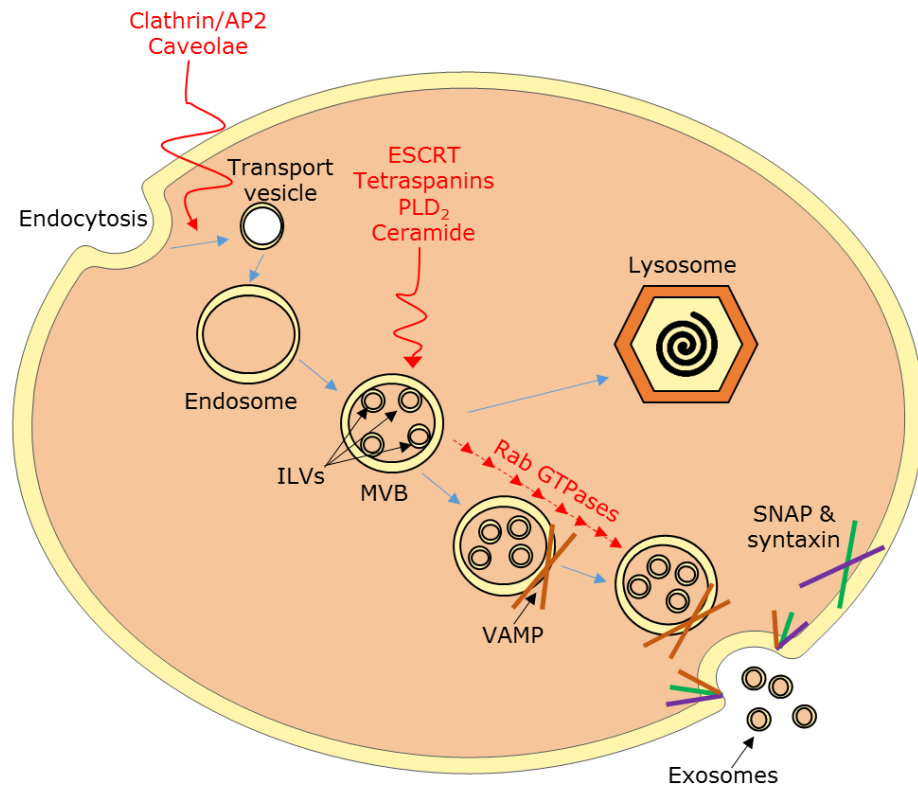


Figure 1.15. The classical pathway of exosome biogenesis. Clathrin and caveolae mediate the endocytosis of plasma membrane components, which are transported to endosomes via small transport vesicles. ILV formation may arise as a result of a number of molecules, including ESCRT complexes, tetraspanins, PLD₂ or ceramide. Rab GTPases then assist the translocation of MVBs toward the plasma membrane, where the SNARE complex assists the docking and fusion of the MVB with the plasma membrane, and subsequent exosome release. AP2 – adapter protein 2, ESCRT – endosomal sorting complex required for transport, PLD₂ – phospholipase D₂ ILV – intraluminal vesicle, MVB – multivesicular body, VAMP – vesicle-associated membrane protein.

1.6.3.2 The direct pathway

The plasma membrane consists of a plethora of proteins embedded in a phospholipid bilayer. Under physiological conditions, these phospholipids are arranged in an asymmetric manner; where the outer leaflet is enriched in phosphatidylcholine (PC) and sphingomyelin, and the inner leaflet predominantly consists of phosphatidylserine (PS) and phosphatidylethanolamine (PE) (235). The distribution of these phospholipids is not fixed, but rather tightly regulated by three phospholipid translocase enzymes embedded within the plasma membrane itself. Floppase is an adenosine triphosphate (ATP)-dependent protein, and a member of the ATP-binding cassette (ABC) transporter family. It mediates the movement of phospholipids to the outer membrane leaflet. Flippase is also an ATPase, which causes rapid translocation of phospholipids from the

outer membrane to the inner membrane leaflet, with a particularly high affinity for PS (236). Finally, scramblase is an ATP-independent enzyme, and causes random, bidirectional transport of phospholipids between membrane leaflets. Under resting conditions, flippase works at a far greater rate than floppase, thus making phospholipid arrangement asymmetric (235).

Typically, activation of a cell leads to an increase in the cytosolic calcium concentration. This leads to activation of the floppase and scramblase enzymes, and inhibition of flippase (236). The result of this is a profound increase in the level of externalised PS on the outer membrane leaflet.

Furthermore, the increased cytosolic calcium levels lead to disruption within the actin cytoskeleton. The cytoskeleton modulates the cell stability via protein-protein and protein-lipid interactions (237). The translocation of membrane phospholipids disturb the covalent links between the membrane and the cytoskeleton, facilitating membrane budding. This subsequently triggers the activation of several calcium-dependent enzymes, including the protease calpain, which is capable of cleaving cytoskeletal proteins and thus remodelling the cytoskeleton. Indeed, there is evidence to suggest that activation of calpain leads to microvesicle release from aggregating platelets (238). Similarly, Rho kinase II has been shown to be essential in endothelial microvesicle formation, with both pharmacologic inhibition and specific silencing preventing their release (239). Furthermore, caspases have also been shown to modulate the actions of calpain, leading to cytoskeletal reorganisation and microvesicle blebbing in neutrophils (240). Additionally, there is some evidence that enhanced permeability to potassium, along with the associated osmotic effects, facilitate microvesicle formation, although this research is dated (241,242). A reduction in cell volume is required to compensate for the loss of plasma membrane surface area as microvesicles are released. This change in cell volume would promote membrane budding due to the stress imposed by a surface area mismatch. Indeed, more recent research has demonstrated that in S49 lymphoma cells, potassium ion efflux, loss of membrane phospholipid asymmetry, and cytoskeletal disruption are all required for microvesicle release (243). Regardless, the exposure of PS and cleavage of the actin cytoskeleton leads to membrane budding, and subsequent shedding in the form of microvesicles, typically between 100-1000 nm in diameter. Although the exact mechanism that governs microvesicle release is not fully elucidated, several key proteins have been identified that play a pivotal role in their release.

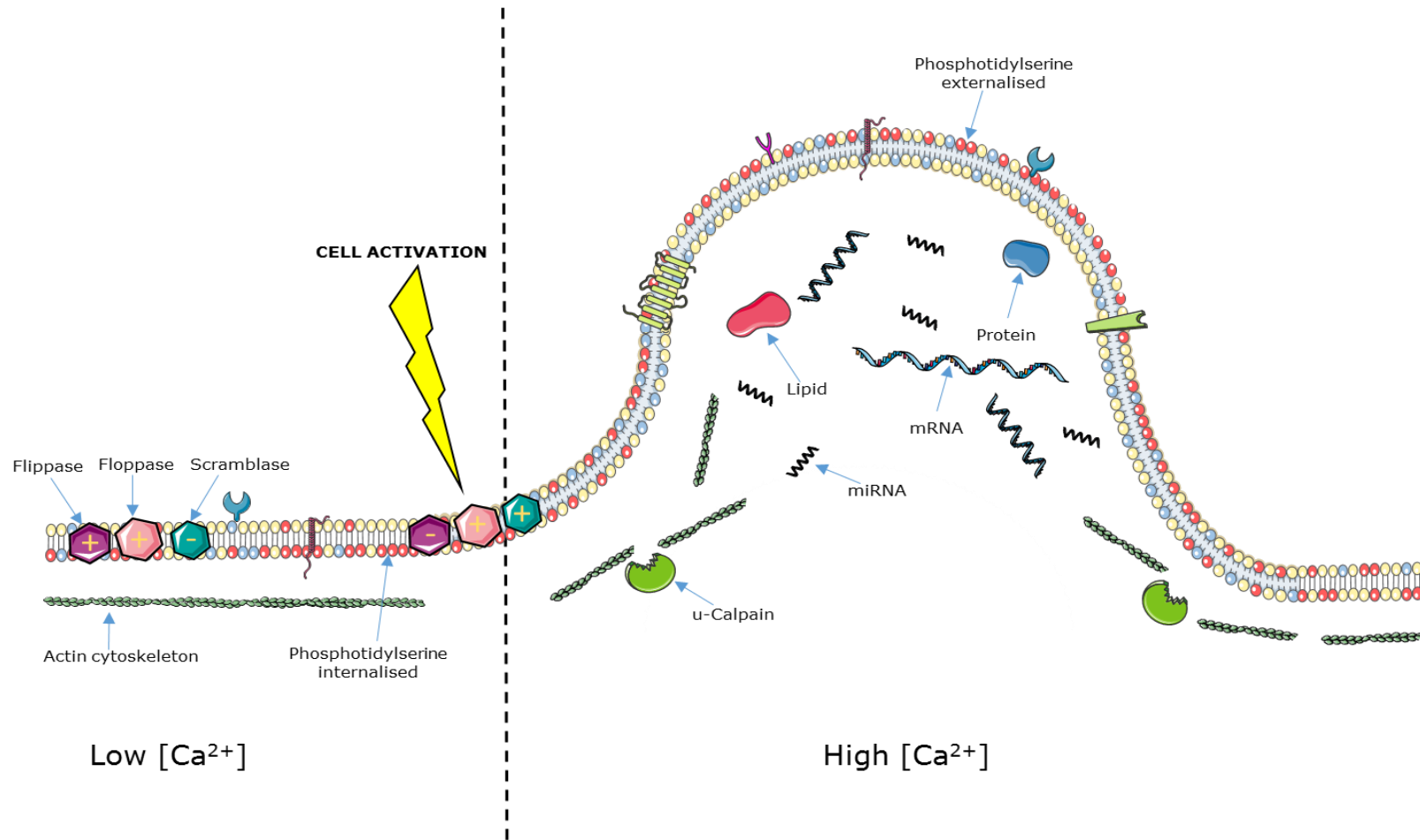


Figure 1.16. Microvesicle biogenesis. Microvesicles are formed via the outward blebbing of the plasma membrane. Biogenesis is mediated by increases in intracellular calcium, and subsequent loss of membrane asymmetry and cytoskeletal rearrangements. This facilitates the budding of the plasma membrane, incorporating both membrane and cytosolic components into the microvesicle.

1.6.4 Composition

Broadly, the content of an EV consists predominately of lipid, protein, and nucleic acids. However, the exact composition varies greatly, and reflects both the content of the parent cell and cellular stimuli leading to their formation (213). During their biogenesis, EVs are capable of engulfing an array of bioactive cargo from their parental cell, including nucleic acids (messenger RNA and micro RNA), bioactive free fatty acids, and protein, both cytosolic and membrane bound.

In vitro studies have shown that the protein and RNA profile of exosomes secreted by endothelial cells cultured under hypoxic conditions, or in the presence of TNF- α , were drastically altered (213). Exosomes derived from TNF- α treated cells contained higher amounts of ICAM-1 and TNF- α protein, and increased NF- κ B and IL-8 mRNA. Exosomes from cells grown under hypoxia contained increase levels of proteins, such as lysyl oxidase 2 (LOXL2), and mRNA encoding N-myc downstream-regulated gene 1 (NDRG1), both of which are involved in the stress response (213). Upregulation of these proteins reflect changes that would also be seen in activated endothelial cells, clearly reflecting the stress condition of their parent cell. Alterations in the protein content of these EVs may dictate their biological function.

EVs derived from specific cell types often constitutively express certain antigens, and can thus be used as a marker to determine the parent cell. Indeed, VE-Cadherin (CD144) is routinely used to determine EVs of endothelial origin (244,245), Integrin α M (CD11b) as a monocyte marker (246), Integrin α Ib (CD41) as a platelet marker (247,248), and glycophorin A (CD235a) as an erythrocyte marker (249,250).

Similarly, there are numerous markers of EVs associated with their biogenesis that are used within the EV field to confirm the presence of EVs within a sample. These can be broadly split into two main categories: intravesicular markers, present within the lumen of an EV, and membrane-associated markers. Transmembrane or lipid-bound extracellular proteins include various tetraspanins (CD9, CD63, CD81) (251), lysosome-associated membrane glycoprotein (LAMPs), and major histocompatibility complex (MHC) I and II (234,252). Intravesicular markers include tumour susceptibility gene 101 (TSG101), Alix, ESCRT complexes and endosomal trafficking proteins, such as Rab GTPases (251,253).

As previously alluded to, research in the EV field is progressing rapidly. Markers once thought of as “exosome specific”, such as the tetraspanin CD9, have since been shown to also be present on microvesicles (254). Furthermore, inhibition of Rab27a modulated exosome secretion, reducing conventional markers CD63, TSG101 and Alix, but had no effect on CD9. CD9 was subsequently confirmed to be present on vesicles of various sizes by electron microscopy (255). As

developments in both proteomic analysis and isolation of EV sub-sets continuously improves, researchers hope that more specific markers will be identified in the near future. Interestingly, EV researchers have created “vesiclepedia”, a regularly updated compendium of proteins identified within differing EV populations (256).

A major breakthrough in the EV field came little over a decade ago, when it was first demonstrated that the cargo of EVs included both mRNA and miRNA, which could subsequently be translated into proteins by target cells (257,258). Since then, the nucleic acid content of EVs has been the subject of much interest. Many RNAs isolated from EVs have been found to be enriched in comparison to the RNA profiles of their parent cells, suggesting that RNA molecules are selectively incorporated into EVs (257–260). It is noteworthy that numerous studies have failed to conclude whether identified extracellular RNAs are present within EVs, or rather RNA-protein complexes are co-isolated with EVs.

Finally, lipids are known to play important roles in not only the stability and rigidity, but also the function of EVs. Sphingomyelin, PC, PE, PS, and phosphatidylinositol are all components of EVs, although the ratios of these lipids will differ according to the originating cell (261). Sphingomyelin and cholesterol are generally enriched in EVs, allowing the tight packing of lipid bilayers and hence increased stability in comparison to cells (262). Aside from a structural role, interest in other functional roles of lipids within EVs is gaining popularity. The lipid content of adipocyte-derived EVs has been shown to reflect the stage of differentiation in the parent cell (263). Additionally, differential lipid compositions within different sub-sets of platelet-derived EVs has been documented recently (264). Prostaglandins bound to EVs have been shown to activate signalling pathways in leukaemia cells (265). Exosomal lipids have been shown to increase Notch signalling, and induce death in pancreatic tumour cells (266). Finally, sphingomyelin present on EVs has been shown to promote endothelial cell migration, tube formation and neovascularisation, which may play a role in tumour growth and metastasis by promoting angiogenesis and tumour invasion (267).

1.6.5 EV internalisation

The biological cargo that EVs carry, outlined above, can drastically alter the function of the recipient cell. However, in order for this alteration to occur, the EV in question must enter the target cell. There is a vast amount of evidence for EV uptake by target cells. A plethora of studies have utilised fluorescent lipid membrane dyes, or membrane permeable compounds to stain EVs, thus allowing the entry of EVs into recipient cells to be visualised (268–272). However, the specific mechanism regarding uptake was not studied. Other groups have loaded EVs with a luciferin substrate, added them to luciferase expressing cells and measured the resulting bioluminescence

(273). It is noteworthy that in some cases, the phenotypic effects of EVs does not require internalisation of the vesicle.

Conversely, the mechanism or mechanisms involved in EV internalisation are poorly understood. The uptake mechanism utilised by an EV is likely to be dependent on surface proteins and glycoproteins found on the surface of both the EV and target cell. Understanding the mechanisms involved in EV trafficking and uptake is of great importance, as utilising the capability of EVs to “deliver” nucleic acids and proteins to target cells offers the potential of using EVs as delivery vectors for therapeutic proteins, nucleic acids and/or drugs.

Many EV surface proteins have been shown to interact with membrane receptors on target cells. Tetraspanins have been implicated in the uptake of EVs by cells; indeed, blockade of CD81 and CD9 can reduce the uptake of EVs by dendritic cells (271). EVs expressing the tetraspanin Tspan8 have been shown to form a complex with integrin $\alpha 4$ (CD49D), which subsequently facilitated internalisation by endothelial cells (274). Indeed, integrins themselves are also thought to play a role in EV internalisation. Blockade of the integrin αL (CD11a) binding site, or its ligand ICAM-1, can reduce dendritic cell uptake of EVs (271). Additionally, the presence of $\alpha 4\beta 1$ integrin on EVs derived from endothelial progenitor cells was essential for their uptake by endothelial cells (275). These interactions may be especially important in facilitating the function of EVs within the immune system. Research has also implicated proteoglycans (276) and lectins (277) with EV uptake. Overall, there are an array of interactions between surface molecules of the EV and target cell that facilitate subsequent internalisation, which appear to be specific to both the target cell type and the composition of the EV.

Following recognition of an EV by the target cell, internalisation ensues. Current knowledge suggests that cells appear to take up EVs by a variety of endocytic pathways, including clathrin-dependent and clathrin-independent (caveolin-mediated) endocytosis, phagocytosis, and pinocytosis (278). It is thought that uptake can be extremely rapid, with EVs being identified inside cells as early as 15 minutes after first exposure (279).

Evidence for the involvement of the endocytic pathway stems from the observation that EV internalisation is an active, energy-dependent process. Uptake has been shown to be drastically reduced in lower temperatures (270,271,276), and significantly lowered following depolymerisation of the actin cytoskeleton by Cytochalasin D, preventing endocytic pathways operating (273,279). As previously mentioned, endocytosis can be mediated by multiple pathways, the most studied being clathrin-mediated endocytosis, which involves assembly of clathrin-coated vesicles within the cell, which can deform the membrane and promote its collapse into a vesicular bud whilst incorporating the EV (280). Inhibition of clathrin-coated pit formation

has been shown to drastically reduce EV uptake in ovarian cancer cells (281). Similarly, inhibition of dynamin2, a GTPase required for clathrin-mediated endocytosis prevents EV internalisation in phagocytic cells (279,282). Endocytosis can also be mediated by clathrin-independent mechanisms, such as caveolin-dependent endocytosis. A key component of caveolae is the protein caveolin-1, which has been shown to suppress EV uptake when knocked-down (283). Lipid rafts are rich in sphingolipids such as sphingomyelin, and can affect membrane fluidity and trafficking (284). Lipid rafts are another example of clathrin-independent endocytosis thought to play a role in EV uptake. Indeed, inhibition of sphingolipids synthesis reduced EV uptake in dendritic cells (285).

Phagocytosis has also been implicated in EV uptake. This receptor-mediated event typically internalises larger particles, however it has been shown that particles as small as 85 nm in diameter can be internalised by phagocytosis, thus it is plausible that EVs may be internalised via this route (286). Inhibition of phosphoinositide 3 kinases (PI3K), which play an integral role in phagocytosis, has been shown to inhibit EV uptake in a dose-dependent manner (279). PS is best known for its role as a signal for the phagocytosis of apoptotic cells. However, the high level of PS on the outer surface of EVs, specifically microvesicles, may facilitate their entry into phagocytic cells. Certainly, blockade of the PS receptor Tim-4 reduced the uptake of EVs in macrophages (279). Treatment of dendritic cells with a soluble PS analogue also reduced EV uptake (271). Treatment of EVs with the PS binding protein annexin-V also reduces the uptake of EVs into macrophages (287).

Finally, macropinocytosis is also thought to play a role in EV internalisation. This process is similar to phagocytosis, but direct contact with any internalised material is not required. Membrane ruffles that protrude from the cell surface encapsulate an area of extracellular fluid, which is subsequently internalised via fusion of the protrusions with themselves. Alternatively, EVs can be macropinocytosed after becoming caught within membrane ruffles. (288). Inhibition of macropinocytosis prevented EV uptake in microglial cells (282). An inhibitor of rac1, a GTPase with a major role in macropinocytosis, also inhibited EV uptake in these cells (282).

The majority of evidence suggests that EV are internalised as intact vesicles. Conversely, Diehl *et al* demonstrated that EVs are capable of direct membrane fusion with target cells, and subsequent delivery of miRNA into the cell (289). The mechanism of membrane fusion is thought to involve similar families of proteins to the exocytosis of MVBs during exosome formation, including SNAREs and Rab GTPases (290).

Whilst the mechanisms of EV uptake remain to be fully elucidated, the majority of research points towards the endocytic pathway as the primary mediator of this event. Cell-specific EV uptake may be mediated by specific surface molecules on both the EV and the target cell membrane. These interactions have been characterised well in some cases; for example, milk-derived EVs can be internalised by dendritic cells due to the interaction between dendritic cell-specific intercellular adhesion molecule-3 grabbing non-integrin (DC-SIGN) and Mucin 1 (MUC1). EVs lacking MUC1 were unable to enter these cells (272). Broadly, it appears that initial interaction between the EV and the target cell is mediated by specific surface ligands, which is followed by endocytosis. Perhaps, the numerous mechanisms of EV internalisation reflect the heterogeneity of EV populations. It is plausible that EVs may utilise a number of different entry routes into a cell, dependent on both the target cell type and molecules expressed on the EV. This would also offer an explanation as to why inhibition of one pathway does not completely abrogate EV entry. Figure 1.17 illustrates the various mechanisms of EV internalisation.

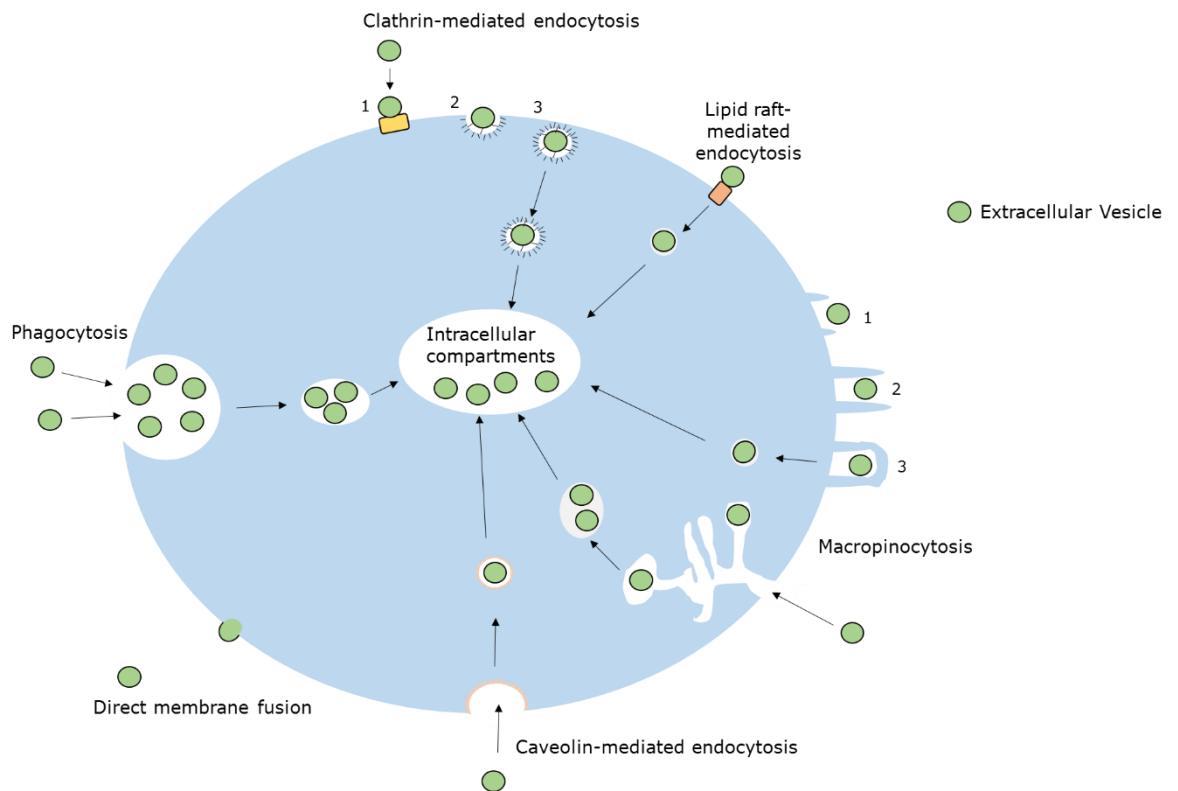


Figure 1.17 EV internalisation by target cells. EVs have been shown to be internalised through a variety of mechanisms, including endocytosis (clathrin and non-clathrin mediated), macropinocytosis, and phagocytosis. Additionally, direct fusion of EV and target cell membranes has been shown to occur, allowing direct delivery of their biogenic cargo, circumventing fusion of intraluminal EVs with the endosome.

1.6.6 EV Processing

Despite the large increase in EV research over the last decade, there is still a fundamental lack of consistency across the field in terms of the isolation, characterisation, and quantification of EVs derived from any extracellular fluid, with no consensus or “gold standard” consistently agreed upon. Thus, comparisons between studies is complex. In an attempt to combat this issue, ISEV released a position statement in 2014 detailing a set of minimal requirements to confirm a true, pure EV population (251), however the field is still in its infancy and it is likely that new requirements and suggestions for EV processing will surface in the future.

1.6.6.1 Sample collection

EVs have been isolated from nearly every biological fluid available, including plasma, sweat, saliva, urine, semen and breast milk (291,292), in addition to cell culture conditioned media. Isolation of EV from whole blood offers numerous challenges, primarily involving preventing activation and subsequent release of EVs from platelets, with the type of needle, vacutainer, and time between collection and processing all having potential effects on the EV concentration and characteristics (293). There is little literature available to suggest which conditions minimise *in vitro* platelet aggregation, although the use of 21-gauge needle for venepuncture has been recommended to minimise shear forces (294). Additionally, following venepuncture it is suggested that the tourniquet should be removed and the first few millilitres of blood discarded, due to the activating effects of pressure, and possible fibroblast contamination (295). The Scientific Standardisation Committee of the International Society on Thrombosis and Haemostasis recommends the use of citrate vacutainers for EV studies (296). Following collection, it is recommended that vacutainers are gently inverted and processed as soon as possible (297). Haematological parameters, such as platelet activation, leukocyte trafficking and cytokine production have been shown to fluctuate throughout the day and follow a circadian rhythm (298,299). In addition, there is some evidence to suggest that EV concentration can vary over the course of 24 hours (300). Further research to facilitate standardisation is essential to allow study to study comparability.

1.6.6.2 EV isolation

The most widely used technique for EV isolation is differential ultracentrifugation; which utilises centrifugal force (g) to sediment or “pellet” matter based on their size and density. The general protocol involves a series of sequential centrifugation speeds at increasing centrifugal force, removing unwanted components from the sample, eventually yielding an EV pellet. Typically, centrifugal accelerations are 200 - 1500 g to remove cells, followed by 10,000 – 20,000 g to pellet any cellular debris, before a final ultracentrifugation of 100,000 – 200,000 g to pellet EVs. Conveniently, this protocol can be altered to selectively isolate an exosome population. However, there is a large amount of variation between the speeds and duration of centrifugation used in different studies and research groups. The popularity of differential ultracentrifugation within the EV field is largely due to both its relative simplicity and short preparation time. However there are several limitations of this technique; the most important being that ultracentrifugation of supernatants derived from blood may co-pellet lipoproteins and soluble protein aggregates, in addition to EVs (301,302). Other concerns include inducing EV fusion, aggregation with protein complexes and increasing PS exposure (303–305).

Recently, size exclusion chromatography (SEC) columns have emerged as a potential solution, removing non-vesicular protein and enriching an EV sample. SEC has risen in popularity in recent years, with evidence that it provides good isolation of EV from lipoprotein and other contaminating protein aggregates (301). However, other studies, in addition to our own unpublished observations, have not been able to replicate these findings, with a high level of lipoprotein markers seen in the “purified” EV sample (302). Additionally, this method is considered labour intensive, with the sample often being heavily diluted, requiring re-concentrating after isolation by ultracentrifugation. Despite this, the potential and increased use of SEC columns for EV isolation has led to commercial SEC columns becoming available, specifically for EV isolation; the Exo-Spin™ Midi Columns (Cell Guidance Systems, United Kingdom) and the qEV™ (IZON Science, New Zealand). Further optimisation and improvement in lipoprotein separation is required before SEC can be considered a “gold-standard” technique.

Density gradient ultracentrifugation has recently emerged as another method of EV isolation. This uses a sucrose gradient to isolate EVs based on their expected density (1.13-1.19 g/mL) from potential protein contaminants, which are denser (306). However, similarly to SEC, there are concerns that the use of a density gradient does not purify EVs from lipoproteins. A study by Yuana *et al* published in the *Journal of Extracellular Vesicles* demonstrated how high-density lipoproteins (HDL) co-isolated with EVs using this method (306).

Finally, immunoaffinity isolation utilises antibodies targeting specific surface proteins on EVs to isolate a select population of EVs. Antibodies are associated with magnetic beads, or beads that pellet at low centrifugal forces (307). Following incubation with a sample, EVs bind to the antibody-bead complex which can thus be physically separated from the rest of the sample either by a magnet or low speed centrifugation. This technique holds promise, especially in positively selecting specific subsets of an EV population. Although, as with other isolation techniques, further validation is required to ensure capture is fully optimised.

In summary, despite advances, there remains a large set of advantages and disadvantages associated with the various isolation techniques currently employed, and further work needs to be carried out before a universal “gold standard” isolation procedure is identified.

1.6.6.3 Measurement of EVs

A range of qualitative and quantitative methods have been utilised for EV research. As the field is rapidly evolving, techniques often become outdated or improvement in a short time frame. Electron microscopy, dynamic light scattering, flow cytometry, and tuneable resistive pulse sensing (TRPS) have all been utilised to quantify EV populations. Within the field, the most commonly used technique for EV size and concentration analysis is nanoparticle tracking analysis. However, the range of methods used throughout the EV field will not be discussed in this thesis, but comprehensive reviews are available within the literature (292). Specific methods used within this thesis are described in detail in chapter 2.

1.6.6.4 Storage of EVs

Ideally, samples should be analysed fresh wherever possible. In many scenarios, however, it is impractical to undertake a comprehensive assessment of EV samples, for example a clinical cohort with multiple time points and/or a large number of participants. Thus, storage and preservation of EVs is of great importance in these studies. The majority of studies store EV samples at -80°C in filtered phosphate-buffered saline (PBS) (292). Some studies have shown that EV size and concentration remain unchanged following storage at this temperature and repeated freeze-thaw cycles (308,309). Conversely, other studies have highlighted that storage at -80°C caused a decrease in EV size. Work from our own laboratory has highlighted how different freezing protocols can affect the measured EV size and concentration (310), suggesting freezing may cause gradual disintegration of EVs over time, regardless of method used. Storage of EVs at 4°C 7 days or less appears to preserve EV number and stability (297).

Overall, despite the huge boom in EV research, there remains a large number of problems in terms of processing, with a limited number of tangible resolutions. Hopefully, the EV field will eventually reach a consensus on a “gold standard” protocol for EV processing from a variety of biological fluids. Until then, caution must be taken when comparing studies utilising differing protocols.

1.6.7 Function of EVs

EVs are today recognised as important signalling molecules capable of mediating cell-cell communication, via transfer of a range of biogenic cargo outlined previously. The specific message delivered to the target cell is dependent on the composition of the EV, which in turn is dependent on the cell of origin. EVs have been implicated in a range of physiological and pathophysiological conditions, thus been the subject to increasing research interest in recent years. Figure 1.18 summarises the variety of roles EVs play within such conditions.

1.6.7.1 EVs in angiogenesis

Endothelial-derived EVs have been demonstrated to both promote and inhibit angiogenesis. Various molecules have been identified as potential mediators, including miRNAs (miR-214, miR-126) which induce proangiogenic signalling (266). Conversely, EVs with high levels of PS exposure leads to interaction with CD36 and subsequent Fyn kinase signalling, leading to increases in oxidative stress and inhibition of angiogenesis (311). Platelet-derived EVs containing pro-angiogenic molecules, such as VEGF and PDGF, have also been shown to induce endothelial cell proliferation and capillary sprouting (312). Mesenchymal stem cells (MSCs) incubated in hypoxia produced EVs capable of stimulating tube formation *in vitro* and promoting angiogenesis *in vivo* (313).

1.6.7.2 EVs in the immune system

As EVs reflect the topology of the cell of origin, antigen-presenting cell (APC)-derived EVs can carry surface MHC molecules and directly stimulate CD8 and CD4 T-cells (314,315). Antigen presentation can also occur indirectly, through the transfer of antigenic peptides present within EVs to APCs (316,317). Dendritic cell-derived exosomes have been shown to contain miRNA, allowing propagation of post-transcriptional regulation between APCs (273). EVs can mediate the immune response independently of antigen transfer or transcriptional regulation however. EVs can stimulate the immune response due to their contents, including microbial antigens, pathogen associated molecular patterns (PAMPs), or pro-inflammatory cytokines such as IL-1 β (318,319). Contrariwise, EVs can also have immunosuppressive effects. Following immunisation, CD11b⁺ EVs

were shown to suppress the immune response in a Fas/Fas ligand-dependent manner (320). MSC-derived EVs also harbour immunosuppressive properties, mimicking their parent cell enhancing regulatory T-cell production (321). Additionally, a recent study by Lo Sicco *et al* demonstrated that MSC derived EVs promote macrophage polarisation towards an anti-inflammatory (M2) phenotype (322).

1.6.7.3 EVs in cancer

Tumour cell derived EVs can act in a paracrine manner and promote tumour cell proliferation, migration and invasion. For example, the transfer of EVs between glioma cells led to proliferation of the recipient cells. These EVs were shown to contain epidermal growth factor receptor (EGFR) mRNA, which is overexpressed in a variety of epithelial tumours, and drives tumour progression (259,323). Tumour cell derived EVs can modulate the immune system, both promoting host protection against cancer (324–326), and also facilitating tumour evasion (327–329). Tumour cells have been shown to selectively package the transmembrane protein natural killer group 2D (NKG2D) into EVs, thereby reducing the recognition of the parent cells by T cells (330). Tumour cells can also secrete EVs that modulate the phenotype of cells surrounding the tumour. For example, EVs derived from tumour cells can convert fibroblasts into myofibroblasts; which produce growth factors and extracellular matrix to support tumour development (331). Taking into account the pleiotropic roles of tumour derived EVs, perhaps it is no wonder that this area continues to attract a significant amount of attention from researchers, in the hope they may facilitate diagnosis and/or treatment of cancer in the future.

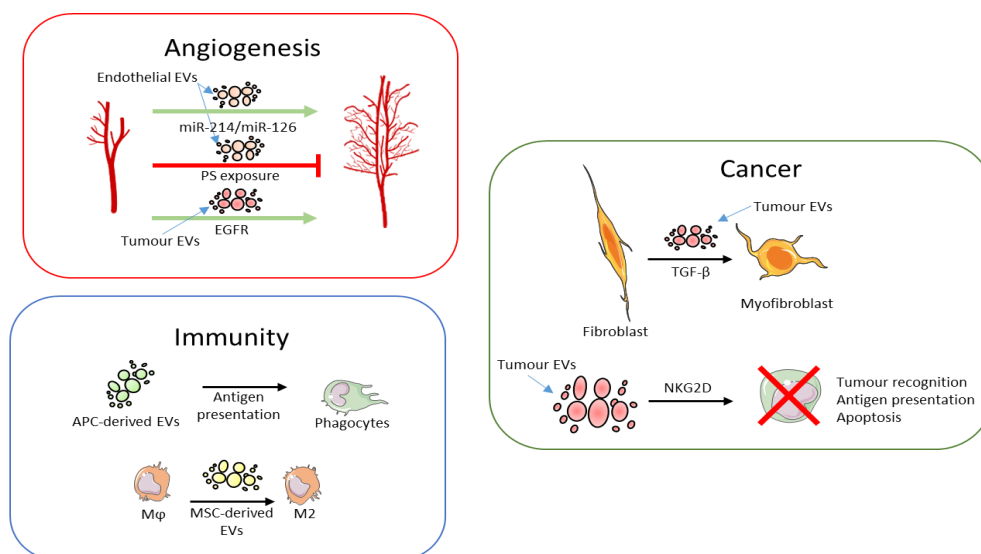


Figure 1.18 The varying roles of EVs in disease. A summary of the differing roles EVs play in angiogenesis, the immune system, and cancer. EGFR – epidermal growth factor receptor. PS – phosphatidylserine, TGF-β – Transforming growth factor-β, APC – antigen presenting cell, MSC – mesenchymal stem cell.

1.6.8 EVs in the cardiovascular system

1.6.8.1 Coagulation

EVs can regulate and actively participate in a variety of processes related to the cardiovascular system, including coagulation, inflammation, and endothelial dysfunction. Perhaps of most clinical interest is the role of EVs in coagulation. *In vivo*, one of the main functions of a platelet is to provide a negatively charged membrane surface that can facilitate acceleration of the coagulation cascade, leading to formation of a fibrin clot. This negative charge facilitates an electrostatic interaction between positively charged γ -carboxyglutamic acid (GLA) domains in the clotting proteins (such as factor VII, IX, X, and II) and PS on the membrane of the platelet (332). It has been claimed that platelet-derived EVs are between 50 to 100-fold *more* procoagulant than the surface of activated platelets themselves (333). This is thought to be primarily due to the enhanced level of negatively charged PS present on the outer leaflet of EV membranes (334). Indeed, platelet-derived EVs have been shown to enhance thrombin generation *in vitro* (335,336). Furthermore, a recent study by Weisel *et al* demonstrated the ability of circulating EVs to alter the structure and stability of fibrin clots; both indirectly through acceleration of thrombin generation, and directly, through physical incorporation of CD61⁺ EVs into the fibrin network (337).

However, it is not only platelet-derived EVs that have been implicated in mediating coagulation. There is evidence to suggest that erythrocyte (338), monocyte (339), and endothelial (340) derived EVs can also contribute to coagulation. Aside from PS exposure, EVs have also been shown to influence coagulation via TF (341). Indeed, TF⁺ EVs derived from endothelial cells and monocytes were shown to accelerate coagulation *in vitro* (342). Interestingly, platelet-derived EVs have been shown to contain small amounts of TF, suggesting that EVs derived from other cell types are the main mediators of this pathway (343). Human monocytes exposed to tobacco smoke have been shown to release TF exposing EVs, and exhibited significantly higher levels of procoagulant activity compared to control EVs, highlighting an additional mechanism by which smoking may affect the progression of CVD (344). Clinically, there are a plethora of publications demonstrating the role of EVs *in vivo*. Circulating EVs have been shown to contribute to coagulation after traumatic brain injury (345). The OASIS-CANCER study found that cancer cell-derived EVs mediate coagulation, potentially contributing to risk of ischemic stroke (346). Leroyer *et al* demonstrated that atherosclerotic plaques had 200-fold higher levels of EVs (derived from leukocyte, erythrocyte, and endothelial cell) in comparison to the blood of the patients, which were highly thrombogenic in nature (347). A study by Huisse *et al* prospectively recruited patients with acute MI, and found that TF-mediated EV activity was increased in patients with persistent

occlusion in comparison to healthy controls (348). Following this, they found that patients who did not achieve thrombolysis had significantly higher TF-mediated EV activity (349).

Intriguingly, it is not only blood-derived EVs that have been shown to play a role in coagulation. Salivary EVs have been shown to expose TF, and initiate coagulation in plasma. It was postulated that this may offer an explanation as to why humans, and many other animals lick their wounds; enhancing coagulation and preventing pathogen entry (350). The role of EVs in coagulation is elegantly demonstrated in individuals with Scott syndrome; a rare autosomal recessive bleeding disorder. It is thought to be caused by a defect in the scramblase enzyme, responsible for externalisation of PS. The result of this defect is an inability to express a functional scramblase enzyme, thus reduced externalisation of PS and EV production (351,352).

1.6.8.2 Endothelial dysfunction

Aside from coagulation, EVs have also been proposed as potential mediators of endothelial dysfunction. It is now widely accepted that endothelial dysfunction or “activation” leads to their release, thus, a multitude of studies have suggested EVs as markers of endothelial dysfunction. Circulating levels of endothelial-derived EVs have been shown to correlate with the degree of impaired vasodilation in a variety of subjects, including patients with type 2 diabetes (353), CAD (354), and end-stage renal failure (355). Additionally, recent studies have indicated that EVs are not only markers of endothelial dysfunction, but are in fact significant mediators of endothelial dysfunction themselves. EVs isolated from myocardial infarction patients have been shown to impair the endothelium-dependent vasodilation *ex vivo*, therefore contributing to endothelial dysfunction (356). Endothelium-derived EVs have been shown to reduce NO generation from eNOS and enhance oxidative stress (357,358). The reduction in NO generation was shown to be mediated by an increase in phosphorylation of eNOS at the inhibitory Threonine-495 site. Contrariwise, there is some evidence to suggest that EVs can promote endothelial function. Human lymphoid T-cell line-derived EVs were shown to contain the morphogen sonic hedgehog on their surface. These EVs preserve NO production by endothelial cells both *in vitro* and *in vivo*, via an interaction of this protein with its complementary receptor, Patched, on the surface of endothelial cells, leading to PI3K signalling (359,360).

1.6.8.3 Inflammation

EVs from various cell types have been shown to modulate inflammation both *in vitro* and *in vivo*. Firstly, bacteria themselves have been shown to release EVs and provoke an inflammatory response. *In vitro*, EVs secreted by *Helicobacter pylori*, *Pseudomonas aeruginosa* and *Neisseria gonorrhoeae* were shown to deliver peptidoglycan to the bacterial recognition protein nucleotide-binding oligomerisation domain-containing protein 1 (NOD1) in epithelial cells, leading to an upregulation of NF- κ B, and NOD1 dependent responses in infected host cells (361). Secondly, studies have demonstrated that EVs derived from atherosclerotic plaques transferred ICAM-1 to endothelial cells, which led to an increase in monocyte adhesion and transendothelial migration (362). Leukocyte-derived EVs have been postulated to stimulate cytokine release in endothelial cells, leading to increased pro-inflammatory activity in these cells. These EVs stimulated an increase in tyrosine phosphorylation of c-Jun N-terminal kinase (JNK1) in endothelial cells (363,364). In addition to their role in coagulation, platelet-derived EVs have been shown to promote leukocyte adhesion to endothelial cells, as well as chemotaxis of monocytes (365). These EVs contain arachidonic acid, which could be transformed to the pro-inflammatory TxA₂ (366). However, these platelet EVs can also induce cyclooxygenase-2 (COX-2) expression and subsequent production of the vasodilatory PGI₂. The increase in leukocyte adhesion has been mirrored in patient studies, whereby hypertensive patients have higher levels of PECAM-1 positive EVs compared to controls (367). Platelet EVs have also been shown to promote leukocyte aggregation, due to interactions between P-selectin on the surface of the EV, and its ligand, P-selectin glycoprotein ligand-1 (PSGL-1) on leukocytes (368). A separate study also found that platelet-derived EVs carried significant levels of RANTES (Regulated on Activation, Normal T-cell Expressed and Secreted), a proinflammatory chemokine that triggered monocyte adhesion in endothelial cells (369). EVs can also mediate inflammation by carrying proinflammatory cytokines. THP-1 monocyte-derived EVs were shown to contain bioactive IL-1 β (319). Conversely, there is some evidence that EVs can reduce inflammation: endothelial-derived EVs have been shown to contain miR-222, which is capable of reducing ICAM-1 expression. However, following hyperglycaemic conditions, these EVs contained significantly lower amounts of miR-222, and showed reduced anti-inflammatory capacity both *in vitro* and *in vivo* (370). This protective miR was completely diminished in patients with CAD. Taken together, this suggests that alterations in endothelial EV composition may reflect CVD status.

1.6.8.4 Arterial stiffness

Arterial stiffness occurs as a result of both biological aging, and atherosclerosis progression. Vascular calcification plays a pivotal role in this process, and is connected with VSMCs transitioning to a synthetic phenotype, associated with bone formation (371). Indeed, under physiological conditions VSMCs release EVs enriched in osteogenic inhibitors, such as matrix Gla protein (372) and fetuin-A (373). In endothelial dysfunction, VSMC-derived EVs contain low levels of these inhibitors (374,375). Additionally, macrophage-derived EVs have been shown to release EVs that promote local microcalcification in atherosclerotic plaques (376). Such microcalcification plays a major role in destabilising atherosclerotic plaques, thereby promoting rupture and consequent MI or stroke (377). *In vivo*, exosomes have been shown to co-localise with calcification in chronic kidney disease patients. A recent publication reviewed the role of EVs in cardiovascular calcification, suggesting that EVs were caught within the extracellular matrix and prevented from reaching their target cells (378). They hypothesise that this leads to dysregulated gene expression and enhanced osteogenic differentiation. Indeed, a number of studies have found that VSMC-derived EVs are enriched in a number of miRs involved in osteogenic differentiation. For example, miR 125-b regulates the expression of the osteogenic transcription factor osterix, involved in osteoblast differentiation (379,380). This, in addition to their role in forming microcalcifications, suggest a dual mechanism of propagating vascular calcification.

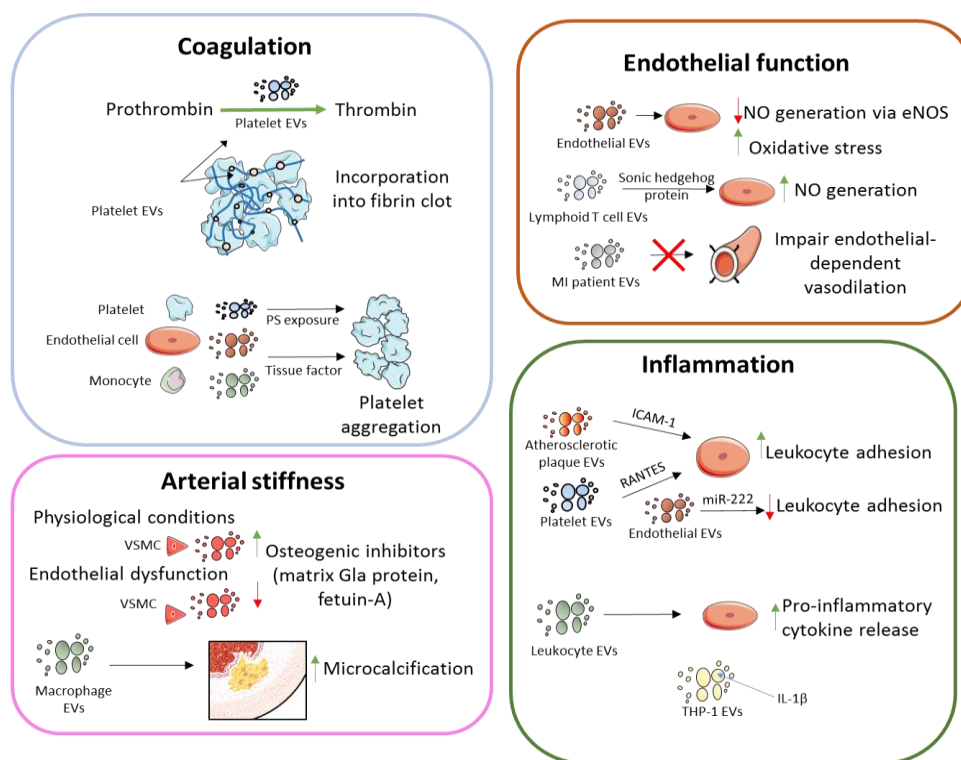


Figure 1.19 Summary of the effects of EVs within the cardiovascular system. Several studies have investigated the role of EVs numerous aspects of cardiovascular disease, including coagulation, endothelial function, inflammation, and arterial stiffness. EVs typically reflect the physiology of their parent cell, hence why EVs derived from differing cells and/or stimuli often have conflicting actions. eNOS – endothelial nitric oxide synthase, VSMC – vascular smooth muscle cell, PS – phosphatidylserine, MI – myocardial infarction, ICAM-1 – intercellular adhesion molecule-1, RANTES - regulated on activation, normal T cell expressed and secreted.

1.6.9 Emerging therapeutic opportunities

1.6.9.1 Biomarkers

Given the mass of evidence suggesting that EVs are reflective of the environment in which they were produced, their potential to detect a pathological disease state has provoked more and more interest in their potential as biomarkers for various diseases. Specific molecules may be present either on or within the EV, serving as an inexpensive and non-invasive method of screening risk patients for a disease prior to the appearance of symptoms (381). Indeed, myeloma-derived EVs express CD44, an antigen shown to be prognostic for the progression of disease (382). Annexin V⁺ endothelial-derived EVs have been shown to correlate with endothelial dysfunction, and have potential as a marker of this (383,384). Similarly, PECAM-1/annexin V⁺ circulating EVs have been shown to correlate with cardiovascular outcomes in CAD patients, suggesting their possible usefulness in risk stratification (385). Standardisation of EV processing is required however before they can feasibly be used in clinical diagnostics.

1.6.9.2 Delivery vectors

Currently, liposomes are routinely used as drug delivery vectors. Liposomes are synthetic vesicles with a phospholipid membrane, and have been utilised to deliver drugs to target cells *in vivo*. However, the ability of a liposome to evade the host immune system and maintain a long half-life remains difficult (386). Thus, the ability of EVs to target specific cells and transfer a message in the form of biogenic cargo has drawn the attention of researchers. EVs possess many of the desirable features of an ideal drug vector; a long circulating half-life, an intrinsic ability to target tissues, and biocompatibility with no toxicity issues (387).

Mesenchymal stem cells transfected with the miR-143 produced EVs containing this miR, which were then able to transfer this to osteocarcinoma cells and inhibit their migration (388). In addition to modulating gene expression via miR delivery, EVs have also been used to deliver proteins directly. Recently, it was shown that exosomes loaded with the antioxidant protein catalase was capable of delivering this across the blood brain barrier, providing significant neuroprotective effects in a mouse model of Parkinson's disease (389). This area of research is still only in its infancy, but is expected to grow rapidly in the coming years. EVs provide huge promise and a novel approach toward the delivery of both synthetic and biological molecules to target cells.

1.6.9.3 Vaccination

A fascinating area of ongoing research is the use of EVs in vaccination. There is some evidence to suggest that vaccinations utilising EVs provoke a more effective immune response than that induced by protein subunit-based vaccines (390). EVs derived from macrophages that had been treated with *Mycobacterium tuberculosis* culture filtrate proteins (CFP) were shown to prime a protective immune response, in addition to boosting prior BCG immunisation. The authors concluded that this EV vaccination conferred decreased growth of *M. tuberculosis* in mouse lungs compared to antigen-based vaccines (391). EV based vaccines offer hope for cases where no effective antigen-based vaccine exists. For example, EVs derived from *Eimeria tenella* antigen-pulsed chicken dendritic cells promoted stronger antibody responses, and led to increased survival rates compared to antigen-vaccinated chickens following an *E. tenella* challenge 10 days post-immunisation (392). Finally, EVs hold promise in vaccination in pregnancy; the vaccination of pregnant mice with EVs from dendritic cells pulsed with *Toxoplasma gondii*-derived antigens increased survival in newborns subsequently challenged with *T. gondii* (393).

EV-based cancer vaccines have recently been investigated in clinical trials. A phase I trial isolated dendritic cells from patients with advanced metastatic melanoma, and incubated them with melanoma peptide antigens, inducing the presentation of the antigen on the cell surface. EVs were collected from the cell culture medium, and reintroduced into patients, promoting an immune response against the melanoma. This trial concluded that patients tolerated administration of EVs for up to 21 months (394). Although the primary purpose of Phase I trials is to assess safety, studies have observed that disease progression halted following EV vaccination (395). A Phase II trial has confirmed the capacity of dendritic cell-derived exosomes to boost the natural killer (NK) cell arm of anti-tumour immunity, in patients with advanced non-small cell lung cancer (396).

Ultimately, the future of EV research holds promise in offering a novel approach to treating pathology. Not only via directed delivery of biogenic molecules or synthetic drugs, but also by controlling their release, and/or function, we may be able to modulate their role in acceleration of disease progression.

1.7 Thesis hypothesis and aims

1.7.1 Hypothesis

Evidence suggests that EVs appear to play a pivotal role in the development of CVD, with roles in coagulation, inflammation, and endothelial dysfunction. Given the mechanism of EV biogenesis, coupled with the protective role of NO in CVD, I hypothesised that increasing NO bioavailability in the form of inorganic $\text{NO}_2^-/\text{NO}_3^-$ would reduce the production of EVs, both *in vitro* and *in vivo*, and possibly alter their biological function.

1.7.2 Aims

In order to test this hypothesis, work was split into several themes, presented within this thesis as individual results chapters. Each chapter contains its own specific aims, however, broadly, the overarching aims of this thesis were as follows:

1. To investigate the effect and mechanism of hypoxia on EV production and size in endothelial cells.
2. Following this, to evaluate the effect of NO_2^- derived NO on endothelial cells exposed to hypoxia, and examine whether this changes the number and/or size of EVs produced.
3. To assess whether hypoxia and/or NO_2^- exposure can alter the function of endothelial-derived EVs in terms of their potential to influence coagulation, inflammation, or cell function/viability using *in vitro* models
4. To examine the influence of a dietary NO_3^- supplement on both NO bioavailability, and EV concentration in healthy volunteers.
5. Finally, to investigate the effect of dietary NO_3^- supplementation on platelet activity, NO bioavailability and circulating EV concentration in CAD patients.

2 GENERAL METHODS

2.1 Cell Culture

2.1.1 Human Vascular Endothelial Cell (HECV) Culture

The human vascular endothelial cell (HECV) line (originally derived from human umbilical vein endothelial cells) was kindly provided by Dr Gareth Willis, previously purchased from Interlab (Milan, Italy) (Figure 2.1). Cells were maintained in Dulbecco's Modified Eagle Medium (DMEM) (PAA Laboratories, UK) containing 10% foetal calf serum (FCS) (PAA Laboratories, UK) and 1% streptomycin/penicillin (Invitrogen, UK). Cells were kept in an incubator at 37°C in 5% CO₂. Cells were sub-cultured at ≈ 90% confluence using Trypsin-EDTA (Invitrogen, UK).

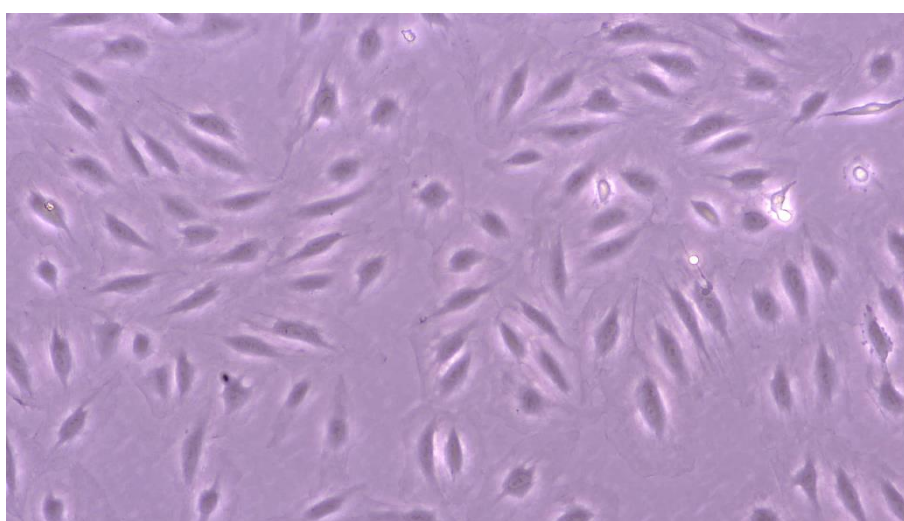


Figure 2.1 Culture of human vascular endothelial cells (HECVs). Cells were grown in DMEM, supplemented with 10% FCS and 1% streptomycin/penicillin. Cell medium was changed regularly (approximately every 48 hours) during cell growth. Image was captured at ≈ 60% confluence and 10x magnification.

2.1.2 Human Umbilical Vein Endothelial Cell (HUVEC) Isolation & Culture

Isolation of HUVECs was performed as previously described, with minor modifications (397). Human umbilical cords were obtained from the Delivery Suite at the University Hospital of Wales. Ethical approval was obtained from the Research Ethics Committee (REC reference: 14/NW/1459). Umbilical cords were cut to around 6 inches, avoiding any damage from clamps used during birth. Umbilical cords were washed with 0.9% saline to remove excess blood and clots. The vein was located and washed through with saline until the solution ran clear. One end of the cord was clamped, and collagenase (diluted 1 mg/ml with complete M199 medium (Table 2.1)) was inserted into the umbilical vein, before incubation at room temperature for 30 minutes

(Figure 2.2). The collagenase solution was removed and placed into a centrifuge tube, gently squeezing the cord to ensure complete cell detachment. The vein was flushed through with sterile PBS three times to ensure maximal yield of HUVECs. The resulting solution was then centrifuged at 300 x g for 5 minutes to pellet HUVECs. HUVECs were then resuspended in complete M199 medium, before being plated onto cell culture plates or flasks pre-coated with 1% gelatin. Medium was changed 2 hours after seeding the cells, and again after \approx 24 hours, in order to remove erythrocyte contamination (Figure 2.3).



Figure 2.2 Isolation of human umbilical vein endothelial cells (HUVECs). Approximately 5 mL of 1 mg/mL collagenase solution was inserted into the umbilical vein, and left for 30 minutes. The umbilical cord and vein was thoroughly washed through with saline before collagenase incubation.

Table 2.1. Constituents of complete M199 Medium.

Reagent	Supplier	Diluent	Final Concentration
M199 Medium	Invitrogen	-	-
Gentamicin	Sigma	ddH ₂ O	35 μ g/mL
Amphotericin B	Sigma	ddH ₂ O	250 ng/mL
10% FCS	Invitrogen	-	-
hEGF	Invitrogen	Filtered PBS	1 ng/mL
Hydrocortisone	Sigma	EtOH	1 ng/mL

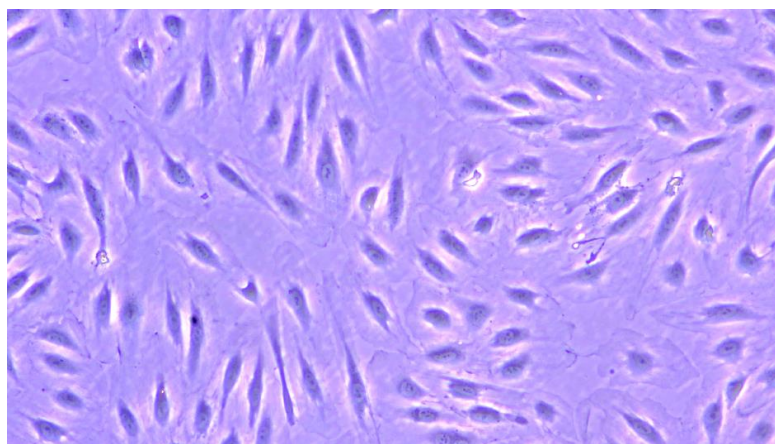


Figure 2.3 Culture of human umbilical vein endothelial cells (HUVECs). Cells were grown in M199 medium, supplemented with gentamicin (35 $\mu\text{g}/\text{mL}$), amphotericin B (250 ng/mL), 10% FCS, hEGF (1 ng/mL) and hydrocortisone (1 ng/mL). Cell medium was changed regularly (approximately every 48 hours) during cell growth. Image was captured at approximately 60% confluency at 10x magnification.

2.1.3 Cellular treatments

Both HECV and HUVEC cultures were exposed to a variety of cellular treatments. Upon cells reaching approximately 80% confluence, cell culture medium was removed. Cells were washed with sterile PBS, and incubated with EV-free serum free medium (SFM) for 24 hours (37°C and 5% CO_2). All cellular treatments were diluted in SFM before addition to cells. The various cellular treatments, stock concentrations, and resuspension diluent are outlined in table 2.2.

Table 2.2 Treatments for HECVs and HUVECs.

Reagent	Supplier	Diluent	Stock Concentration	Final Concentration
Sodium Nitrite (NaNO_2)	Sigma	H_2O	10 mM	3-300 μM
Sodium Nitrate (NaNO_3)	Sigma	H_2O	10 mM	3-300 μM
Allopurinol	Sigma	H_2O	100 mM	100 μM
S-Nitrosoglutathione (GSNO)	SantaCruz Biotechnology	H_2O	10 mM	100 μM
Desferrioxamine (DFO)	Sigma	H_2O	10 mM	100 μM
Calpain Inhibitor I (ALLN)	Sigma	EtOH	100 mM	100 μM
TNF- α	ThermoFisher Scientific	SFM	1 $\mu\text{g}/\text{mL}$	0.1 $\mu\text{g}/\text{mL}$

In some experiments, a combination of treatments were given. The supplier, diluent, stock concentration and final concentration are shown. Chemical were made to the stock concentration using the diluent shown, then further diluted to the final concentration in SFM.

2.1.4 Hypoxia exposure

Cells were transferred from the incubator to an Invivo2 hypoxic workstation 400 (Baker Ruskin, UK), and maintained under a range of oxygen concentrations (1-20% O₂) for 24 hours. The oxygen concentration was monitored using an i-CO₂N₂ gas mixing system (Baker Ruskin, UK).

2.1.5 Cell Counting & Viability

2.1.5.1 Trypan blue exclusion

Cells were detached from flasks by adding trypsin-EDTA and incubating at 37°C for ≈ 5 minutes. Cell medium was added to neutralise the trypsin, before centrifugation at 300 x *g* for 5 minutes. The resultant cell pellet was resuspended in cell medium, and mixed with trypan blue solution (final concentration 0.2%, Sigma Aldrich, UK) (1:1 v/v) before being counted using a Cellometer Auto T4 (Nexcelom Biosciences, USA) (Figure 2.4). Trypan blue utilises the fact that live cells possess intact cell membranes, and thus will not take up the dye. Dead cells have compromised cell membranes, and thus will take up the dye, allowing them to be excluded from the viable cell count.

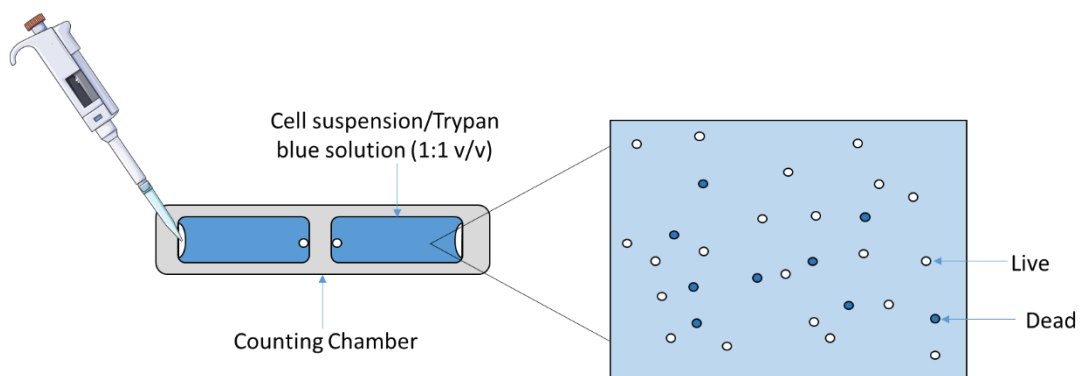


Figure 2.4. Trypan Blue Exclusion. Cells in suspension were mixed (1:1 v/v) with trypan blue solution. This suspension was then added to a Cellometer® counting chamber for automated cell counting.

2.1.5.2 Haemocytometer

Cells were also counted manually using a haemocytometer. The haemocytometer was first prepared by cleaning with alcohol. The coverslip was moistened with water and affixed to the haemocytometer. Cell suspension was diluted 1:1 (vol/vol) with trypan blue solution (final concentration 0.2%). Next, 100 μ L of this trypan blue treated cell suspension was added to the haemocytometer. Using a microscope, the grid lines of the haemocytometer were focussed on with a 10x objective. Using a hand tally counter, the cells were counted in one set of 16 squares. This was repeated until all 4 sets of 16 squares were counted. The number was then multiplied by 10^4 and adjusted for dilution, giving a final viable cells / mL of the original cell suspension.

2.1.5.3 MTS assay

In order to comprehensively assess the effect of hypoxia on cell viability, a MTS assay was undertaken (CellTiter 96[®] AQueous one solution cell proliferation assay; Promega, Southampton, UK), following the manufacturers protocol. This colorimetric method utilises the tetrazolium compound 3-(4,5-dimethylthiazol-2-yl)-5-(3-carboxymethoxyphenyl)-2-(4-sulfophenyl)-2H-tetrazolium (MTS) and the electron coupling reagent phenazine ethosulfate (PES). The enhanced chemical stability of PES allows it to be combined with MTS to form the stable “one solution” reagent. In the presence of PES, the tetrazolium compound is reduced by dehydrogenase enzymes, such as NADH or NADPH in metabolically active cells, into a formazan product (398). Approximately 1×10^4 cells were seeded in a 96 well plate. 24 hours later, cell culture medium was replaced with the CellTiter 96[®] AQueous One Solution Reagent, diluted in cell culture medium (20 μ L:80 μ L), and incubated for 2 hours. The formazan product produced is purple in colour, and soluble in cell culture medium, allowing the quantity to be measured by absorbance at 490 nm, which is directly proportional to the number of living cells in culture (399). Absorbance was measured using a BMG CLARIOstar OPTIMA (BMG Labtech, USA).

2.1.5.4 Caspase-Glo[®] 3/7 assay

In order to assess the effect of hypoxia on apoptosis, a Caspase-Glo[®] 3/7 assay (Promega, Southampton, UK) was used. This luminescent assay measures caspase-3 and -7 activity, which are activated during the early stages of apoptosis. This assay utilises a luminogenic caspase-3/7 substrate containing the tetrapeptide DEVD. This substrate was diluted 1:1 (v/v) in a buffer optimised for caspase activity, luciferase activity, and cell lysis provided by the company. 1×10^4 cells were seeded in a 96 well plate. 24 hours later, 100 μ L of this reagent was added to wells and incubated for 3 hours at 37°C. Following caspase-3/7 cleavage of the lumogenic substrate, the DEVD peptide is cleaved, and a luciferase substrate (aminoluciferin) is released, resulting in the luciferase

reaction, and production of a stable luminescent signal. Luminescence was measured using a BMG CLARIOstar OPTIMA (BMG Labtech, USA).

2.1.6 Silencing RNA

In order to investigate the effect of hypoxia-inducible factor (HIF)-1 α and -2 α in endothelial cells, silencing RNA was utilised.

For HIF-1 α , 5x10⁵ HECVs were seeded in a T25 flask and grown to approximately 50% confluency. HIF-1 α siRNA (Dharmacon SMARTpool, UK) was mixed with a siRNA transfection reagent (Dharmacon RNAi Technologies, UK) at a ratio of 20:1, and incubated at room temperature for 20 minutes. This mix was added to 4 mL of antibiotic free medium (DMEM, 10% FCS), and added to the cells, yielding a final siRNA concentration of 100 nM. Control experiments consisted of transfection with the ON-TARGETplus non-targeting siRNA control (100 nM; Dharmacon RNAi Technologies). Cells were incubated in medium containing either HIF-1 α siRNA or control siRNA for 48-72 hours prior to hypoxia exposure for 24 hours.

For HIF-2 α silencing, 2x10⁵ HECVs were seeded in a 6 well plate in 2 mL antibiotic-free medium (DMEM, 10% FCS). Cells were incubated until they were approximately 50% confluent. Prior to transfection, HECVs were incubated in 2x DMEM (2% P/S, 20% FCS), as per the manufacturer's instructions. The HIF-2 α siRNA duplex was mixed with the siRNA transfection reagent (Santa Cruz Biotechnology, USA) (1:1 ratio) in transfection medium (antibiotic and FCS free) (Santa Cruz Biotechnology, USA), yielding a final siRNA concentration of 10 μ M, and incubated at room temperature for 30 minutes before being added to cells. Cells were incubated in the transfection medium containing the siRNA for 24 hours before replacing the medium with fresh 1 x DMEM. Cells were incubated for an additional 48-72 hours prior to hypoxia exposure. Control experiments were performed using a non-targeting siRNA (final concentration 10 μ M).

Successful silencing of both HIF-1 α and HIF-2 α was confirmed via Western blotting, as described in section 2.15.

2.2 Electron Microscopy

Electron microscopy (EM) of HECVs was undertaken in collaboration with Dr Christopher Von Ruhland (Central Biotechnology Services - Cardiff University). Scanning electron microscopy was used to visualise HECVs at normoxia (21% O₂) and hypoxia (1% O₂). Transmission electron microscopy was used to confirm a true EV population after isolation, and assess EV morphology and purity. Scanning electron microscopy was also used to visualise fibrin clots, which was kindly performed by Vanessa Evans of Swansea University.

2.2.1 Scanning electron microscopy

HECVs were grown on a 35 mm glass bottom dish (Cellvis, USA), maintained in DMEM supplemented with 10% FCS and 1% penicillin/streptomycin at 37°C and 5% CO₂. Cells were washed three times in sterile PBS, before being fixed in 1% glutaraldehyde in PBS (v/v) for 1 hour at room temperature. Once fixed, cells were kept in PBS at 4°C until imaging. Cell samples were subjected to dehydration through graded isopropanol (IPA) at 50%, 70%, 90% and 100% for 10 minutes at each grade, followed by three exchanges in hexamethyldisilazane (HMDS) for 5 minutes per exchange. Excess HMDS was then removed and any remaining residue was allowed to evaporate by air drying for 1 hour. Samples were then sputter coated with gold, and imaged at 5 kV using a JEOL 840 scanning electron microscope (JEOL, USA). SEM images of fibrin clots were obtained using a similar protocol, with minor modifications. Fibrin clots were formed at 37°C for 2 hours by adding calcium chloride (CaCl₂, 20 mM). Clots were washed three times with sodium cacodylate buffer (0.2M), before being fixed in 2% glutaraldehyde in PBS (v/v) for 1 hour at room temperature. Clots were subjected to dehydration through graded ethanol (30-100%), and then fixed using HMDS. Finally, the fibrin clot was sputter coated with gold, and imaged using a Hitachi Ultra-high resolution FE-SEM S-4800.

2.2.2 Transmission electron microscopy

EVs were isolated from HECVs incubated at normoxia (21% O₂) and hypoxia (1% O₂) as described in section 2.4.1. EVs were resuspended in 1x sterile PBS and stored at 4°C until analysis. 50 µL of EV droplets were adsorbed onto carbon-coated grid for 30 minutes before fixation with 1% glutaraldehyde (v/v) for 1 hour at room temperature. These grids were then washed in PBS 3 times for 1 minute, and 6 times for 10 minutes in water. EVs were negatively stained with 2% (w/v) uranyl acetate for 20 minutes. Surplus stain was shaken off and allowed to air dry at room temperature. EVs were then visualised in a Philips CM12 TEM (FEI Ltd, UK) at 80 kV.

2.3 Nanoparticle tracking analysis

2.3.1 Background

Nanoparticle tracking analysis (NTA) is currently the most widely used and accepted method in the EV field to determine EV size and concentration. Past EV research has been hindered by limitations of previous methods, such as flow cytometry, or electron microscopy. Although these methods confirm the presence of EVs, electron microscopy is non-quantitative and requires significant sample preparation, and flow cytometry has a limit of detection of approximately > 300 nm, an obvious stumbling block considering given a large portion of microvesicles are < 300 nm, and all exosomes are < 100 nm (400).

NTA allows for direct and real-time visualization of nanoparticles, utilising a finely focussed laser beam to illuminate a diluted sample of particles in a suspension. The beam refracts at a low angle through a glass prism (or “optical flat”) resulting in a thin beam of laser light at the interface of the glass-liquid layer, allowing the illumination of particles within the sample. Illumination of the sample results in the particles scattering light, which is collected by an objective lens, and then focussed by a second lens onto a sensitive electron multiplying charge coupled device (EMCCD) camera (Figure 2.5). This camera captures video of the movement of particles at 30 frames per second with a field of view of $100\ \mu\text{m} \times 80\ \mu\text{m}$ (401).

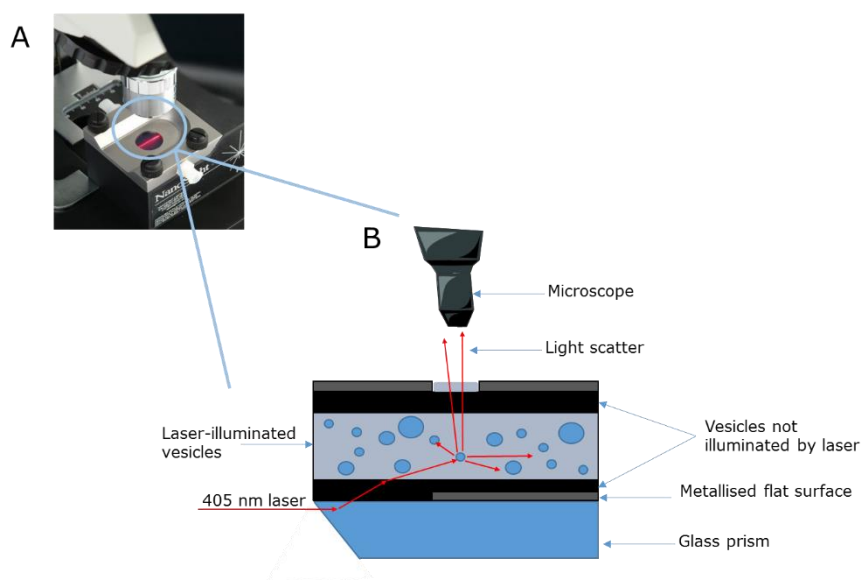


Figure 2.5. Nanoparticle Tracking Analysis. A. NanoSight laser illumination module. B. EVs in a suspension are illuminated by a laser refracted into the fluid via a glass prism, causing the EVs to scatter light. This light scattering is then visualised by a microscope with a video camera attached, allowing the tracking of illuminated EVs to determine the particle size. Image (A) ©Malvern Instruments Ltd.

This camera records the EVs moving under Brownian motion, which allows the velocity and distance travelled of individual EVs to be tracked in order to calculate their size and concentration using NTA software. The lower limit of particle size measurable is dependent on the refractive index (R_i) of the sample. For colloidal gold, which has a high R_i , accurate determination of size is possible down to ≈ 15 nm. For particles of biological origin with a lower R_i , such as EVs, this limit is ≈ 30 nm (401). Software is optimised to track EVs on a frame by frame basis (Figure 2.6), allowing the calculation of the hydrodynamic diameter using a modified Stokes-Einstein equation. Particles move under Brownian motion in three dimensions, however the Brownian motion is only tracked in two dimensions (x and y) by NTA software. Thus, a modified Stokes-Einstein equation is used (equation 2.1) (402). The average distance moved of each particle in two dimensions is determined from NTA software. This, along with the particle diffusion coefficient Dt , the sample temperature T , and solvent viscosity η , allows the hydrodynamic diameter (particle size) to be calculated.

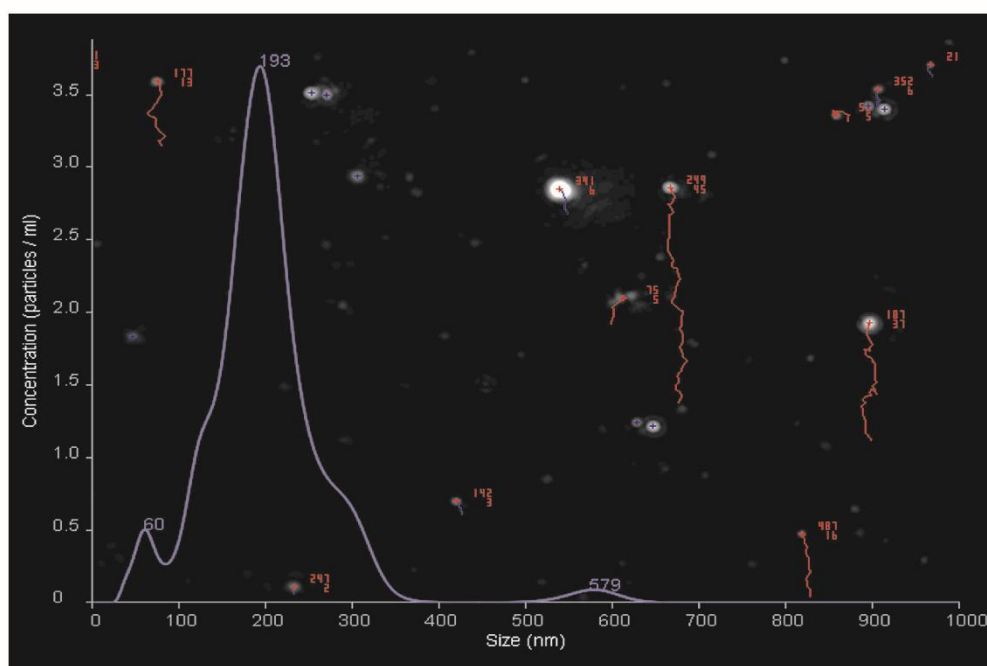


Figure 2.6. Example of NTA tracking individual particles. EVs are illuminated by a fine laser beam. The velocity and distance travelled of each individual EV is tracked frame-by-frame allowing EV size and concentration to be determined by a modified Stokes-Einstein equation.

$$\mathbf{A} \quad Dt = \frac{T_t K_B}{3\pi\eta d}$$

$$\mathbf{B} \quad \frac{(x, y)^2}{4} = Dt = \frac{T_t K_B}{3\pi\eta d}$$

Equation 2.1 Stokes-Einstein equation. The original equation (A) only accounts for movement in two dimensions, therefore a modified equation (B) is used. (x,y) is the mean displacement moved in two dimensions, Dt is the diffusion coefficient, K_B is Boltzmann's constant, T is the temperature of the sample in Kelvin, t is the sampling time, η is the viscosity of the sample, and d is the hydrodynamic diameter, or particle size.

2.3.2 Experimental methodology

NTA analyses were undertaken using a NanoSight LM10 microscope (Malvern Instruments, UK), with a 488 nm (blue) laser installed. 100 nm polystyrene beads were measured prior to sample analysis in order to ensure correct functioning of the microscope, and accurate size determination by the NTA software (v3.0). The system was washed through between samples with sterile water until no particles were detectable. EV samples were diluted in sterile water to the range 10^7 - 10^9 per mL, in order to allow NTA software to accurately track each individual particle and thus accurately determine size and concentration. EV size is represented as the mean of the population (nm). Pre- and post- analytical settings were kept consistent between experiments, summarised in table 2.3.

Table 2.3 Pre- and post- analytical settings used for EV sample analysis by NTA.

	Setting	Value
Pre-analytical	Camera shutter	450
	Camera level	12-16
	Camera gain	200-300
	Syringe Pump Speed	20
Post-analytical	Temperature	21-25 °C
	Screen gain	10-15
	Detection threshold	5-8

2.4 EV Isolation & Storage

2.4.1 Isolation of cell-derived EVs

Our research group (263) and others (403) have previously shown that isolation of EVs from cells grown in media supplemented with FCS overestimates EV concentration when analysed by NTA, due to the calf serum also containing EVs which are co-pelleted upon ultracentrifugation. Thus, cells were incubated in serum-free media for 24 hours prior to EV isolation. Cell-conditioned culture medium was then removed directly from the culture flask/well, and subjected to a differential ultracentrifugation method, as described previously (404). First, cell media was centrifuged at 1000 x *g* for 5 minutes to remove any detached cells in suspension. This supernatant was taken and subjected to a second centrifugation at 15,000 x *g* for 15 minutes at 4°C in order to pellet any cellular debris or apoptotic bodies. This supernatant was isolated and subjected to a third and final ultracentrifugation at 100,000 x *g* for 60 minutes at 4°C in order to pellet EVs. This pellet was then resuspended in 1x PBS, which had been filtered with a 0.22 µm filter (Millex®, Merck Millipore, Ireland) (Figure 2.7A). EVs were suspended in a 10-fold concentrate, for example, EVs were resuspended in 100 µL of filtered PBS for every 1 mL of cell-conditioned media ultracentrifuged.

2.4.2 Isolation of plasma-derived EVs

Blood samples were drawn gently from an antecubital vein using a 21G butterfly needle (Hospira, UK) into citrate vacutainers® (BD, UK). Blood was immediately centrifuged at 2,500 x *g* for 15 minutes at 4°C to isolate platelet-poor plasma (PPP) from whole blood. This PPP was subjected to a second identical centrifugation in order to pellet any remaining platelets, rendering the supernatant platelet-free plasma (PFP). This PFP was then ultracentrifuged at 100,000 x *g* and resuspended in a 10-fold concentrate (Figure 2.7B).

2.4.3 Storage of EVs

Once isolated, EV suspensions were stored at 4°C for up to 5 days. Where possible, EV suspensions were utilised immediately. For long term storage (>5 days) of EVs, EVs were slowly frozen at 1°C per minute to -80°C using a Cryogenic “Mr. Frosty™” Freezing Container (ThermoScientific, UK).

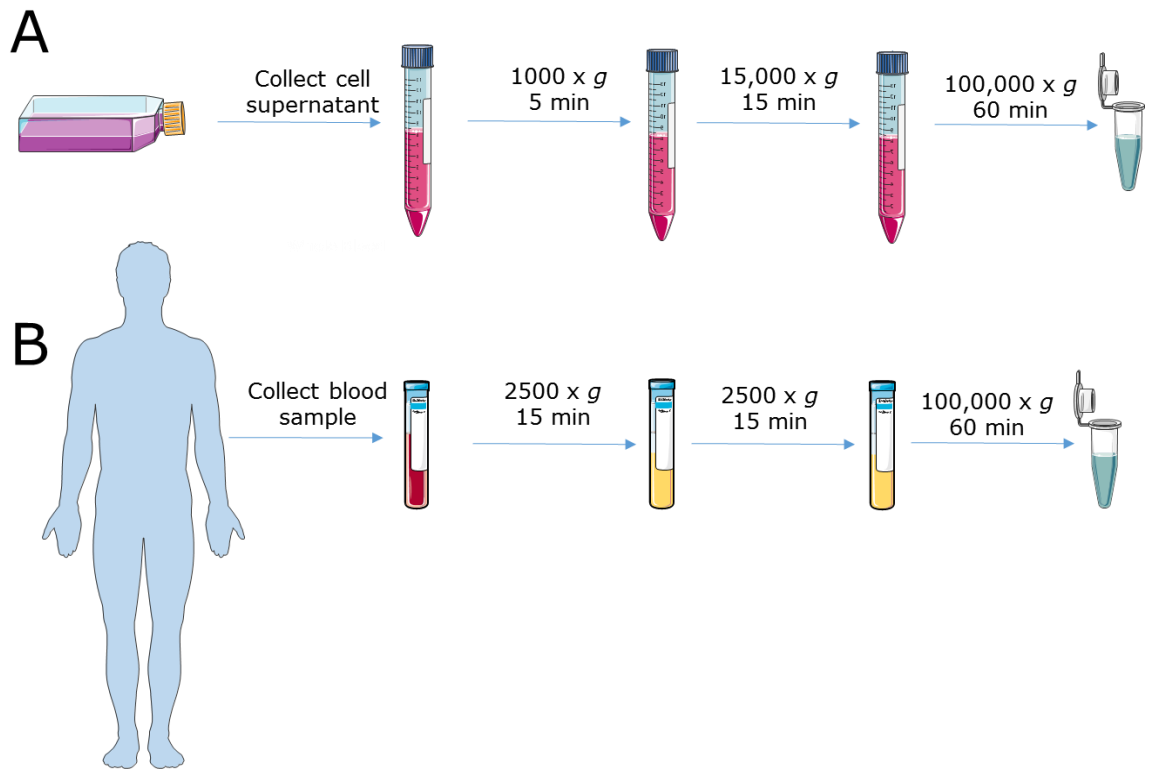


Figure 2.7. Isolation of EVs. A. Isolation of cell culture derived EVs. B. Isolation of plasma derived EVs.

2.5 Time resolved fluorescence

2.5.1 Background

A time-resolved fluorescence assay developed in the laboratory of Professor Aled Clayton (405) was used to measure the protein expression of EVs isolated from both plasma and cell culture, with minor modifications. Time-resolved fluorescence utilises “long-life” fluorophores, called lanthanides, such as europium. Lanthanides emit light over a much longer period of time after excitation (microseconds) compared to traditional fluorophores (nanoseconds). This allows a minimum amount of background noise by delaying the beginning of the measurement window until after background signal has decayed (Figure 2.8).

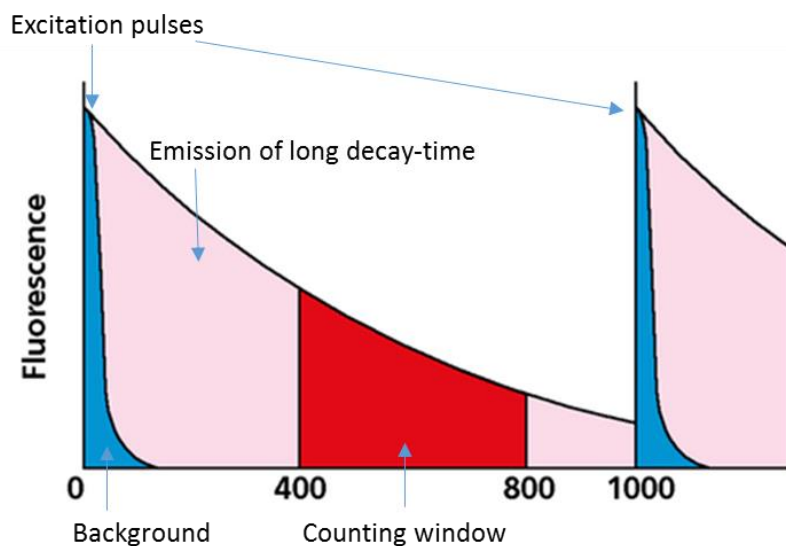


Figure 2.8 Time resolved fluorescence. Fluorescence is measured 400 μs after the last excitation flash, and measured for a 400 μs window, minimising background fluorescence. Diagram adapted from (406).

2.5.2 Experimental method

EVs were first isolated as outlined in section 2.4, before their size and concentration was determined as outlined in section 2.3. 5×10^9 (plasma) or 5×10^8 (cell culture) EVs per well were loaded onto a high-protein binding 96-well plate (Greiner Bio-One) and allowed to settle overnight at 4°C. Wells were blocked with 1% BSA in PBS (w/v) for 2 hours at room temperature. In order to analyse intravesicular protein content, a lysis buffer (RIPA buffer, Santa Cruz, CA) was added for 1 hour at room temperature, in order to permeabilise EVs. EVs were then probed with primary antibodies overnight at 4°C on a plate shaker. Details of primary antibodies are given in table 2.4. Next, a biotin-labelled anti-rabbit IgG (Goat) secondary antibody (Perkin Elmer, UK) was added and incubated for 1 hour at room temperature on a plate shaker. Finally, a streptavidin-europium conjugate (Perkin Elmer, UK) was added and incubated for 1 hour at room temperature. Three washes were performed between each stage in the assay (6 washes after addition of europium) using DELFIA® wash buffer (Perkin Elmer, UK). Plates were read using a BMG FLUOstar OPTIMA or a BMG CLARIOstar (BMG Labtech, UK). Each well received 400 flashes, with the measurement beginning 400 μ s after the last flash, and was recorded for 400 μ s. A set of europium standards were ran in order to set the gain adjustment, allowing for comparison between multiple plate reads. Data were analysed using MARS software (BMG Labtech, UK) and presented in relative fluorescence units (RFU). All data was adjusted to account for background fluorescence using a negative control (EVs with IgG control antibody added).

Table 2.4 Primary antibodies used for TRF.

Antibody	Type	Source	Product Code
CD9	Rabbit	Cell Signaling	13174
Alix	Rabbit	Abcam	Ab88388
TSG101	Rabbit	Abcam	Ab30871
HIF-1 α	Rabbit	Abcam	Ab51608
CD144	Rabbit	Abcam	Ab33168
CD41	Rabbit	Abcam	Ab63983
CD11b	Rabbit	Abcam	Ab133357
CD235a	Rabbit	Abcam	Ab129024
vWF	Rabbit	Abcam	Ab6994
Tissue factor	Rabbit	Abcam	Ab48647
Thrombomodulin	Rabbit	Abcam	Ab109189
TFPI	Rabbit	Abcam	Ab180619
TNF- α	Rabbit	Abcam	Ab6671
IL-1 α	Rabbit	Abcam	Ab9614
IL-6	Rabbit	Abcam	Ab6672
IL-8	Rabbit	Abcam	Ab18672
NF- κ B (p65)	Rabbit	Abcam	Ab16502
VCAM-1	Rabbit	Abcam	Ab134047
ICAM1	Rabbit	Cell Signaling	4915
E-Selectin	Rabbit	Abcam	Ab18981
P-Selectin	Rabbit	Abcam	Ab6632
PECAM	Rabbit	Abcam	Ab28364

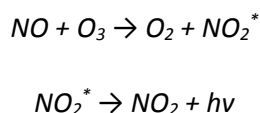
Antibody type, source and product code are given. All antibodies were diluted to 3 μ g/mL and incubated overnight at 4°C on a plate shaker. All antibodies were detected using a biotin-labelled anti-rabbit IgG (goat) secondary antibody, followed by a streptavidin-europium conjugate.

2.6 Plasma NO metabolites: Ozone Based Chemiluminescence

2.6.1 Background

Given the highly reactive nature of free NO, direct measurement is extremely difficult. Therefore, metabolites of NO are determined to obtain information about the *in vivo* production, consumption, and bioavailability of NO. NO_3^- , NO_2^- and RSNO were determined using well established ozone based chemiluminescence (OBC) techniques, which were developed and have been described in detail previously by our laboratory (173). In order to measure these metabolites, they must first be reduced back to NO. This is performed using chemical cleavage agents specific to the metabolite of interest. The NO produced is carried in a flow of inert gas (O_2 -free N_2) at a constant flow rate ($\approx 150\text{-}200\text{ cm}^3/\text{min}$), passed through a 1M sodium hydroxide (NaOH) trap, and fed into a nitric oxide analyser (NOA) (Sievers NOA 280i, Analytix, UK).

The NOA uses O_2 to generate ozone (O_3) in a reaction cell, which subsequently reacts with the NO entering the NOA, to form an excitable form of nitrogen dioxide (NO_2^*). The electrons in this state are unstable, and release excess energy as a photon in the process of returning to their original ground state. These photons are focused via a low-pass filter lens ($< 900\text{ nm}$ wavelength) into a photomultiplier tube, which amplifies the signal to allow an accurate, recordable electrical signal (mV) where the potential difference is recorded in real time (Sievers, Liquid NO analysis software). Upon injection of a sample, a peak is produced and the area-under-the-curve (AUC) is calculated, from which the NO metabolite concentration can be determined by comparing to a set of relevant reference standards. A standard curve was performed daily to account for fluctuations in temperature and other performance variations. The reactions of the NOA are summarised in equation 2.2.

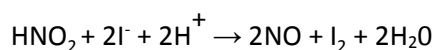


Equation 2.2

Despite the ability to utilise this technique to investigate a range of NO metabolite concentrations, there have been discrepancies in the NO concentrations in whole blood reported. It is likely that this variation is due to disparity in the set-up of nitric oxide analysis equipment, or the level of NO_2^- contamination due to inadequate cleaning and/or washing of equipment, in particular the Hamilton syringes used for sample injection. This contamination was minimised throughout the experiments described in this thesis by implementing specific protocols to ensure the accuracy of readings. HPLC grade water is used for washing all equipment and diluting reagents and chemicals, which has been shown to reduce standard error by approximately 5% (407). The timing of measuring samples is also important, especially when dealing with blood; therefore consistency is key. Blood samples are immediately centrifuged allowing isolation of the plasma, which is subsequently snap frozen in liquid nitrogen before being stored at -80°C until analysis. Our own findings have shown the baseline levels of NO_2^- and RSNO in plasma of healthy individuals range from 150-300 nM and 20-40 nM, respectively. In comparison, the baseline levels of NO_3^- seen in the blood are typically 20-40 μM (124).

2.6.2 Plasma NO_2^-

Tri-iodide was used as a cleavage reagent to reduce NO_2^- to NO. The solution was made by dissolving 650 mg of iodine crystals in 70 mL of 13.5 M glacial acetic acid in a fume hood. 1g of potassium iodide (KI) dissolved in 20 mL HPLC grade water was then added to this solution. This solution was left to mix for approximately 30 minutes. 5 mL was added into the purge vessel with 30 μL of antifoam, to prevent foaming of plasma proteins. The tri-iodide solution was changed after approximately 500 μL of plasma had been injected to prevent foaming. The purge vessel was heated to 50°C in a water bath that was heated by a thermostatically controlled hot plate with a magnetic stirrer. The purge vessel was connected to the N_2 gas inlet and NaOH trap, using Nalgene® clear plastic PVC tubing. Typically, 200 μL of a sample was injected directly into the purge vessel through a rubber septum injection inlet (Figure 2.9). Results were compared to a NaNO_2 standard curve, performed daily, to account for fluctuations in room temperature and equipment performance. The reduction power of tri-iodide reduces both RSNO and NO_2^- to NO. Therefore, it is necessary to measure RSNO levels (see section 2.6.3) and subtract this from the total measurement to give a true NO_2^- concentration. The limit of sensitivity of this assay is $< 10\text{nM}$ and the intra-assay coefficient of variation was $< 5\%$. The reaction catalysed by the tri-iodide cleavage reagent can be seen below.



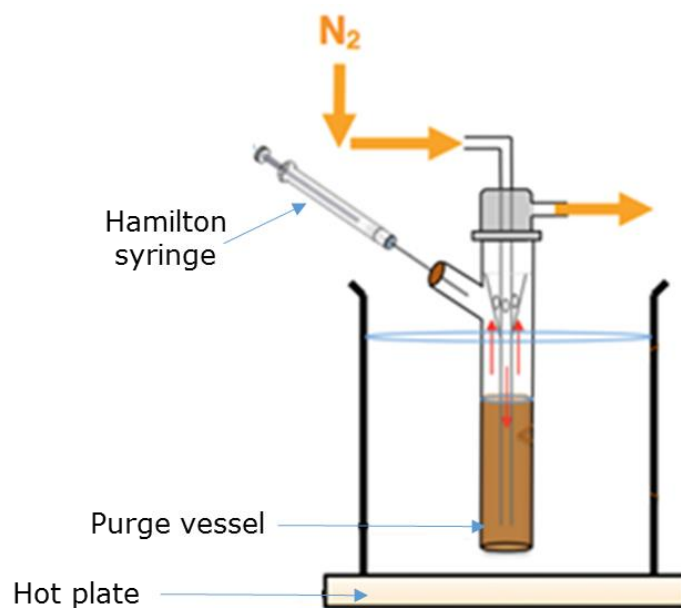


Figure 2.9 Schematic representation of the tri-iodide set up for plasma NO_2^- detection. 200 μL of sample or standard is injected through the rubber septum directly into the purge vessel containing 5 mL tri-iodide solution. The chemical cleavage reagent was heated to 50°C in a water bath thermostatically regulated by a hot plate. The subsequent NO produced from the reduction of NO_2^- was then carried via the inert N_2 stream into a NaOH trap (15 mL, 1M) to prevent any acid vapour entering the NOA.

2.6.2.1 NO₂⁻ standard curve

Prior to measurement of plasma samples, a NaNO₂ standard was made by adding 69 mg of NaNO₂ to 100 mL HPLC grade water. A serial dilution was then performed to produce standards of varying concentrations; 1000 nM, 500 nM, 250 nM, 125 nM and 62.5 nM. 200 μL of each standard were injected into the purge vessel to produce an AUC (Figure 2.10A). A sample of HPLC grade water was also injected to allow the standards to be “blank-adjusted”. The standard curve was then generated by plotting the NaNO₂ concentration against AUC (Figure 2.10B).

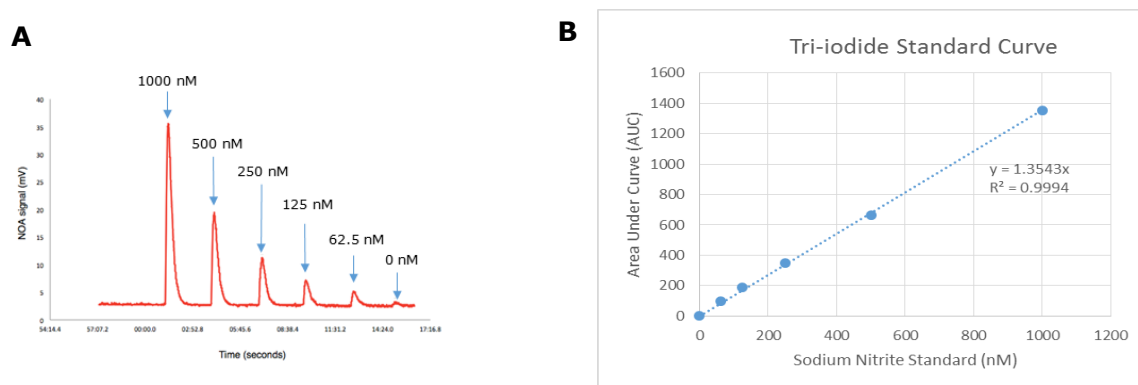
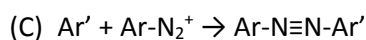
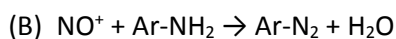


Figure 2.10 NO₂⁻ Standard Curve. A. A Typical millivolt signal obtained from running a series of standards. 1000 nM, 500 nM, 250 nM, 125 nM and 62.5 nM standards were diluted in HPLC grade H₂O. AUC was determined using Liquid analysis software. B. The AUC was then plotted against concentration to generate a standard curve.

2.6.3 Plasma RSNO

In order to determine the concentration of RSNO present in the samples, 540 μL plasma was incubated with 60 μL 5% acidified sulphanilamide (9:1 ratio) for 15 minutes in the dark prior to injection into the tri-iodide reagent. 5% acidified sulphanilamide was made by mixing 500 mg sulphanilamide with 10 mL 1 M hydrochloric acid (HCl), and kept in the dark at room temperature. In an acidic environment, NO₂⁻ forms the nitrosonium cation (NO⁺)^(A), which can react with sulphanilamide to form a diazonium salt^(B/C). These reactions can be seen below in equation 2.3. This diazonium salt is undetectable by OBC when injected into the tri-iodide solution (Figure 2.11) (407,408). 400 μL of the plasma/acidified sulphanilamide solution was injected directly into the purge vessel, and the resultant peak was measured and AUC calculated. Increased accuracy of RSNO measurement was obtained by a 50-point adjacent averaging algorithm, improving the signal to noise ratio, using Origin 7.0 (OriginLab, Massachusetts, USA).



Equation 2.3. Sulphanilamide reactions when added to plasma. A. Formation of the nitrosonium cation NO^+ . B/C. This nitrosonium cation can react with sulphanilamide to form a diazonium salt.

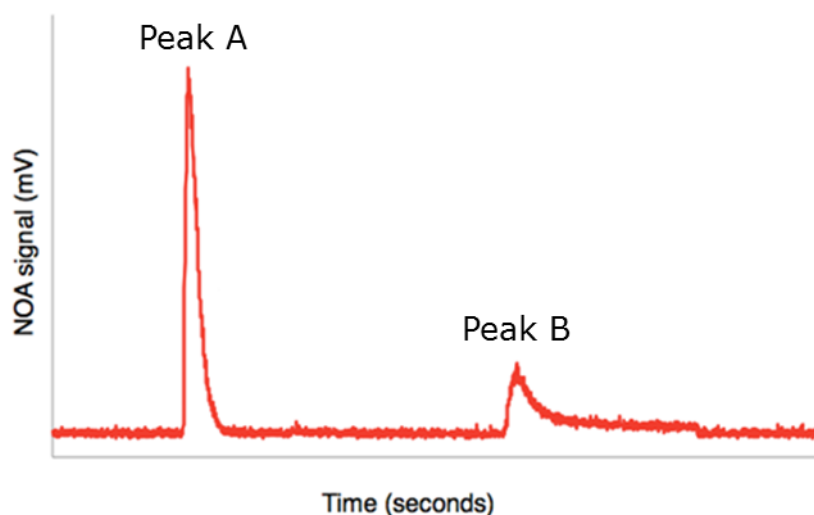


Figure 2.11. Typical NO_2^- and RSNO Signal from the NOA. Exemplar chemiluminescence trace from an injection of plasma (peak A) into tri-iodide, followed by an injection of a parallel plasma sample incubated with acidified sulphanilamide for 15 minutes (peak B). Peak A is largely composed of NO_2^- which is rendered undetectable after incubation with acidified sulphanilamide, and thus the remaining signal (Peak B) can be attributed to RSNO.

2.6.4 Plasma NO_3^-

In order to reduce NO_3^- to NO, a stronger reductive agent than tri-iodide is required. Vanadium III chloride (VCl_3) is capable of measuring all of the NO metabolites that tri-iodide can detect, with the additional ability to reduce NO_3^- to NO to allow measurement by the NOA. Thus, values obtained from vanadium chloride represent the total NO_x in the plasma sample. In order to determine the true NO_3^- value, the AUC obtained from tri-iodide must be subtracted from the AUC obtained from vanadium chloride. The vanadium chloride solution was made by dissolving 0.785 g of VCl_3 in 100 mL of 0.8 M hydrochloric acid, final concentration 49.9 mM. This solution is left to mix for approximately 30 minutes before being filtered through a 0.22 μm Millex-GP syringe filter (Merck Millipore, Germany), giving a final solution that is turquoise in colour. 30 mL of this solution was added to the puffer vessel and heated in a water bath to 90°C via a

thermostatically controlled hot plate. Maintaining acid at these high temperatures has required a specific custom glassware set-up; using a Liebig condenser prevents the loss of reagent and damage from acid vapour (Figure 2.12). Additionally, the glassware allows for a larger volume of vanadium chloride to be added in comparison to tri-iodide, therefore multiple plasma injections can be performed before the reagent must be changed due to foaming. The Liebig condenser is attached to the NaOH trap using Nalgene® clear plastic PVC tubing, which subsequently fed into the NOA. 20 µL of a plasma sample was injected through a rubber septum injection inlet. Results were compared to a NaNO₃ standard curve, performed daily to account for variation in room temperature and machine performance. Typically, room temperature was 18±2°C. The limit of sensitivity for NO₃⁻ measurement is > 500nM, and the intra-assay coefficient of variation was < 8%. The reaction catalysed by vanadium chloride cleavage reagent can be seen below.

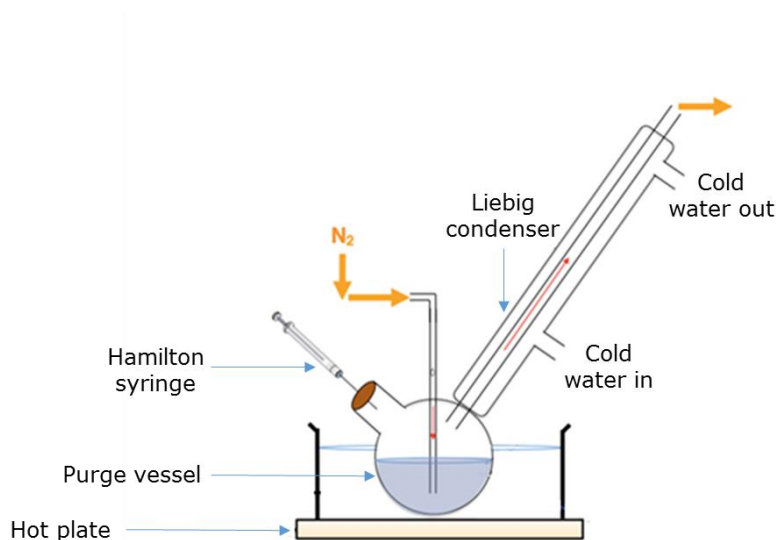
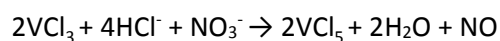


Figure 2.12 Schematic representation of the vanadium chloride set up for plasma NO₃⁻ detection. 20 µL of sample, or standard, is injected through the rubber septum into the round bottom flask containing 30 mL vanadium chloride. The vanadium chloride was heated to 90°C in a water bath controlled by a hot plate. The NO produced from the reduction of NO_x was carried through the Liebig condenser via the N₂ stream into the NaOH trap (15 mL, 1M), then into the NOA.

2.6.4.1 NO₃⁻ standard curve

A NaNO₃ standard curve was produced by adding 85 mg of NaNO₃ to 100 mL HPLC grade water. Known NaNO₃ concentrations were then added to the vanadium chloride solution (100 μM, 50 μM, 25 μM, 12.5 μM, and 6.25 μM). 20 μL of each standard was injected to produce an AUC (Figure 2.13A). The standards were then “blank-adjusted” by subtracting the AUC of a HPLC grade water injection (0 μM). The standard curve was generated by plotting the known NO₃⁻ concentration against AUC (Figure 2.13B)

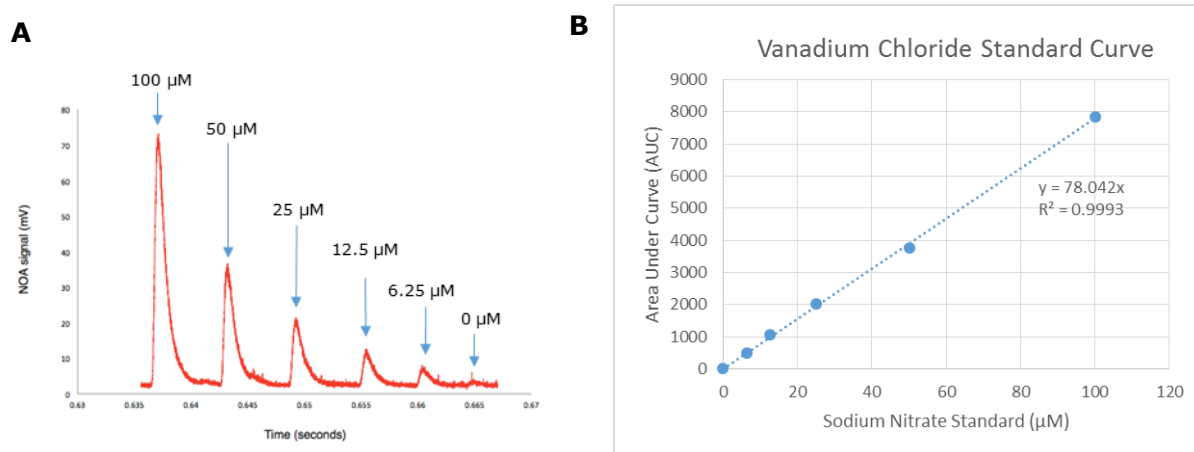


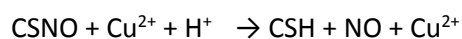
Figure 2.13. NO₃⁻ standard curve. (A) Typical millivolt signal obtained from running a series of NaNO₃ standards (100 μM, 50 μM, 25 μM, 12.5 μM, 6.25 μM) diluted in HPLC grade H₂O. AUC was determined using Liquid analysis software. (B) The AUC was then plotted against concentration to generate a standard curve.

2.7 *Ex vivo* platelet EV production

In order to evaluate the effect of RSNO on platelet-derived EV *ex vivo*, platelet-rich plasma (PRP) was isolated from the blood of healthy volunteers via sodium citrate vacutainers® (300 x g, 15 minutes). Platelet poor plasma was also isolated (300 x g, 15 minutes, followed by 2 2500 x g spins, both for 15 minutes) for use as a control. Platelets (in platelet-rich plasma) were stimulated with ADP (6.5 μM final concentration) and incubated for 5 minutes before NaNO₂, clopidogrel, GSNO or clopidogrel-SNO (all 10 μM) were added and left to incubate for 1 hour at 37°C. This concentration was chosen to compare directly with *ex vivo* platelet aggregation studies performed by our research group, showing the IC₅₀ for GSNO/clopidogrel-SNO was ≈7.5 μM (409). Clopidogrel-SNO was produced as described in detail previously (409). Briefly, crushed clopidogrel tablets were dissolved in HPLC grade water, to yield a 10 mM suspension. 10 mM NaNO₂ was then added to this (1:1 v/v), and was then neutralised by NaOH (0.1 M) addition. The RSNO produced from this was then quantified by 2C's ozone based chemiluminescence (section 2.7.1.1) and diluted appropriately. EVs were then isolated as described previously (section 2.4.2), and the resultant pellet was resuspended in filtered PBS, stored at 4°C overnight and analysed using NTA (section 2.3) and time-resolved fluorescence (TRF) (section 2.5) within 24-48 hours of isolation.

2.7.1.1 RSNO measurement

To determine the concentration of clopidogrel-SNO produced, a specialist cleavage reagent; Cuprous (I) chloride (CuCl) and cysteine (CSH), also known as the 2C's reagent, was used. This was produced by dissolving 47.25 mg of cysteine in 390 mL of HPLC grade water. Next, a 40 mM solution of CuCl was produced by adding 39.59 mg of CuCl in 10 mL HPLC grade water. A 1:10 dilution of this solution was made, producing a 4 mM solution, 10 mL of which was then added to the 390 mL cysteine solution. This solution was then neutralised to pH 7 using 1 M NaOH. This solution was left to mix for approximately 30 minutes. The 2C's reagent is specific for RSNO measurement due to its neutrality. This prevents the reduction of both NO₃⁻ and NO₂⁻ which require acidic conditions (pH < 6) to be reduced. Upon injection of a sample, the excess of cysteine in this solution generates CSNO due to transnitrosation from RSNO compounds present in the sample. The copper ions then homolytically cleave the NO moiety from CSNO (410). 5 mL of the CuCl/CSH solution was added into the purge vessel with 30 μL of antifoam, with the glassware set-up identical to that of the tri-iodide reagent. 400 μL of sample was injected directly into the purge vessel. The reaction catalysed by the 2C's cleavage reagent is shown below.



Results were compared to a RSNO standard curve, performed daily to account for fluctuations in room temperature. The limit of sensitivity of this measurement was < 200 nM, and the intra-assay variation was < 10%.

2.7.1.1.1 RSNO standard curve

RSNO concentrations using the 2Cs reagent were determined using a set of Acetyl-cysteine-SNO (NACSNO) standards. NACSNO was prepared by dissolving 1.63 g of N-acetyl cysteine (NAC) in 10 mL of 1 M HCl, forming a 1 M solution. Separately, 759 mg of NaNO₂ was dissolved in 10 mL HPLC grade water, forming a 1.1 M solution. 500 µL of the NAC solution was then added to a small brown glass bottle, with an injection port covered with a rubber septum. 500 µL of the 1.1 M NaNO₂ solution was then injected through this septum, allowing the production of NACSNO and turning the mixture red. As NACSNO is subject to both thermal and photochemical decomposition, the solution is kept on ice, in the dark.

In order to determine the concentration of NACSNO produced, the solution was diluted 1:200 in HPLC grade water, and the absorbance at 335 nm was measured using a spectrophotometer. Typically, absorbance was ≈ 1.5-2. The concentration was then determined according to the Beer-Lambert law, using the formula below.

$$[\text{NACSNO}] = (\text{Light absorbance } 335 \text{ nm} / \text{Absorption coefficient } (\epsilon = 727)) \times 200$$

2.8 Leukocyte Adhesion Assay

2.8.1 Leukocyte Isolation

The leukocyte isolation protocol was based on that of Pettit and Hallett, 1998 (411). Whole blood was drawn (approximately 10 mL) gently from an antecubital vein of healthy volunteers using a 21G butterfly needle (Hospira, UK) into a sterile syringe. Blood was gently added directly into a universal container containing 100 μ L of heparin at 5000 I.U./mL (Wockhardt, UK). Next, 2.5 mL of dextran (or $\frac{1}{4}$ the volume of blood) was added and the container was gently inverted once. Whole blood was transferred to a clean UC using a Pasteur pipette, taking care not to smear any blood on the side of the UC, or introduce any air bubbles. Blood was then left for 30-45 minutes at room temperature, until blood had separated into its constituent parts; plasma, the buffy coat, and erythrocyte layers. The buffy coat layer (approximately 1 – 1.5 mL) was carefully isolated using a Pasteur pipette and placed into a new UC. This was then centrifuged at 1000 RPM for 1 minute at brake speed 3, pelleting leukocytes and erythrocytes. The supernatant was discarded and the resultant pellet suspended in deionised water for 10 seconds, in order to lyse any contaminating erythrocytes. The UC was then “flooded” with balanced salt solution (BSS) and centrifuged again at 1000 RPM for 2 minutes. The supernatant was again discarded and the resultant leukocyte pellet was resuspended in 1 mL Krebs-BSA. Leukocytes were isolated the same day as experiments were performed, and were thus used “fresh” and not stored.

2.8.2 Leukocyte Adhesion Assay

HUVECs were isolated and grown in a 96-well plate, as outlined in section 2.1.2. Once HUVECs were approximately 90% confluent, cell medium was removed. HUVEC-derived EVs from various conditions were diluted in 100 μ L SFM and added to HUVECs (final concentration 2×10^8 EVs/mL) for 6 hours at 37°C, 5% CO₂. TNF α was added to HUVECs (diluted in SFM) as a positive control at a final concentration of 0.1 μ g/mL, for 1 hour. The negative control consisted of SFM only, with no EVs present. Whilst HUVECs were incubating with EVs, leukocytes were isolated as described in section 2.8.1.

1 μ L of CellTrace™ Calcein Red-Orange (ThermoFisher Scientific, UK) was added to leukocytes and incubated in the dark for 10 minutes at room temperature. Leukocytes were centrifuged at 1000 RPM for 2 minutes, and the supernatant discarded, in order to minimise background fluorescence from excess dye not taken up by the cells. Leukocytes were once again resuspended in 1 mL of Krebs-BSA, before being diluted in SFM to a total volume of 10 mL. EVs that were incubating with HUVECs were washed off with SFM, before leukocytes in SFM were added and incubated for 1 hour at 37°C. HUVECs were then washed three times with Krebs-BSA, before leaving cells in the buffer to be visualised.

The extent of leukocyte adhesion to HUVECs was visualised by fluorescence microscopy. AxioVision software was used to take 5 high resolution images of each well. For each experiment, 5 wells were used per condition, allowing a total of 25 images. Images were analysed using ImageJ (version 1.50i). First, images were converted to “8 bit” and “binary”, before setting contrast to maximum, in order to fully distinguish between leukocytes and HUVECs. This allowed the proportion of the image the leukocytes covered to be measured and expressed as a percentage of the total field of view (Figure 2.14).

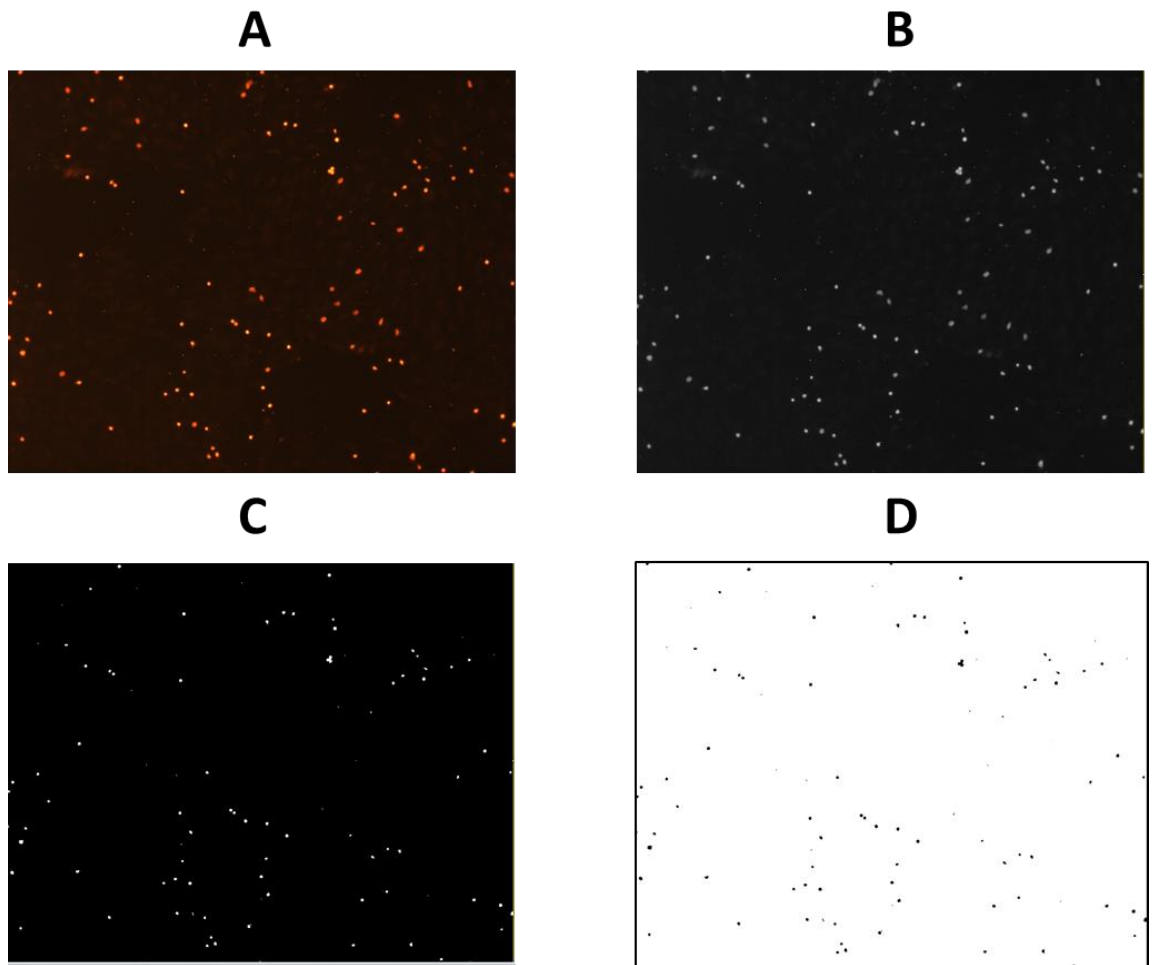


Figure 2.14 Leukocyte Adhesion Assay Analysis. (A) Images are obtained using AxioVision Imaging System. (B) Images are converted to 8 bit. (C) Contrast is set to maximum. (D) Images are converted to binary and assessed for percentage coverage.

2.9 Platelet Function

2.9.1 Background

Multiple electrode aggregometry (Multiplate[®], Roche Diagnostics Ltd, Switzerland) measures the ability of platelets to adhere to an artificial surface. The assay is based on Cardinal and Flower's 1979 impedance aggregometry method (412). Impedance aggregometry is based on the principle that in their resting state, platelets are non-thrombogenic, but once activated expose receptors on their surface, which allow them to attach to both vascular injuries and artificial surfaces (413). Multiple electrode aggregometry (MEA) analysis occurs in a single use test cell, which contains two pairs of silver coated electrode sensors. The assay measures the impedance of a current which is applied across a pair of these electrodes. When platelets adhere to the electrode wires, they increase the electrical impedance between them, which is continuously recorded. Automated quality control is achieved by comparison of the two simultaneously recorded impedance readings between the two electrode pairs. The magnitude of adhesion from platelets to the artificial electrode is determined by a change in impedance over a set time (Figure 2.15).

2.9.2 Experimental methodology

Whole blood (300 μL) collected into a hirudin BD Vacutainer[®] was diluted 1:1 with 0.9% NaCl preheated to 37°C in a single use test cell for 3 minutes. Samples were continuously homogenised using a Teflon coated stirring bar. Platelet activation was then initiated by the addition of either ADP (20 μL , final concentration 6.5 μM) or TRAP (Thrombin receptor activating peptide, 20 μL , final concentration 32 μM) (Roche Diagnostics Ltd, Switzerland). An increase in electrical impedance was recorded for 6 minutes, and expressed as arbitrary aggregation units (AU*min).

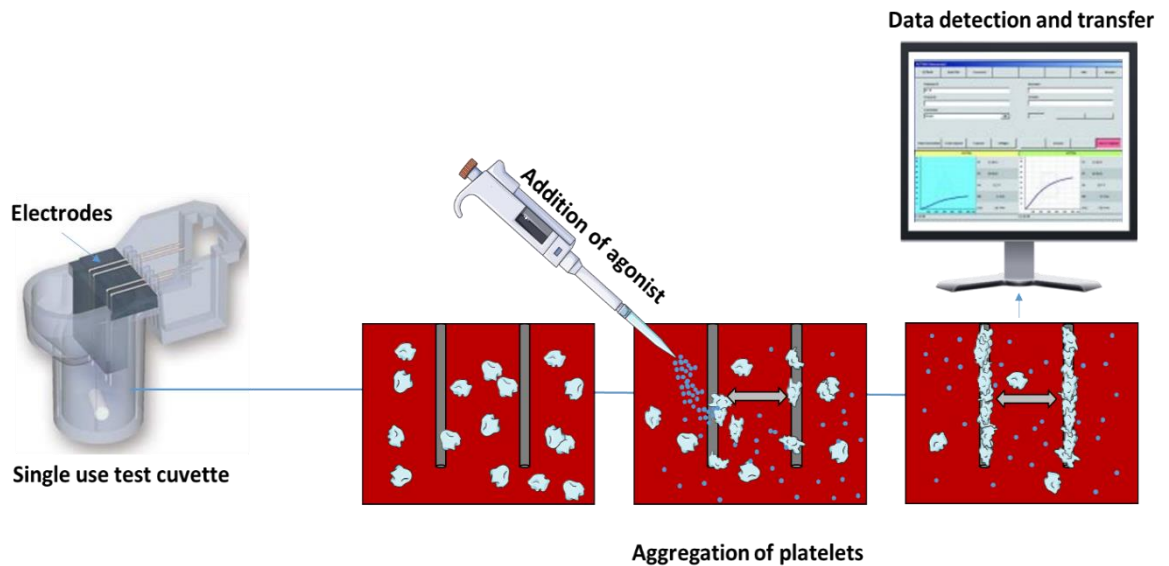


Figure 2.15 Multiple electrode aggregometry. Blood is added to a single use test cuvette and stimulated with an agonist (ADP/TRAP). Platelets then adhere to the artificial electrodes, increasing the impedance between them. The extent of platelet aggregation is quantified by the increase in impedance.

2.10 Rheology

2.10.1 Background

Rheology was performed by Dr Matthew Lawrence on site at Morriston Hospital, Swansea University. The haemorheological gel point (GP) technique has been described in detail previously (414,415). Briefly, blood is placed within a controlled stress rheometer where it is confined between two surfaces (Figure 2.16A). Oscillatory stress is applied to one plate and the resultant strain experienced by the second plate is measured. The difference between the applied stress and measured strain waveforms is calculated, termed phase angle (δ) (Figure 2.16B). δ can range between 0 (a perfect solid response) and 90° (a perfect liquid response) with all values in between indicating the material is visco-elastic. The δ alters as the blood transitions from a viscoelastic liquid to a viscoelastic solid, which is used to identify the gel point (GP). The GP marks the formation of the incipient blood clot; the first point at which a sample spanning haemostatic structure can be identified. The value of δ at the GP is related to the organisation of the fibrin clot, and can be quantified using fractal analysis to give a fractal dimension (d_f), where a low d_f represents a less branched, weaker clot, and a high d_f represent a dense, branched, stronger clot (414–416).

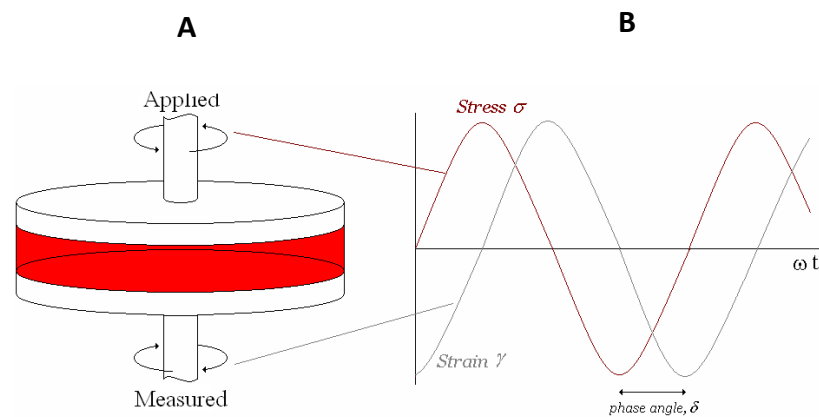


Figure 2.16 Rheology experimental set up. A. Blood is confined between two surfaces. B. The phase angle is a measure of the difference between the stress applied to one plate and the strain experienced by the other. Image courtesy of Dr Matthew Lawrence.

2.10.2 Experimental methodology

In this study, blood from healthy volunteers was taken into sodium citrate vacutainers[®], aliquoted into 7 mL vials and incubated at 37°C with EVs (final concentration 2×10^8 /mL) for 15 minutes. Citrated blood samples were then re-calcified by adding 333 μ L 0.2 M CaCl_2 , before being immediately loaded into the rheometer. The process from re-calcifying the blood to initialization of the measurement was performed in less than 60 seconds. Samples were allowed to run for sufficient time to reach the GP, never exceeding more than 10 minutes.

2.11 Thrombin activity assay

A thrombin activity assay (Abcam, Cambridge, UK) was utilised to assess the effect of EVs derived from hypoxia and/or NaNO_2 on thrombin activity in plasma. This assay utilises thrombin present in the sample to proteolytically cleave a synthetic substrate, releasing the fluorophore AMC, which can subsequently be quantified using a fluorescence reader. The assay was undertaken as per the manufacturer's instructions. Firstly, a set of thrombin standards were prepared, before plasma (isolated from the blood of healthy volunteers) was diluted and added to the microplate. EVs were added to plasma samples (final concentration 2×10^8 /mL) and incubated for 1 hour at 37°C, before a reaction mix (containing a fluorogenic thrombin substrate and buffer) was added to both plasma and standard wells. Fluorescence was measured at $\text{Ex/Em} = 350/450$ nm every minute for 60 minutes at 37°C. Following completion of this incubation period, two time points were chosen within the linear portion of the time course in order to calculate the change in fluorescence and

thus thrombin activity. This change in fluorescence was then used to calculate ng of thrombin, allowing thrombin activity to be expressed as ng/mL.

2.12 ROS detection

In order to assess the effect of EVs on oxidative stress in target endothelial cells, a cellular reactive oxygen species detection assay was utilised (Abcam, Cambridge, United Kingdom). This used 2'7'-dichlorofluorescein diacetate (DCFDA), a fluorogenic dye that can measure hydroxyl, peroxy and other ROS. Once diffused into the cell, DCFDA is deacetylated by cellular esterases into a non-fluorescent compound, which is subsequently oxidised by ROS into 2'7'-dichlorofluorescein (DCF), a highly fluorescent compound.

This assay was performed following manufacturer's instructions. Firstly, approximately 25,000 cells/well were seeded in a 96-well plate, and allowed to adhere overnight. Cells were then stained with a DCFDA solution and incubated for 45 minutes at 37°C in the dark. The DCFDA solution was removed and cells were washed three times with buffer. EVs were then added to cells (final concentration 2×10^8 /mL) and incubated for 3 hours at 37°C in the dark. Fluorescence was then measured at Ex/Em = 485/535 nm in end point mode.

2.13 Calpain activity assay

A calpain activity assay (Abcam, Cambridge, UK) was used to further elucidate the role of the calcium-dependent cysteine protease in EV biogenesis. HECVs were incubated with their treatments for 24 hours in a T75 flask, before being washed with ice cold filtered PBS. 100 μ L extraction buffer was added and cells were gently removed using a cell scraper, before being centrifuged at top speed (approximately 13,000 $\times g$) for 5 minutes to remove any insoluble material. The cell supernatants were isolated and placed on ice, before their protein concentration was determined using Nanodrop (as described in section 2.14.2).

Cell lysates were diluted to 100 μ g using the extraction buffer, to a final volume of 85 μ L in a black, clear bottom 96 well plate. Positive control wells consisted of active calpain diluted in extraction buffer at a range of concentrations. Negative controls consisted of an untreated cell lysate with the calpain inhibitor (2mM, Z-LLY-FMK) added. 10 μ L of reaction buffer, followed by 5 μ L of calpain substrate (1mM) was added to each well. The 96 well plate was incubated at 37°C in the dark for 1 hour, before measuring the fluorescence (Ex/Em = 400/505 nm) on a BMG CLARIOstar.

2.14 Protein Assay

2.14.1 Bicinchoninic acid (BCA) assay

2.14.1.1 Background

The Bicinchoninic acid assay, or BCA assay, is used to determine the total concentration of protein in a sample, by comparison to a set of known standards. This assay utilises the reduction of cupric ions (Cu^{2+}) to cuprous (Cu^{1+}) ions by protein in an alkaline medium. The first step involves chelation of Cu^{2+} ions with protein, known as the biuret reaction. The BCA present in the solution then reacts with the reduced cuprous (Cu^{1+}) cations formed in the previous step. Two molecules of BCA chelate with one Cu^{1+} cation, forming a deep purple solution. This solution can be measured using colorimetry (absorbance at 562 nm). The BCA assay was used to determine the protein concentration cell derived samples for Western blotting.

2.14.1.2 Procedure

The Pierce BCA Protein Assay Kit was used following manufacturer's instructions. Briefly, a set of bovine serum albumin (BSA) standards were produced by diluting in PBS. 25 μL of each standard, or sample was added into a well of a 96 well plate, containing 200 μL of working reagent (Grenier, Germany) in quintuplicate. A range of sample dilutions were performed if necessary. The plate was gently shaken for 1 minute before being wrapped in foil and left to incubate at 37°C for 30 minutes. The absorbance of samples at 562 nm was then measured using a microplate reader (ClarioSTAR, BMG Labtech, UK) and compared to the standard curve (figure 2.17).

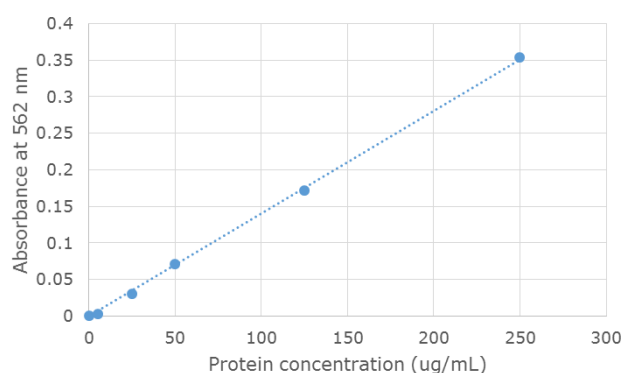


Figure 2.17 Exemplar BCA assay standard curve. A 6 point standard curve was produced using samples of known concentration (250, 125, 50, 25, 5 and 0 $\mu\text{g}/\text{mL}$, $R^2 = 0.9994$). Samples with unknown protein concentration were then determined by utilising the equation; $y = 0.0014x$.

2.14.2 NanoDrop Spectrophotometer

NanoDrop technology utilises the natural surface tension properties of liquids to hold microvolume samples in place during measurement without the need for any containment device, such as a cuvette or plate. With the arm open, 1 μL of sample is directly pipetted onto the pedestal. After the arm is closed, a sample column is formed. The arm automatically adjusts to an optimal path length, typically between 0.05 – 1 mm) (Figure 2.18). Proteins in solution absorb ultraviolet light at 280 nm, and using the Beer-Lambert law (below), the protein concentration can be determined.

$$A = \epsilon \times B \times C$$

Where A is absorbance, ϵ is the extinction coefficient, b in path length in centimetres, and c is the analyte concentration.

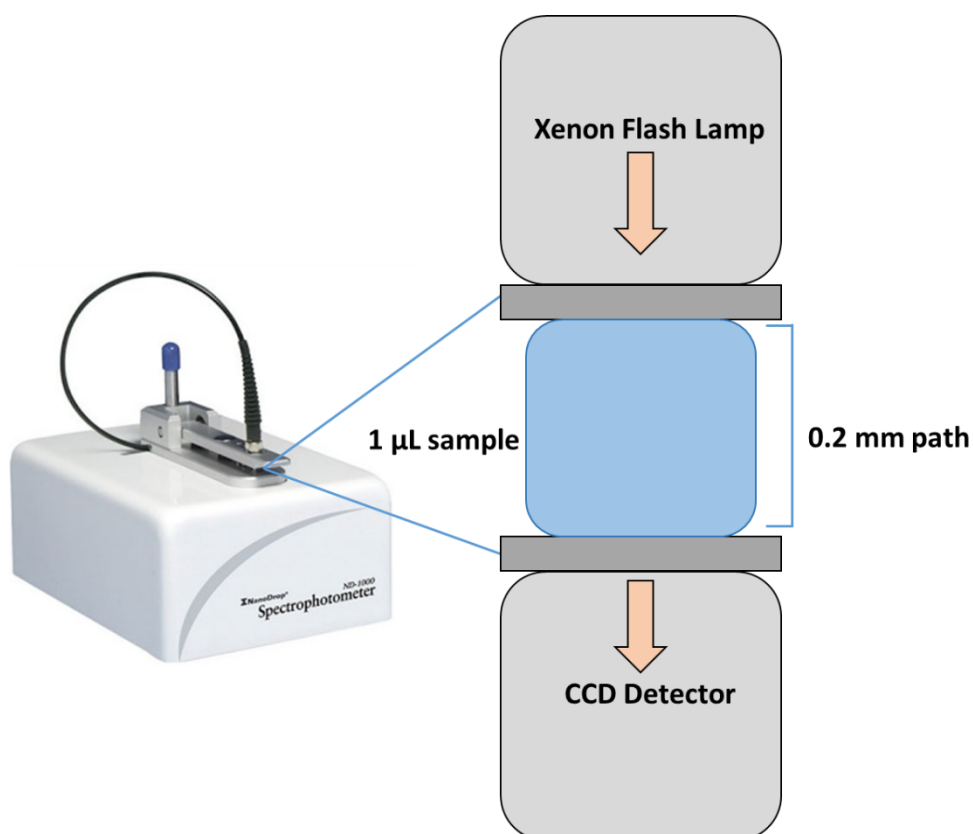


Figure 2.18 NanoDrop Spectrophotometer. The sample is added to the pedestal and the arm is closed. A magnet on the pedestal draws the arm down to generate the 0.2 mm liquid column, and absorbance through the sample column is measured using a xenon flash lamp and a charge coupled device (CCD) detector.

2.15 Western Blotting

2.15.1 Background

Western blotting is an analytical technique used to detect specific proteins in a sample. It uses gel electrophoresis to separate the denatured proteins by their size, before the proteins are transferred to a nitrocellulose membrane. The membrane is then probed using antibodies specific for the protein of interest, before detection using chemiluminescence.

2.15.2 Cell Lysis

Cells were grown to \approx 90% confluency in T25 flasks. Cell culture medium was removed and cells were washed with ice cold 1X sterile PBS (Fischer-Scientific) three times on ice. 10 μ L of ice cold lysis buffer (table 2.5) per 1 cm² was added to the cells. Cells were carefully removed from the flask using a cell scraper. Samples were transferred to a sterile Eppendorf and promptly centrifuged at 13,300 x g for 20 minutes at 4°C in order to pellet any insoluble material. The supernatant was taken and stored in sterile Eppendorf tubes at -20°C until further analysis.

Table 2.5 Constituents and concentrations of the lysis buffer.

Constituents (pH 7.5)	
Tris buffer 50 mM	Phenylmethylsulfonylfluoride 1 mM
EGTA 5 mM	Sodium flurodioxide 50 mM
NaCl 150 mM	Phenylarsine oxide 20 μ M
Triton 1%	Sodium molybdate 10 mM
Sodium orthovanadate 2 mM	Leupeptin 10 μ g/ml
Aprotinin 10 μ g/ml	

2.15.3 Sodium Dodecyl Sulfate-Polyacrylamide Gel Electrophoresis (SDS-PAGE)

The polyacrylamide gels, both stacking gel (4%) and resolving gel (7.5%), were assembled in a glass plate sandwich held in place with a casting frame and stand. Constituents of the gels are detailed in table 2.6.

Table 2.6 Polyacrylamide gels

Constituent	Resolving gel	Stacking gel
Deionised H ₂ O	4.8 ml	6.1 ml
Tris Buffer	2.5 ml	2.5 ml
30 % Acrylamide solution	2.5 ml	1.3 ml
10 % (w/v) SDS	0.1 ml	0.1 ml
10% (w/v) ammonium persulphate (APS)	0.1 ml	0.1 ml
TEMED	6 µl	10 µl

The components and volumes of both the resolving (7.5%) and stacking (4%) gels. SDS - sodium dodecyl sulphate. APS - ammonium persulphate. TEMED - tetramethylethylenediamine.

Reagents were added in order from largest to smallest volume. APS and TEMED were added last to trigger the polymerisation process of the acrylamide. The solution was gently inverted to mix and left to set between the glass plates. Once the resolving gel had set, the stacking gel was added, the gel comb put in place and left to set (approximately 30 minutes).

Once the gels had set, the glass plates were slotted into the electrode assembly unit, fixed in place with a clamp and added into the tank. The reservoir between the 2 sets of glass plates was filled with running buffer. 20-80 µg of protein sample was mixed with loading buffer and reducing agent (ThermoFisher Scientific, UK) before being denatured by heating at 95°C for 10 minutes.

Protein samples were loaded onto the polyacrylamide gel and separated by electrophoresis. A pre-stained protein standard ladder (3.5–260 kDa, ThermoFisher Scientific, UK) was also added for reference. Proteins were resolved at 180 V for approximately 1 hour in 1X running buffer (Table 2.7).

Table 2.7. 10X Running Buffer.

Constituent	Weight (g)
Tris	30
Glycine	144
SDS	10

The constituents of the running buffer were made up in 1 L of HPLC grade water and diluted 1:10 before running the gels.

2.15.4 Electroblotting

After SDS-PAGE, wet electroblotting was used to transfer proteins from the gel to a 0.45 μm nitrocellulose membrane (Bio-Rad, UK). The nitrocellulose membrane was soaked in methanol for 1 minute prior to transfer. Both the gel and the nitrocellulose membrane were “sandwiched” between blotting paper and foam pads, encased within a blotting cassette (Figure 2.18). Proteins were transferred for 1 hour at 100 V in ice cold 1X transfer buffer (Table 2.8) with a magnetic stirrer and ice pack.

Table 2.8 Transfer buffer.

Constituent	Weight (g)
Tris	3.025
Glycine	13.66

The constituents were diluted in 1 L of water and stored on ice before use.

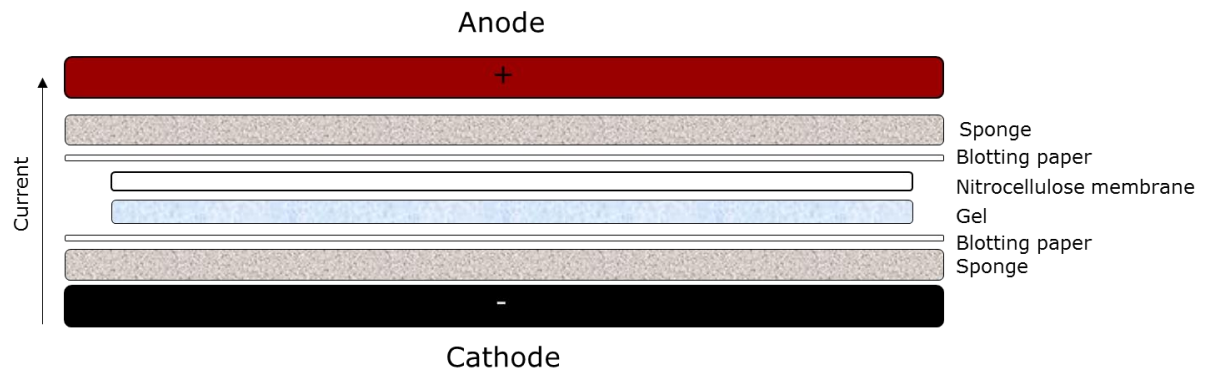


Figure 2.19 Transfer of proteins via electroblotting. Schematic showing the arrangement of components for transfer in Western blotting.

2.15.5 Incubation of antibodies

Following transfer, the gel was discarded and the nitrocellulose membrane was soaked in Ponceau S solution to assess equal loading of protein and the presence of any air bubbles. The membrane was then washed in tris-buffered saline-tween (TBS/T) 3 times for 5 minutes on a plate shaker. The 1X TBS/T solution was produced by diluting a 10X TBS stock (table 2.9) and adding 500 μ L of tween.

Table 2.7 10X TBS buffer.

Constituent	Amount
Tris base	60.6 g
NaCl	87.6 g
HPLC grade water	1 L

A 10X stock of TBS was made by diluting both the tris base and NaCl in 900 mL of HPLC grade water. This solution was then adjusted to pH 7.6 with 12 M HCl, before adding HPLC grade water to a final volume of 1 L.

Blocking of non-specific sites on the nitrocellulose membrane was achieved by incubating the membrane in 5% (w/v) skimmed milk powder (Marvel, UK) in TBS/T for 1 hour. The membrane was then incubated with the primary antibody in 1% milk- TBS/T (table 2.8), overnight at room temperature. The membrane was then washed 3 times for 5 minutes before adding an ECL peroxidase labelled secondary antibody; either 1:2000 goat anti-mouse (Sigma Aldrich, UK), or 1:4000 donkey anti-rabbit (GE healthcare) diluted in 1% milk-TBS/T for 1 hour at room temperature.

Table 2.8 Antibodies used for Western blotting.

Antibody	Dilution	Type	Source	Product Code
HIF-1 α	1:1000	Mouse	BD Biosciences	610958
HIF-2 α (EPAS-1)	1:500	Rabbit	SantaCruz Biotech	sc-46691
VCAM-1	1:1000	Rabbit	Abcam	ab134047
ICAM1	1:500	Mouse	ThermoScientific	MA5407
E-Selectin	1:1000	Rabbit	Abcam	ab18981
P-Selectin	1:1000	Rabbit	Abcam	ab6632
PECAM	1:2500	Rabbit	Abcam	ab28364
Rab22a	1:2000	Rabbit	Abcam	ab137093
eNOS (total)	1:1000	Mouse	Abcam	ab5589
eNOS (Ser1177)	1:500	Rabbit	SantaCruz Biotech	sc-81510
eNOS (Thr495)	1:500	Rabbit	SantaCruz Biotech	sc-136519
β -Actin	1:5000	Rabbit	Cell Signalling Technology	sc-47778

The details of primary antibodies used for the detection of specific proteins are listed above, including the dilution. Following incubation in secondary antibodies, the membrane was thoroughly washed; at least 5 times for 5 minutes in TBS/T prior to developing.

2.15.6 Developing

In order to detect protein bands, equal volumes of Western blot detection reagents (SuperSignal™ West Pico/Femto Chemiluminescent Substrate (ThermoFisher Scientific, UK)) were mixed in an Eppendorf before 250 µL was added to the membrane. The membrane was then exposed to photographic film (Amersham™ Hyperfilm ECL, GE Healthcare) in a dark room (exposure time varied between antibodies). The film was then soaked in developer (Kodak, UK) until bands began to appear, before being soaked in water, and then finally soaked in fixer (Kodak, UK). Films were washed thoroughly with water and left to air dry.

2.15.7 Densitometry

Densitometry of the Western blots was performed in order to semi-quantitatively analyse the amount of protein present in the samples. Densitometry was performed using Image-J version 1.50i (National Institutes of Health, USA). Densitometry values were normalised to an appropriate control, and expressed as arbitrary densitometry units (ADU).

2.16 Statistical analysis

Data were analysed using Graphpad Prism (version 5.0, GraphPad Software Inc., San Diego, USA). The Kolmogorov-Smirnov test or D'Agostino's K-squared test were used to check data for normality. A one-way ANOVA followed by a Dunnett's post-test was used to compare all groups to the relevant control. A one-way ANOVA followed by a Tukey's test was used to compare all groups with each other. A student's unpaired t-test was used to compare means from two groups. For clinical studies, data was analysed according to "Practical Statistics for Medical Research" by Altman et al (417). All data were assessed for both a period effect and a treatment-period interaction. The change in measurement before and after NO₃⁻ supplementation/placebo was calculated and compared directly using a paired t-test. Results are expressed as mean ± SEM. A *p* value of < 0.05 was regarded as statistically significant. Further details of the statistical tests applied can be found in each individual results chapter.

3 RESULTS I: PRODUCTION OF EXTRACELLULAR VESICLES BY ENDOTHELIAL CELLS: THE EFFECT OF HYPOXIA AND NITRITE

3.1 Perspective

The work detailed within this chapter was conducted at the beginning of my PhD, and enabled me to learn the techniques required for research within the EV field. This chapter aimed to delineate the effect of hypoxia on EV production by endothelial cells, and, furthermore, whether inorganic nitrite (NaNO_2) could provide a source of NO under these hypoxic conditions and reduce the production of EVs. The link between hypoxia and EV production was investigated, including the roles of HIF-1 α and -2 α .

3.2 Introduction

As discussed in Chapter 1, EVs are secreted by numerous cell types into their extracellular space. The endothelium is a highly metabolically active organ, occupying a unique interface between circulating blood and the extravascular tissues, where it plays a pivotal role in the regulation of haemostasis. The endothelium modulates many pathophysiological processes, such as barrier function, the control of vasomotor tone, leukocyte adhesion, and inflammation (418). In physiological circumstances endothelial cells carefully prevent thrombosis by numerous anticoagulant and antiplatelet mechanisms (39). In contrast, under pathological stresses, the endothelium undergoes modifications which allow it to participate in the inflammatory response; a state known as endothelial cell activation (419).

Endothelial cell activation can be characterised by four core changes: Loss of vascular integrity; expression of adhesion molecules; change in phenotype from anti-thrombotic to pro-thrombotic and increased cytokine production (419). The loss of vascular integrity can expose the subendothelium, promoting adhesion and aggregation of platelets. Upregulation of adhesion molecules such as ICAM-1 and VCAM-1 allows leukocyte extravasation into the surrounding tissues (420). The shift in phenotype from anti- to pro-thrombotic is highlighted by the downregulation of the anti-coagulant molecules thrombomodulin and heparin sulphate on the surface of endothelial cells, and a concomitant elevation in pro-coagulant components such as TF (421,422). Finally, the synthesis of cytokines such as IL-6, IL-8 and MCP-1 by endothelial cells regulate the acute phase response and promote movement of leukocytes to the area via chemotaxis.

Endothelial cell activation and dysfunction precedes the development of atherosclerosis and can lead to further acceleration and development of CVD. It is important to note, however, that endothelial cells may be activated without being dysfunctional (423). The endothelium is constantly sensing and responding to alterations in the extracellular environment (424,425). Interestingly, it has previously been shown that activation of endothelial cells leads to augmented release of EVs (426,427).

Hypoxia is known to be a strong activator of endothelial cells (428), and it has previously been demonstrated that in healthy volunteers, temporary hypoxia exposure enhances EV secretion by endothelial cells (429). Additionally, hypoxia exposure has been shown to enhance EV secretion in breast cancer cells (231,430). It is generally well accepted that the bioactive cargo of EV reflects the stimulus which triggered their formation, with hypoxia-derived EVs displaying a markedly altered RNA and protein composition (213). The adaptation of cellular physiology in response to

hypoxia is largely mediated by the transcription factor HIF-1, which promotes the transcription of genes involved in cell proliferation, metastasis, angiogenesis and vascular remodelling (431,432). HIF is comprised of an oxygen regulated HIF- α subunit (HIF-1 α or HIF-2 α) and the constitutively expressed HIF- β . The HIF- α subunit is targeted for degradation under normoxic conditions by the O₂-dependent HIF- α prolyl hydroxylase enzymes [26]. Inhibition of these enzymes in hypoxia prevents the degradation of HIF- α , allowing it to regulate its target genes (433). HIF has been shown to increase expression of several proteins involved in cytoskeletal changes (434), a mechanism shown to be implicated in augmented EV release (243). Thus, selective targeting of HIF- α could modulate endothelial cell EV release.

Endothelial-derived NO plays a pivotal role in vascular homeostasis, highlighted by the deficiency of NO prevalent in CVD states (435). NO can modulate the cellular response to hypoxia by preventing the stabilisation of HIF- α via an increase in prolyl hydroxylase-mediated degradation (436,437). Previously, impaired endogenous NO production in HUVECs has been shown to increase EV formation (438). The inorganic anions NO₃⁻ and NO₂⁻ can be considered reservoirs for NO bioactivity, particularly during hypoxia (124,439). *In vivo*, NO₃⁻ is reduced to NO₂⁻ via commensal bacteria present in the oral cavity. NO₂⁻ can subsequently be reduced to NO on exposure to acidic conditions, or through reaction with various proteins that possess NO₂⁻ reductase activity, including xanthine oxidoreductase (XOR) (440,441), heme globins (144,442), and components of the mitochondrial electron transport chain (147,443).

Here, I hypothesised that endothelial EV release *in vitro* was enhanced by HIF-1 α and/or HIF-2 α in hypoxia. Furthermore, the addition of NaNO₂ may be able to modulate this enhancement via selectively targeting the expression of these transcription factors.

3.3 Aims

The aims of this chapter were as follows:

1. Investigate the effect of hypoxia on EV production by endothelial cells *in vitro*.
2. Characterise differences in EVs produced under hypoxic or normoxic conditions.
3. Investigate the role of HIF-1 α and HIF-2 α in hypoxic EV production.
4. Assess the role of NO₂⁻ derived NO on hypoxic EV production
5. Evaluate the role of the calcium-dependent protease calpain in EV production.

3.4 Methods

3.4.1 Cell culture

HECVs were cultured as described in section 2.1.1. Primary HUVECs were isolated and cultured as detailed in section 2.1.2. Cells were counted as outlined in section 2.1.5.1

3.4.2 Hypoxia exposure

HECVs were subjected to a range of oxygen concentrations (1% O₂ – 20% O₂) using an Invivo2 hypoxic workstation 400, as outlined in section 2.1.4

3.4.3 Cell viability and apoptosis

To assess the effect of various pathological insults on cell viability and apoptosis, numerous assays were undertaken. Both trypan blue exclusion and an MTS assay were used to assess cell viability, and a Caspase-Glo[®] 3/7 assay was used to assess apoptosis, as outlined in sections 2.1.5.1, 2.1.5.3 and 2.1.5.4, respectively.

3.4.4 Cellular treatments

Both HECV and HUVEC cultures were treated with a variety of conditions, detailed in section 2.1.3. All stressors were diluted in SFM and incubated for 24 hours, unless stated otherwise. Control cells were treated with SFM alone.

3.4.5 EV Isolation

EVs were isolated using differential ultracentrifugation as detailed in section 2.4.1. EV samples were stored at 4°C and used within 48-72 hours of isolation.

3.4.6 EV size, concentration and distribution

EV size and concentration were determined using nanoparticle tracking analysis, as outlined in section 2.3. 5 x 60 second videos were recorded and analysed, and the mean was subsequently used in further analysis. Size distribution graphs were generated by totalling the number of EVs/cell in each 50 nm range (bin width).

3.4.7 Electron microscopy

Scanning electron microscopy was used to visualise HECVs in both normoxia and hypoxia, as outlined in section 2.2.1. Transmission electron microscopy was also used to visualise HECV-derived EV to confirm a true EV sample and assess purity and morphology, as detailed in section 2.2.2.

3.4.8 Time resolved fluorescence

Time resolved fluorescence was used to measure differences in protein expression between endothelial cells that had been exposed to hypoxia (1% O₂) and normoxia (21% O₂), as outlined in section 2.5.

3.4.9 siRNA transfection

In order to deduce the role of both HIF-1 α and HIF-2 α in hypoxia-mediated EV production, siRNA targeting both of these sub-types was undertaken, as described in section 2.1.6.

3.4.10 Calpain activity assay

A fluorometric calpain activity assay was performed to quantify calpain activity following a range of cellular treatments, and is described in detail in section 2.13.

3.4.11 Western blotting

Western blotting was performed to assess the expression of various proteins in endothelial cells following a variety of treatments, as outlined in section 2.15.

3.4.12 Statistics

Data were analysed using GraphPad Prism (version 5.0: GraphPad Software Inc., San Diego, USA). The Kolmogorov-Smirnov test was used to determine if the data were normally distributed. A two-way ANOVA with Bonferroni correction was used to compare size distribution differences between hypoxia and normoxia. A one-way ANOVA was used followed by either a Dunnett's post-test to compare all groups to the relevant control, or a Tukey's test to compare all pairs of columns with each other. A Kruskal-Wallis test with a Dunn's multiple comparisons post-hoc test was used for non-normally distributed data. A student's unpaired *t*-test was used to compare means from two groups. Results are expressed as mean \pm SEM unless stated. A *p* value of < 0.05 was regarded as statistically significant.

3.5 Results

3.5.1 Electron microscopy

Scanning electron microscopy visualised HECVs under normoxic (21% O₂) and hypoxic (1% O₂) conditions. Cells were approximately 10-15 µm in diameter. Figure 3.1A shows HECVs incubated in normoxic conditions. Figure 3.1B shows HECVs incubated in hypoxia for 24 hours. Transmission electron microscopy confirmed successful isolation of EVs from cell culture medium. The diameter of EVs appears to be between 200-500 nm for both normoxia-derived EVs (Figure 3.1C) and hypoxia-derived EVs (Figure 3.1D).

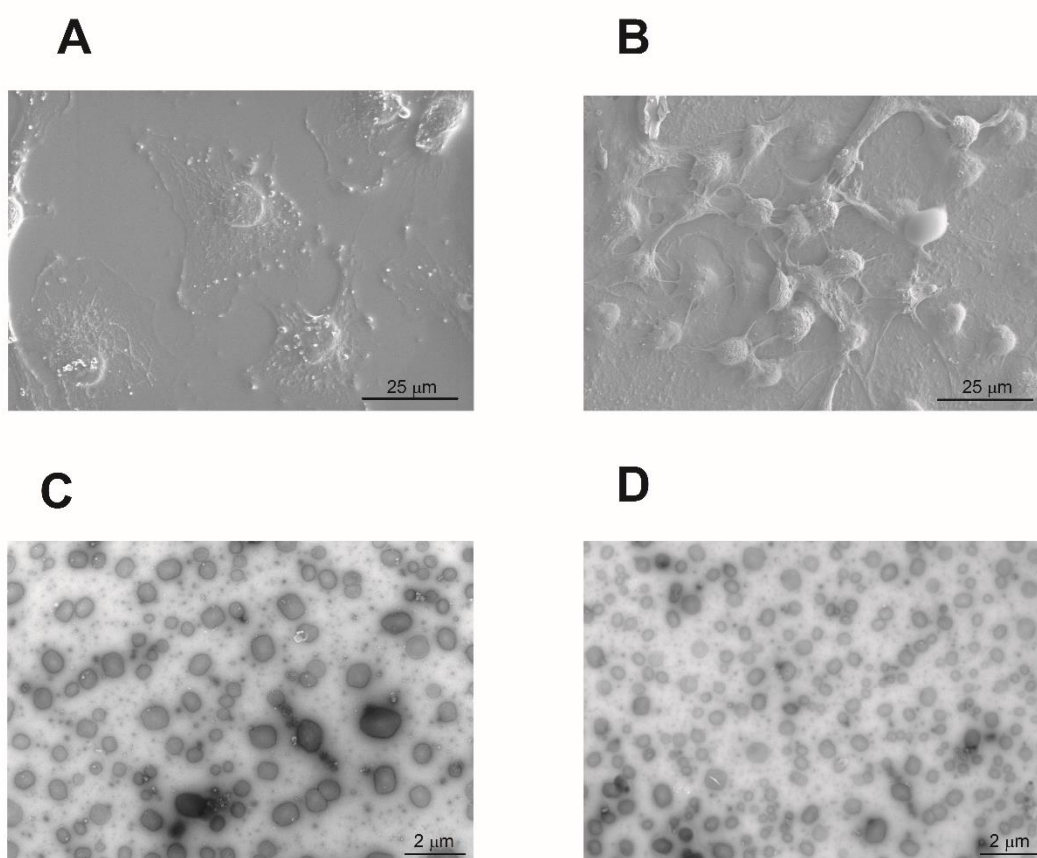


Figure 3.1 Morphology of HECVs and HECV-derived EVs. Scanning electron microscopy images: HECVs maintained in normoxia (A) vs HECVs exposed to hypoxic conditions (1% O₂) (B) for 24 hrs. Transmission electron microscopy images: submicron heterogeneous population of spherical EVs derived from HECVs maintained in normoxia (C) and hypoxia (1% O₂) (D). Scale bars: (A, B) 25 µm; (C, D) 2 µm. Results represent [n=3].

3.5.2 The effect of hypoxia on EV size, concentration and distribution

Hypoxia exposure (1%, 2% and 5% O₂) enhanced EV production in comparison to HECVs maintained in normoxia (1% O₂: 1766 ± 63 EVs/cell, 2% O₂: 1179 ± 59 EVs/cell, 5% O₂: 659 ± 48 EVs/cell vs 21% O₂: 133 ± 15 EVs/cell, $p < 0.001$). However, 10% and 20% O₂ did not change EV production (10% O₂: 190.2 ± 40 EVs/cell, 20% O₂: 218 ± 57 EVs/cell, $p > 0.05$) compared to normoxia (Figure 3.2A). Hypoxic conditions did not affect EV size (21% O₂: 134 ± 8 nm; 1% O₂: 131 ± 27 nm; 2% O₂: 133 ± 33 nm; 5% O₂: 143 ± 38 nm; 10% O₂: 133 ± 38 nm, 20% O₂: 132 ± 30 nm, $p > 0.05$ for all comparisons) (Figure 3.2B).

On assessment of EV size distribution (split by 50 nm bin size for analysis), no differences were observed for EVs exposed to both 10% and 20% O₂ compared to the 21% O₂ control. HECVs exposed to 1%-5% O₂ produced an altered EV size distribution compared to control EVs however, displaying an elevated EV concentration within a diameter range of 51-400 nm, 51-350 nm and 101-250 nm for 1% O₂, 2% O₂ and 5% O₂, respectively, as outlined in Table 3.1. Figure 3.3 summarises these results.

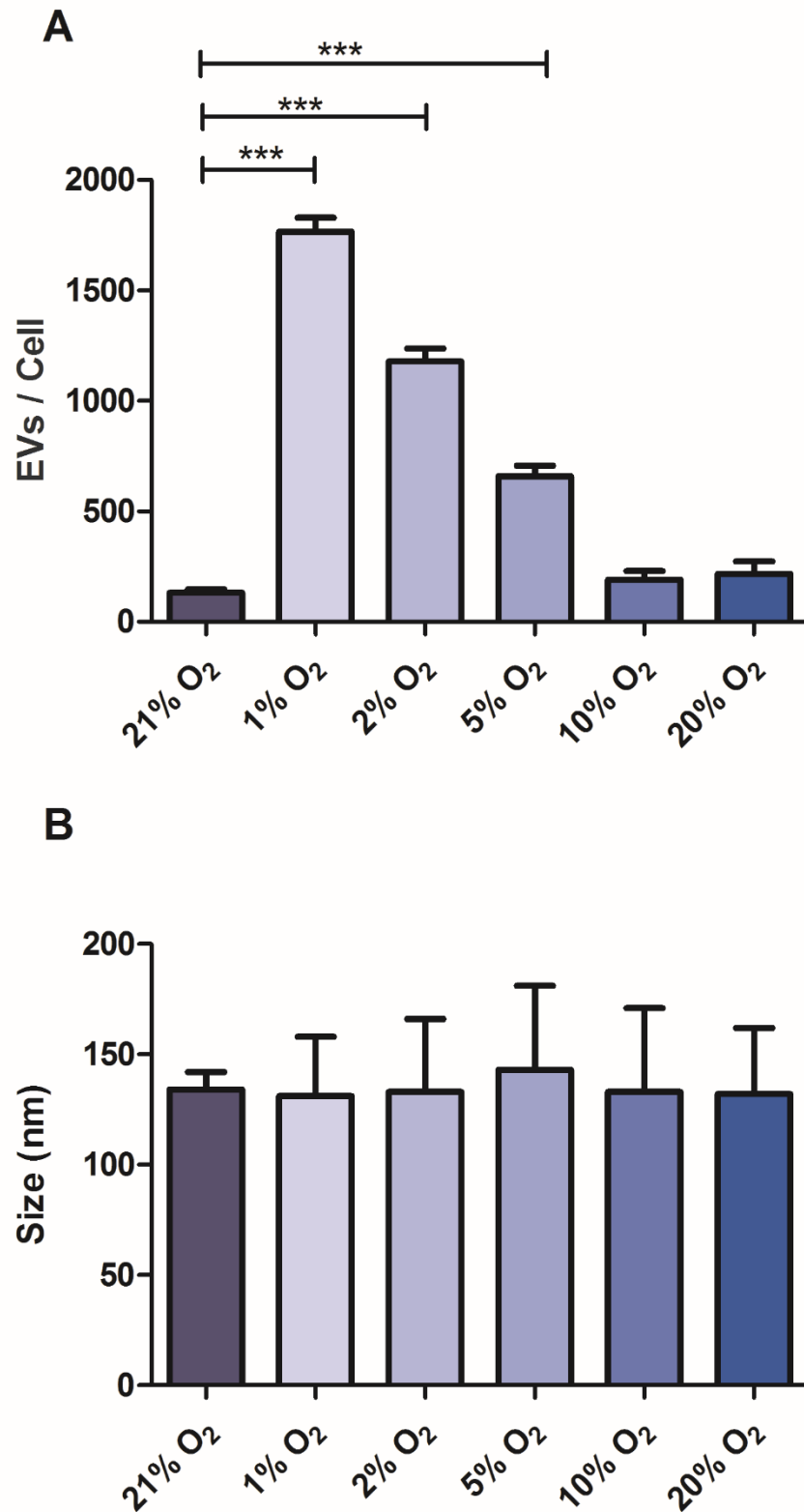


Figure 3.2 The effect of hypoxia on EV production and size in HECVs. (A) EV production per cell after 24 hours exposure to varying O₂ concentrations (1%-21% O₂). (B) The mean size (particle diameter) of EVs following hypoxia exposure. Results represent [n=5]. Data are expressed as mean ± SEM. *** reflects $p < 0.001$.

Table 3.1 The effect of hypoxia (1% - 20% O₂) on HECV-derived EV size distribution.

EV Size	Control (21% O ₂)	1% O ₂	2% O ₂	5% O ₂	10% O ₂	20% O ₂
0-50	1 ± 0	11 ± 3	8 ± 2	3 ± 1	2 ± 1	2 ± 1
51-100	16 ± 5	195 ± 42 ***	147 ± 23 ***	67 ± 13	24 ± 7	27 ± 8
101-150	33 ± 8	419 ± 61 ***	362 ± 43 ***	185 ± 26 ***	49 ± 11	55 ± 13
151-200	29 ± 5	380 ± 24 ***	260 ± 11 ***	152 ± 3 ***	42 ± 7	48 ± 8
201-250	22 ± 4	285 ± 18 ***	162 ± 12 ***	99 ± 12 **	31 ± 5	36 ± 6
251-300	14 ± 3	199 ± 28 ***	98 ± 14 ***	68 ± 15	21 ± 4	24 ± 5
301-350	7 ± 2	125 ± 21 ***	66 ± 16 *	40 ± 11	11 ± 2	12 ± 3
351-400	4 ± 1	69 ± 14 *	38 ± 11	21 ± 6	6 ± 1	6 ± 1
401-450	4 ± 1	55 ± 13	30 ± 8	16 ± 4	5 ± 1	6 ± 2
451-500	1 ± 0	15 ± 4	7 ± 2	4 ± 1	1 ± 0	2 ± 1
501-550	1 ± 0	7 ± 1	4 ± 1	2 ± 1	1 ± 0	1 ± 0
551-600	1 ± 0	4 ± 1	2 ± 1	1 ± 0	0 ± 0	0 ± 0

NTA was used to assess the size distribution of EVs, split into 50 nm bin sizes for analysis and normalised to cell count. Samples were measured in quintuplicate and the mean was used in further analysis. Data are expressed as the group mean ± SEM. Results represent [n=5]. **, and *** reflects p < 0.01 and 0.001 respectively, compared to the 1% O₂

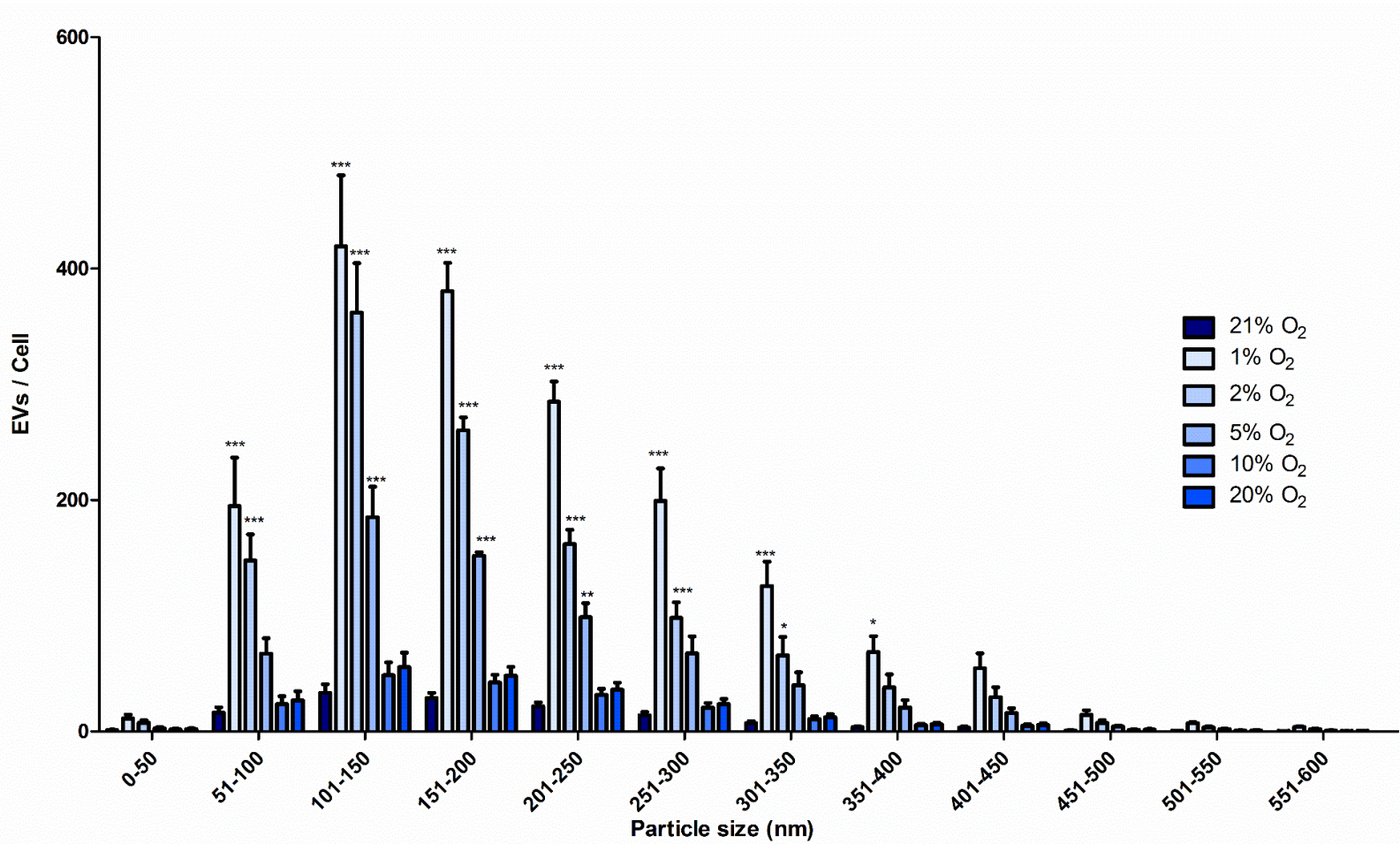


Figure 3.3 The effect of hypoxia (1%-20% O₂) on HECV-derived EV size distribution. Assessed in 50 nm bin sizes, results represent [n=5]. Each sample was analysed in quintuplicate and the mean was used in further analysis. Data are expressed mean ± SEM. *, ** and *** reflect p < 0.05, 0.01 and 0.001, respectively, compared to the 21% O₂ normoxia control.

3.5.3 Viability and apoptosis

As EV production has been linked to apoptosis, cell viability and apoptosis assays were undertaken on HECVs. Hypoxic conditions had no effect on cell viability compared to the normoxic control (21% O₂: 1.73 ± 0.24 vs 1% O₂: 1.99 ± 0.04, 2% O₂: 1.85 ± 0.43, 5% O₂: 1.79 ± 0.21, 10% O₂: 1.80 ± 0.32, 20% O₂: 1.84 ± 0.18, $p > 0.05$) (Figure 3.4A). Hypoxia exposure also had no effect on apoptosis compared to normoxia (21% O₂: 688 ± 7 RLU vs 1% O₂: 612 ± 73 RLU, 2% O₂: 658 ± 58 RLU, 5% O₂: 691 ± 14 RLU, 10% O₂: 714 ± 26 RLU, 20% O₂: 751 ± 23 RLU, $p > 0.05$ for all comparisons) (Figure 3.4B).

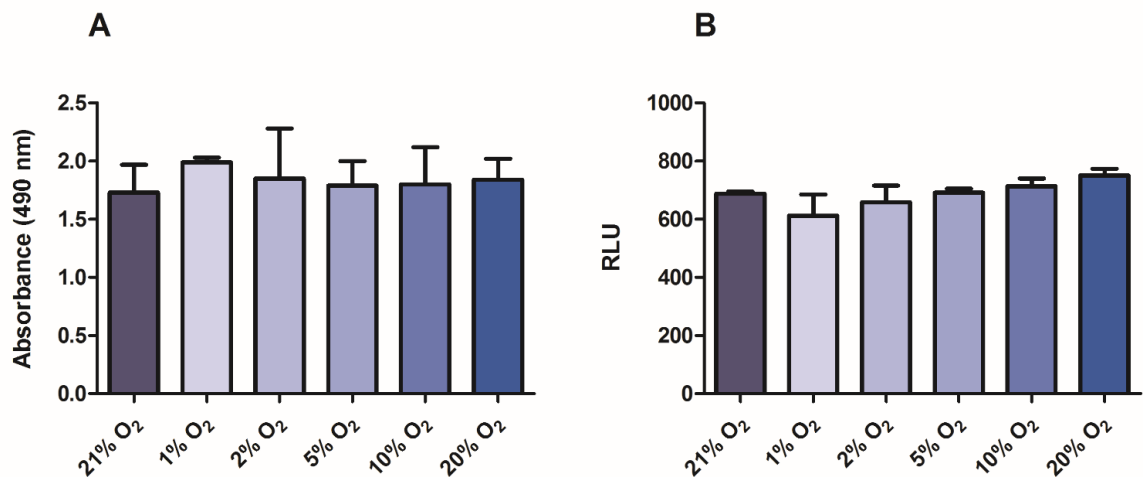


Figure 3.4 The effect of hypoxia exposure on cell viability (A) and apoptosis (B). No significant differences were seen between cells grown in hypoxia and normoxia for both cell viability (A) and caspase 3/7 activity (B). RLU – Relative luminescence units. Absorbance – arbitrary units. $P > 0.05$ for all comparisons, [n=5].

3.5.4 Characterisation of EV

TRF revealed no difference between the level of the exosomal markers CD9, TSG101 or Alix and the endothelial marker VE-Cadherin (CD144) in EVs isolated from normoxia and hypoxia (CD9: 21% O₂; 37651 ± 1724 RFU vs 1% O₂; 39528 ± 2507 RFU. TSG101: 21% O₂; 14495 ± 549 RFU vs 1% O₂; 15979 ± 1953 RFU. Alix: 21% O₂; 8683 ± 818 RFU vs 1% O₂; 10310 ± 510 RFU. CD144: 21% O₂; 2182 ± 178 RFU vs 1% O₂; 2601 ± 234 RFU, $p > 0.05$) (Figure 3.5). HIF-1 α was present in EVs isolated from hypoxic HECVs and absent in those isolated from normoxia (21% O₂; 115 ± 25 RFU vs 1% O₂; 10310 ± 520 RFU, $p < 0.001$).

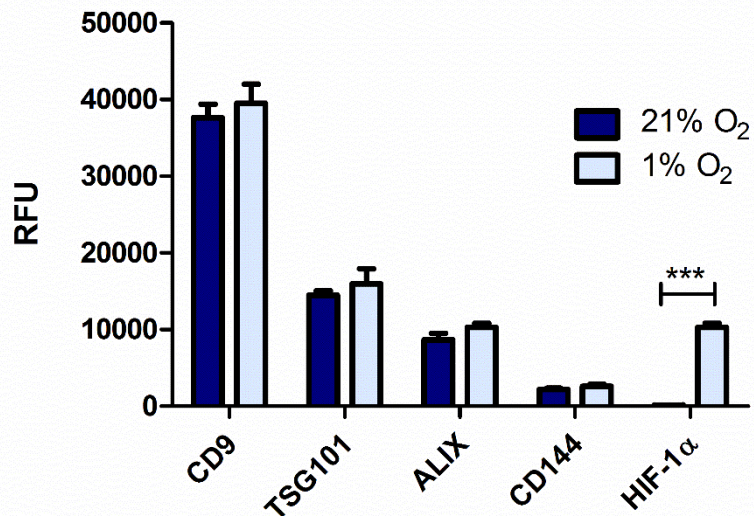


Figure 3.5 The effect of hypoxia on EV protein content. The content of vesicular (CD9, Alix, TSG101), endothelial (CD144), and HIF-1 α proteins in HECVs incubated in normoxia (21% O₂) and hypoxia (1% O₂). Proteins were detected using a streptavidin-europium conjugate and measured using time-resolved fluorescence. RFU – Relative fluorescence units. Data are expressed as mean ± SEM. *** reflects $p < 0.001$. Results represent [n=4].

3.5.5 HIF-1 α expression

Following an increase in EV production upon hypoxia exposure, HECV lysates were subsequently analysed for HIF-1 α expression. Western blotting revealed the presence of HIF-1 α in cells exposed to 1-5% O₂ for 24 hours. HIF-1 α was not detected in cells exposed to 10% or 20% O₂ (Figure 3.6A). Densitometry showed no significant difference in the levels of HIF-1 α observed in cell lysates from 1%, 2% and 5% O₂ (Figure 3.6B).

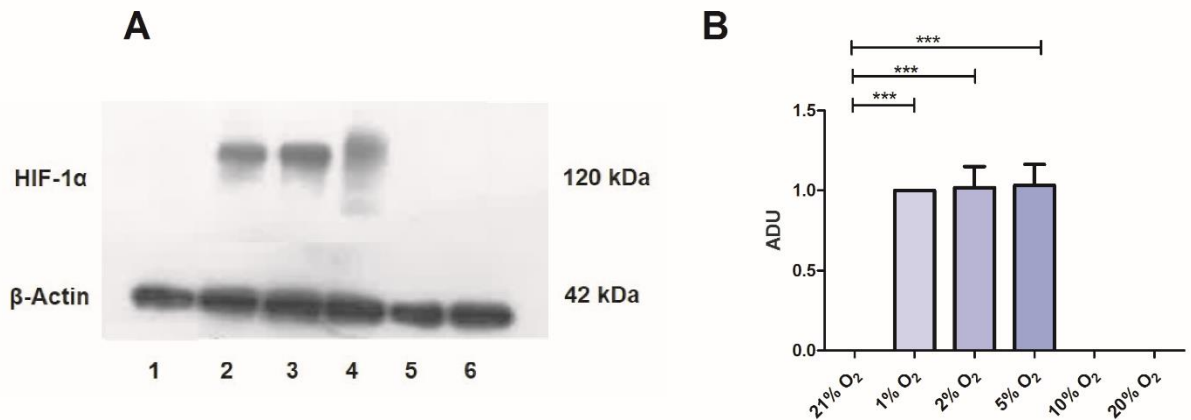


Figure 3.6 The expression of HIF-1 α at varying O₂ concentrations in HECVs. (A) Western blotting confirming the presence or absence of HIF-1 α . Lane 1: 21% O₂. Lane 2: 1% O₂. Lane 3: 2% O₂. Lane 4: 5% O₂. Lane 5: 10% O₂. Lane 6: 20% O₂. (B) Densitometry quantifying levels of expression of HIF-1 α . Values were compared to the loading control β -Actin and normalised to 1% O₂. ADU - arbitrary densitometry units. Results represent [n = 3].

3.5.6 Silencing RNA

To confirm the role of HIF-1 α and/or HIF-2 α in the hypoxic enhancement of EV release, HECVs were transfected with a siRNA targeting either HIF-1 α or HIF-2 α . Cells transfected with HIF-1 α siRNA failed to show an enhancement in EV release following hypoxia, compared to cells transfected with control siRNA or cells exposed to hypoxia alone (HIF-1 α siRNA in 1% O₂: 243 \pm 20 EVs/cell, control siRNA in 1% O₂: 1680 \pm 473 EVs/cell, 1% O₂: 1680 \pm 250 EVs/cell, $p < 0.001$) (Figure 3.7A). EV production in cells transfected with HIF-1 α siRNA in hypoxia was similar to that of the normoxia control (158 \pm 38 EVs/cell, $p > 0.05$). HECVs were also transfected with HIF-2 α siRNA. Unlike HIF-1 α siRNA transfection, HIF-2 α silencing had no effect on EV production compared to cells transfected with control siRNA or

exposed to hypoxia alone (HIF-2 α siRNA in 1% O₂: 1549 \pm 46 EVs/cell, control siRNA in 1% O₂: 1608 \pm 69 EVs/cell, 1% O₂: 1774 \pm 132 EVs/cell, $p > 0.05$) (Figure 3.7B). Western blotting confirmed that cells transfected with HIF-1 α and HIF-2 α siRNA successfully inhibited protein expression, whilst the control siRNA had no impact on HIF-1 α /-2 α expression (Figure 3.7C, 3.7D).

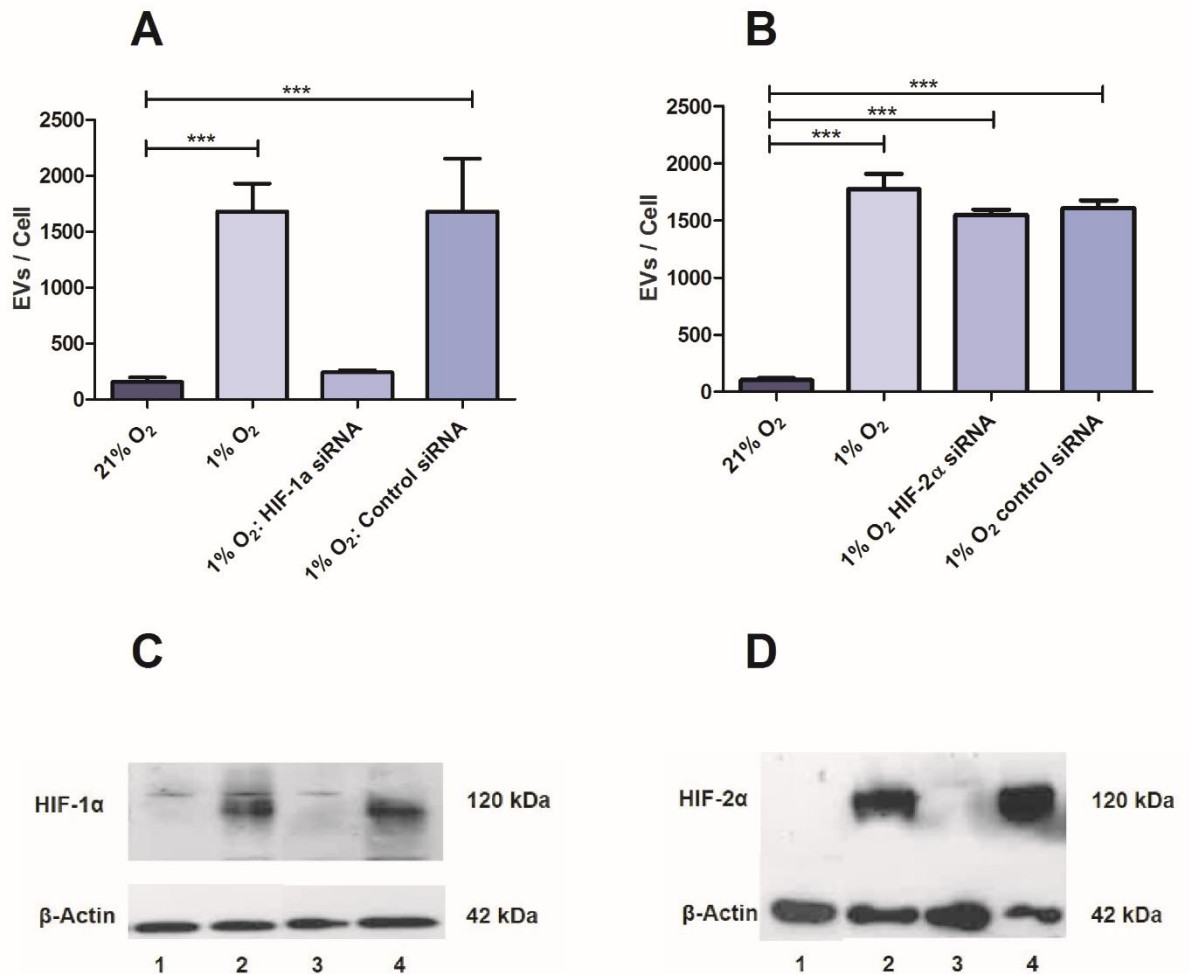


Figure 3.7 The role of HIF-1 α and HIF-2 α on EV production in HECVs. (A) The effect of HIF-1 α siRNA on EVs produced. (B) The effect of HIF-2 α siRNA on EVs produced. (C) Western blot confirming successful silencing of HIF-1 α . Lane 1: 21% O₂. Lane 2: 1% O₂. Lane 3: 1% O₂ & HIF-1 α siRNA. Lane 4: 1% O₂ & control siRNA. (D) Western blot confirming successful silencing of HIF-2 α . Lane 1: 21% O₂. Lane 2: 1% O₂. Lane 3: 1% O₂ & HIF-2 α siRNA. Lane 4: 1% O₂ & control siRNA. Results represent [n = 5]. Each sample was analysed in quintuplicate and the mean was used in further analysis. Data are expressed as mean \pm SEM. *** reflects $p < 0.001$.

3.5.7 Desferrioxamine mesylate (DFO) addition

The hypoxia mimetic agent desferrioxamine mesylate (DFO) was added to HECVs incubated in normoxia to confirm the role of hypoxia in EV production. Cells incubated in normoxia exposed to DFO produced a significantly higher number of EVs compared to cells exposed to normoxia alone (1212 ± 109 EVs/cell vs 133 ± 15 EVs/cell, $p < 0.001$), respectively. The addition of DFO to cells already exposed to hypoxia (1% O₂) had no influence on EV production compared to hypoxia exposure alone (1% O₂ & DFO: 1733 ± 87 EVs/cell vs 1% O₂: 1673 ± 60 EVs/cell, $p > 0.05$) (Figure 3.8A). Chemically induced hypoxia by DFO was confirmed by Western blot detection of HIF-1 α in cells incubated in normoxia. (Figure 3.8B). Densitometry revealed the relative levels of HIF-1 α expression between conditions (Figure 3.8C).

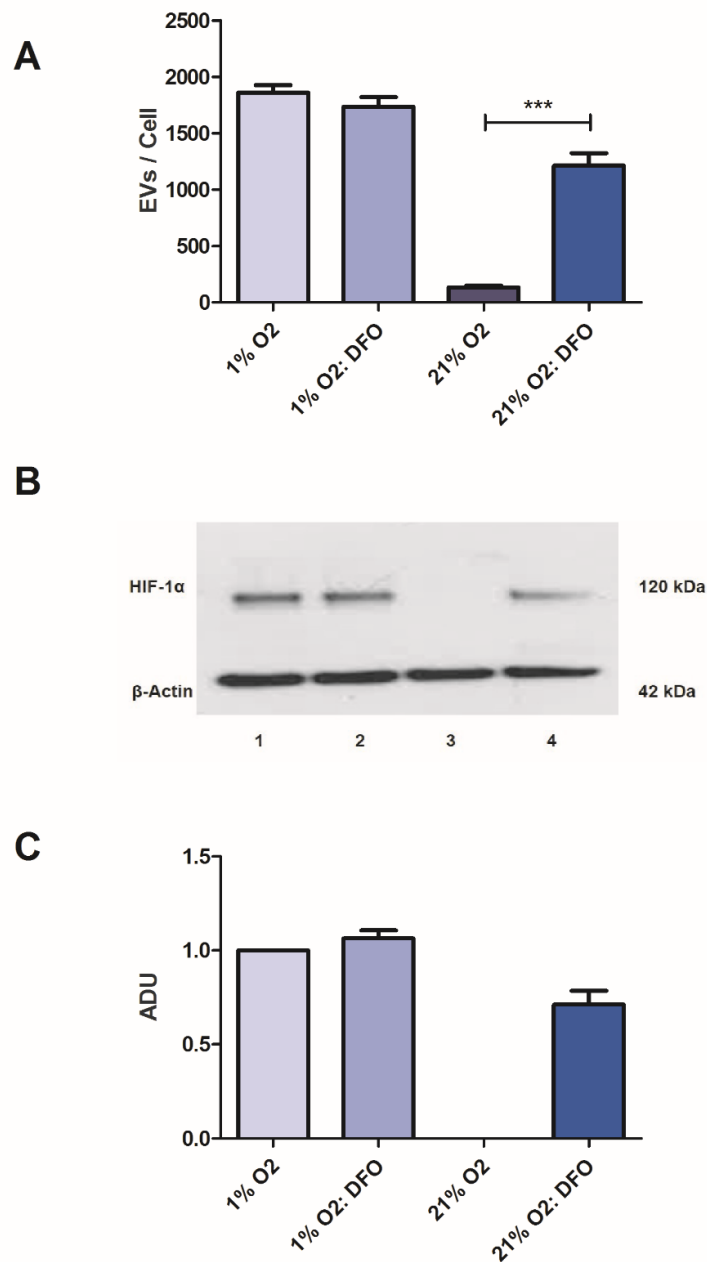
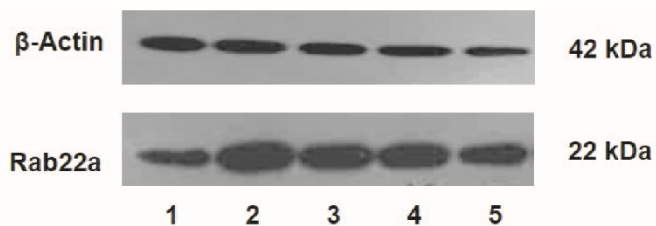


Figure 3.8 The effect of the hypoxia mimetic agent DFO on EV production and HIF-1 α expression. (A) EVs produced per cell. (B) Western blot confirming successful stabilisation of HIF-1 α in normoxia. Lane 1: 1% O₂. Lane 2: 1% O₂ & DFO. Lane 3: 21% O₂. Lane 4: 21% O₂ & DFO. (C) Densitometry quantifying levels of expression of HIF-1 α , normalised to 1% O₂. Results represent [n=4]. Each sample was analysed in quintuplicate and the mean was used in further analysis. ADU – Arbitrary densitometry units. Data are expressed as mean \pm SEM. *** reflects p < 0.001.

3.5.8 Rab22a expression in hypoxia

Rab22a expression was assessed under a range of oxygen concentrations, as a possible downstream mechanism and link between hypoxia and EV production. It has previously been shown that hypoxia induces HIF-dependent Rab22a expression in cancer cell lines (231). Western blotting and subsequent densitometry revealed that Rab22a expression was incrementally higher in lower oxygen concentrations, with cells exposed to 1%, 2%, 5% and 10% O₂ being significantly higher than the 21% O₂ control (21% O₂: 1.0 ± 0.0 ADU, 1% O₂: 2.20 ± 0.15 ADU, 2% O₂: 2.01 ± 0.11 ADU, 5% O₂: 1.6 ± 0.05 ADU, 10% O₂: 1.52 ± 0.15 ADU) (Figure 3.9).

A



B

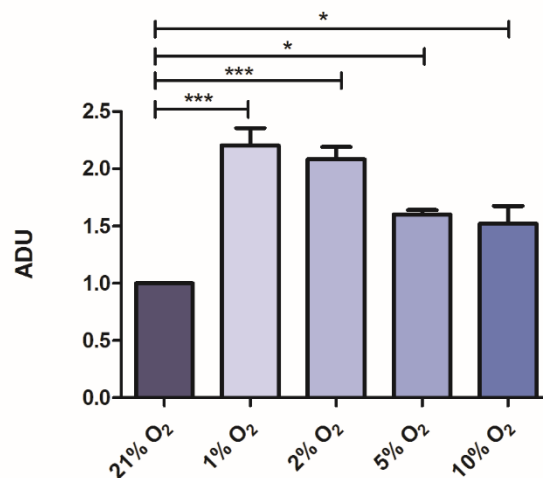


Figure 3.9 Rab22a expression in hypoxic conditions. (A) Western blot representing higher levels of Rab22a expression in hypoxic cell lysates. (B) Densitometry quantifying expression levels of Rab22a, normalised to 21% O₂. Data are expressed as mean ± SEM. Results represent [n=3]. *** and * reflect p < 0.001 and p < 0.05, respectively. Lane 1: 21% O₂. Lane 2: 1% O₂. Lane 3: 2% O₂. Lane 4: 5% O₂. Lane 5: 10% O₂.

3.5.9 Sodium nitrate (NaNO₃) and sodium nitrite (NaNO₂) addition

3.5.9.1 NaNO₃

HECVs exposed to hypoxia (1% O₂) received varying concentrations of NaNO₃ (0.3-300 μM) for 24 hours. At all concentrations, NaNO₃ administration had no effect on EV production compared to control (1% O₂: 1530 ± 64 EVs/cell, 0.3 μM NaNO₃: 1509 ± 21 EVs/cell, 3 μM NaNO₃: 1480 ± 111 EVs/cell, 30 μM NaNO₃: 1530 ± 64 EVs/cell, 300 μM NaNO₃: 1467 ± 128 EVs/cell, *p* > 0.05) (Figure 3.10A). NaNO₃ administration, at a range of concentrations, did not alter the size of EVs produced under hypoxic conditions (1% O₂: 121 ± 5 nm, 0.3 μM NaNO₃: 112 ± 8 nm, 3 μM NaNO₃: 113 ± 10 nm, 30 μM NaNO₃: 117 ± 14 nm, 300 μM NaNO₃: 110 ± 12 nm, *p* > 0.05) (Figure 3.10B). Finally, NaNO₃ administration had no effect on HECV viability (1% O₂: 86.9 ± 2.8% viable, 0.3 μM NaNO₃: 89.5 ± 2.5% viable, 3 μM NaNO₃: 87.2 ± 4.2% viable, 30 μM NaNO₃: 80.4 ± 2.2% viable, 300 μM NaNO₃: 83.9 ± 1.9% viable, *p* > 0.05) (Figure 3.10C).

3.5.9.2 NaNO₂

HECVs exposed to hypoxia (1% O₂) were also exposed to varying concentrations of NaNO₂. Administration of NaNO₂ at 0.3 μM and 3 μM had no effect on EV production (1% O₂: 1569 ± 63 EVs/cell, 0.3 μM NaNO₂: 1430 ± 47 EVs/cell, 3 μM NaNO₂: 1344 ± 69 EVs/cell, *p* > 0.05). However, NaNO₂ administered at higher doses (30-300 μM) significantly reduced EV production in hypoxia (1% O₂: 1569 ± 63 EVs/cell, 30 μM NaNO₂: 1015 ± 67 EVs/cell, 300 μM NaNO₂: 974.8 ± 49 EVs/cell, *p* < 0.001) (Figure 3.10D). NaNO₂ administration did not alter the size of EVs produced under hypoxic conditions at any of the concentrations used (1% O₂: 131 ± 5 nm, 0.3 μM NaNO₂: 116 ± 4 nm, 3 μM NaNO₂: 128 ± 3 nm, 30 μM NaNO₂: 118 ± 7 nm, 300 μM NaNO₂: 132 ± 3.7 nm, *p* > 0.05) (Figure 3.10E). Finally, NaNO₂ had no effect on cell viability at concentrations between 0.3-30 μM (1% O₂: 84.2 ± 2.9% viable, 0.3 μM NaNO₂: 84.2 ± 2% viable, 3 μM NaNO₂: 86.7 ± 1.6% viable, 30 μM NaNO₂: 79.4 ± 1.5% viable, *p* > 0.05). However, at 300 μM, NaNO₂ significantly reduced cell viability (1% O₂: 84.2 ± 2.9% viable vs 300 μM NaNO₂: 74.17 ± 0.8% viable, *p* < 0.05) (Figure 3.10F).

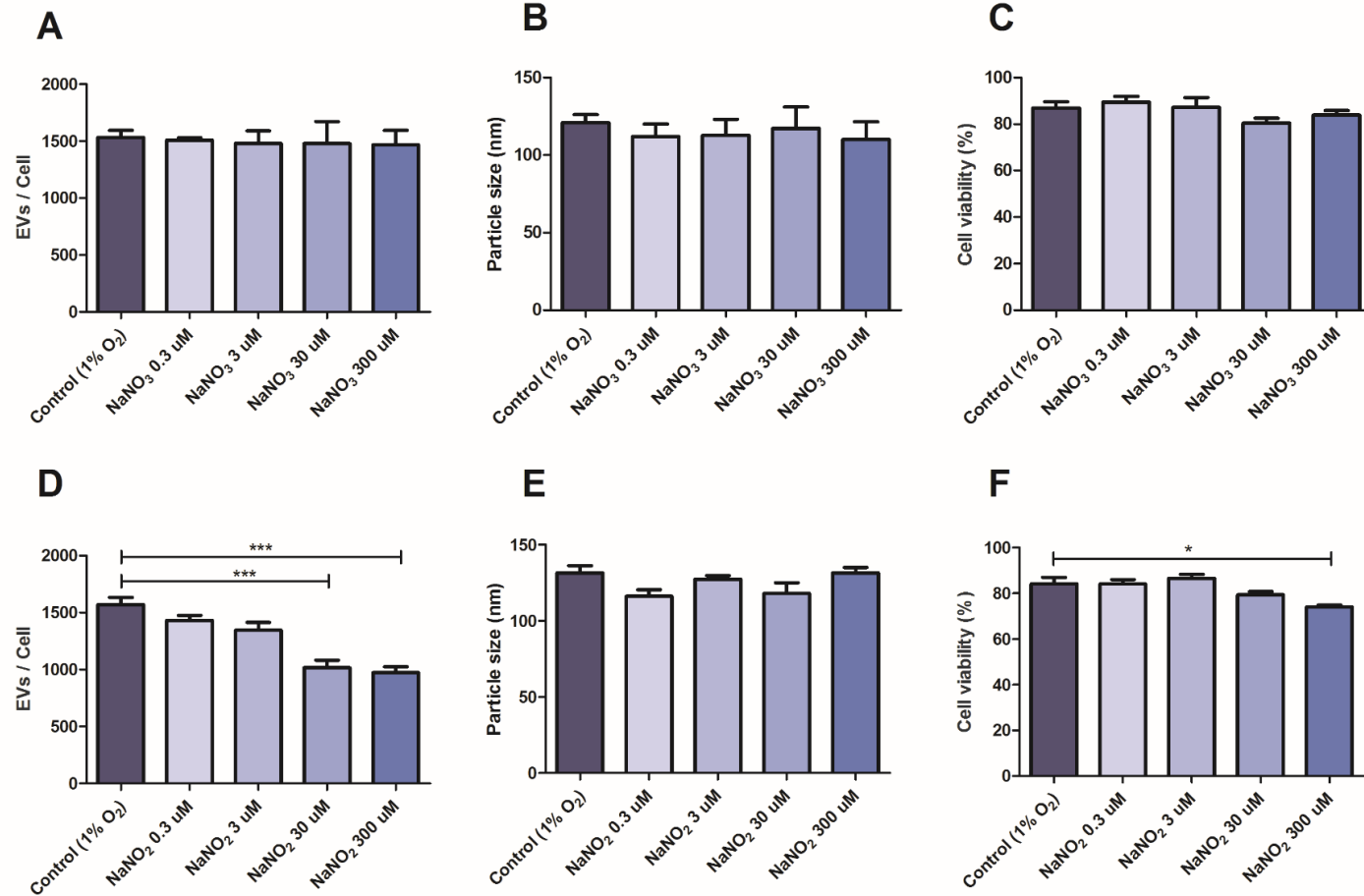


Figure 3.10 The effect of NaNO₃ and NaNO₂ on EV production, size, and cell viability. (A,D) EVs produced per cell. (B,E) Mean size of vesicles produced. (C,F) Effect of NaNO₃/NaNO₂ treatment on cell viability, measured by trypan blue exclusion. Data are expressed as mean ± SEM. Results represent [n=4]. *** and * reflect $p < 0.001$ and $p < 0.05$, respectively.

3.5.10 Sodium nitrite & xanthine oxidoreductase inhibition

Following the identification of the optimal NaNO_2 concentration (30 μM), HECVs incubated in both normoxia and hypoxia were exposed to NaNO_2 for 24 hours. Additionally, the xanthine oxidoreductase inhibitor allopurinol was added (100 μM), to prevent the conversion of NO_2^- to NO under hypoxic conditions. NaNO_2 had no effect on EV production in HECVs incubated in normoxic conditions (21% O_2 : 133 ± 15 EVs/cell vs 21% O_2 + NaNO_2 : 125 ± 19 EVs/cell, $p > 0.05$). However, NaNO_2 significantly reduced the hypoxic enhancement of EV production (1% O_2 : 1859 ± 67 EVs/cell vs. 1% O_2 + NaNO_2 : 905 ± 78 EVs/cell, $p < 0.001$). Interestingly, treatment of HECVs in hypoxia with allopurinol in addition to NaNO_2 significantly attenuated the reduction of EV production seen with NaNO_2 alone (1% O_2 + NaNO_2 ; 905 ± 78 EVs/cell vs 1% O_2 , NaNO_2 + allopurinol; 1414 ± 141 EVs/cell, $p < 0.001$). Allopurinol alone had no effect on EV production in hypoxia (1% O_2 : 1859 ± 67 EVs/cell vs 1% O_2 + allopurinol: 1824 ± 69 EVs/cell, $p > 0.05$) (Figure 3.11A). Western blots showed that the presence of NaNO_2 in hypoxia reduced the expression of HIF-1 α . The addition of allopurinol in the presence of NaNO_2 appeared to restore HIF-1 α expression in HECVs (Figure 3.11B, 3.11C).

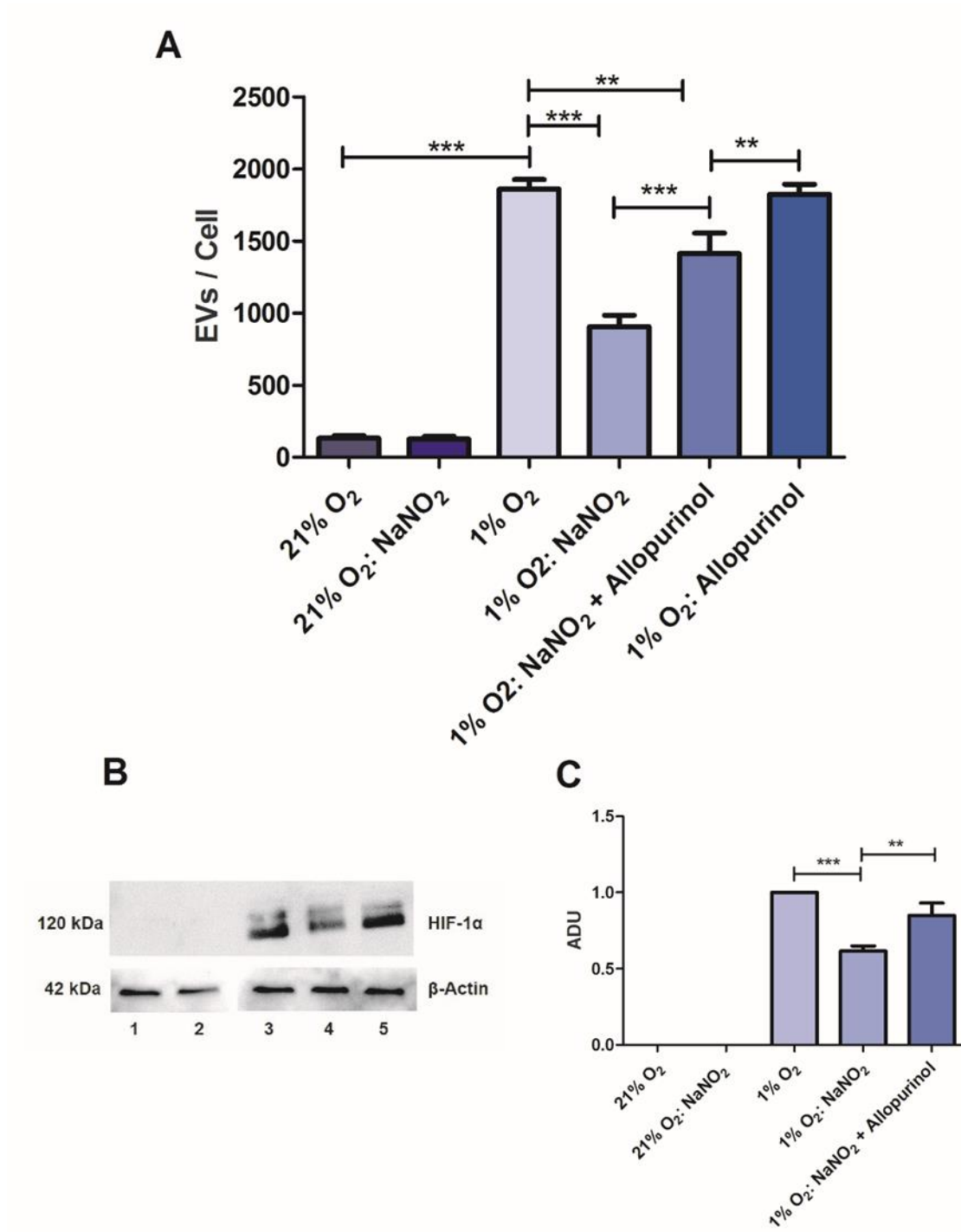


Figure 3.11 The effect of NaNO₂ on EV production. (A) EVs produced from HECVs following exposure to various conditions. (B) Western blot showing the expression of HIF-1α under various conditions. Lane 1: 21% O₂. Lane 2: 21% O₂ + NaNO₂ (30 μM). Lane 3: 1% O₂. Lane 4: 1% O₂ + NaNO₂. Lane 5: 1% O₂, NaNO₂ and allopurinol (100 μM). (C) Densitometry quantifying levels of expression of HIF-1α, normalised to 1% O₂. Results represent [n = 5]. Data are expressed as mean ± SEM. ** and *** reflect p < 0.01, and p < 0.001 respectively.

Treatment with NaNO₂ in both hypoxia (1% O₂: 127 ± 31 nm vs. 1% O₂ + NaNO₂: 133 ± 18 nm, *p* > 0.05) and normoxia (21% O₂: 128 ± 15 nm vs. 21% O₂ + NaNO₂: 123 ± 17 nm, *p* > 0.05) had no effect on the size of EV produced. Similarly, allopurinol had no effect on the size of EV compared to hypoxia alone (1% O₂, NaNO₂ + allopurinol: 119 ± 19 nm, 1% O₂ + allopurinol: 127 ± 9 nm, *p* > 0.05) (Figure 3.12A).

There was no change in overall cell viability following all cellular treatments (21% O₂: 88.0 ± 2.4 % viable, 21% O₂ + NaNO₂: 84.9 ± 2.5 % viable, 1% O₂: 83.9 ± 2.2 % viable, 1% O₂ + NaNO₂: 88.1 ± 2.8 % viable, 1% O₂, NaNO₂ + allopurinol: 89.4 ± 1.8 % viable, 1% O₂ + allopurinol: 87.7 ± 2.8 % viable, *p* > 0.05) (Figure 3.12B).

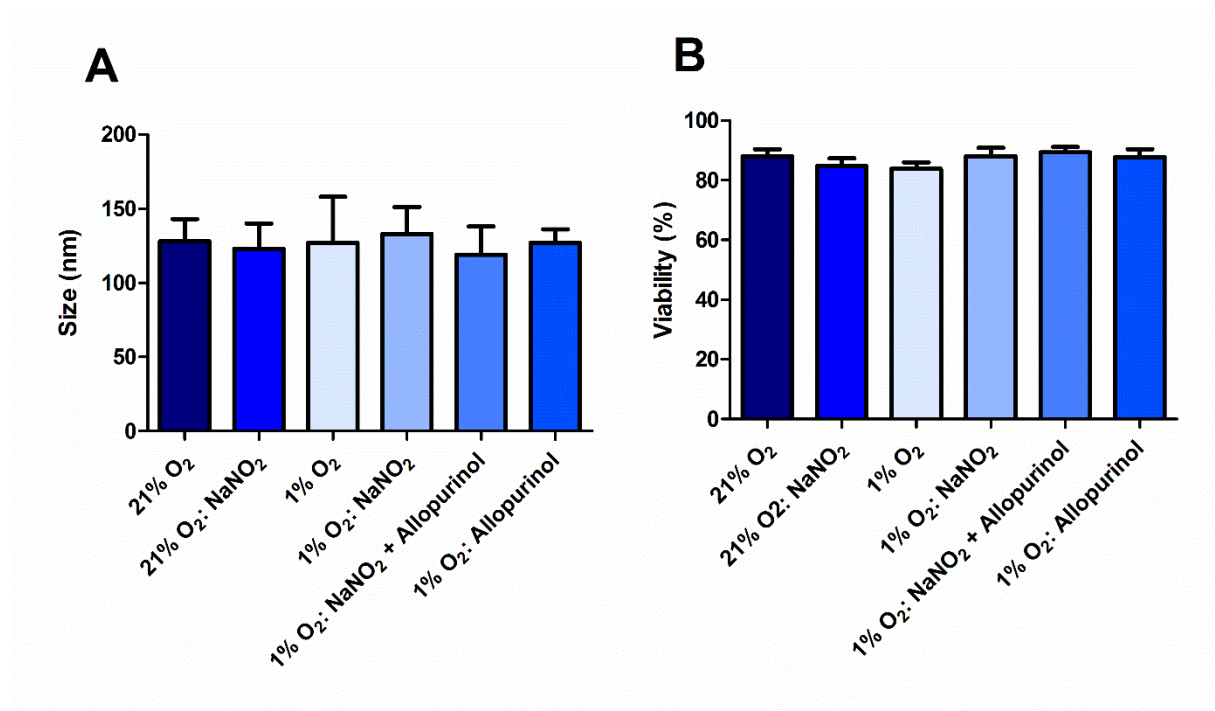


Figure 3.12 The effect of NaNO₂ on EV size and cell viability. (A) The effect of hypoxia, NaNO₂, and allopurinol on the mean size of EV produced. (B) The effect of hypoxia, NaNO₂, and allopurinol on cell viability, measured by trypan blue exclusion. Data are expressed as mean ± SEM. Results represent [n = 5].

On assessment of EV size distribution (split by 50 nm bin size for analysis), the addition of NaNO₂ to HECVs in normoxia had no effect on the size distribution profile compared to normoxia alone. However, the addition of NaNO₂ in hypoxia significantly reduced the EVs between 101-300 nm in diameter compared to hypoxia alone (101 – 150 nm: 1% O₂; 441 ± 65 EVs/cell vs 1% O₂ + NaNO₂; 233 ± 51 EVs/cell. 151 – 200 nm: 1% O₂; 401 ± 26 EVs/cell vs 1% O₂ + NaNO₂; 202 ± 38 EVs/ cell. 201 – 250 nm: 1% O₂; 300 ± 18 EVs/cell vs 1% O₂ + NaNO₂; 133 ± 18 EVs/ cell. 251-300 nm: 1% O₂; 210 ± 30 EVs/cell vs 1% O₂ + NaNO₂; 54 ± 10 EVs/ cell) (Figure 3.13). This reduction was prevented when allopurinol was added in combination with NaNO₂. The full size distribution profile for all conditions can be seen in table 3.2 and figure 3.13.

Table 3.2 The effect of hypoxia, NaNO₂ and allopurinol on EV size distribution.

EV Size	21% O ₂	21% O ₂ : NaNO ₂	1% O ₂	1% O ₂ : NaNO ₂	1% O ₂ : NaNO ₂ + Allopurinol	1% O ₂ : Allopurinol
0-50	1 ± 0	1 ± 0	12 ± 3	11 ± 5	11 ± 2	34 ± 24
51-100	16 ± 5 ^{***}	21 ± 1 ^{***}	205 ± 44	114 ± 32	148 ± 20	182 ± 64
101-150	33 ± 8 ^{***}	44 ± 3 ^{***}	441 ± 65	233 ± 51 ^{***}	372 ± 34	563 ± 104 ^{**}
151-200	29 ± 5 ^{***}	32 ± 2 ^{***}	401 ± 26	202 ± 38 ^{***}	329 ± 8	428 ± 34
201-250	22 ± 4 ^{***}	14 ± 1 ^{***}	300 ± 18	133 ± 18 ^{**}	218 ± 28	259 ± 21
251-300	14 ± 3 ^{***}	7 ± 0 ^{***}	210 ± 30	91 ± 14 [*]	152 ± 32	158 ± 21
301-350	7 ± 2 ^{**}	3 ± 0 ^{**}	132 ± 22	54 ± 10	86 ± 26	88 ± 19
351-400	4 ± 1	2 ± 0	72 ± 15	27 ± 6	46 ± 15	47 ± 13
401-450	4 ± 1	1 ± 0	58 ± 14	20 ± 5	35 ± 10	34 ± 8
451-500	1 ± 0	1 ± 0	15 ± 4	5 ± 1	9 ± 3	9 ± 2
501-550	1 ± 0	1 ± 0	8 ± 1	2 ± 1	4 ± 1	4 ± 1
551-600	1 ± 0	1 ± 0	4 ± 1	2 ± 1	2 ± 1	2 ± 1

NTA was used to assess the size distribution of EVs, split into 50 nm bin sizes for analysis and normalised to cell count. Samples were measured in quintuplicate and the mean was used in further analysis. Data are expressed as the group mean ± SEM. Results represent [n=5]. **, and *** reflects p < 0.01 and 0.001 respectively, compared to the 1% O₂

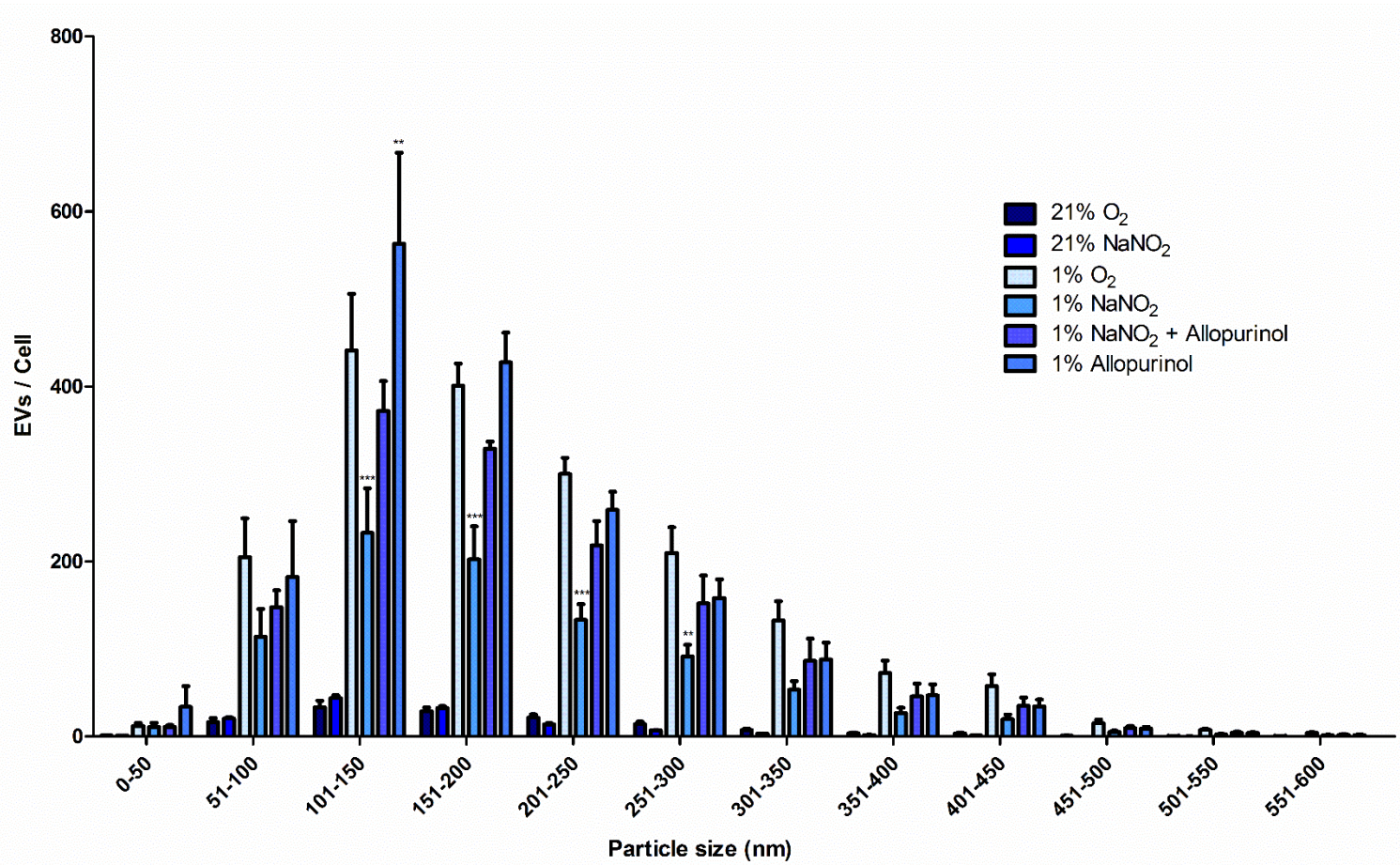


Figure 3.13 The effect of hypoxia, NaNO₂ and allopurinol on EV size distribution. NTA was used to assess the size distribution of EVs, split into 50 nm bin sizes for analysis and normalised to cell count. Samples were measured in quintuplicate and the mean was used in further analysis. Data are expressed as the group mean ± SEM. Results represent [n=5]. **, and *** reflects p < 0.01 and 0.001 respectively, compared to the 1% O₂

3.5.11 S-Nitrosoglutathione addition

S-Nitrosoglutathione (GSNO) (100 μ M) was also added to HECVs as an NO donor. GSNO addition in normoxia had no effect on EV production (21% O₂: 150 \pm 25 EVs/cell vs 21% O₂ + GSNO: 119 \pm 18, $p > 0.05$). GSNO addition in hypoxia however significantly reduced EV production (1% O₂: 1797 \pm 48 EVs/cell vs 1% O₂ + GSNO: 896 \pm 27, $p < 0.001$) (Figure 3.14A). GSNO addition had no effect on EV size when added in both normoxia (21% O₂: 108 \pm 14 nm vs 21% O₂ + GSNO: 105 \pm 21 nm, $p > 0.05$) and hypoxia (1% O₂: 130 \pm 24 nm vs 1% O₂ + GSNO: 123 \pm 14 nm, $p > 0.05$) (Figure 3.14B). HECV viability was not altered following GSNO addition (21% O₂: 88.9 \pm 5.2 % viable, 21% O₂ + GSNO: 89.1 \pm 4.8 % viable, 1% O₂: 91.5 \pm 7.8 % viable, 1% O₂ + GSNO: 88.2 \pm 17, $p > 0.05$) (Figure 3.14C).

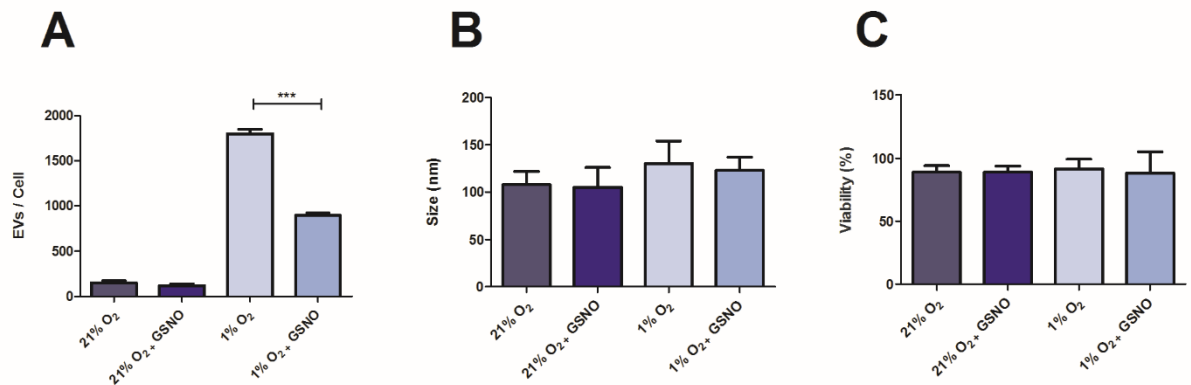


Figure 3.14 The effect of GSNO on EV production. (A) EVs produced per cell. (B) Mean size of EVs produced. (C) Cell viability, as measured by trypan blue exclusion. Data are expressed as mean \pm SEM. Results represent [n=5]. *** reflects $p < 0.001$. GSNO concentration – 100 μ M.

3.5.12 Hypoxia exposure and NaNO₂ addition in HUVECs

HUVECs were obtained in order to validate the findings in the HECVs, and compare the effect of hypoxia and NaNO₂ in a primary cell compared to a cell line. Hypoxia exposure greatly enhanced EV production compared to normoxia (21% O₂: 43 ± 6 EVs/cell vs 1% O₂: 292 ± 23 EVs/cell, *p* < 0.001). NaNO₂ had no effect on EV production in normoxia (21% O₂: 43 ± 6 EVs/cell vs 21% O₂ + NaNO₂: 41 ± 4 EVs/cell, *p* > 0.05). However, the addition of NaNO₂ significantly reduced EV production in hypoxia (1% O₂: 291 ± 23 EVs/cell vs 1% O₂ + NaNO₂: 153 ± 11 EVs/cell, *p* < 0.001) (Figure 3.15A). Western blots confirmed that NaNO₂ addition in hypoxia reduced the expression of HIF-1α in HUVECs (Figure 3.15B and C), as seen in HECVs.

NaNO₂ addition had no effect on EV size (21% O₂: 108 ± 14 nm vs 21% O₂ + NaNO₂: 97 ± 16 nm, *p* > 0.05) and hypoxia (1% O₂: 107 ± 22 nm vs 1% O₂ + NaNO₂: 129 ± 18 nm, *p* > 0.05) (Figure 3.16A). HECV viability was not altered following GSNO addition (21% O₂: 80.5 ± 7.6 % viable, 21% O₂ + NaNO₂: 84.6 ± 13.6 % viable, 1% O₂: 87.9 ± 9.1 % viable, 1% O₂ + NaNO₂: 79.8 ± 8.0, *p* > 0.05) in both hypoxia and normoxia (Figure 3.16B).

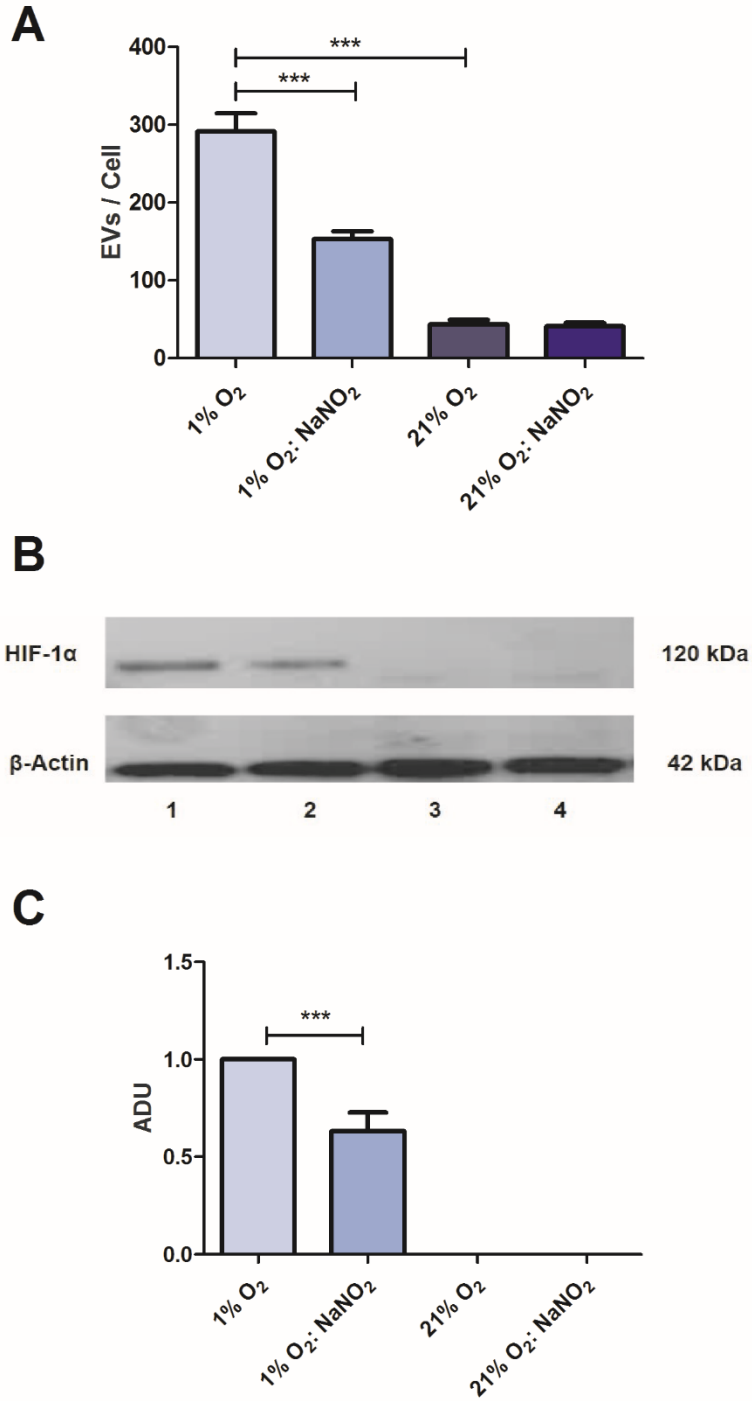


Figure 3.15 The effect of hypoxia and NaNO₂ on EV production in HUVECs. (A) EVs produced by HUVECs following exposure to hypoxia and/or NaNO₂. (B) Western blotting showing the expression of HIF-1α following exposure to hypoxia and/or NaNO₂. Lane 1: 1% O₂. Lane 2: 1% O₂ + NaNO₂. Lane 3: 21% O₂. Lane 4: 21% O₂ + NaNO₂. Results represent [n=5]. Each sample was analysed in quintuplicate and the mean was used in further analysis. Data are expressed as mean ± SEM. *** reflects p < 0.001.

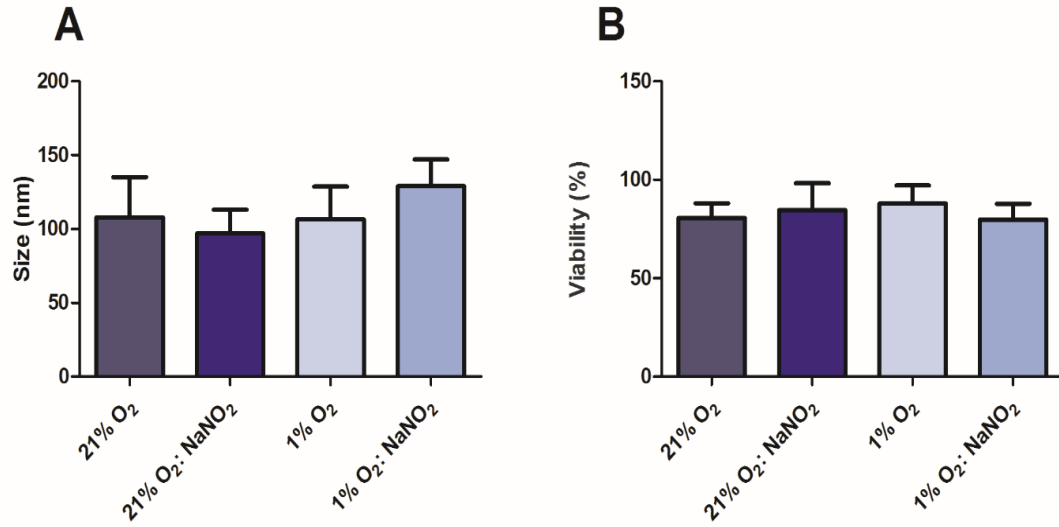


Figure 3.16. Effect of hypoxia exposure and NaNO₂ addition on HUVEC-derived EV size and viability. (A) Mean size of EVs produced from HUVECs. (B) Cell viability of HUVECs, as measured by trypan blue exclusion. Data are expressed as mean ± SEM. Results represent [n=5].

3.5.13 TNF- α addition

TNF- α was added to HECVs as an alternative stimulus to hypoxia in order to activate endothelial cells. TNF- α addition significantly increased EV production (control: 240 ± 57 EVs/cell vs TNF- α : 833 ± 100 EVs/cell, $p < 0.001$). NaNO₂ failed to reduce this TNF- α mediated enhancement in EV production (TNF- α : 833 ± 100 EVs/cell vs TNF- α + NaNO₂: 947 ± 81 EVs/cell). The addition of GSNO however did significantly reduce EV production following TNF- α addition (TNF- α : 833 ± 100 EVs/cell vs TNF- α + GSNO: 508 ± 75 EVs/cell, $p < 0.05$) (Figure 3.17A).

TNF- α addition did not affect EV size (control: 121 ± 21 nm vs TNF- α : 108 ± 18 nm, $p < 0.05$). The addition of both NaNO₂ and GSNO also had no effect on the mean EV size compared to TNF- α alone (TNF- α + NaNO₂: 121 ± 34 nm, TNF- α + GSNO: 139 ± 31 nm, $p > 0.05$) (Figure 3.17B). The viability of HECVs was not altered following TNF- α treatment (control: 92.5 ± 9.0 % viable. TNF- α : 82.3 ± 14 % viable. TNF- α + NaNO₂: 95.6 ± 10.0 % viable, TNF- α + GSNO: 88.4 ± 13.0 % viable, $p > 0.05$) (Figure 3.17C).

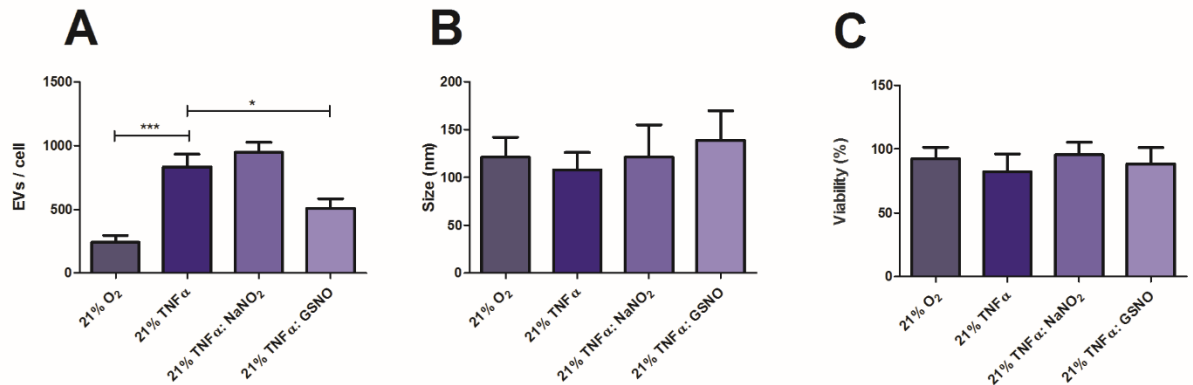


Figure 3.17 The effect of TNF- α on EV production. (A) EVs produced per cell. (B) Mean size of vesicles produced in nm. (C) Cell viability, as measured by trypan blue exclusion. Data are expressed as mean \pm SEM. Results represent [n=5]. *** and * reflect $p < 0.001$ and $p < 0.05$, respectively.

3.5.14 Calpain inhibition

To assess the role of the calcium-dependent cysteine protease calpain in EV biogenesis, Calpain Inhibitor I (ALLN) was added to HECVs in both normoxia and hypoxia. The addition of ALLN in normoxia had no effect compared to the vehicle control (21% O₂ vehicle control: 214 ± 27 EVs/cell vs 21% O₂ + ALLN: 126 ± 20 EVs/cell, $p > 0.05$). However, calpain inhibition did reduce EV production in hypoxic conditions (1% O₂ vehicle control: 1552 ± 184 EVs/cell vs 1% O₂ + ALLN: 883 ± 138 EVs/cell, $p < 0.01$) (Figure 3.18A). Calpain inhibition did not alter the size of EV produced in either normoxia (21% O₂ vehicle control: 165 ± 23 nm vs 21% O₂ + ALLN: 149 ± 14 nm, $p > 0.05$) or hypoxia (1% O₂ vehicle control: 158 ± 19 nm vs 1% O₂ + ALLN: 126 ± 14 nm, $p > 0.05$) (Figure 3.18B). Cell viability was not affected by any cellular treatment (21% O₂ vehicle control: 93.1 ± 1.2 % viable, 21% O₂ + ALLN: 88.9 ± 2.0 % viable, 1% O₂ vehicle control: 89.2 ± 2.3 % viable vs 1% O₂ + ALLN: 90.4 ± 1.2 % viable, $p > 0.05$) (Figure 3.18C).

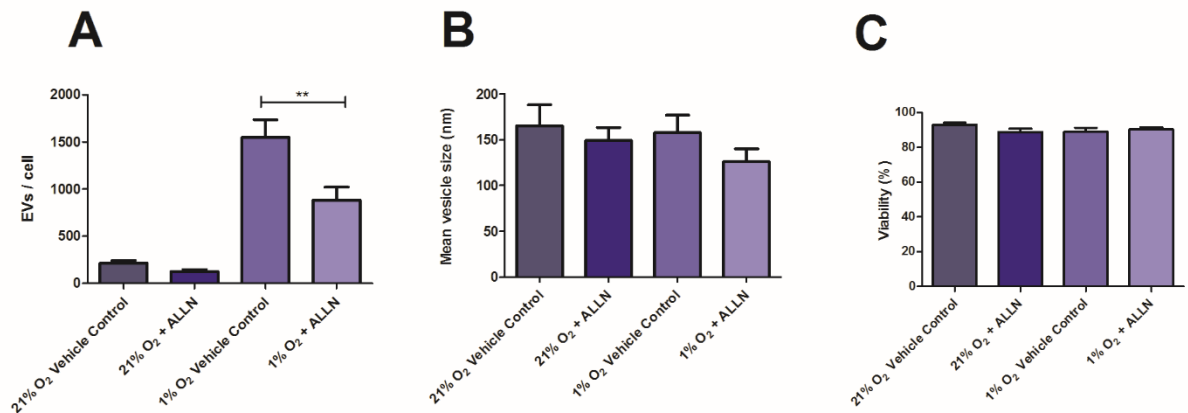


Figure 3.18 The effect of calpain inhibition on EV production in HECVs. (A) EVs produced per cell. (B) Mean size of vesicles produced. (C) Cell viability, as measured by trypan blue exclusion. Data are expressed as mean ± SEM. Results represent [n=5]. ** reflects $p < 0.01$.

On assessment of EV size distribution (split by 50 nm bin size for analysis), no differences were observed for EVs produced from HECVs exposed to the calpain inhibitor ALLN compared to the normoxic (21% O₂) control. HECVs incubated in hypoxia exposed to ALLN showed a reduction in EV produced specifically within the diameter range of 50-199 nm, compared to the hypoxic control (50 – 99 nm: 1% O₂ control; 252 ± 77 EVs/cell vs 1% O₂ + ALLN; 63 ± 7 EVs/cell. 100 – 149 nm: 1% O₂ control; 631 ± 28 EVs/cell vs 1% O₂ + ALLN; 248 ± 29 EVs/cell. 150 – 199 nm: 1% O₂ control; 333 ± 57 EVs/cell vs 1% O₂ + ALLN; 223 ± 26 EVs/cell, *p* < 0.001) (Figure 3.19). The full size distribution profile for all cellular treatments is outlined in table 3.3.

Table 3.3. The effect of calpain inhibition on EV size distribution.

EV Size	21% O ₂ vehicle control	21% O ₂ + ALLN	1% O ₂ vehicle control	1% O ₂ + ALLN
0-50	1 ± 0	0 ± 0	1 ± 1	0 ± 0
51-100	52 ± 7	10 ± 1	252 ± 77	63 ± 7***
101-150	87 ± 8	27 ± 2	631 ± 29	248 ± 29***
151-200	39 ± 2	32 ± 3	332 ± 57	223 ± 26***
201-250	21 ± 3	18 ± 1	142 ± 11	129 ± 16
251-300	8 ± 1	10 ± 2	86 ± 17	60 ± 7
301-350	3 ± 1	8 ± 1	38 ± 8	42 ± 6
351-400	1 ± 0	6 ± 1	20 ± 5	37 ± 5
401-450	2 ± 1	9 ± 1	33 ± 9	47 ± 6
451-500	1 ± 0	3 ± 0	8 ± 2	15 ± 2
501-550	0 ± 0	2 ± 0	5 ± 2	10 ± 1
551-600	0 ± 0	1 ± 0	2 ± 1	5 ± 2

NTA was used to assess the size distribution of EVs, split into 50 nm bin sizes for analysis and normalised to cell count. Samples were measured in quintuplicate and the mean used in further analysis. Data are expressed as the group mean ± SEM. Results represent [n=5]. *** reflects p < 0.001 respectively, compared to the relative oxygen concentration control.

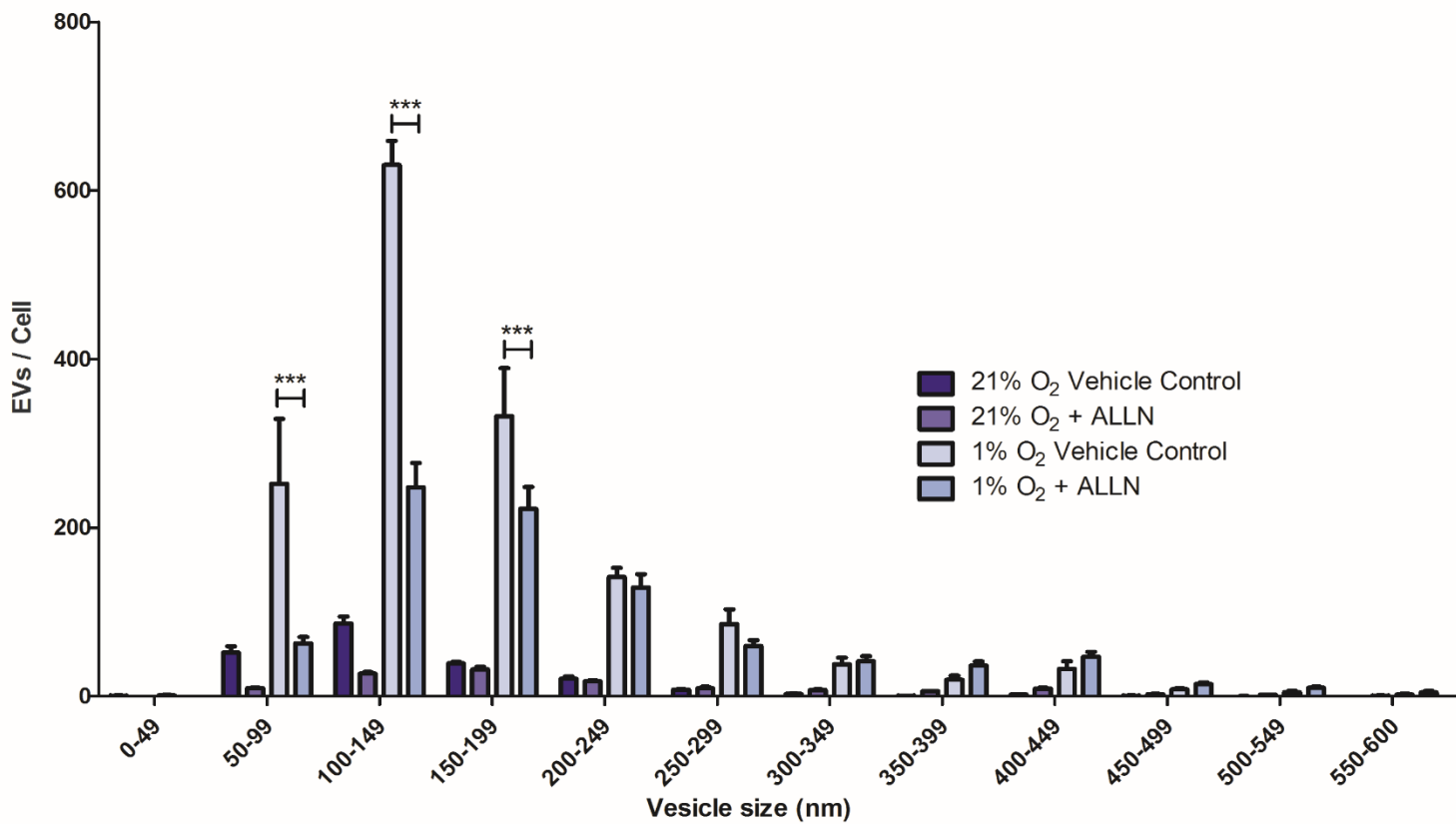


Figure 3.19 The effect of calpain inhibition on EV size distribution. NTA was used to assess the size distribution of EVs, split into 50 nm bin sizes for analysis and normalised to cell count. Samples were measured in quintuplicate and the mean used in further analysis. Data are expressed as the group mean \pm SEM. Results represent [n=5]. *** reflect $p < 0.001$ respectively, compared to the relative O₂ control.

3.5.15 Calpain activity

Calpain activity was assessed to further elucidate the role of the calcium-dependent cysteine protease in EV biogenesis. HECVs exposed to hypoxia had significantly higher levels of calpain activity compared to those incubated in normoxia (1% O₂: 841 ± 47 RFU vs 21% O₂: 363 ± 16 RFU, $p < 0.001$). Following NaNO₂ or GSNO addition, calpain activity significantly reduced in hypoxia (1% O₂: 841 ± 47 RFU vs 1% O₂ + NaNO₂: 518 ± 41 RFU, 1% O₂ + GSNO: 545 ± 25 RFU, $p < 0.001$). In contrast, the addition of NaNO₂ or GSNO had no effect on calpain activity in normoxia (21% O₂: 363 ± 16 RFU vs 21% O₂ + NaNO₂: 432 ± 25 RFU, 21% O₂ + GSNO: 357 ± 53 RFU, $p > 0.05$) (Figure 3.20A). Varying amounts of positive control (Calpain I) treated with and without 1 μL of inhibitor (Z-LLY-FMK) were also measured for calpain activity (Figure 3.20B).

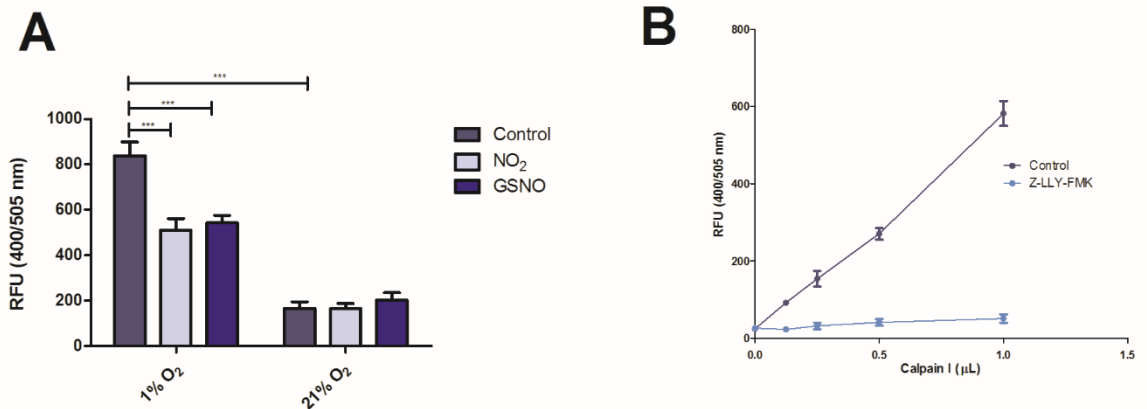


Figure 3.20 Calpain activity in hypoxia and normoxia. (A) Calpain activity was assessed following the addition of both NaNO₂ and GSNO in both normoxia (21% O₂) and hypoxia (1% O₂). (B) Active Calpain I treated with or without inhibitor were assayed for calpain activity. Samples were analysed in triplicate and the mean used in further analysis. Results represent [n = 4]. Data are expressed as mean ± SEM. *** reflects $p < 0.001$.

3.6 Discussion

3.6.1 Key findings

- Hypoxia increases EV production in endothelial cells (both primary cells and a cell line).
- This increase is mediated by HIF-1 α , but not HIF-2 α
- NO₂⁻ derived NO increases HIF-1 α degradation, and consequently reduces EV production.
- This effect is attenuated by inhibition of xanthine oxidoreductase, preventing the conversion of NO₂⁻ to NO.
- Calpain activity is increased in hypoxia and corresponds with an increase in EV release.

3.6.2 Main discussion

During pathological conditions, cellular O₂ levels are often insufficient to meet physiological demands. The resulting hypoxia is a key feature in various disease states including CVD and cancer, and is associated with poor patient outcomes (67,444). HECVs that were exposed to hypoxia for 24 hours had markedly enhanced EV production at 5% O₂ or lower. This is in agreement with previous studies which have demonstrated that hypoxia is associated with increased endothelial-derived EV production *in vivo* (429,445). Arterial blood pO₂ is normally within the range 10-14% O₂ (75-100 mmHg), with venous levels approximately 4-5.5% O₂ (30-40 mmHg). At an arterial O₂ of 8% (60 mmHg) there is a steep decline in oxygen saturation, and a human would require supplemental breathing, whereas < 4% O₂ (26 mmHg) can be considered extreme hypoxia (446). Given these reference ranges, we rationalised 5% O₂ in our studies represents an accurate model of a hypoxic condition for cells in culture, whereas less than 1% O₂ reflects severe hypoxia. Indeed, the expression of HIF-1 α in HECVs incubated at 5% O₂ confirms this can be considered a hypoxic environment, in contrast to previous considerations from the group (447).

Endothelial-derived EV have previously been shown to enhance platelet activation and adhesion, promoting the formation of a thrombus (448). It has also been shown that in patients with a history of stroke, activated endothelial cells increased EV release, which were associated with an increased frequency of cardiovascular events. This suggests that widespread endothelial cell activation may increase the risk of cardiovascular morbidity (449). Elevated EV levels have been observed in many conditions associated with both coagulation and inflammation (340). EVs have been shown to contain TF and vWF (450,451), which may partially explain their procoagulant properties. Additionally, the high level of PS exposure on endothelial-derived EVs allows

acceleration of the coagulation cascade via activation of factors Xa and Va (452,453).

Interestingly, we detected HIF-1 α present within our EV samples isolated from endothelial cells exposed to hypoxia, potentially allowing paracrine signalling to nearby cells. Nuclear translocation is not essential for the stabilisation of HIF-1 α following translation within the cytoplasm (454), and therefore could possibly be packaged into EV during their formation.

Results within this chapter suggest that HIF-1 α is pivotal in the hypoxic enhancement of EV production in endothelial cells. The hypoxia mimetic agent desferrioxamine (DFO) stabilised HIF-1 α expression in normoxia and subsequently significantly increased EV production. Silencing of HIF-1 α further confirmed its role within EV formation. In contrast, silencing of HIF-2 α had no effect on EV production in endothelial cells, suggesting the enhancement seen in hypoxia is solely HIF-1 α mediated. This result is in agreement with a previous study by King *et al*, showing that a hypoxic enhancement of EV release in breast cancer cell lines was HIF-1 α mediated (430). This suggests that regardless of cell type, hypoxia-mediated EV production may share common cellular pathways. These results are consistent with the previous suggestion that HIF-1 α is thought to be involved in acute hypoxia (2-24 hours), whereas HIF-2 α is thought to have a role in cellular adaptation to chronic hypoxia (> 24 hours) (455,456). A third, poorly defined HIF isoform, HIF-3 α , also regulates the cellular response to hypoxia, but was not investigated within this chapter. HIF-3 α differs from the other two isoforms in both structure and regulation of gene expression (457). HIF-3 α lacks the transactivation domain found in both HIF-1 α and HIF-2 α , and is thought of as a negative regulator of HIF-regulated genes by competing with HIF-1 α and HIF-2 α in binding to transcriptional elements in target genes (458).

Following hypoxia exposure (1%- 20% O₂), we saw no change in the size of EVs produced. However, on analysis of the size distribution profile, EVs were increased specifically within the range 50-400 nm. This diameter spans the definition of both exosomes (30-100 nm), and microvesicles (100-1000 nm), suggesting hypoxia does not selectively enhance only 1 subtype of EV, but instead increases EV release regardless of their mechanism of formation.

Additionally, we saw no change in both cell viability and apoptosis. Indeed, acute hypoxia increases cytosolic calcium concentration in endothelial cells to a similar level to those observed following agonist stimulation (428,459). This level is considered too low however to induce apoptosis or a reduction in viability (460). The formation of EV appears to be initiated by an increase in cytosolic concentrations of calcium, and subsequent activation of scramblase (allowing translocation of PS) (243,461), calpain (allowing for remodelling of the cytoskeleton) (462–464) and an enhanced permeability to potassium, with associated osmotic effects (241,465). Indeed, HIF-1 α activation has been shown to permit cytoskeleton reorganisation in endothelial cells (466).

Results in this chapter complement this, showing an increase in calpain activity under hypoxic conditions. Inhibition of calpain by ALLN significantly reduced EV production in hypoxia, but not in normoxia in endothelial cells. This is consistent with previous reports showing an alternative calpain inhibitor, calpeptin, reduced EV formation in platelets (462). ALLN specifically reduced EVs 50-200 nm in size, suggesting it plays a role in both exosome and microvesicle production. Moreover, the small GTPase Rab22a has previously been shown to be a mediator of HIF-1 α induced EV release in breast cancer cells (231). This study demonstrated knockdown of Rab22a completely eliminated EV generation in hypoxia, but had only a modest effect on EV generation in normoxia. Results within this chapter agree with this, as Western blotting confirmed Rab22a expression was higher in hypoxic endothelial cells compared to normoxia. This may offer some explanation as to the link between hypoxia and EV release.

NO₃⁻ and NO₂⁻ were once thought of as inactive end products of NO metabolism, but are now seen as a bioactive storage pool of NO, that under certain conditions – such as hypoxia - may be reduced back to the bioactive NO molecule. The utilisation of NO₃⁻ from dietary/endogenous sources first requires reduction to NO₂⁻, which is predominantly carried out by commensal bacteria within the gastrointestinal tract, as mammals do not possess specific NO₃⁻ reductase enzymes (134,140). This clarifies why a reduction in EV production was seen only following the addition of NaNO₂, and not NaNO₃, as endothelial cells do not possess NO₃⁻ reductase capability. Treatment of endothelial cells with allopurinol, in the presence of NaNO₂, largely inhibited the NO₂⁻ attributed suppression of EV production. This complements the hypothesis that under hypoxic conditions, xanthine oxidoreductase plays an important role in the reduction of NO₂⁻ to NO (467). However, the addition of allopurinol failed to completely restore EV production seen in hypoxia alone, and therefore likely that multiple mechanisms are responsible for NO₂⁻ reduction, including aldehyde dehydrogenase and mitochondrial reduction (468,469). The importance of hypoxia in NO₂⁻ reduction is further emphasised by the absence of a decrease in EV production seen following a non-hypoxic, inflammatory stimulus (TNF- α). This pathway has been dubbed the “nitrate, nitrite, nitric oxide pathway”, and is said to complement the traditional L-arginine eNOS pathway perfectly, ensuring an alternative source of NO production in hypoxia, during conditions where the oxygen dependent eNOS is compromised. Both our group and others have shown that NO₂⁻ administration can improve functional responses in ischemic myocardium, preventing ischemia-reperfusion injury (156,470).

This chapter has shown that NO can reduce the hypoxic augmentation of EV release in endothelial cells (both primary endothelial cells and an endothelial cell line), via the hypoxia-selective reduction of NO₂⁻ to NO. This is complemented by previous studies which showed that impaired

NO production in HUVECs leads to enhanced endothelial EV release (438). The oxygen-regulated subunit of HIF, HIF-1 α , is stabilised only in cells exposed to hypoxic conditions, in contrast to the constitutively active β -subunit of HIF. Under normoxic conditions, the HIF-1 α subunit is promptly and continuously degraded by the ubiquitin-proteasome system. Hydroxylation of proline residues (Pro⁴⁰² and Pro⁵⁶⁴) within an oxygen-dependent degradation domain of HIF-1 α allows the von Hippel-Lindau protein to bind, ubiquitinating the protein for degradation. However, the hydroxylation of these key proline residues is oxygen-dependent, hence under hypoxic conditions hydroxylation is impaired, leading to increased HIF-1 α stability (454,471).

Modulation of HIF-1a by NO is well documented (437,472–474). The mechanism of modulation is thought to involve the mitochondrial cytochrome c oxidase (CcO). NO can readily modulate the activity of CcO, and therefore the cells oxygen consumption. Competitive binding of NO under hypoxia inhibits CcO, allowing the redistribution of cellular oxygen. This leads to an increased availability for the oxygen dependent prolyl hydroxylase, and consequent degradation of HIF-1 α (436,437). This effect has been mimicked by all inhibitors of mitochondrial respiration, indicating it is indeed dependent on an action within the respiratory chain (475). Interestingly, our data suggest that although HIF-1 is the master hypoxic regulator which governs hypoxia-induced EV release, under hypoxic conditions NO₂⁻ is metabolised to NO, promoting the degradation of HIF-1 α and subsequent suppression of EV release.

Conversely, there have also been some reports that NO can increase HIF-1 α stability in normoxia (476–478). This accumulation of HIF-1 α occurs rapidly (\approx 30 minutes), and occurs in a mitochondria-independent manner (475). The exact mechanism of this is poorly understood, although hypotheses include that stabilisation is a result of S-nitrosylation of thiol groups in HIF-1 α (479), or a result of free-radical formation (480); however, these remain controversial.

3.6.3 Limitations

There are several limitations associated with this chapter. Firstly, the endothelial cell line HECVs were used throughout the majority of this work. Although HECVs are an established cell line, their cellular physiology can alter over time, and may not be truly reflective of an *in vivo* scenario. Importantly, our main findings that hypoxia enhances EV release, which can subsequently be attenuated by NaNO₂ addition, were also validated in primary HUVECs isolated directly from umbilical cord. Interestingly, HUVECs produced significantly less EVs per cell compared to the cell line. These differences may be simply due to physiological differences between cell lines and primary cells, or due to differences in cell culture medium (DMEM vs M199).

This chapter assessed EV production after 24 hours' exposure to hypoxia. HIF-1 α is said to be involved in acute adaptations to hypoxia (up to 24 hours). We did not assess increases in EV production at various timepoints in this study. Thus, future studies should assess EV production in hypoxia at several timepoints over a 24-hour period to elucidate the kinetics of EV release following hypoxia in endothelial cells. Certain proteins, such as TNF- α , have rapid responses to hypoxia (approximately 2 hours), which may have returned to baseline after 24 hours. However, 24-hour exposure was required to generate enough EVs for subsequent analysis.

Finally, "normoxic" conditions within this chapter refer to a standard cell incubator conditions of 95% air (approximately 21% O₂) and 5% CO₂. Arterial pO₂ is typically between the range 10-14%, and thus, "normoxic" conditions used in this chapter may actually represent a marginally hyperoxic environment.

3.6.4 Conclusions

In summary, this chapter highlights the effect of hypoxia on EV production in endothelial cells. This increase is mediated selectively by HIF-1 α , but not HIF-2 α , confirmed by siRNA. The hypoxic enhancement in EV production can be attenuated via NO₂⁻ derived NO. This attenuation is blocked by the addition of the xanthine oxidoreductase inhibitor allopurinol, preventing the reduction of NO₂⁻ to NO. GSNO also reduced EV production in hypoxia, confirming the inhibition was NO-mediated. Hypoxia exposure had no effect on the size of EVs produced, but reduced EVs within both the exosome and microvesicle range. Finally, the activity of the calcium-dependent protease calpain, involved in cytoskeletal rearrangements, is upregulated in hypoxia.

**4 RESULTS II: THE INFLUENCE OF HYPOXIA AND NITRITE
ON THE FUNCTION OF ENDOTHELIAL-DERIVED
EXTRACELLULAR VESICLES**

4.1 Perspective

Following the detailed investigation into the effect of hypoxia and NaNO_2 on EV production by endothelial cells in Chapter 3 (Results I), the next question was whether NaNO_2 treatment could also alter the biological function of EVs, or simply reduce the number produced. Thus, this chapter utilises a series of functional experiments relating to coagulation, inflammation, and cell viability, in order to assess whether NO_2^- may be able to modulate the pathogenic potential of EVs *in vitro*.

4.2 Introduction

A reduction in oxygen availability leads to physiological adaptations by numerous cell types, resulting in differential expression of specific genes, often mediated by HIF. Hypoxia affects endothelial cellular physiology in a variety of ways, resulting in alterations in their role in coagulation, inflammation, and other pathophysiological processes, as outlined in section 1.4.2. Previous work from our own research group, and others, have established that hypoxia is a potent stimulator of EV production from various cell types (430,481,482). Despite changes in cellular adaptations to hypoxia being well documented, it remains unclear whether hypoxia alters the function of EVs produced under such conditions.

Given that the bioactive cargo EVs harbour is typically reflective of the stimuli which triggered their release from the parent cell, it seems reasonable to assume that hypoxia-derived EVs may have altered in function in comparison to those derived from “normoxia” (305). Excitingly, evidence is beginning to emerge that this is indeed the case. A recent study by Gohner *et al.* assessed the coagulation capacity of EVs derived from syncytiotrophoblasts incubated under normoxic and hypoxic conditions (483). They found hypoxia-derived EVs led to elevated thrombin generation, and increased the rate of fibrinogenesis. They concluded that these effects were likely due to alterations in phenotype, but did not investigate this further. Additionally, a separate study concluded that hypoxia led to enhanced secretion of ovarian cancer cell-derived EVs with pro-coagulant TF-fVIIa activity, leading to accelerated activation of the extrinsic pathway of the coagulation cascade (484).

Aside from coagulation, there is also evidence that hypoxia-derived EVs can mediate inflammatory responses. *In vitro*, a more intense and rapid inflammatory response was observed by peripheral blood mononuclear cells following incubation with hypoxic trophoblast-derived EVs, in comparison to normoxic controls. There is also *in vivo* evidence supporting this claim; healthy volunteers breathing hypoxic air for 80 minutes had significantly elevated levels of VCAM-1⁺ endothelial-derived EVs (445).

Finally, there is accumulating evidence that hypoxic-EVs can also influence endothelial structure and function. Hypoxic exosomes from breast cancer cells have a significantly higher level of miR-210 than normoxic exosomes (430), which promotes endothelial cell tubulogenesis, and could thus represent a mechanism of tumour progression in response to hypoxia. Indeed, exosomes derived from hypoxic leukaemia cells have been shown to enhance tube formation in endothelial cells (485). Furthermore, EVs derived from rats exposed to hypoxia induced endothelial dysfunction, via a reduction in NO production and an increase in oxidative stress (486).

NO_2^- is capable of eliciting vasoprotective effects via its reduction to NO, which is greatly accelerated in hypoxia. In murine models, NO_2^- protects against hypoxic pulmonary arterial hypertension and ischemia-reperfusion damage, via its conversion to NO (487,488). Our research group has previously shown that low-dose NaNO_2 can protect against ischemia-reperfusion injury in humans, only when given before the onset of ischemia (470). NO_2^- can modulate platelet activation via its erythrocyte-mediated reduction to NO, which is promoted by hypoxia (165). Endogenous NO_2^- also regulates hypoxic vasodilation, via its reduction to NO, enhancing blood flow and matching O_2 supply to the increased metabolic demands under hypoxic conditions.

Taken together, I hypothesised that NaNO_2 , via an NO-based mechanism, may influence the function of HUVEC-derived EV isolated from hypoxic conditions.

4.3 Aims

The aims of this chapter were to:

1. Investigate the influence of NaNO_2 on the coagulation capacity of hypoxic HUVEC-derived EVs.
2. Assess the effect of these EVs on leukocyte adhesion to the endothelium
3. Identify potential changes in expression of cellular adhesion molecules by the endothelium following incubation with EVs derived from hypoxia/normoxia, with and without NaNO_2 .
4. Determine whether EVs can influence eNOS expression or post-translational eNOS modification (Serine-1177 and Threonine-495 phosphorylation) in HUVECs
5. Evaluate whether these EVs are pro-apoptotic, and assess their ability to induce oxidative stress in HUVECs.
6. Finally, examine the biogenic cargo of the EVs that may be upregulated in hypoxia and could explain any changes in function.

4.4 Methods

4.4.1 Cell culture

Primary HUVECs were isolated and cultured as detailed in section 2.1.2. Cells were counted as outlined in section 2.1.5.2.

4.4.2 Cellular treatments

HUVECs were treated with EVs derived from HUVECs that had been incubated under the following conditions: 21% O₂, 21% O₂ & NaNO₂, 1% O₂, and 1% O₂ & NaNO₂. Controls consisted of EV-free filtered PBS. NaNO₂ was added to HUVECs as outlined in section 2.1.3. HUVECs were subjected to hypoxic conditions (1% O₂, 24 hours) using an Invivo2 hypoxic workstation 400, as outlined in section 2.1.4.

4.4.3 EV Isolation

EVs were isolated from HUVECs using differential ultracentrifugation as detailed in section 2.4.1. EV samples were stored at 4°C and used within 48-72 hours of isolation.

4.4.4 EV concentration

EV concentration was determined using NTA, as outlined in section 2.3. 5 x 60 second videos were recorded analysed and the mean was subsequently used in further analysis. Size distribution graphs were generated by totalling the number of EVs/cell in each 50 nm range (bin width).

4.4.5 Cell viability and apoptosis

Two assays were undertaken to assess the effect of EVs on HUVEC viability and apoptosis. EVs were added to HUVECs (final concentration of 2x10⁸/mL) for 24 hours. A MTS assay was used to assess cell viability, and the Caspase-Glo[®] 3/7 assay was used to assess apoptosis, as outlined in sections 2.1.5.3 and 2.1.5.4, respectively.

4.4.6 Electron microscopy

Scanning electron microscopy was used to visualise the effect of HUVEC-derived EV on fibrin clot formation, as outlined in section 2.2.1. SEM was kindly performed by Miss Vanessa Evans of Swansea University.

4.4.7 Reactive oxygen species detection

The ability of EVs to induce oxidative stress within HUVECs was assessed using a DFCDA detection assay kit, as outlined in section 2.12.

4.4.8 Leukocyte adhesion assay

Leukocytes were isolated from whole blood of healthy volunteers, as outlined in section 2.8.1. The effect of EVs on the adhesion of leukocytes to the endothelium was assessed using an adhesion assay outlined in section 2.8.2.

4.4.9 Western blot

Western blotting was utilised to assess the effect of EVs on expression of total eNOS, and eNOS phosphorylation. Additionally, the expression of adhesion molecules on HUVECs was investigated. HUVECs were incubated with EVs (final concentration 2×10^8 /mL) for 24 hours, before cells were lysed with ice-cold lysis buffer and frozen at -20°C . Western blotting was performed as outlined in section 2.15. Details of antibody conditions and dilutions are given in Table 2.8.

4.4.10 Rheology

Rheology was used to quantify the organisation of fibrin clot formation and measure the time taken for the clot to form, as outlined in section 2.10.

4.4.11 Platelet aggregation

Platelet activity was assessed using multiple electrode aggregometry, as outlined in section 2.9, with minor modifications. Whole blood was diluted 1:1 with EVs in PBS (final concentration 2×10^8 /mL) and incubated at 37°C for 3 minutes. Samples were then stimulated with ADP/TRAP and the increase in electrical impedance recorded for 6 minutes.

4.4.12 Thrombin activity

The effect of EVs on thrombin activity was assessed using a thrombin activity assay kit, as outlined in section 2.11.

4.4.13 Time resolved fluorescence

Time resolved fluorescence was used to measure differences in protein expression between HUVEC-derived EVs derived from hypoxia (1% O₂) or normoxia (21% O₂), with or without NaNO₂ treatment, as outlined in section 2.5.

4.4.14 Statistics

Data were analysed using GraphPad Prism (version 5.0; GraphPad Software Inc., San Diego, USA). D'Agostino's K-squared test was used to check data for normality. For normally distributed data, a 1-way ANOVA was used followed by a Tukey's test to compare all pairs of columns with each other. For non-normally distributed data, a Kruskal-Wallis test was used followed by a Dunns post-test. Results are expressed as mean \pm SEM unless stated. A *p*-value of < 0.05 was regarded as statistically significant.

4.5 Results

4.5.1 Platelet aggregation

Platelet aggregation stimulated via the ADP receptor was significantly increased following whole blood incubation with 1% O₂ EVs (888.0 ± 32.2 AU*min vs 647.2 ± 38.1 AU*min, $p < 0.01$) compared to control. 1% O₂ EVs also increased platelet activity following stimulation by ADP in comparison to 21% O₂ EVs (671.5 ± 28.3 AU*min, $p < 0.01$) and 21% O₂ & NaNO₂ EVs (616.0 ± 44.9 AU*min, $p < 0.001$). 1% O₂ & NaNO₂ EVs significantly reduced platelet aggregation stimulated via ADP in comparison to 1% O₂ EVs (716.5 ± 44.3 AU*min vs 888.0 ± 32.2 AU*min, $p < 0.001$), respectively. 21% O₂ EVs and 21% O₂ & NaNO₂ EVs had no effect on platelet activity stimulated via ADP in comparison to control (21% O₂ EVs: 671.5 ± 28.3 AU*min, 21% O₂ & NaNO₂ EVs: 616.0 ± 44.9 AU*min, control: 647.2 ± 38.1 AU*min, $p > 0.05$) (Figure 4.1A).

Following stimulation via the thrombin receptor, 1% O₂ EVs were elevated in comparison to 21% O₂ derived EVs (922.2 ± 30.1 AU*min vs 641.2 ± 25.2 AU*min, $p < 0.05$), respectively. 1% O₂ & NaNO₂ EVs significantly reduced platelet aggregation in comparison to 1% O₂ EVs (650.3 ± 45.4 AU*min vs 922.2 ± 30.1 AU*min, $p < 0.05$). EVs derived from normoxia had no effect platelet aggregation stimulated by TRAP compared to control (21% O₂ EVs: 641.2 ± 25.2 AU*min, 21% O₂ & NaNO₂ EVs: 612.3 ± 115.2 AU*min, control: 616.8 ± 45.1 AU*min, $p > 0.05$) (Figure 4.1B).

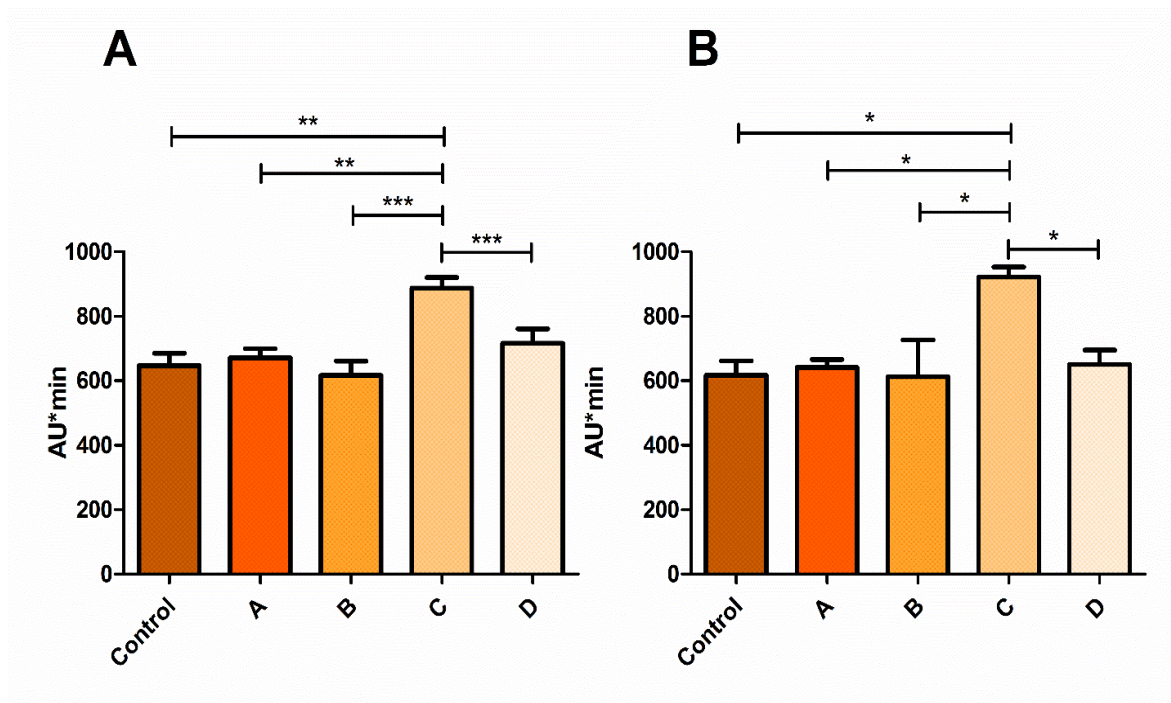


Figure 4.1 The effect of HUVEC derived EVs on ADP- and TRAP- mediated platelet aggregation. HUVEC derived EVs were incubated with whole blood for 3 minutes, before platelets were stimulated with either ADP (A) or TRAP (B). Aggregation units calculated as area under the curve after 6 minutes (impedance:time). Control – EV-free filtered PBS. Group A – 21% O₂ EVs, Group B – 21% O₂ & NaNO₂ EVs, Group C – 1% O₂ EVs, Group D – 1% O₂ & NaNO₂ EVs. Results represent [n=6]. ***, ** and * reflect p < 0.001, 0.01 and 0.05, respectively.

4.5.2 Thrombin activity

Thrombin activity in the plasma of healthy volunteers was not affected by 21% O₂ EVs or 21% O₂ & NaNO₂ EVs in comparison to control (21% O₂ EVs: 128.9 ± 4.2 ng/mL, 21% O₂ & NaNO₂ EVs: 131.6 ± 9.5 ng/mL, control: 114.6 ± 15.6 ng/mL, *p* > 0.05). 1% O₂ EVs significantly increased thrombin activity in comparison to both 21% O₂ EVs and 21% O₂ & NaNO₂ EVs (1% O₂ EVs: 187.1 ± 14.8 ng/mL, 21% O₂ EVs: 128.9 ± 4.2 ng/mL, 21% O₂ & NaNO₂ EVs: 131.6 ± 9.5 ng/mL, *p* < 0.05). 1% O₂ & NaNO₂ EVs did not significantly reduce thrombin activity in comparison to 1% O₂ EVs alone (190.7 ± 18.1 ng/mL vs 187.1 ± 14.8 ng/mL, *p* > 0.05). 1% O₂ & NaNO₂ EVs significantly increased thrombin activity in comparison to 21% O₂ EVs and 21% O₂ & NaNO₂ EVs (1% O₂ & NaNO₂ EVs: 190.7 ± 18.1 ng/mL, 21% O₂ EVs: 128.9 ± 4.2 ng/mL, 21% O₂ & NaNO₂ EVs: 131.6 ± 9.5 ng/mL, *p* < 0.05). Figure 4.2A shows differences in thrombin activity. Figure 4.2B shows increases in thrombin activity measures over 60 minutes. Figure 4.2C shows a representative standard curve used to calculate thrombin activity.

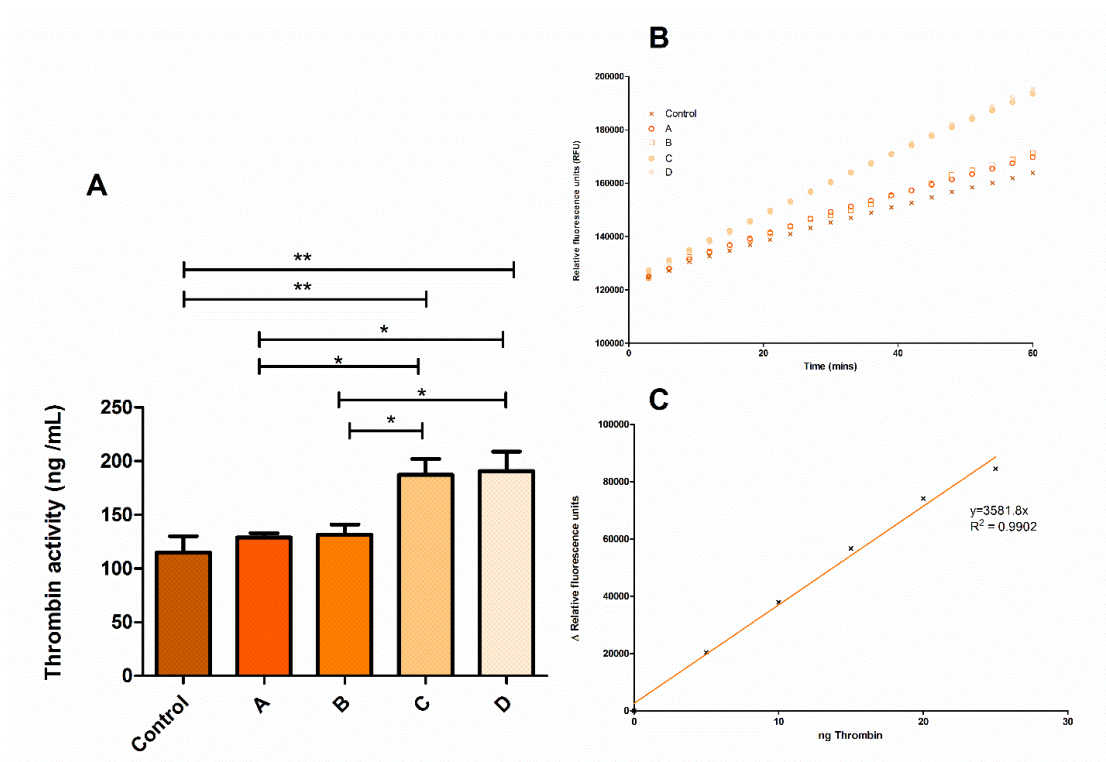


Figure 4.2 The effect of HUVEC-derived EVs on thrombin activity. A. Thrombin activity in plasma of healthy volunteers following a 60 minute incubation with HUVEC-derived EVs. B. Fluorescence was measured every 3 minutes for 60 minutes, generating a thrombin activity curve. C. Thrombin activity was calculated using a standard curve generated by wells with a known thrombin concentration. Data are expressed as mean ± SEM. Control – EV-free filtered PBS. Group A – 21% O₂ EVs. Group B – 21% O₂ & NaNO₂ EVs. Group C – 1% O₂ EVs. Group D – 1% O₂ & NaNO₂ EVs. Results reflect [n=8], ** and * reflect *p* < 0.01 and 0.05, respectively.

4.5.3 Fractal dimension (d_f) and clot formation time (T_{GP})

Fractal dimension (d_f) was significantly elevated following the addition of 1% O₂ EVs to whole blood, in comparison to control ($d_f = 1.030 \pm 0.0067$ vs 1.00 ± 0.00 , $p < 0.001$). These 1% O₂ EVs also significantly increased d_f in whole blood in comparison to incubation with 21% O₂ EVs, and 21% O₂ & NaNO₂ EVs ($d_f = 1\% \text{ O}_2 \text{ EVs: } 1.030 \pm 0.0067$, $21\% \text{ O}_2 \text{ EVs: } 1.012 \pm 0.0029$, $21\% \text{ O}_2 \text{ \& NaNO}_2 \text{ EVs: } 1.007 \pm 0.0027$, $p < 0.05$ and $p < 0.01$, respectively). Interestingly, 1% O₂ & NaNO₂ EVs significantly reduced d_f in comparison to 1% O₂ EVs alone ($d_f = 1.005 \pm 0.0017$ vs 1.030 ± 0.0067 , $p < 0.001$), respectively. d_f was not significantly different between 21% O₂ EVs and control ($d_f = 1.012 \pm 0.0030$ vs 1.00 ± 0.00 , $p > 0.05$). NaNO₂ treatment of HUVECs had no effect on the function of the EVs produced in 21% O₂, with similar d_f measurements being observed ($d_f = 21\% \text{ O}_2 \text{ EVs: } 1.012 \pm 0.0030$ vs $21\% \text{ O}_2 \text{ \& NaNO}_2 \text{ EVs: } 1.007 \pm 0.0026$, $p > 0.05$) (Figure 4.3A).

Clot formation time (T_{GP}) was significantly reduced by 21% O₂ EVs in comparison to control ($T_{GP} = 221.4 \pm 19.71$ seconds vs 273.4 ± 12.31 seconds, $p < 0.05$), respectively. 21% O₂ & NaNO₂ EVs had no effect on T_{GP} in comparison to the control, but was significantly increased in comparison to 21% O₂ EVs ($T_{GP} = 278.6 \pm 7.78$ secs vs 221.4 ± 18.71 secs, $p < 0.05$). 1% O₂ EVs significantly reduced T_{GP} in comparison to control ($T_{GP} = 181.6 \pm 8.98$ seconds vs 273.4 ± 12.31 seconds, $p < 0.05$), respectively. Interestingly, 1% O₂ EVs did not significantly alter T_{GP} in comparison to 21% O₂ EVs ($T_{GP} = 181.6 \pm 8.98$ seconds vs 221.4 ± 19.71 seconds, $p > 0.05$), respectively. 1% O₂ & NaNO₂ EVs appeared to reverse the effect of 1% O₂ EVs on T_{GP} , with 1% O₂ & NaNO₂ EVs restoring T_{GP} to a similar level as the control ($T_{GP} = \text{control: } 273.4 \pm 12.31$ seconds, $1\% \text{ O}_2 \text{ \& NaNO}_2 \text{ EVs: } 250.8 \pm 4.2$ seconds vs $1\% \text{ O}_2 \text{ EVs: } 181.6 \pm 8.99$ seconds, $p < 0.01$) (Figure 4.3B).

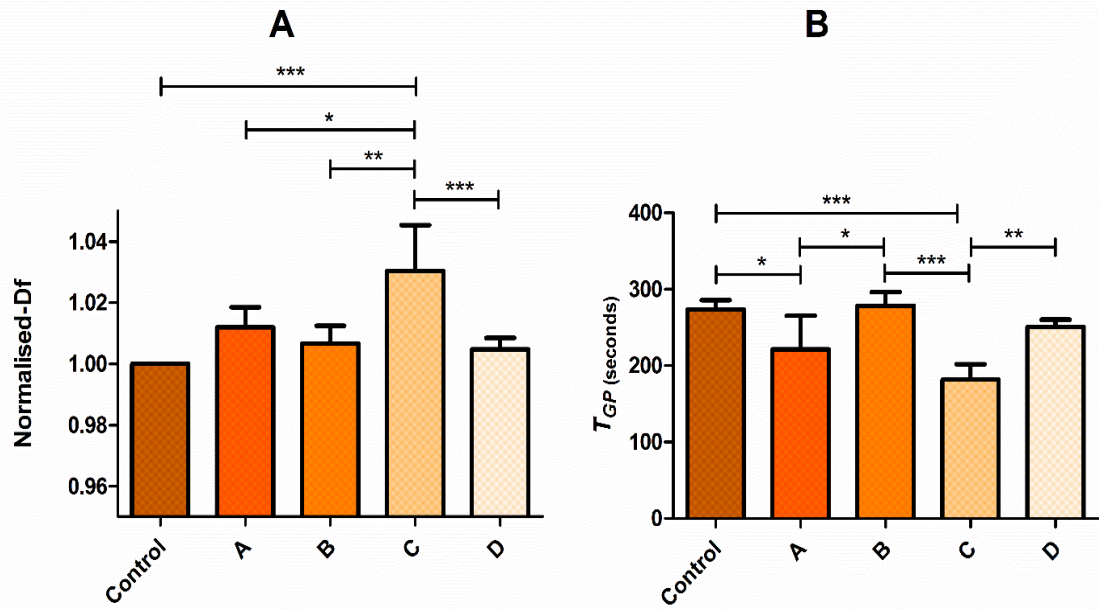


Figure 4.3 The effect of hypoxia and NaNO₂ treated HUVEC-derived EVs on d_f and T_{GP} . A. EVs were added to whole blood and incubated for 15 minutes before blood was tested to obtain the d_f . Results are normalised to an EV-free PBS control. B. T_{GP} represents the time taken for a blood clot to form, in seconds. Results represent mean \pm SEM. Control – EV-free filtered PBS. Group A – 21% O₂ EVs. Group B – 21% O₂ & NaNO₂ EVs. Group C – 1% O₂ EVs. Group D – 1% O₂ & NaNO₂ EVs. Results represent [n=5]. ***, ** and * reflect $p < 0.001$, 0.01 and 0.05, respectively.

4.5.4 Electron microscopy

Scanning electron microscopy (Figure 4.4) highlighted structural differences in fibrin clots produced following whole blood incubation with HUVEC-derived EV isolated from various conditions. The addition of EV appeared to lead to their incorporation into the fibrin clot in all treatments, with multiple sub-micron particles visibly attached to the fibres. Clots formed in the presence of 1% O₂ EVs and 1% O₂ & NaNO₂ EVs appear denser, with thicker fibrin strands. 21% O₂ & NaNO₂ EVs appear to reduce the density of the clot in comparison to normoxic EVs.

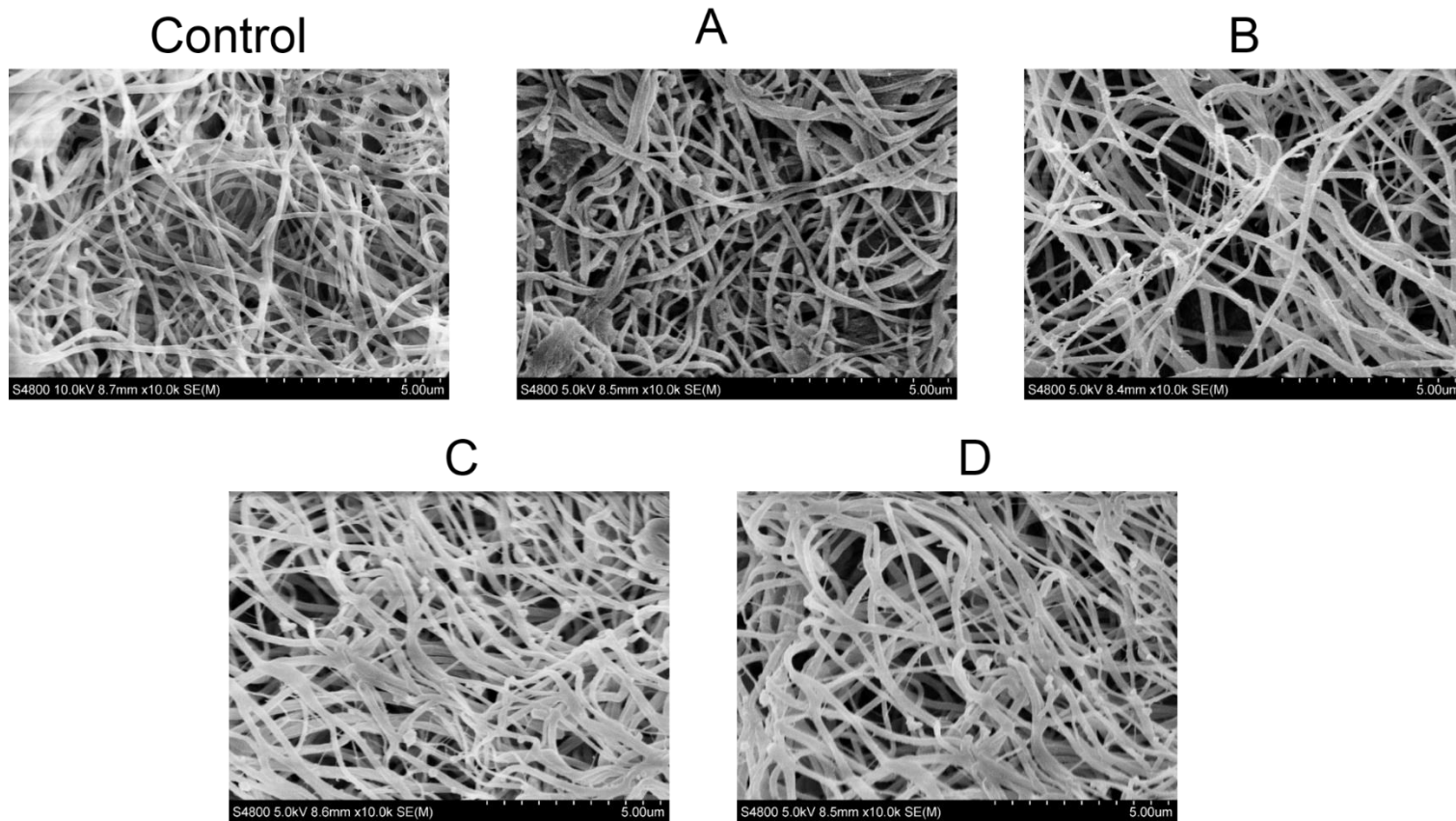


Figure 4.4 Typical scanning electron micrographs of fibrin clots. HUVEC derived EVs appear to be incorporated within the fibrin network. Control – Filtered PBS. Group A – 21% O₂ EVs. Group B – 21% O₂ & NaNO₂ EVs. Group C – 1% O₂ EVs. Group D – 1% O₂ & NaNO₂ EVs. The magnification bar is 5 µm for all images, shown in 500 nm increments. Images represent [n=3].

4.5.5 Leukocyte Adhesion

HUVEC incubation with TNF- α significantly elevated leukocyte adhesion in comparison to all other treatments (6.76 ± 0.54 %, $p < 0.001$). Leukocyte adhesion was significantly elevated following HUVEC incubation with 1% O₂ EVs in comparison to control (3.65 ± 0.79 % vs 0.64 ± 0.13 %, $p < 0.001$). These 1% O₂ EVs also significantly increased leukocyte adhesion in comparison to 21% O₂ EVs (3.65 ± 0.79 % vs 0.84 ± 0.20 %, $p < 0.01$) and 21% O₂ & NaNO₂ EVs (0.82 ± 0.20 %, $p < 0.001$). 1% O₂ & NaNO₂ EVs were not significantly different to 1% O₂ EVs (3.65 ± 0.79 % vs 2.94 ± 0.29 %, $p > 0.05$), respectively (Figure 4.5). Figure 4.6 displays typical images captured following incubation with EVs.

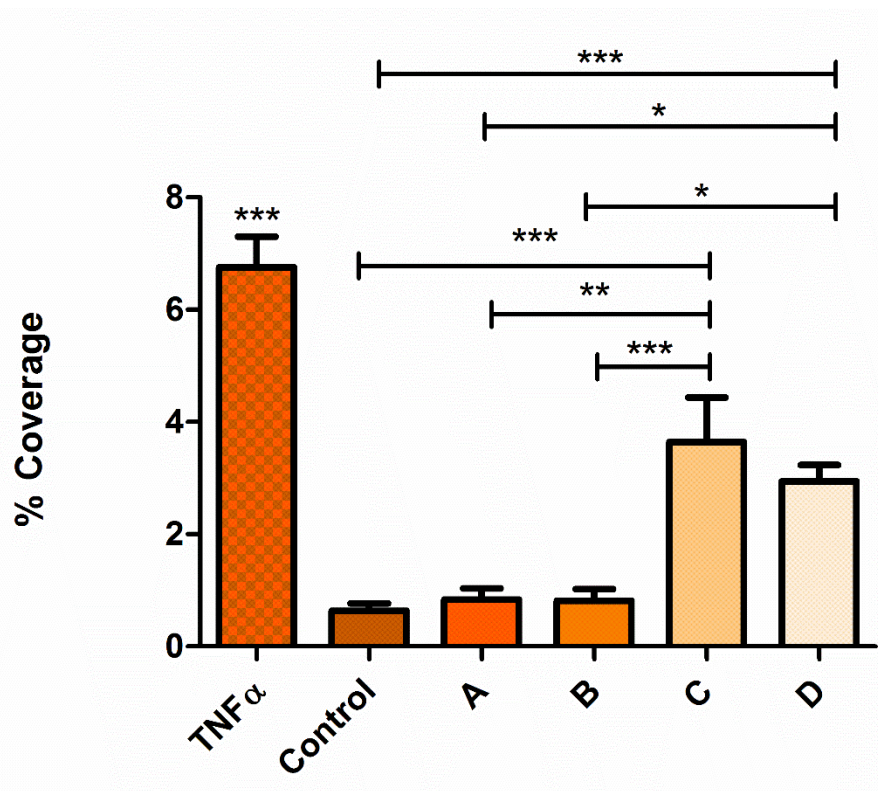


Figure 4.5 The effect of hypoxia and/or nitrite treated HUVEC-derived EVs on leukocyte adhesion. HUVECs were pre-incubated with EVs for 6 hours (TNF- α for 1 hour). Fluorescence microscopy was used to visualise leukocyte adhesion to endothelial cells. Control – Filtered PBS. Group A – 21% O₂ EVs. Group B – 21% O₂ & NaNO₂ EVs. Group C – 1% O₂ EVs. Group D – 1% O₂ & NaNO₂ EVs. Results represent [n=6]. Data are expressed as mean \pm SEM. ***, ** and * reflect $p < 0.001$, 0.01 and 0.05, respectively.

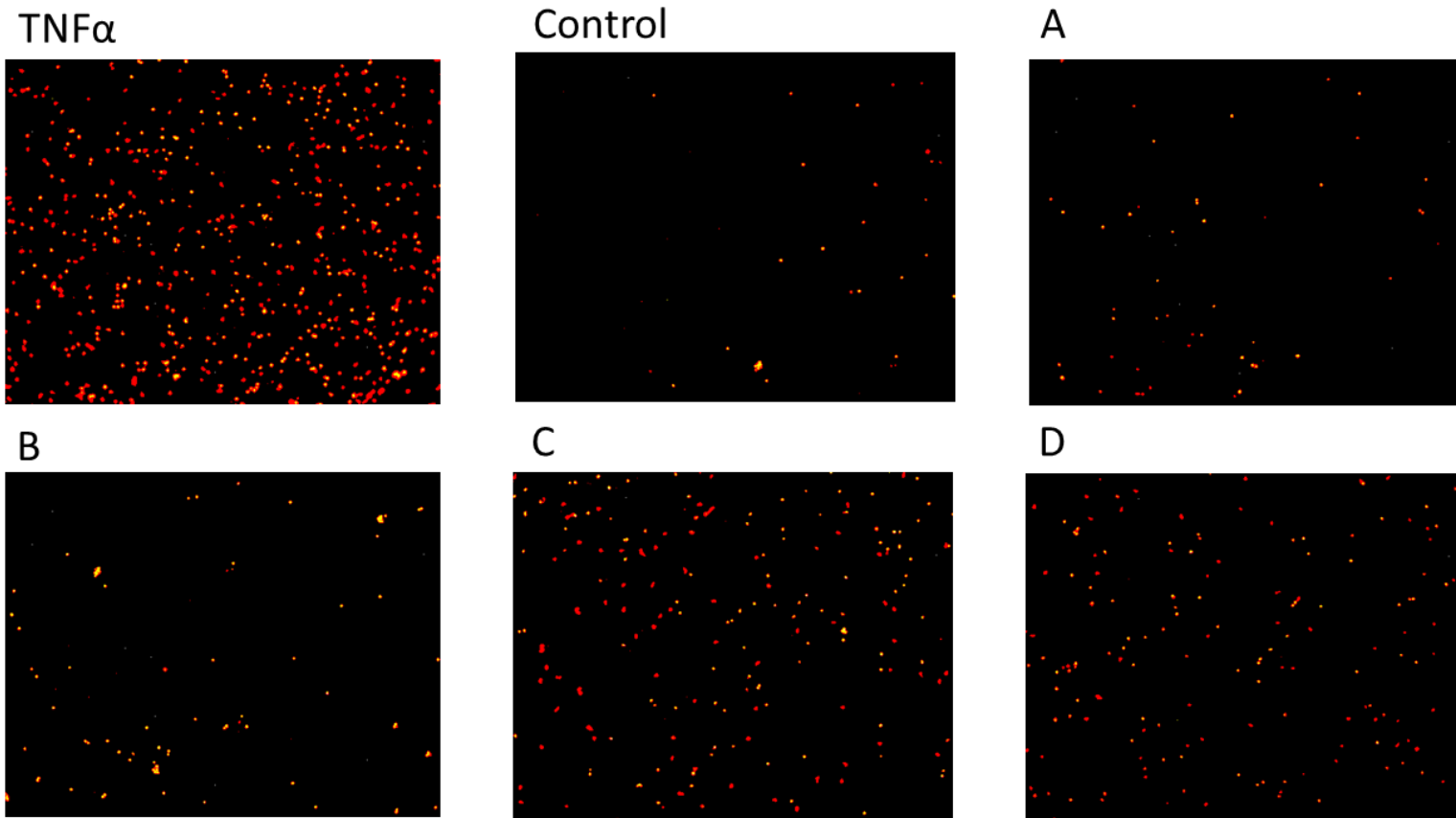


Figure 4.6 The effect of HUVEC-derived EV on leukocyte adhesion to the endothelium. Typical images obtained using fluorescence microscopy. Fresh leukocytes were isolated from whole blood and stained with Calcein red-orange. Leukocytes were incubated with HUVECs for 1 hour before HUVECs were washed with Krebs-BSA. Axiovision software was used to take high resolution images of each condition. A – 21% O₂ EV treated HUVECs. B - 21% O₂ & NaNO₂ EV treated HUVECs. C - 1% O₂ EV treated HUVECs. D - 1% O₂ & NaNO₂ EV treated HUVECs. Control HUVECs were incubated with filtered PBS.

4.5.5.1 Adhesion molecule expression

Having demonstrated an increase in leukocyte adhesion, the effect of EVs on HUVEC adhesion molecule expression was investigated. Western blot analysis revealed that ICAM-1 was significantly elevated in HUVECs incubated with 1% O₂ EVs in comparison to both 21% EVs, and 21% O₂ & NaNO₂ EVs (1% O₂ EVs: 0.36 ± 0.90 ADU vs 21% O₂ EVs: 0.04 ± 0.01 ADU, 21% O₂ & NaNO₂ EVs: 0.01 ± 0.02 ADU, $p < 0.05$). No differences in ICAM-1 expression were observed between HUVECs incubated with 1% O₂ EVs and 1% O₂ & NaNO₂ EVs (0.36 ± 0.90 ADU vs 0.22 ± 0.10 ADU, $p > 0.05$). Minimal amounts of ICAM-1 expression were observed in HUVEC lysates treated with normoxic EVs, in addition to control (filtered PBS) treatment (Figure 4.7A, 4.7B).

VCAM-1 expression was elevated following exposure to 1% O₂ EVs in comparison to HUVEC incubated with 21% O₂ EVs (0.76 ± 0.05 ADU vs 0.32 ± 0.07 ADU, $p < 0.01$), 21% O₂ & NaNO₂ EVs (0.26 ± 0.04 ADU, $p < 0.01$) and control (0.34 ± 0.11 , $p < 0.05$). VCAM-1 expression was not significantly altered following incubation with 1% O₂ & NaNO₂ EVs in comparison to 1% O₂ EVs alone (0.76 ± 0.05 ADU vs 0.62 ± 0.09 ADU, $p > 0.05$), respectively (Figure 4.7C, 4.7D).

Similarly, E-selectin expression was elevated in HUVECs exposed to 1% O₂ EVs compared to 21% O₂ EVs (0.70 ± 0.01 ADU vs 0.32 ± 0.02 ADU, $p < 0.01$), 21% O₂ & NaNO₂ EVs (0.30 ± 0.03 ADU, $p < 0.01$) and control (0.30 ± 0.10 ADU, $p < 0.05$), respectively. E-selectin levels were similar between HUVECs incubated with 1% O₂ EVs and 1% O₂ & NaNO₂ EVs (0.70 ± 0.01 ADU vs 0.54 ± 0.03 ADU, $p > 0.05$) (Figure 4.7E, 4.7F).

P-selectin expression was elevated in HUVECs incubated with 1% O₂ EVs compared to 21% O₂ EVs (0.65 ± 0.08 ADU vs 21% O₂ EVs: 0.27 ± 0.01 ADU, $p < 0.05$), 21% O₂ & NaNO₂ EVs (0.19 ± 0.04 ADU, $p < 0.05$) and control (0.22 ± 0.08 ADU, $p < 0.05$). P-selectin levels did not differ between HUVECs incubated with 1% O₂ EVs and 1% O₂ & NaNO₂ EVs (0.65 ± 0.08 ADU vs 0.59 ± 0.14 , $p > 0.05$), respectively (Figure 4.7G, 4.7H).

Finally, PECAM-1 expression remained unaltered following HUVEC incubation with hypoxic EVs, with no significant differences being observed (1% O₂ EVs: 0.87 ± 0.01 ADU, 1% O₂ & NaNO₂ EVs: 0.67 ± 0.24 ADU, 21% O₂ EVs: 0.79 ± 0.06 ADU, 21% O₂ & NaNO₂ EVs: 0.74 ± 0.04 ADU, control: 0.76 ± 0.04 , $p > 0.05$ for all comparisons) (Figure 4.7I, 4.7J).

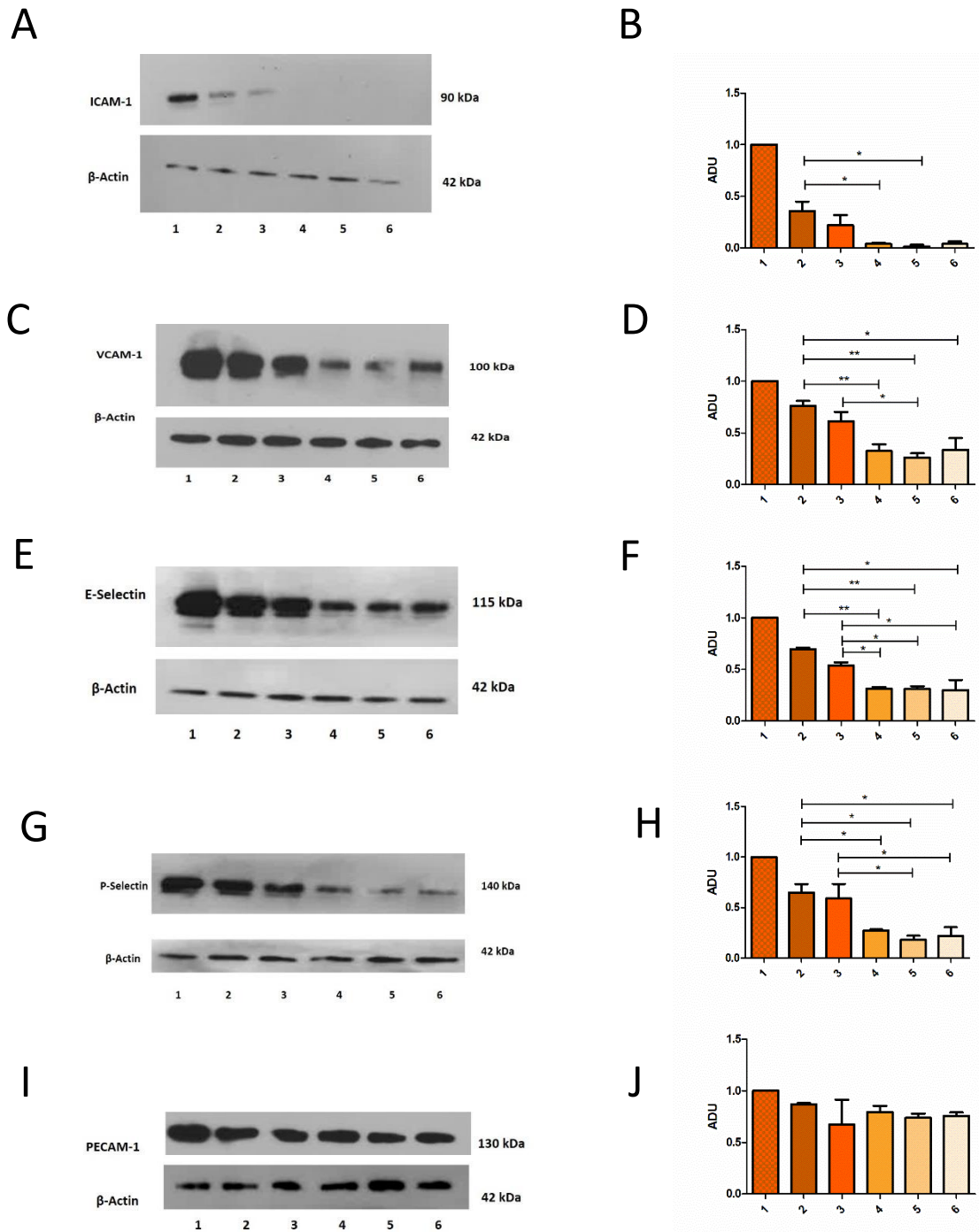


Figure 4.7 Adhesion molecule expression. Representative Western blots and densitometry for HUVECs incubated with various EV treatments. Values were normalised to TNF α treated HUVECs. Key: 1 – TNF α treated HUVECs, 2 – 1% O₂ EV treated HUVECs, 3 - 1% O₂ & NaNO₂ EV treated HUVECs, 4 - 21% O₂ EV treated HUVECs, 5 - 21% O₂ & NaNO₂ EV treated HUVECs, 6 – control (filtered PBS) treated HUVECs. Results represent [n=4]. Data are represented as mean \pm SEM. ** and * represent p < 0.01 and 0.05, respectively.

4.5.6 Viability and apoptosis

EVs derived from HUVECs incubated in both hypoxia and normoxia, with or without NaNO₂ treatment, had no effect on cell viability in comparison to control (control: 1.56 ± 0.03 , 21% O₂ EVs: 1.49 ± 0.03 , 21% O₂ & NaNO₂ EVs: 1.55 ± 0.17 , 1% O₂ EVs: 1.53 ± 0.14 ADU, 21% O₂ & NaNO₂ EVs: 1.40 ± 0.19 , $p > 0.05$ for all comparisons). Hydrogen peroxide (as a positive control) significantly reduced cell viability compared to EV treatments (0.56 ± 0.03 , $p < 0.001$ for all comparisons) (Figure 4.8A).

Similarly, EVs did not significantly alter apoptosis in HUVECs, with similar levels of caspase 3/7 activity being observed between treatment groups (control: 984.3 ± 117.4 RLU, 21% O₂ EVs: 1011.0 ± 86.9 RLU, 21% O₂ & NaNO₂ EVs: 965.0 ± 47.0 RLU, 1% O₂ EVs: 920.3 ± 42.6 RLU, 21% O₂ & NaNO₂ EVs: 981.5 ± 112.6 RLU, $p > 0.05$ for all comparisons). Hydrogen peroxide significantly increased caspase 3/7 activity compared to EV treatments (5553.0 ± 94.1 RLU, $p < 0.001$ for all comparisons) (Figure 4.8B).

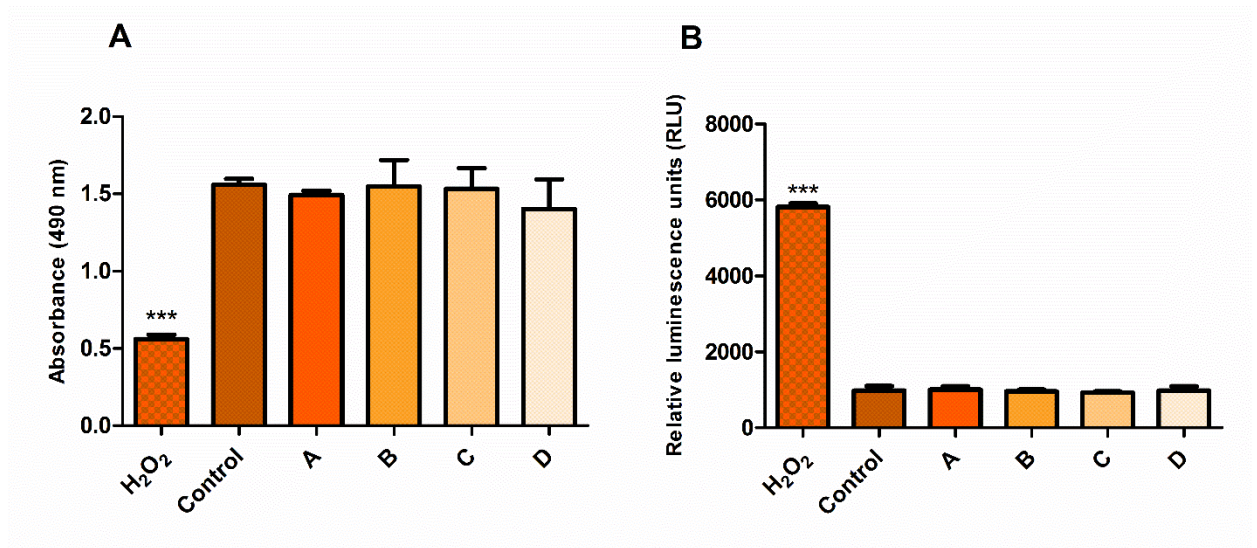


Figure 4.8 The effect of EVs on endothelial cell viability (A) and apoptosis (B). EV treatment had no effect on both cell viability and apoptosis (caspase 3/7 activity), regardless of their origin. Results represent [n=5]. *** reflects $p < 0.001$. Control – Filtered PBS. Group A – 21% O₂ EVs. Group B – 21% O₂ & NaNO₂ EVs. Group C – 1% O₂ EVs. Group D – 1% O₂ & NaNO₂ EVs.

4.5.7 Oxidative stress

Incubation of HUVECs with EVs did not significantly alter oxidative stress within cells in comparison to the control (control: 1617 ± 166 RFU, 21% O₂ EVs: 1695 ± 165 RFU, 21% O₂ & NaNO₂ EVs: 1557 ± 221 RFU, 1% O₂ EVs: 1915 ± 147 RFU, 1% O₂ & NaNO₂ EVs: 1950 ± 90 , $p > 0.05$ for all comparisons).

Incubation of HUVECs with tert-Butyl hydroperoxide (TBHP) as a positive control did significantly induce oxidative stress in HUVECs in comparison to the control (6314 ± 404 RFU vs. 1617 ± 166 RFU, $p < 0.001$) (Figure 4.9).

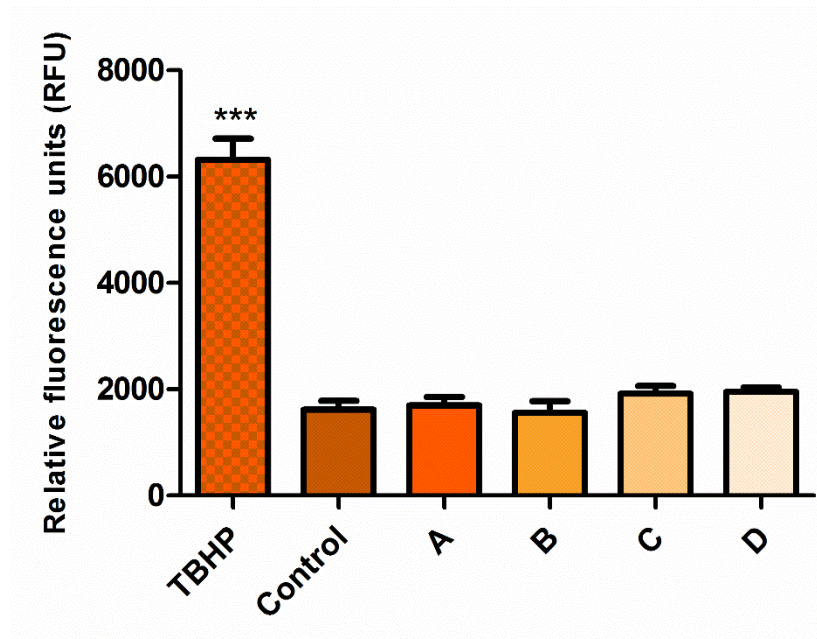


Figure 4.9 The effect of EVs on oxidative stress in endothelial cells. EVs derived from HUVECs incubated under hypoxia/normoxia, with or without NaNO₂ treatment, had no effect on inducing oxidative stress in endothelial cells. Control – Filtered PBS. Group A – 21% O₂ EVs. Group B – 21% O₂ & NaNO₂ EVs. Group C – 1% O₂ EVs. Group D – 1% O₂ & NaNO₂ EVs. TBHP - tert-Butyl hydroperoxide. Results represent [n=6]. Data are expressed as mean \pm SEM. *** reflects $p < 0.001$.

4.5.8 eNOS function

Western blotting revealed that incubation of HUVECs with EVs had no effect on total eNOS expression in comparison to control treatment (1% O₂ EVs: 1.12 ± 0.22 ADU, 1% O₂ & NaNO₂ EVs: 1.15 ± 0.25 ADU, 21% O₂ EVs: 1.07 ± 0.15 ADU, 21% O₂ & NaNO₂ EVs: 1.1 ± 0.07 ADU, control: 1.0 ± 0.0, $p > 0.05$ for all comparisons) (Figure 4.10A, 4.10B).

Similarly, no changes in the Serine-1177 phosphorylation of eNOS were observed following incubation with EVs in comparison to control (1% O₂ EVs: 1.02 ± 0.17 ADU, 1% O₂ & NaNO₂ EVs: 1.04 ± 0.11 ADU, 21% O₂ EVs: 0.97 ± 0.23 ADU, 21% O₂ & NaNO₂ EVs: 1.08 ± 0.19 ADU, control: 1.0 ± 0.0, $p > 0.05$ for all comparisons) (Figure 4.10C, 4.10D).

Additionally, no changes in Threonine-495 phosphorylation of eNOS were seen following incubation with EVs (1% O₂ EVs: 1.07 ± 0.22 ADU, 1% O₂ & NaNO₂ EVs: 1.22 ± 0.06 ADU, 21% O₂ EVs: 1.23 ± 0.25 ADU, 21% O₂ & NaNO₂ EVs: 1.02 ± 0.09 ADU, control: 1.0 ± 0.0, $p > 0.05$ for all comparisons) (Figure 4.10E, 4.10F).

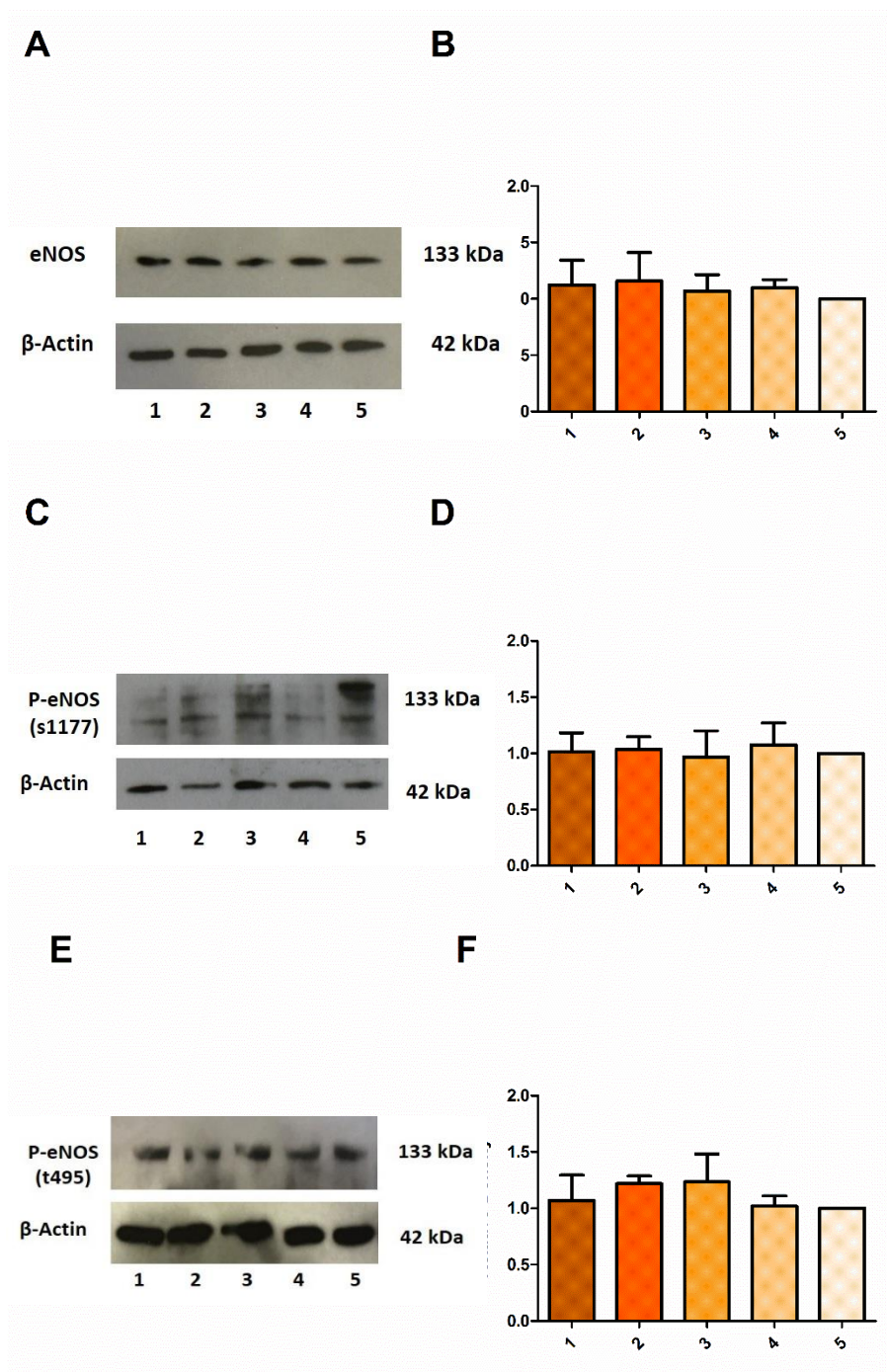


Figure 4.10 The effect of EVs on eNOS expression and phosphorylation in HUVECs. Representative Western blots and corresponding densitometry for HUVECs incubated with various EV treatments. Values were normalised to control treated HUVECs. (A,B) Total eNOS. (C,D) S1177 P-eNOS. (E,F) T495 P-eNOS. Key: 1 – 1% O₂ EV treated HUVECs, 2 - 1% O₂ & NaNO₂ EV treated HUVECs, 3 - 21% O₂ EV treated HUVECs, 4 - 21% O₂ & NaNO₂ EV treated HUVECs, 5 – control (filtered PBS) treated HUVECs. Results represent [n=3]. Data are represented as mean ± SEM.

4.5.9 Characterisation of EV

No significant differences in the levels of vWF or TF were observed between EV samples.

Thrombomodulin and TFPI levels were both significantly reduced in 1% O₂ EVs in comparison to 21% O₂ EVs. NaNO₂ treated HUVECs had no effect on thrombomodulin and TFPI expression in both normoxic EVs and hypoxic EVs (Figure 4.11A). Appendix 1.1A summarises these results.

1% O₂ EVs had significantly elevated levels of TNF- α in comparison to 21% O₂ EVs. 1% O₂ & NaNO₂ EVs had significantly lower TNF- α levels compared to 1% O₂ EVs. IL-6 levels were also elevated in 1% O₂ EVs compared to 21% O₂ EVs. NaNO₂ had no effect on these levels in both normoxia and hypoxia. The transcription factor NF- κ B was also elevated in 1% O₂ EVs compared to 21% O₂ EVs (Figure 4.11B). Appendix 1.1B summarises these results.

Analysis of adhesion molecule expression in HUVEC-derived EVs revealed no significant differences in VCAM-1, ICAM-1, PECAM-1, P-selectin and E-selectin levels between EVs isolated from hypoxia, normoxia, with or without NaNO₂ treatment (Figure 4.11C). Appendix 1.1C summarises these results.

Finally, levels of exosomal markers (CD9, Alix and TSG101) and the endothelial marker (CD144) were similar within all EV groups. HIF-1 α was significantly higher in 1% O₂ EVs in comparison 21% O₂ EVs (Figure 4.11D). Appendix 1.1D summarises these results.

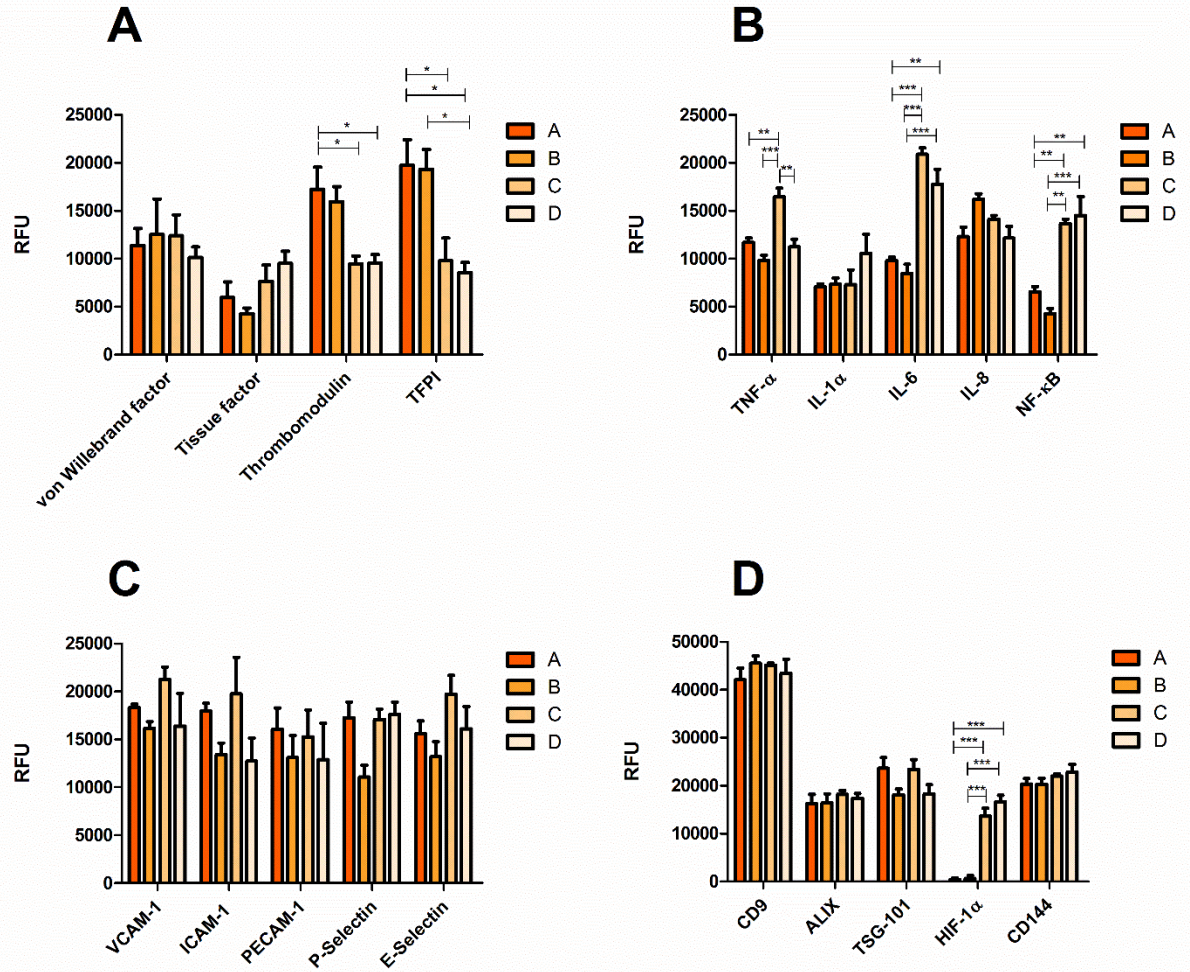


Figure 4.11 The effect of hypoxia and NaNO₂ on the protein content of HUVEC-derived EV. A. The relative levels of coagulation proteins. B. Inflammatory cytokines and transcription factors. C. Levels of adhesion molecule expression. D. Levels of exosomal, endothelial and hypoxia markers. Proteins were detected using a streptavidin-europium conjugate and measured using time-resolved fluorescence. Control – Filtered PBS. Group A – 21% O₂ EVs. Group B – 21% O₂ & NaNO₂ EVs. Group C – 1% O₂ EVs. Group D – 1% O₂ & NaNO₂ EVs. Data are expressed as mean ± SEM. Results reflect n=5. ***, ** and * reflect p < 0.001, 0.01 and 0.05, respectively.

4.6 Discussion

4.6.1 Key Findings

- EVs derived from hypoxic HUVECs significantly augment ADP- and TRAP- mediated platelet aggregation, an effect which is not observed in EVs derived from hypoxic HUVECs treated with NaNO₂.
- EVs derived from hypoxic HUVECs increase thrombin generation in comparison to normoxia-derived EVs.
- Hypoxic EVs increase the clot microstructure (as measured by *d_f*), and the speed of formation of the clot. This effect was not seen in EVs derived from hypoxia and NaNO₂ treated HUVECs.
- Leukocyte adhesion is enhanced following incubation of endothelial cells with hypoxic EVs. These EVs increase the expression of various adhesion molecules (ICAM-1, VCAM-1, E-Selectin, P-Selectin) in comparison to normoxic EVs.
- Finally, analysis of the biogenic cargo of the EVs revealed hypoxia increases the expression of numerous inflammatory markers (TNF- α , IL-1 α , IL-6, and NF- κ B) and decreases thrombomodulin and TFPI, proteins involved in modulation of the coagulation cascade.

4.6.2 Main discussion

This chapter revealed that EVs derived from hypoxic conditions exhibit enhanced pathological potential in comparison to EVs derived from normoxic conditions. *In vivo*, the presence of an atherosclerotic plaque in the wall of an artery reduces the perfusion of downstream tissues. Ischemia is defined as the inability of the vasculature to supply adequate O₂ and nutrients to tissues. This, in turn, leads to tissue hypoxia (reduced oxygen), or in severe cases, anoxia (absence of oxygen). Indeed, EVs produced by cells under these challenging conditions appear to have a differential function in a variety of pathological scenarios, in comparison to EVs released under “healthy” normoxic conditions.

EVs derived from hypoxic conditions exhibited potent pro-coagulant activity, with increases in clot microstructure being observed. Furthermore, the time taken for the formation of a blood clot was reduced following hypoxic EV incubation. The mechanical properties of blood clots are essential for the prevention of blood loss. It is thought that clots composed of compact fibrin strands are more resistant to lysis, and can predispose individuals to thrombotic events (489–493). Indeed, alterations

in clot structure have been implicated in various thrombotic diseases, including ischemic stroke (489,492), heart failure (494) and CAD (495,496). The structural composition of the clot defines its fibrinolytic properties, with a compact, tight fibrin network suppressing fibrinolytic components from penetrating the clot. Conversely, a loose structure is more susceptible to lysis due to high plasmin penetration (497,498). Thus, hypoxic EVs promote the formation of a clot which could increase the risk of future thrombotic events. These results are in agreement with other findings in this chapter, including the observations that hypoxic EVs can enhance both platelet aggregation to an artificial electrode, and thrombin generation, in comparison to EVs derived from normoxia.

Scanning electron microscopy revealed small particles between 200-500 nm in diameter are incorporated into fibrin clots. These spherical particles are attached to fibrin strands, but are not visible in the fibrin clot formed in the presence of the PBS control, suggesting they may be HUVEC-derived EVs. The fibrin clot formed in the presence of hypoxic EVs appears denser, and thus may be more resistant to fibrinolysis. Previous work by Weisel *et al* has shown that platelet-derived EVs attach to fibrin and incorporate themselves within the clot network, altering the clot microstructure (337).

Hypoxia has previously been shown to modulate the expression of various proteins involved in coagulation in cells. TF is upregulated in rat glioma cell lines following hypoxia exposure (80). Similarly, PAI-1, which inhibits the degradation of fibrin clots, is also upregulated in hypoxia, promoting the stability of fibrin clots (81). In endothelial cells, hypoxia exposure has been shown to enhance the expression of TF (76), and decrease the expression of thrombomodulin (78) and TFPI (499). Characterisation of the EVs in this chapter suggests that EVs reflect the conditions and character of their parent cells, as suggested by Van der pol *et al* (305). We observed significant reductions in both TFPI and thrombomodulin levels in hypoxic EVs in comparison to those derived from normoxia. We also observed small increases in TF in hypoxic EVs, although this was not statistically significant. Such modulation of gene expression in hypoxia is largely mediated by HIF. Indeed, HIF has been shown to repress TFPI expression by directly binding to the hormone response element (HRE) (499,500). The effect of hypoxia on TF expression remains to be fully elucidated, however there is evidence to suggest that HIF may regulate TF expression in some capacity (501,502). It is possible that changes in the levels of these molecules are responsible for the increases in pro-coagulant activity observed in hypoxic EVs.

Interestingly EVs derived from hypoxic HUVECs incubated with NaNO_2 did not exhibit the same pro-coagulant activity as EVs derived from hypoxic HUVECs alone, suggesting a protective role for NO_2^- . However, the biogenic cargo did not alter between EVs derived from hypoxic HUVECs with or without NaNO_2 pre-treatment. No differences in levels of vWF, TF, thrombomodulin or TFPI were observed in this chapter. This is in contrast to other studies which have shown that increases in NO bioavailability can reduce the expression of TF in endothelial cells, and therefore the pro-thrombotic phenotype of the cell (503). It is possible that reductions in the cellular expression of TF in HUVECs were not translated into the EVs produced, however the mechanism underpinning the protective effect of NO_2^- against the production of pro-coagulant EVs in hypoxia remains elusive. The high level of PS exposure on the surface of EVs is thought to be highly pro-coagulant, providing a negatively charged surface for formation of the prothrombinase complex (453). PS exposure is in turn mediated by the calcium-dependent floppase and scramblase membrane bound enzymes (236). NO elicits many of its effects, including modulation of platelet activation and vasodilation, via a reduction in intracellular calcium (504). Thus NO_2^- derived NO may have elicited its protective effects via a reduction in PS exposure on the surface of EVs produced. The anti-platelet effects of NO_2^- are already well documented (162,505), however this chapter extends these observations to an additional protective role of NO_2^- in the prevention of the production of pro-coagulant EVs under hypoxic conditions.

Aside from their influence on coagulation, hypoxic EVs also enhanced leukocyte adhesion to the endothelium. Extravasation is a pivotal stage in the formation of atherosclerotic plaques, allowing leukocytes to move through the endothelium and engulf the deposited LDL, leading to foam cell formation, the hallmark of the “fatty streak” (506). This study observed increases in the expression of numerous adhesion molecules (VCAM-1, ICAM-1, E-selectin and P-selectin) following incubation of HUVEC with hypoxic EVs. EVs derived from atherosclerotic plaques are capable of transferring ICAM-1 to endothelial cells (362). Adhesion molecules were present on EVs, but did not differ depending on the conditions of their parental cell. Interestingly, exosome-bound ICAM-1 has been shown to bind leukocytes and exhibit anti-leukocyte adhesion activity, suggesting EVs may be capable of both positively and negatively regulating leukocyte adhesion (507).

One possible explanation for the effect of hypoxic EVs on leukocyte adhesion is the increased levels of pro-inflammatory cytokines $\text{TNF-}\alpha$, $\text{IL-1}\alpha$ and IL-6 . These cytokines are capable of activating $\text{NF-}\kappa\text{B}$ (508–510), which itself was also upregulated in hypoxic EVs. $\text{NF-}\kappa\text{B}$ is a well-known ubiquitous transcription factor involved in the regulation of many inflammatory genes. Indeed, activation of the $\text{NF-}\kappa\text{B}$ pathway has been shown to increase the expression of ICAM-1 (511), VCAM-1 (512), E-selectin

(513) and P-selectin (514), by binding to specific binding motifs within their promoters. Interestingly, endothelial EVs have previously been shown to bind to and activate monocytes directly, increasing ICAM-1 expression and drastically increasing transendothelial migration (515). However, in this chapter, EVs were incubated with endothelial cells which were washed thoroughly prior to the addition of leukocytes, so this mechanism is unlikely to explain the effects observed.

NaNO₂ treatment of HUVECs did not affect the cargo of the EVs produced, with similar levels of pro-inflammatory cytokines present on EVs derived from hypoxia alone. This is perhaps mirrored in the similar level of leukocyte adhesion to endothelial cells following incubation with both 1% O₂ EVs and 1% O₂ & NaNO₂ EVs. Indeed, the expression of adhesion molecules was similar between HUVECs incubated with these EVs. NO has previously been shown to modulate the effects of NF-κB, by post-translational modification. Specifically, NO can modify a conserved C62 residue by S-nitrosylation, inhibiting the ability of NF-κB to bind to promoters (99). Furthermore, NO can induce and stabilize the NF-κB inhibitor IκBα (100). It is well documented that NO can modulate leukocyte recruitment via this mechanism in endothelial cells (97,516,517). However, this was not mirrored in the effects of EVs on leukocyte adhesion, with EVs derived from NaNO₂ treated HUVECs not altering the extent of leukocyte adhesion in comparison to EVs derived from cells without NaNO₂ treatment.

EVs derived from all conditions had no effect on viability and apoptosis in comparison to the control. When cells are exposed directly to hypoxia, the severity and length of exposure determines whether cells become apoptotic, or adapt and survive (518). Acute hypoxia (≤24 hours) raises intracellular calcium to a level considered too low to induce apoptosis (519). However, the PS exposure that occurs as a result of this is commonly used as a signal for macrophages to engulf the cell (520). EVs derived from hypoxia did not influence apoptosis or viability in endothelial cells, suggesting the absence of any apoptotic signals within the vesicles. In contrast to this, monocyte-derived EVs have previously been shown to induce apoptosis in HUVECs via caspases 3, 6 and 7 (521). Additionally, EVs did not alter oxidative stress within endothelial cells. Other studies have shown that endothelial-derived EVs are capable of affecting angiogenesis *in vitro*, via an increase in superoxide production (522). Furthermore, these EVs have been shown to express NADPH oxidase subunit p22^{phox}, and are capable of producing superoxide directly (523). EVs derived from hypoxia/reoxygenation-treated HUVECs have also been shown to be pro-apoptotic, pro-oxidative and directly pathogenic to cardiomyocytes *in vitro* (524). These effects were mediated by the ability of EVs to phosphorylate p38 and JNK1/2. Despite this, there is no evidence within this chapter that EVs, regardless of pre-treatment, have any effect on cell viability, apoptosis, or oxidative stress.

Endothelial EVs have also been shown to impair endothelial function, diminishing acetylcholine-induced vasorelaxation and NO production by rat aortic rings (522). Hypoxia has previously been shown to modulate eNOS expression, via destabilising eNOS mRNA and subsequently decreasing transcription of the gene (88). However, post-translational modifications have also been reported, including a reduction in the phosphorylation site Serine-1177, and an increase in phosphorylation at the inhibitory site Threonine-495 (89,90). However, any cellular adaptations of eNOS activity in hypoxia were not transferred via the EVs produced, as EVs had no effect on eNOS expression when incubated with HUVECs.

4.6.3 Limitations

Firstly, this chapter used the blood of healthy volunteers when analysing the effects of EVs on coagulation. This sample may not be truly reflective of a diseased individual, which may have altered properties which in turn may have influenced coagulation measures. Secondly, the level of PS exposure on EVs was not measured, which may have mediated some of the effects on coagulation observed in this study. Previous colleagues have observed no differences in Annexin V⁺ between normoxia and hypoxia-derived EVs (525), however the effect of NO₂⁻ was not investigated here.

Additionally, no mRNA or miRNA analysis was undertaken on the content of the EVs used in this chapter. This is a rapidly expanding area of research within the EV field which may be responsible, at least in part, for the alterations in expression of adhesion molecules observed in this chapter. Future studies should investigate how hypoxia and NaNO₂ treatment of HUVECs may alter the genetic content of the EVs released.

4.6.4 Conclusions

In summary, this chapter highlights the pro-coagulant and pro-inflammatory effects of hypoxia-derived endothelial EVs. Furthermore, the addition of NaNO_2 to hypoxic HUVECs appears to partially alleviate some of the pro-coagulant effects of the EVs produced, although this had no effect on the ability of EVs to influence leukocyte adhesion. EVs derived from HUVECs incubated under normoxia have no effect on coagulation or inflammation. Additionally, HUVEC-derived EVs have no effect on endothelial cell function; with no influence on eNOS expression, oxidative stress, or overall viability. Taking these results, future studies should assess the effect of NO_3^- supplementation in CVD patients on the function of circulating EVs.

**5 RESULTS III: THE EFFECT OF CHRONIC DIETARY
NITRATE SUPPLEMENTATION ON EXTRACELLULAR
VESICLES IN HEALTHY VOLUNTEERS**

5.1 Perspective

At the time of investigation, there was limited data on the effect of chronic dietary NO_3^- supplementation on plasma NO metabolites (NO_3^- , NO_2^- and RSNO). Thus, in collaboration with the Norwegian University of Science and Technology, I investigated the effect of NO_3^- supplementation (in the form of beetroot juice (BR juice)) on NO metabolites and EV concentration in healthy volunteers, over a 6 day period. This would allow us to investigate whether the results seen in the *in vitro* model used in previous chapters could be mirrored in an *in vivo* scenario. This study also investigated differences between acute and chronic plasma NO metabolite changes, and parallel changes in circulating EV number, which would be important for future use in CAD patients.

5.2 Introduction

The vascular endothelium was once considered the inactive packaging of the vascular network, with no particular functions other than selective permeability to water and electrolytes. Today, the endothelium is thought of as a large, endocrine organ with a wide range of homeostatic functions, capable of responding to environmental changes (418). Exposure to cardiovascular risk factors, or mechanical injury, can compromise endothelial cells leading to their dysfunction. Endothelial dysfunction has been linked with an increase in endothelial-derived EVs (353). Endothelial-derived EVs have previously been shown to independently predict cardiovascular events in CAD patients (526).

Given the growing body of evidence for EVs playing a functional role in the pathogenesis of various disease types, they represent an attractive target for therapeutic intervention. Thus far, the majority of research within the EV field has sought to characterise and fully elucidate the roles of EVs from various cellular origins within a range of disease states (527,528). However, there have been a small number of studies exploring the effect of several different interventions targeting EV production, both *in vitro* and *in vivo*.

A study by Tramonano *et al.* in 2004 assessed the effect of statins on EV concentration. *In vitro*, fluvastatin was shown to suppress TNF- α induced endothelial EV release (529). In this study, the Rho kinase inhibitor Y-27632 reproduced the effects seen by fluvastatin, suggesting a possible role for this pathway. Inactivation of the Rho/Rho kinase pathway indeed leads to impaired actin cytoskeletal organisation, which in turn leads to suppression of EV release (243). NO elicits many of its effects through cGMP/PKG signalling, with PKG phosphorylating Rho kinase, thus regulating Rho-mediated effects on the cytoskeleton (530,531). However, a separate group have since investigated the effect of cholesterol-lowering drugs on EV generation *in vivo* in CAD patients, where no significant changes were observed in the amount of circulating endothelial or platelet-derived EVs following simvastatin or ezetimibe treatment (532).

A second intervention that has been investigated involved the administration of dietary flavanols to CAD patients over a 30 day period (533). They found endothelial-derived EVs significantly decreased following ingestion of a “high flavanol” drink but remained unchanged following a “low flavanol” drink. The mechanism of this reduction was not described; however, it is possible that the reduction may be mediated by an enhancement in NO bioavailability, thus improving endothelial function. The modulation of NO bioavailability by flavanoids has been well documented previously, thought to be due to an increase in eNOS activity (534–536).

Interestingly, various lifestyle alterations have been investigated as to their effect on EV concentration. A 6 month aerobic-exercise training intervention successfully reduced both endothelial-derived EVs and the inflammatory mediator IL-6 in African Americans (537). The positive changes in inflammatory markers in this study were coupled with an increase in flow-mediated dilation (FMD). FMD is, at least in part, mediated by NO (538). Aerobic exercise is well documented to increase NO bioavailability (539–542), and thus may offer some mechanistic explanation as to the results seen in this study.

Finally, ingestion of a Mediterranean diet for 4 weeks has been shown to reduce total circulating EVs in elderly subjects. This diet was also shown to reduce endothelial damage and improve the regenerative capacity of the endothelium (543). Typically, a Mediterranean diet consists of NO_3^- rich vegetables (125). Indeed, the diet used in this study included significant amounts of swiss chard, a vegetable known for its high NO_3^- content, as demonstrated by its inclusion as a key ingredient in many dietary NO_3^- supplements widely used in sports and exercise medicine.

The unifying link between these interventions appears to be increases in NO bioavailability. Despite this, there are currently no studies assessing the effect of NO_3^- supplementation on EV production. Indeed, impaired NO production in HUVECs has previously been shown to enhance EV generation (438). NO_3^- supplementation offers a direct route of greatly increasing NO bioavailability via conversion to NO_2^- , and other bioactive NO metabolites (124,544). Additionally, no study has assessed the effect of long-term NO_3^- supplementation on RSNO formation in humans, with only acute increases being observed following a one-off dose of KNO_3 (545). However, 7 days of NO_3^- administration in mice has been shown to lead to significant increases in RSNO (546).

Here, I hypothesised that dietary NO_3^- supplementation would increase plasma NO metabolites and subsequently reduce circulating EVs in healthy volunteers.

5.3 Aims

The aims of this chapter were to

1. Investigate the effect of 6 days NO_3^- supplementation on NO metabolites (NO_3^- , NO_2^- and RSNO) in healthy volunteers
2. Assess the effect of this supplementation on the concentration and size of circulating plasma EVs
3. Analyse the protein content of the EVs before and after supplementation for markers of cellular origin

5.4 Methods

5.4.1 Subjects and protocol

This study was performed in collaboration with the Norwegian University of Science and Technology (NTNU), in Trondheim, Norway. A total of 8 healthy volunteers were recruited for this randomised, single-blind placebo controlled cross-over study. Subjects were included if they were healthy, recreationally active males, over the age of 18 with no prior history of pulmonary or CVD. Subjects were excluded if they were tobacco users, or took any dietary supplements. Subjects were instructed to refrain from alcohol and caffeine intake over the duration of the study, and were also instructed to avoid NO_3^- rich food and anti-bacterial mouthwash. Participants were instructed to arrive at the laboratory (NTNU) in a rested and hydrated state, at least 3 hours postprandial. Subjects were randomly allocated either 2 x 70 mL BEET IT Organic beetroot juice (BR juice, 12.88 mmol), or a NO_3^- depleted placebo of identical appearance, to be ingested once daily, for a total of 6 days. The subjects then had a wash-out period of 8 days prior to receiving the alternate treatment. Blood samples were obtained from the antecubital vein through an 18g IV cannula into EDTA and citrate vacutainers[®]. Blood samples were taken immediately prior to ingestion of the BR juice, and two hours post-ingestion, on day 1 and day 6 of supplementation. Ethical approval was given by the Regional Committees for medical and health research ethics (REK) (Reference: 2014/2095/REK-midt). The study conformed to the ethical principles contained in the Declaration of Helsinki.

5.4.2 Plasma NO metabolites

NO metabolites were measured as described in section 2.6. Briefly, blood samples were collected into EDTA vacutainers and immediately centrifuged at 2,500g for 15 min. Plasma was subsequently isolated and snap frozen in liquid nitrogen, and stored at -80°C until analysis.

5.4.3 EV isolation

EVs were isolated from platelet-poor plasma using differential ultracentrifugation, as outlined in section 2.4.2, with minor amendments. Plasma was rendered acellular following 2 x 15 min. 2,500g centrifugations and slow-frozen at a rate of 1°C a minute to -80°C in NTNU. Following material transfer of acellular plasma from NTNU to Cardiff, plasma was thawed and ultracentrifuged at 100,000g for 1 hour. The resultant pellet was resuspended in filtered PBS, stored at 4°C and used within 48-72 hours of isolation.

5.4.4 EV size and concentration

EV size and concentration were determined using nanoparticle tracking analysis, as described in section 2.3. 5 x 60 second videos were recorded and analysed for each sample, with the mean values being used in subsequent analysis. EV concentration was expressed as EVs/mL.

5.4.5 Time resolved fluorescence

The surface protein expression of EVs was analysed using an immunophenotyping assay as outlined in section 2.5. Markers of the main producers of circulating EVs (platelet, leukocyte, erythrocyte, endothelial) were used as an indication of the cell-of-origin of the EVs.

Measurements were made using a BMG CLARIOstar (BMG Labtech, UK).

5.4.6 Statistics

Data were analysed according to “Practical Statistics for Medical Research” by Altman et al (417). All data were assessed for both a period effect and a treatment-period interaction, and checked for normality using the Kolmogorov-Smirnov test. The change in measurement between time points was calculated and compared directly to placebo using a 2-way ANOVA. Data were analysed using GraphPad Prism version 5.0 (GraphPad Software, San Diego, USA). Data are expressed as mean \pm standard error of the mean (SEM) unless stated.

5.5 Results

5.5.1 Patient Characteristics

A total of 8 males participated in the study with an average age of 33.5 ± 3.0 years, an average height of 182.5 ± 3.0 cm, an average weight of 83.9 ± 4.5 kg and an average body mass index (BMI) of 25.1 ± 1.0 kg/m². No period effects or treatment-period interactions were observed for any of the parameters determined in this study.

5.5.2 Plasma NO metabolites

5.5.2.1 Plasma NO₃⁻

There was no difference in baseline plasma NO₃⁻ levels between placebo and BR juice (23.5 ± 1.2 μM vs 24.0 ± 1.5 μM, $p > 0.05$) (Figure 5.1A). As anticipated, following BR juice, plasma NO₃⁻ levels significantly increased compared to placebo 2 hours after ingestion of the supplement (Δ NO₃⁻: 489.6 ± 41.9 μM vs 0.4 ± 1.4 μM, $p < 0.001$). However, there was no significant increase in plasma NO₃⁻ after 5 days of BR juice supplementation (24 hours after last ingestion) compared to placebo (Δ NO₃⁻: 68.3 ± 11.6 μM vs 18.4 ± 7.5 μM, $p > 0.05$). 2 hours after BR juice ingestion on day 6, plasma NO₃⁻ levels again increased significantly compared to placebo (Δ NO₃⁻: 354.5 ± 81.8 μM vs -1.1 ± 1.1 μM, $p < 0.001$) (Figure 5.1B) to a similar level observed on day 1 of supplementation (510.1 ± 58.4 μM vs 493.1 ± 42.1 μM, $p > 0.05$) (Figure 5.1A).

5.5.2.2 Plasma NO₂⁻

Baseline levels of plasma NO₂⁻ were similar between placebo and BR juice treatments (161.1 ± 22.8 nM vs 145.5 ± 17.0 nM, *p* > 0.05) (Figure 5.1C). 2 hours following ingestion of BR juice, plasma NO₂⁻ levels rose significantly in comparison to placebo (ΔNO₂⁻: 339.2 ± 54.3 nM vs -7.7 ± 18.6 nM, *p* < 0.001). After 5 days of BR juice, basal plasma NO₂⁻ did not significantly increase compared to placebo (ΔNO₂⁻: 65.7 ± 42.5 nM vs 31.6 ± 31.5 nM, *p* > 0.05). On day 6 of BR juice supplementation, plasma NO₂⁻ increased significantly compared to placebo (ΔNO₂⁻: 259.9 ± 68.0 nM vs -30.1 ± 36.1 nM, *p* < 0.001) (Figure 5.1D). Peak plasma NO₂⁻ measured 2 hours post-BR juice was similar on both day 1 and day 6 of supplementation (484.7 ± 8.2 nM vs 471.1 ± 90.0 nM, *p* > 0.05) (Figure 5.1C).

5.5.2.3 Plasma Nitrosothiol (RSNO)

Plasma RSNO levels were similar at baseline in both treatment groups (placebo: 24.1 ± 3.8 nM vs BR juice: 16.2 ± 2.0 nM, *p* > 0.05) (Figure 5.1E). Plasma RSNO levels increased significantly 2 hours after BR juice, compared to placebo (ΔRSNO: 125.9 ± 16.8 nM vs 0.6 ± 2.5 nM, *p* < 0.001). Basal levels of RSNO did not increase significantly between day 1 and day 6 compared to placebo (ΔRSNO: 7.2 ± 4.0 nM vs -2.9 ± 3.0 nM, *p* > 0.05). 2 hours following BR juice on day 6, plasma RSNO again significantly increased compared to placebo (ΔRSNO: 128.45 ± 32.0 nM vs -2.1 ± 2.5 nM, *p* < 0.001) (Figure 5.1E) to a similar level observed on day 1 of supplementation (151.9 ± 32.6 nM vs 142.1 ± 17.0 nM, *p* > 0.05) (Figure 5.1F).

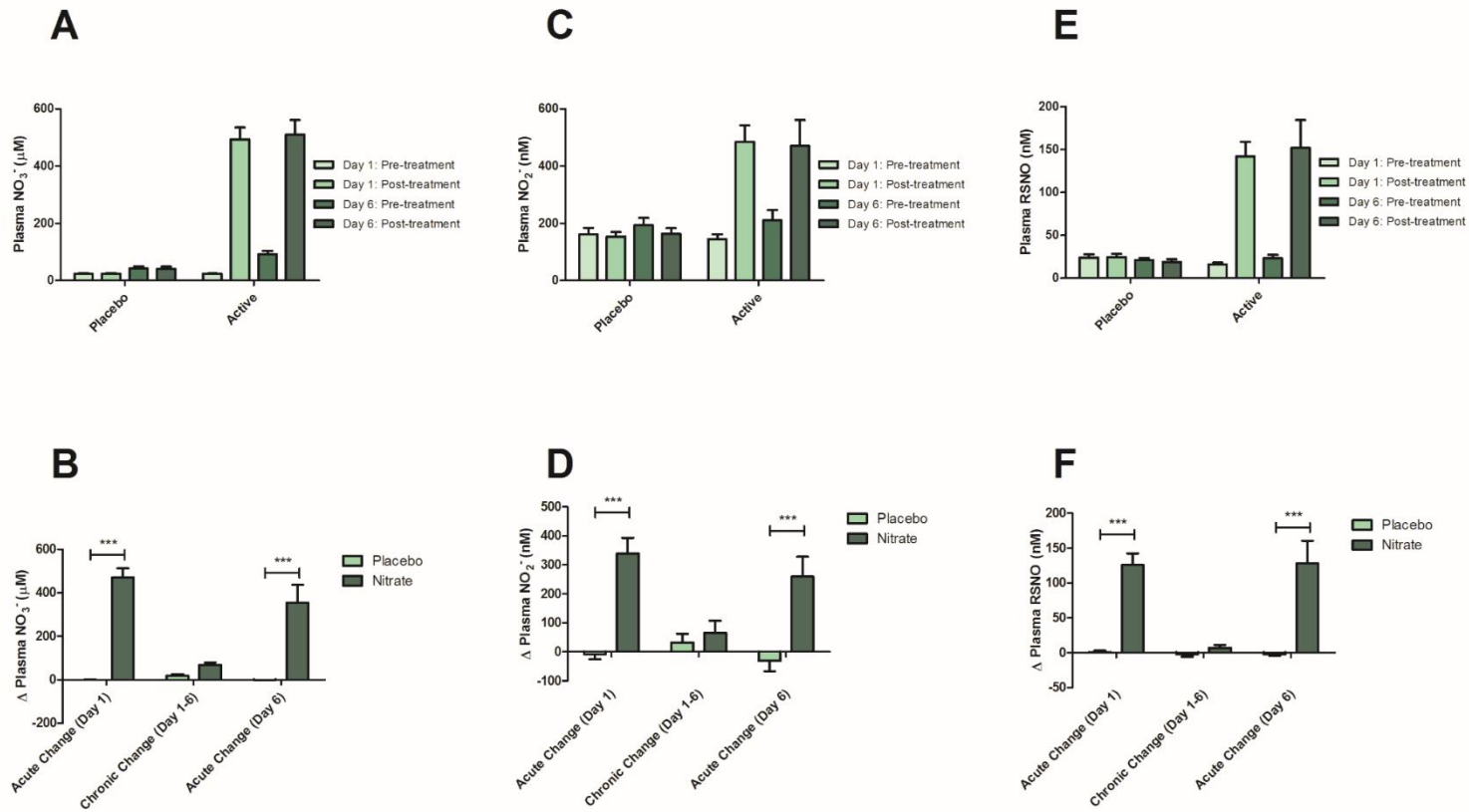


Figure 5.1 Plasma NO metabolites following 6 days BR juice supplementation. Plasma NO₃⁻ (μM) (A) NO₂⁻ (nM) (C) and RSNO (nM) (E) values following both placebo and BR Juice. (B) Comparison of the change in plasma NO₃⁻ (B) NO₂⁻ (D) and RSNO (F) following BR Juice or placebo. Data are represented as mean ± SEM [n=8]. *** reflects p < 0.001

5.5.3 EV size and concentration

Baseline plasma EV levels did not differ significantly between BR juice and placebo (BR Juice: $3.21e^{11} \pm 2.69e^{10}$ EVs/mL plasma vs placebo: $2.72e^{11} \pm 3.41e^{10}$ EVs/mL plasma, $p > 0.05$) (Figure 5.2A). 2 hours following supplementation, plasma EV concentrations did not alter significantly compared to placebo (Δ EVs: $-2.5e^9 \pm 2.58e^{10}$ EVs/mL vs $4.375e^9 \pm 2.64e^{10}$ EVs/mL, $p > 0.05$), respectively. After 6 days of BR juice, there was no significant change in EV concentration compared to placebo (Δ EVs: $1.88e^{10} \pm 5.02e^{10}$ EVs/mL vs $-4.82e^{10} \pm 4.83e^{10}$ EVs/mL, $p > 0.05$), respectively. Finally, on day 6, 2 hours following the final BR juice supplementation, plasma EV levels did not alter significantly in comparison to the placebo (Δ EVs: $-4.00e^{10} \pm 4.12e^{10}$ EVs/mL vs $-3.38e^{10} \pm 3.93e^{10}$ EVs/mL, $p > 0.05$), respectively (Figure 5.2B).

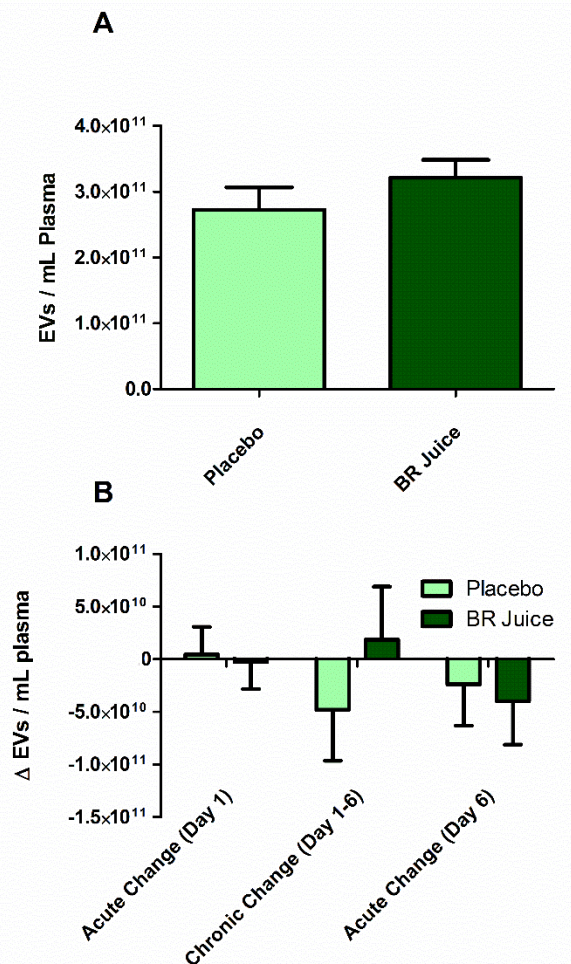


Figure 5.2 Plasma EV concentrations following 6 days BR juice / placebo. (A) EV concentrations at baseline for both placebo and BR juice. (B) Changes in circulating EV concentration following BR juice or placebo between various time points. Data are represented as mean \pm SEM [n=8].

Similarly, no differences in EV size were observed prior to treatment (BR Juice: 117.3 ± 7.6 nm vs placebo 136.5 ± 9.4 nm, $p > 0.05$), nor indeed over the entire course of the study, in either placebo or BR juice groups (Figure 5.3A). No change in mean EV size was observed following either BR juice or placebo over the course of the study ($p > 0.05$ for all comparisons) (Figure 5.3B). Furthermore, no changes in the size distribution profile of EVs were observed between BR juice and placebo at the acute change (day 1) (Figure 5.4A), chronic change (day 1-6) (Figure 5.4B) or acute change (day 6) (Figure 5.4C) time points. Appendix 1.2A-C details the changes in size distribution profile following BR juice or placebo.

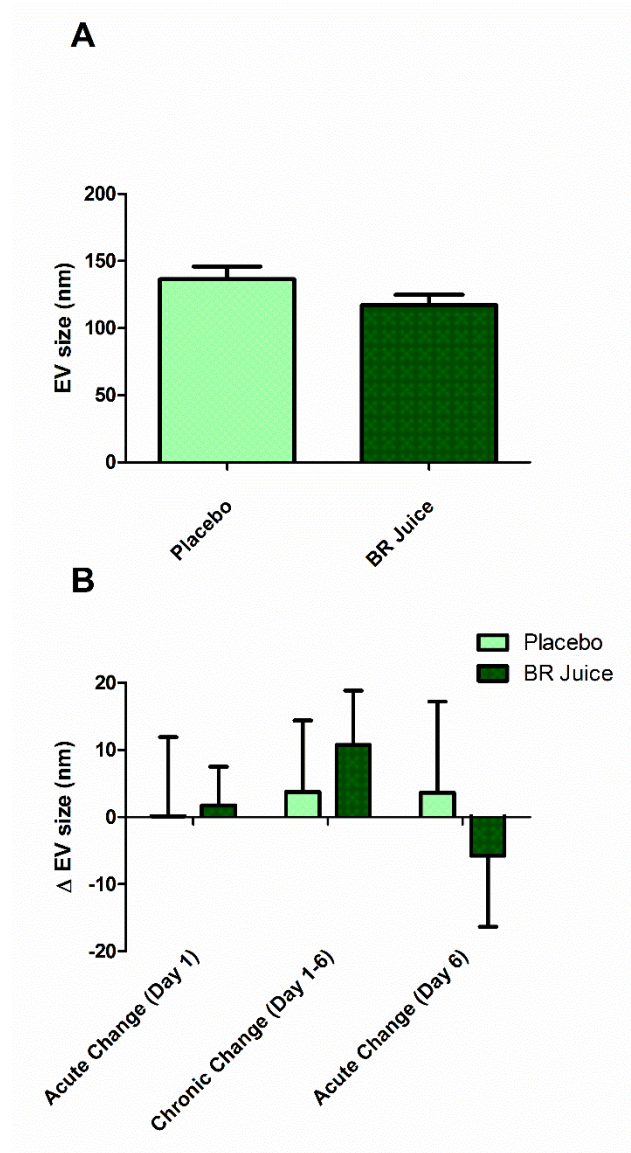


Figure 5.3 Plasma EV size following 6 days BR juice or placebo. (A) Mean EV size at all baseline for placebo and BR juice. (B) Changes in mean EV size following BR juice or placebo between various time points. Data are represented as mean \pm SEM [n=8].

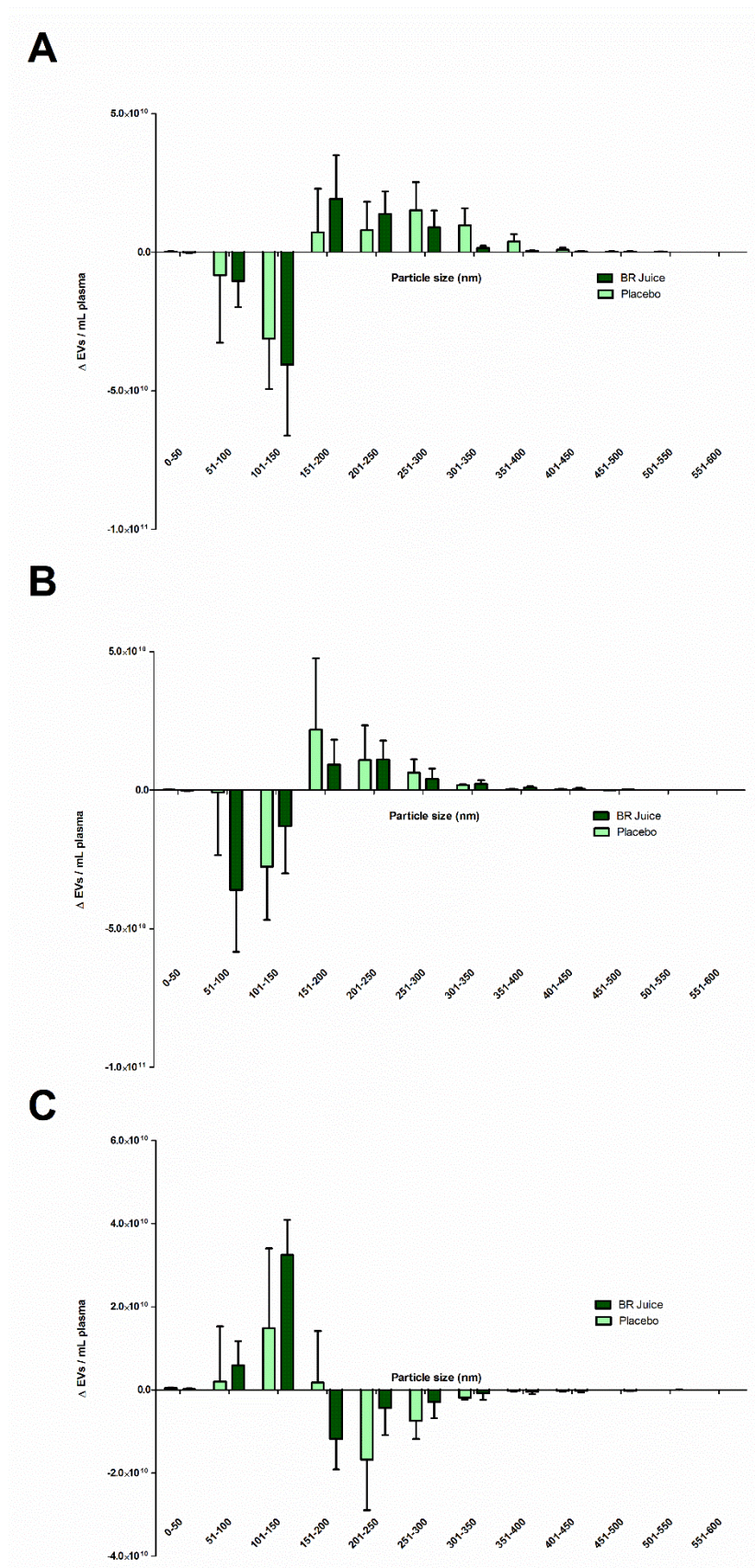


Figure 5.4 The effect of BR juice on size distribution profile of EVs. (A) Acute change (Day 1). (B) Chronic change (Day 1-6). (C) Acute change (Day 6). Data are represented as mean ± SEM [n=8].

5.5.4 EV immunophenotyping

Comparison between BR juice and placebo groups revealed that there was no significant difference between any of the markers at baseline (Appendix 1.3). Comparing the change in expression of markers observed between BR juice and placebo treatment revealed no significant changes across all time points for CD9 (Figure 5.5A), CD41 (Figure 5.5B), CD11b (Figure 5.5C), CD235a (Figure 5.5D) and CD144 (Figure 5.5E) ($p > 0.05$ for all comparisons).

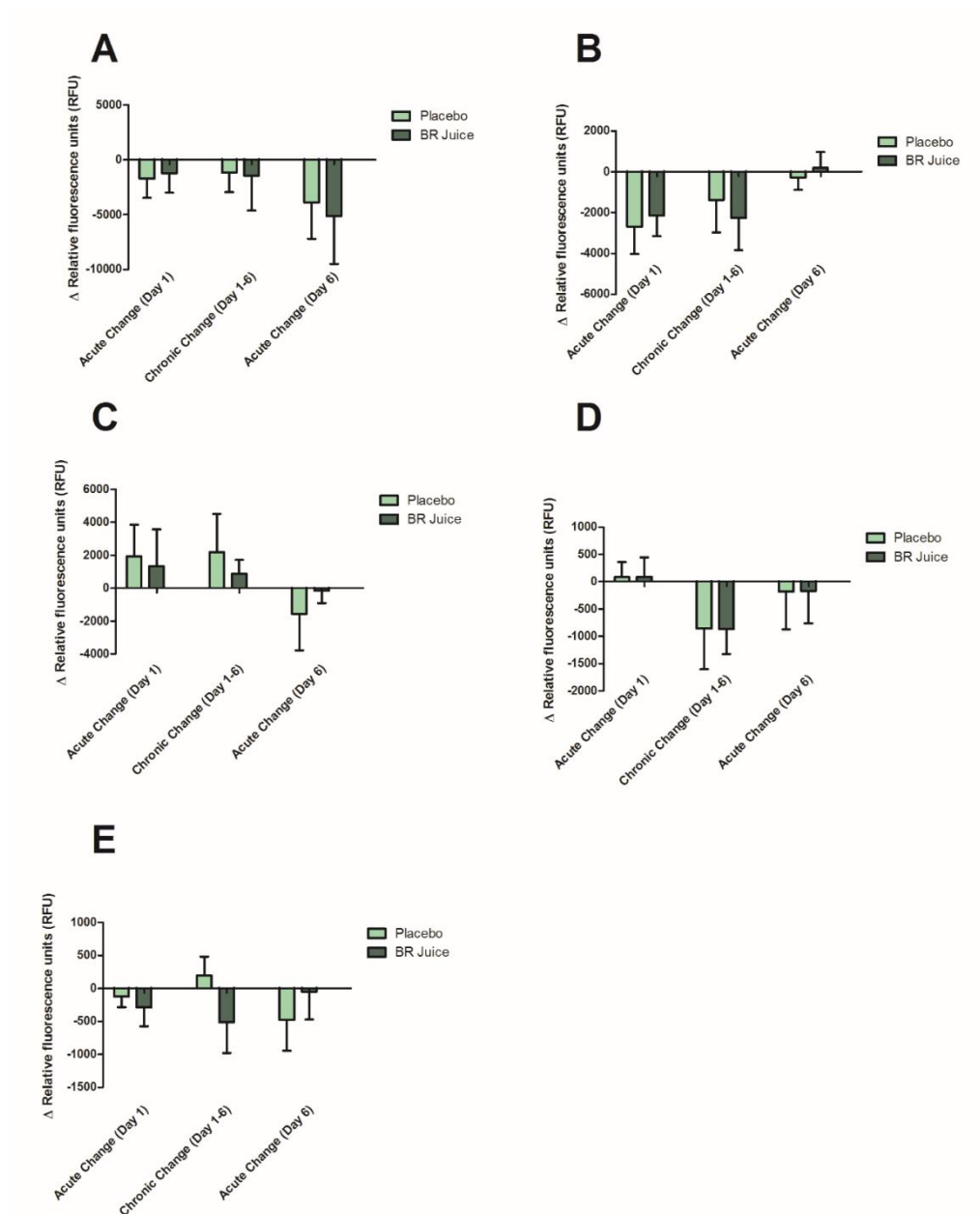


Figure 5.5 Changes in EV surface proteins following BR juice or placebo. (A) CD9, (B) CD41, (C) CD11b, (D) CD235a, (E) CD144. Proteins were detected using a streptavidin-europium conjugate and measured using time resolved fluorescence (relative fluorescence units). Data are represented as mean \pm SEM [n=8].

5.6 Discussion

5.6.1 Key Findings

- BR juice significantly elevated plasma NO_3^- , NO_2^- and RSNO 2 hours following supplementation.
- After 5 days of BR juice, 24 hours following the last supplement, plasma NO metabolites reverted back to near-baseline levels, suggesting an inability to elicit an “accumulative” effect.
- Daily BR juice supplementation had no effect on total circulating EVs in healthy volunteers over 6 days.
- Within the EV sample, no change in parental cell markers were observed following BR juice supplementation.

5.6.2 Main discussion

Diets rich in fruit and vegetables have long been associated with a reduced risk of developing CVD (157). Determining how these foods provide protection against CVD could potentially allow for therapeutic gain. Previously, this has been attributed to the anti-oxidant vitamin content of vegetables. However, a large scale meta-analysis of randomised trials did not support this hypothesis (547). More recently, evidence is accumulating suggesting that the NO_3^- content in vegetables, such as beetroot, are responsible for beneficial cardiovascular outcomes, such as a reduction in blood pressure, a reduction in platelet aggregation, and an improvement in revascularisation following chronic ischemia (162,163,548,549).

Dietary NO_3^- supplementation results in subsequent increases in plasma NO_2^- , as our group and others have previously established (156,163,550,551). In this study, a total NO_3^- load of 12.88 mmol from BR juice resulted in a peak plasma NO_3^- concentration of approximately 480 μM (an increase of approximately 460 μM) 2 hours post-supplementation. This is in agreement with previous studies which have shown a 350 μM increase (25-375 μM) following a 11.2 mmol NO_3^- load (162), and a 570 μM increase (30-600 μM) following a 16.8 mmol NO_3^- load (552). As shown by James *et al*, the relationship between NO_3^- dose given and peak plasma NO_3^- appears to be linear (124). Furthermore, the resulting increase in plasma NO_2^- following BR juice was approximately 340 nM (145-485 nM). Again, this is within the range expected given the NO_3^- dose in comparison to other studies (124).

In contrast to NO_3^- and NO_2^- , only a few studies have assessed the effect of NO_3^- supplementation on RSNO formation. Hendgen-Cotta *et al* have shown in mice that dietary NO_3^- over 7 days (150 μmol per day) can significantly increase plasma RSNO levels (in addition to NO_3^- and NO_2^-), reaching 349 nM (546). Interestingly, NO_2^- and RSNO concentrations were markedly lower in mice that underwent an antibacterial mouthwash, supporting the hypothesis that RSNO is produced from NO_2^- rather than NO_3^- . Furthermore, this study showed that NO_3^- supplementation attenuated apoptosis of regenerative myoblasts in ischemic tissue, an effect which was abolished by preventing the conversion of NO_3^- to NO_2^- via antibacterial mouthwash (549). Pinheiro *et al* have shown similar increases in RSNO in a rat model of renovascular hypertension. Treatment with a thiol-depleting agent buthionine sulfoximine attenuated the increase in plasma RSNO, and also blunted the antihypertensive effects of NO_2^- previously observed (553). Despite differences between humans and rodents in their metabolism (554), these studies, in combination with my results, suggest that the beneficial effects of NO_3^- supplementation in humans may be, in part, due to formation of RSNO. Specifically, under conditions whereby the optimal conditions for NO_2^- reduction to NO are not met, RSNO may offer an alternative route, or an additional step, within the nitrate, nitrite, nitric oxide pathway.

To my knowledge, the only previous study assessing the effect of dietary NO_3^- supplementation on plasma RSNO levels in humans is by Richardson *et al* (545). They showed that KNO_3 (2mmol) in healthy volunteers increased gastric RSNO and inhibited platelet function in humans over 2 hours. Baseline plasma RSNO levels were similar to those seen in this chapter (≈ 25 nM), and did not alter following KNO_3 ingestion. RSNO molecules have been shown to have potent anti-platelet effects in numerous studies (555–557), via both a cGMP dependent (558) and independent mechanism (559). Unfortunately, platelet function was not measured in this study, however no reduction in the platelet marker CD41 was observed in the EV population of this healthy cohort.

No significant change in the circulating EV concentration was observed following BR juice over a 6 day period. This is in contrast to previous studies which have observed a reduction in plasma EVs following an increase in NO bioavailability, albeit indirectly (537,543). Interestingly, basal levels of plasma EVs in these healthy volunteers were notably lower than those observed in a disease cohort (hypercholesterolaemia) measured previously by our research group ($\approx 3e^{11}$ vs $\approx 2e^{12}$) (560). This is in agreement with the literature which states that EVs are greatly elevated in various CVD states (561,562). Specifically, EVs derived from platelets and endothelial cells appear to be most commonly elevated (385,562–564). This elevation can be explained by continuous platelet and endothelial cell activation in CVD states, as EV release is synonymous with cell activation (243). The EV concentrations observed in this study likely reflect healthy individuals with a low level of disease, and hence reduced inflammatory cellular activation. It is possible that this represents a

“basal” level of EV release which is elevated in disease, and only following this can NO_3^- supplementation alleviate the enhancement. Additionally, no changes within both the mean size of EVs, and the size distribution profile of the EVs, were observed. This confirms that BR juice did not selectively reduce either the exosome or microvesicle portion of the EV sample, which may have been masked looking at the overall EV concentration. Furthermore, no reductions in any of the parental cell markers were observed following beetroot juice. The lack of change of these markers suggests that the BR juice had no effect on EV production, regardless of cellular origin.

These results, in combination with other studies, are supportive of a hypothesis that NO_3^- supplementation can increase circulating RSNO levels, which may subsequently be able to elicit advantageous effects in CVD.

5.6.3 Limitations

A major limitation of this study is the small sample size ($n=8$). This study was performed in collaboration with the Norwegian University of Science and Technology (NTNU), with NTNU providing the samples. Recruitment of suitable volunteers proved challenging. Additionally, two volunteers had to be discounted and removed from the final results due to receiving an incorrect combination of BR juice / placebo. Secondly, the process of EV isolation was slightly compromised. Typically, platelet-free plasma (PFP) is isolated from whole blood and immediately centrifuged at $100,000 \times g$ for 1 hour. However, this was not possible at NTNU, therefore PFP was frozen at -80°C upon isolation and transferred to Cardiff upon completion of the study. Thus, some plasma samples had been frozen for > 3 months prior to EV isolation. Although this was not an issue for NO metabolite analysis, our research group have shown that long term storage of EVs in the freezer can alter their concentration (565). Additionally, there are concerns within the field that ultracentrifugation may co-pellet soluble proteins and lipoproteins, which can be detected by NTA. However, there is currently a lack of a standardised protocol within the EV field and methods are continuously being updated, each with its own advantages and disadvantages. Finally, no assessment of platelet function was performed in this study. Previous studies have shown a potent anti-platelet effect of RSNO. Despite a lack of reduction in circulating EVs, it is possible that RSNO may have had an effect on platelet activity.

5.6.4 Conclusions

In summary, this chapter has shown that dietary NO_3^- supplementation can significantly increase NO metabolites in the plasma of healthy volunteers, notably RSNO. Furthermore, after 5 days of BR juice, NO_3^- , NO_2^- , and RSNO values appear to return to near-baseline levels 24 hours following the last supplementation, suggesting that a build-up of an “NO-reservoir” is not possible.

However, future studies should assess the effect of longer term NO_3^- supplementation on NO metabolites. No effect on EV concentration, size, or size distribution was observed following BR juice over a 6 day period. These results suggest that increasing NO bioavailability has no effect on circulating EVs in healthy volunteers.

**6 RESULTS IV: THE EFFECT OF ACUTE DIETARY
NITRATE SUPPLEMENTATION ON EXTRACELLULAR
VESICLES IN CORONARY ARTERY DISEASE PATIENTS**

6.1 Perspective

Following the lack of a reduction in circulating EV in healthy volunteers, a randomised, double-blind, placebo controlled study was designed to assess the effect of dietary NO_3^- supplementation on EV concentration in CAD patients. As per chapter 5, NO metabolites (NO_3^- , NO_2^- , RSNO) were assessed, in addition to plasma EV concentration, platelet activity and EV surface content. CAD patients were split into 2 groups based on whether they were currently prescribed clopidogrel. Our research group has shown previously that clopidogrel, with NO_2^- , can produce an RSNO derivative (clopidogrel-SNO). This study allowed comparison of the effects of NO_3^- supplementation in CAD patients on and off clopidogrel.

6.2 Introduction

EVs have been implicated as a biomarker in many disease states, including CVD, as discussed in Chapter 1. EVs have been shown to play a role in promotion of coagulation, inflammation, and cell survival (340,566–568). Elevated levels of EVs have been reported in a number of CVD states, such as CAD and ischemic stroke (354,569,570). Furthermore, elevated levels of EVs in CAD patients have been shown to correlate with cardiovascular outcomes. Sinning *et al* showed that EVs were significantly higher in patients with major adverse cardiovascular and cerebral events (MACCE) compared to patients without an event (385). Therefore, EVs within a CVD setting represent an attractive target for pharmacological or dietary intervention.

Arguably, within the EV field, platelet-derived EVs have received the most attention, primarily due to their relative abundance and reactivity (247). Elevated platelet EV levels have been associated with numerous disease states, including heparin-induced thrombocytopenia, arterial thrombosis, sickle cell disease and rheumatoid arthritis (571–574). Furthermore, platelet-derived EVs have been implicated in the pathogenesis of atherosclerosis, playing an important role in the thrombotic process, in addition to eliciting pro-inflammatory effects (575). Thus, the central role of platelets in the development of atherosclerosis is further accelerated by the EVs they produce. It is said that the surface of platelet-derived EVs is between 50- to 100-fold more pro-coagulant than the surface of an activated platelet, primarily due to high level of PS exposure, as well as other surface markers that stimulate fibrin clot formation (333).

Anti-platelet therapy plays a fundamental role in the management of CVD. Thienopyridines (clopidogrel, prasugrel, ticlopidine) act primarily via irreversible inhibition of the P₂Y₁₂ receptor, a subtype of the ADP receptor, preventing the activation of platelets. Interestingly, in addition to their anti-platelet actions, pleiotropic effects of thienopyridines have been reported, independent of the P₂Y₁₂ receptor, especially for clopidogrel (576). These include increases in NO bioavailability, anti-inflammatory effects and reductions in endothelial dysfunction (577–579). A study by Behan *et al* showed that clopidogrel treatment reduced EV formation in parallel with a reduction in platelet activation and pro-coagulant activity (580).

NO plays a pivotal role in maintaining both platelet and endothelial cell homeostasis. However, NO bioavailability is compromised in CVD, leading to the progression of atherosclerosis and vascular dysfunction (581). NO can inhibit platelet activation via the cGMP pathway, offering an alternative route of inhibition to thienopyridines. When both pathways are activated, *ex vivo* studies have highlighted a synergistic antiplatelet effect is achieved, culminating in a reduction in intracellular calcium (582,583).

The effect of dietary NO_3^- supplementation is well documented in exercise physiology, and more recently in CVD, where it has been shown to reduce blood pressure, improve vascular function and reduce platelet aggregation (162,167,584). Moreover, previous studies have shown that sustained release (organic) nitrates can act synergistically with clopidogrel, augmenting platelet inhibition in patients undergoing PCI (585).

RSNOs are formed by the nitrosation of reduced sulphydryl groups, and appear to play a role in many aspects of cardiac function, including inflammation and platelet function (555,557,586,587). RSNOs represent a means for the storage and transport of NO within the circulation (588,589). Our group have previously demonstrated that thienopyridines are capable of forming RSNO molecules, dependent on both NO_2^- availability and a low pH, both of which are present in the stomach (409,590). These “thienopyridine-SNO” (Th-SNO) molecules are able to donate NO *in vivo*, hence increasing NO availability.

In light of these collective observations, I hypothesised that dietary NO_3^- supplementation, in combination with clopidogrel therapy, would increase circulating RSNO levels, and subsequently reduce circulating EVs in individuals with CAD.

6.3 Aims

The aims of this chapter were to

1. Investigate the effect of acute dietary NO_3^- supplementation on NO bioavailability, by measuring plasma NO_3^- , NO_2^- , and RSNO levels compared to placebo.
2. Assess the effect of acute dietary NO_3^- supplementation, both alone and in combination with clopidogrel, on platelet function.
3. Investigate the effect of acute dietary NO_3^- supplementation on circulating EV levels in CAD patients compared to placebo.
4. Assess the cellular origin of the EVs before and after NO_3^- supplementation.
5. Investigate the role of “clopidogrel-SNO” on platelet-derived EV *ex vivo*.

6.4 Methods

6.4.1 Subjects and protocol

20 CAD patients consented to participate in this randomised, double-blind, placebo-controlled, cross-over study of dietary NO_3^- vs placebo, in two groups of patients: Those receiving 75 mg clopidogrel daily (n=10), and those receiving no thienopyridine treatment, referred to henceforth as “naïve” (n=10). Patients attended the Cardiology Day Case Unit at the University Hospital of Wales (UHW). All patients were randomly allocated either 2 x 60 mL (8.1 mmol total) of dietary NO_3^- supplement (Science in Sport Go⁺ Nitrates gel), followed by a placebo of identical appearance, or placebo followed by NO_3^- supplementation. We adopted a wash-out period of at least 7 days, in agreement with several other groups (591,592). Our group have shown previously that 24 hours following ingestion of this dose of NO_3^- , plasma NO_3^- and NO_2^- values have returned to baseline (124). Figure 6.1 summarises the study design. Blood samples were obtained from the antecubital vein through an 18g IV cannula into EDTA, citrate, and hirudin vacutainers[®]. Samples were taken both before ingestion of the supplement and two hours post-supplementation. The pharmacokinetics of blood NO metabolite both before and for 24 hrs following ingestion of NO_3^- have been well characterised (124). Patients were fasted for at least 12 hours prior to attendance and took their prescribed medication at least 1 hour prior to the study. Patients were included if they were male, over the age of 18 with stable CAD, were attending the cardiology day case unit and had been fasted for > 12 hours. Patients in the clopidogrel group must have been receiving clopidogrel for > 1 month prior to commencement of the study. Patients were excluded if they had a clopidogrel intolerance or contraindication, were on other long-term oral anticoagulant drugs, or receiving intravenous or subcutaneous antithrombin therapy. Patients were also excluded if they had any ischemic event (ACS, stroke or TIA) or revascularisation procedure (PCI or CABG) within the preceding 3 months, chronic renal or liver disease, or an inability to give informed consent. Ethical approval was provided by the South East Wales Research Ethics Committee (IRAS Project ID 102427).

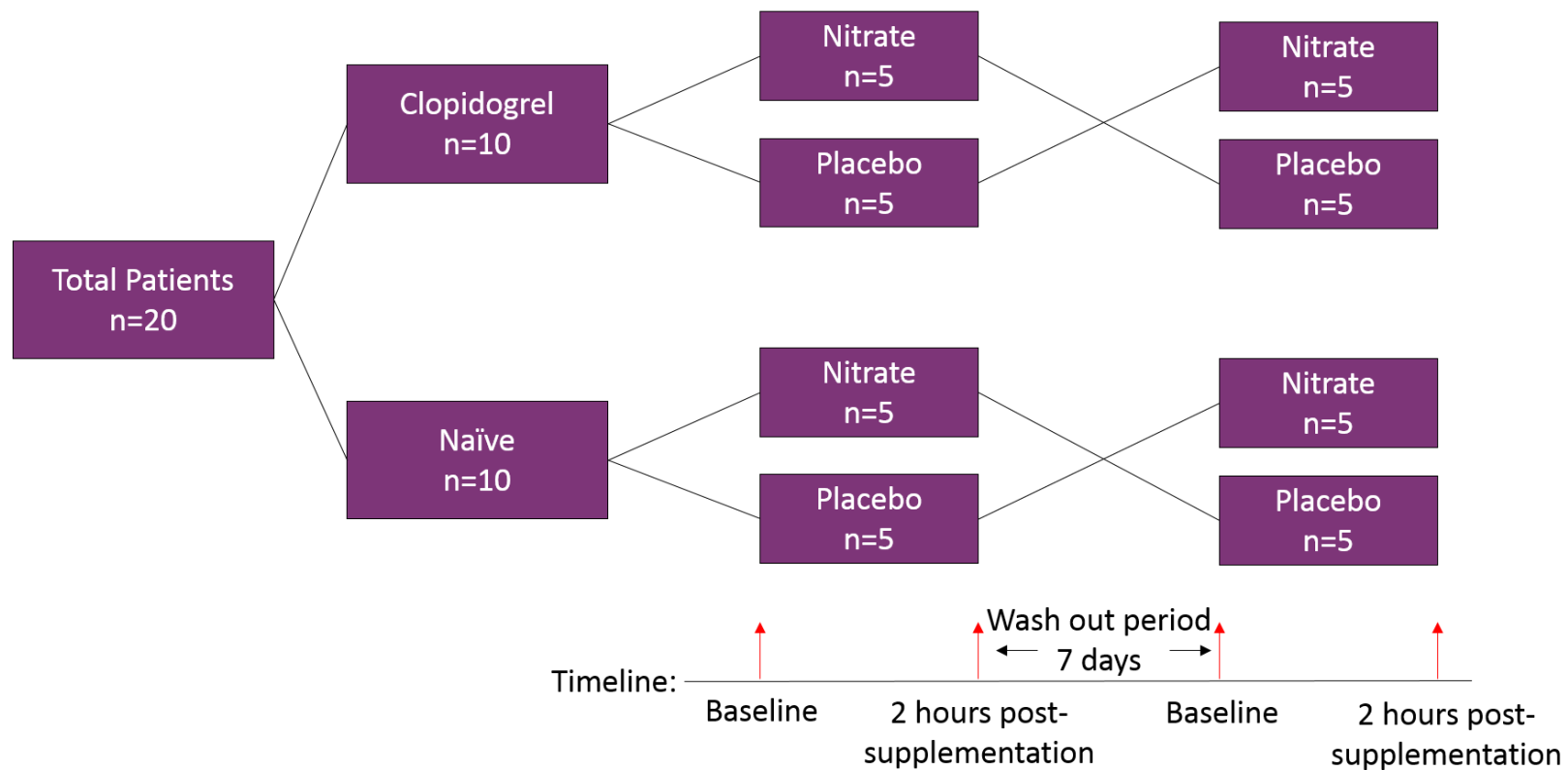


Figure 6.1 Study design. Patients were split into those receiving clopidogrel 75 mg daily (n=10) and those receiving no thienopyridine treatment (naïve, n=10). Patients were randomly assigned to either NO₃⁻ supplementation (Science in Sport Go⁺ Nitrates gel), followed by a placebo of identical appearance, or vice-versa. A washout interval of a minimum of seven days separated the two treatment periods. Blood samples were taken immediately before ingestion of the supplement and two hours post-supplementation, as indicated by red arrows.

6.4.2 Biochemical measurements

A full blood count was measured on an ABX-Pentra X120 haematology blood analyser (Horiba, Northampton, UK). Serum cholesterol and triglycerides were assessed using an Aeroset automated analyser (Abbott Diagnostics, Berkshire, UK). LDL-cholesterol was calculated using Friedewald's formula. C-reactive protein was assayed by nephelometry (BN-II system, Dade Behring, Milton Keynes, UK). The intra- and inter-assay coefficients of variation were all less than 9%. All biochemical measurements were carried out by the Department of Medical Biochemistry, UHW.

6.4.3 Plasma NO metabolites

Plasma NO metabolites (NO_3^- , NO_2^- , and RSNO) were measured as outlined in section 2.6. Blood samples were collected into EDTA vacutainers and immediately centrifuged at 2,500 *g* for 15 minutes. The plasma was then isolated and subsequently snap frozen in liquid nitrogen, and stored at -80°C until analysis.

6.4.4 Platelet aggregation

Whole blood aggregation was assessed by multiple electrode aggregometry, as described in section 2.9. Whole blood was collected into hirudin vacutainers® and analysed within 30 minutes of blood drawing.

6.4.5 EV isolation

EVs were isolated from platelet-poor plasma using differential ultracentrifugation as detailed in section 2.4.2. EV samples were stored at 4°C and used within 48-72 hours of isolation.

6.4.6 EV size and concentration

EV size and concentration were determined using nanoparticle tracking analysis, as outlined in section 2.3. 5 x 60 second videos were recorded and analysed, with the mean subsequently used in further analysis. EV concentration was expressed as EVs/mL.

6.4.7 Time-resolved fluorescence

The surface protein expression of EVs was assessed using an immunophenotyping assay, as outlined in section 2.5. Markers of the main producers of circulating EVs (platelet, leukocyte, erythrocyte, endothelial) were used as an indication of the cell-of-origin of the EVs. Measurements were made using a BMG FLUOstar OPTIMA (BMG Labtech, UK).

6.4.8 *Ex vivo* platelet EV production

The effect of RSNO on platelet EV production was investigated *ex vivo*, as outlined in section 2.7. Briefly, platelets (in platelet-rich plasma) were stimulated with ADP (6.5 μ M) and incubated with NaNO₂, clopidogrel, GSNO or clopidogrel-SNO (all 10 μ M) for 1 hour at 37°C. EVs were then isolated as described in section 2.4.2, and analysed using NTA and TRF, as described in sections 2.3 and 2.5, respectively.

6.4.9 Statistics

A power calculation based on unpublished prior results from CAD patients from our laboratory showed that 9 subjects would provide 90% power for detecting a 20% difference in circulating EVs between placebo and NO₃⁻ supplementation, assuming 10% variation, with $\alpha=0.05$. Data were analysed using GraphPad Prism version 5.0 (GraphPad Software, San Diego, USA). Data are expressed as mean \pm standard error of the mean (SEM) unless stated. Data were analysed and assessed for both a period effect and treatment-period interaction according to “Practical Statistics for Medical Research” by Altman *et al* (417). Data were assessed for normality using the Kolmogorov-Smirnov test. Baseline values were compared using a repeated measures ANOVA. The change in measurement before and after NO₃⁻ supplementation or placebo was calculated and compared directly using a paired t test. For *ex vivo* experiments, a 1-way ANOVA was performed to determine differences within groups, with Bonferroni’s multiple comparison post-hoc test.

6.5 Results

6.5.1 Patient characteristics

Of the 20 males that participated in the study, 10 were taking clopidogrel (>1 month) and 10 were not receiving anti-platelet therapy (naïve group). The average ages of the groups were 63.2 ± 3.6 years and 62.7 ± 3.2 years, respectively. Biochemical measurements are summarized in table 6.1. Importantly, no differences were observed in platelet count at baseline or at the follow up visit. No differences were seen in age, BMI, and biochemical parameters between groups. Notably, patients on clopidogrel had a higher prevalence of cardiovascular risk factors (diabetes mellitus, smoking, hypertension), previous acute ischaemic events (MI, stroke/TIA) and revascularisation procedures (PCI/CABG) compared to the naïve group (Table 1). No significant period effects and treatment-period interaction were observed for any of the parameters determined in this study, performed following Altman *et al* (417).

Table 6.1 Patient characteristics.

Participant Characteristics	Naïve group (n=10)		Clopidogrel group (n=10)		P-value
Age	62.7 ± 3.19		63.2 ± 3.66		> 0.05
BMI (kg/m ²)	29.9 ± 1.49		28.2 ± 1.18		> 0.05
Cardiovascular Risk Factors					
Diabetes Mellitus	1 (10%)		2 (20%)		
Past/Current Smoking	3 (30%)		6 (60%)		
Hypertension	7 (70%)		8 (80%)		
Dyslipidaemia	10 (100%)		8 (80%)		
Family History of Premature Heart					
Disease (<65 years)	4 (40%)		2 (20%)		
Stroke/TIA	1 (10%)		2 (20%)		
Peripheral Vascular Disease	1 (10%)		1 (10%)		
History of MI	4 (40%)		7 (70%)		
Previous Revascularisation					
PCI	4 (40%)		7 (70%)		
CABG	2 (20%)		4 (40%)		
Respiratory Disease (Asthma/COPD)	0 (0%)		3 (30%)		
Medications					
Aspirin	7 (70%)		4 (40%)		
Clopidogrel	0 (0%)		10 (100%)		
Proton Pump Inhibitor	5 (50%)		7 (70%)		
Beta Blockers	4 (40%)		6 (60%)		
ACEi/ARB	6 (60%)		8 (80%)		
Statins	10 (100%)		8 (80%)		
GTN	1 (10%)		1 (10%)		
Thyroxin	1 (10%)		0 (0%)		
NSAIDs	0 (0%)		2 (20%)		
Oral Anti-Coagulants	1 (10%)		0 (0%)		
Calcium Channel Blockers	2 (20%)		1 (10%)		
Diuretics	2 (20%)		2 (20%)		
Biochemical Measures					
CRP (mg/L)	5.3 ± 4.27		4.90 ± 4.63		> 0.05
Total Cholesterol (mmol/L)	4.58 ± 0.77		4.30 ± 0.82		> 0.05
Triglycerides (mmol/L)	2.1 ± 1.80		1.47 ± 0.90		> 0.05
HDL (mmol/L)	1.11 ± 0.26		1.07 ± 0.13		> 0.05
LDL (mmol/L)	2.61 ± 0.54		2.57 ± 0.68		> 0.05
Total Cholesterol:HDL Ratio	4.13 ± 1.69		4.02 ± 0.57		> 0.05
Haematological Measures					
	Visit 1	Visit 2	Visit 1	Visit 2	
White Cell Count (x10 ⁹ /L)	6.0 ± 0.50	6.3 ± 0.6	6.7 ± 0.6	6.4 ± 0.3	> 0.05
Haemoglobin (g/L)	149.1 ± 3.1	151.5 ± 3.6	147.5 ± 3.4	144.9 ± 3.4	> 0.05
Platelet Count (x10 ⁹ /L)	232.8 ± 25.0	219.4 ± 16.1	234.7 ± 13.4	237.8 ± 18.2	> 0.05

Summary of patient characteristics including age, BMI, cardiovascular risk factors, medications, biochemical and haematological measurements. Haematological measures were taken at the beginning of both patient visits, prior to any treatment.

6.5.2 Plasma NO metabolites

There was no significant difference between plasma NO_3^- , NO_2^- and RSNO levels between the naïve and clopidogrel groups at baseline (NO_3^- : $31.14 \pm 2.5 \mu\text{M}$ vs $31.34 \pm 5.1 \mu\text{M}$. NO_2^- : 92.3 ± 9.0 nM vs 118.9 ± 15.7 nM. RSNO: 6.4 ± 0.5 nM vs 11.9 ± 3.4 nM, all $p > 0.05$) (Figure 6.2). Following NO_3^- supplementation, plasma NO_3^- levels were significantly elevated in both the naïve (ΔNO_3^- : $252.1 \pm 17.4 \mu\text{M}$ vs $3.7 \pm 1.9 \mu\text{M}$, $p < 0.001$) (Figure 6.3A) and clopidogrel (ΔNO_3^- : $252.1 \pm 17.4 \mu\text{M}$ vs $3.7 \pm 1.9 \mu\text{M}$, $p < 0.001$) (Figure 6.3B) groups compared to placebo. Plasma NO_2^- also significantly increased in both the naïve (ΔNO_2^- : 167.8 ± 40.1 nM vs 18.5 ± 22.6 nM, $p < 0.05$) (Figure 6.3C) and clopidogrel (ΔNO_2^- : 164.8 ± 68.5 nM vs -5.2 ± 12.2 nM, $p < 0.05$) groups following NO_3^- supplementation, compared to placebo (Figure 6.3D). Interestingly, increases in plasma RSNO levels were not significantly different following NO_3^- supplementation compared to placebo (ΔRSNO : 0.9 ± 1.3 nM vs -1.3 ± 0.6 nM, $p > 0.05$) (Figure 6.3E). However, in the clopidogrel group, plasma RSNO was significantly increased following NO_3^- supplementation compared to placebo (ΔRSNO : 4.7 ± 0.8 nM vs 0.2 ± 0.5 nM, $p < 0.001$) (Figure 6.3F).

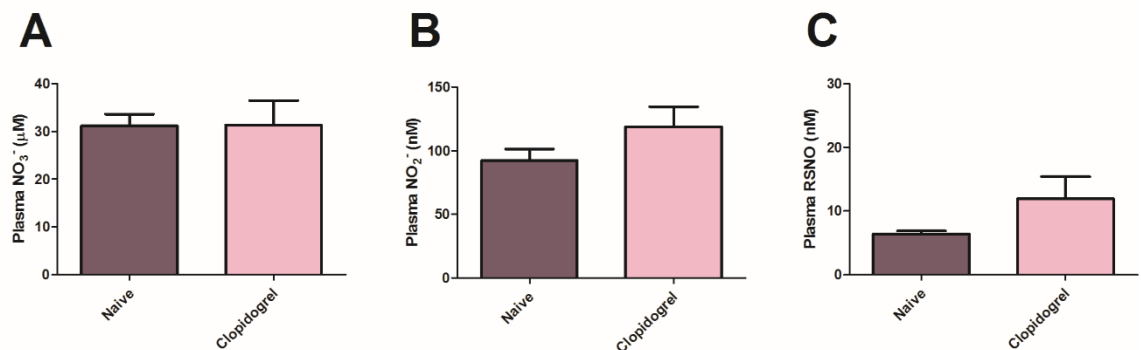


Figure 6.2 Baseline plasma NO metabolites. The difference in NO metabolites between the naïve and clopidogrel group. (A) Plasma NO_3^- levels, μM . (B) Plasma NO_2^- levels, nM. (C) Plasma RSNO levels, nM. Baseline refers to an average value for each patient calculated from blood samples taken from both visits prior to ingestion of either the NO_3^- supplement or placebo [n=10].

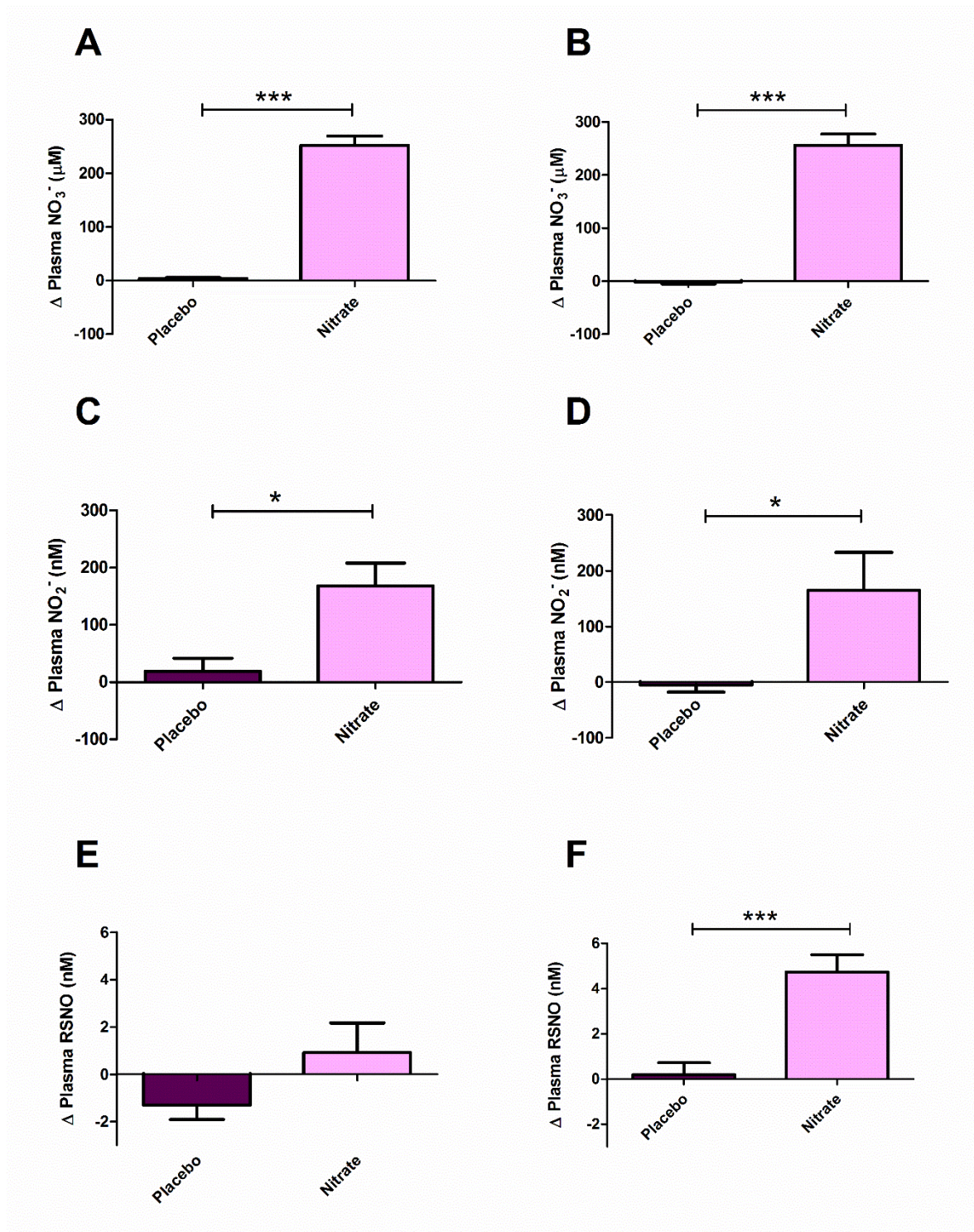


Figure 6.3. NO metabolite measurements. The change in plasma NO metabolites two hours post NO₃⁻ supplementation or placebo. (A) Naïve group plasma NO₃⁻, µM. (B) Clopidogrel group plasma NO₃⁻, µM (C) Naïve group NO₂⁻, nM. (D) Clopidogrel group plasma NO₂⁻, nM. (E) Naïve group plasma RSNO, nM. (F) Clopidogrel group plasma RSNO, nM. Data are expressed as mean ± SEM [n=10]. * and *** represent p < 0.05 and p < 0.001 respectively.

6.5.3 Platelet Aggregation

Platelet aggregation stimulated via the thrombin receptor (TRAP) was not significantly different between the naïve and clopidogrel groups at baseline (1081 ± 71 AU*min vs 1037 ± 66 AU*min, $p > 0.05$), respectively (Figure 6.4A). However, platelet activation stimulated via the ADP receptor was markedly lower in the clopidogrel group in comparison to the naïve group (395 ± 43 AU*min vs 636 ± 55 AU*min, $p < 0.001$) (Figure 6.4B).

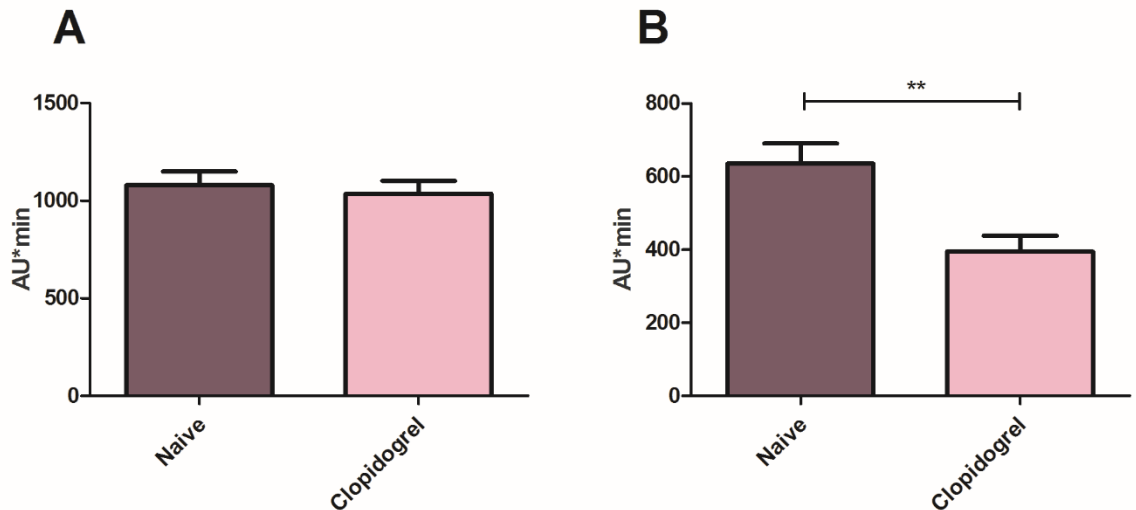


Figure 6.4 Baseline platelet aggregation. The difference in TRAP (A) and ADP (B) mediated platelet aggregation between the naïve and clopidogrel group. Baseline refers to an average value for each patient obtained from both visits prior to ingestion of either the NO_3^- supplement or placebo [n=10]. ** represents $p < 0.01$.

Within the naïve group, NO_3^- supplementation did not significantly reduce ADP-mediated platelet aggregation compared to placebo (ΔADP : -78.2 ± 57.5 AU*min vs 20.6 ± 48.7 AU*min, $p > 0.05$), respectively (Figure 6.5A). Similarly, TRAP-mediated platelet aggregation was also unaltered following NO_3^- supplementation within the naïve group compared to placebo (ΔTRAP : -214.7 ± 83.9 AU*min vs -37.6 ± 92.4 AU*min, $p > 0.05$), respectively (Figure 6.5B). In the clopidogrel group, NO_3^- supplementation also failed to significantly reduce ADP-mediated platelet aggregation in comparison to placebo (ΔADP : -21.7 ± 22.4 AU*min vs 1.3 ± 18.0 AU*min, $p > 0.05$) (Figure 6.5C). However, NO_3^- supplementation did significantly reduce TRAP-mediated platelet aggregation within the clopidogrel group compared to placebo (ΔTRAP : -198.9 ± 63.2 AU vs -39.5 ± 63.5 AU, $p < 0.05$) (Figure 6.5D)

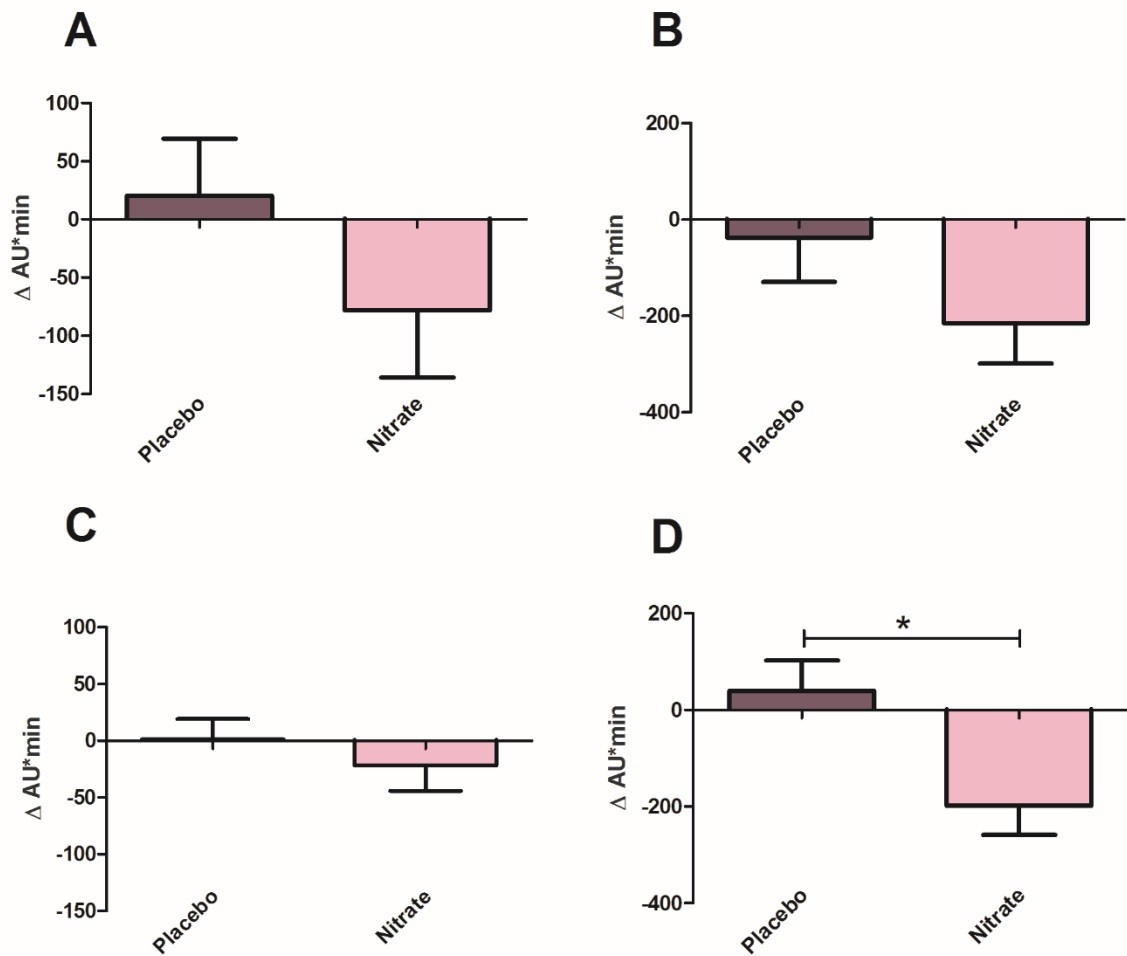


Figure 6.5 Changes in platelet aggregation following NO_3^- supplementation. (A) ADP-stimulated platelet aggregation in the naïve group. (B) TRAP-stimulated platelet aggregation in the naïve group. (C) ADP-stimulated platelet aggregation in the clopidogrel group. (D) TRAP-stimulated platelet aggregation in the clopidogrel group. Aggregation units calculated as area under the curve after 6 minutes. Data are expressed as mean \pm SEM [n=10]. * represents $p < 0.05$.

6.5.4 EV size and concentration

The basal circulating plasma EV concentration was not significantly different between the naïve and clopidogrel groups ($5.03e^{11} \pm 4.17e^{10}$ EVs/mL vs $4.67e^{11} \pm 3.67e^{10}$ EVs/mL, $p > 0.05$) (Figure 6.6A). Similarly, no difference in EV size was observed between patient groups (Naïve: 138 ± 19.5 nm vs clopidogrel: 132 ± 26.5 nm, $p > 0.05$) (Figure 6.6B). Within the naïve group, NO_3^- supplementation did not significantly reduce circulating EV concentration compared to placebo (ΔEVs : $-2.78e^{10} \pm 4.22e^{10}$ EVs/mL vs $1.76e^{10} \pm 1.23e^{10}$ EVs/mL) (Figure 6.7A). However, NO_3^- supplementation did significantly reduce circulating EVs compared to placebo within the clopidogrel group (ΔEVs : $-1.18e^{11} \pm 3.15e^{10}$ EVs/mL vs $-9.93e^9 \pm 1.84e^{10}$ EVs/mL, $p < 0.05$) (Figure 6.7B). EV size did not alter between ingestion of the NO_3^- supplement or placebo in both the naïve (before placebo: 135 ± 21 nm, after placebo: 158 ± 33 nm, before NO_3^- : 140 ± 18 nm, after NO_3^- : 132 ± 11 nm, $p > 0.05$) (Figure 6.7C) nor the clopidogrel (before placebo: 118 ± 30 nm, after placebo: 129 ± 12 nm, before NO_3^- : 145 ± 23 , after NO_3^- : 124 ± 26 , $p > 0.05$) (Figure 6.7D) groups.

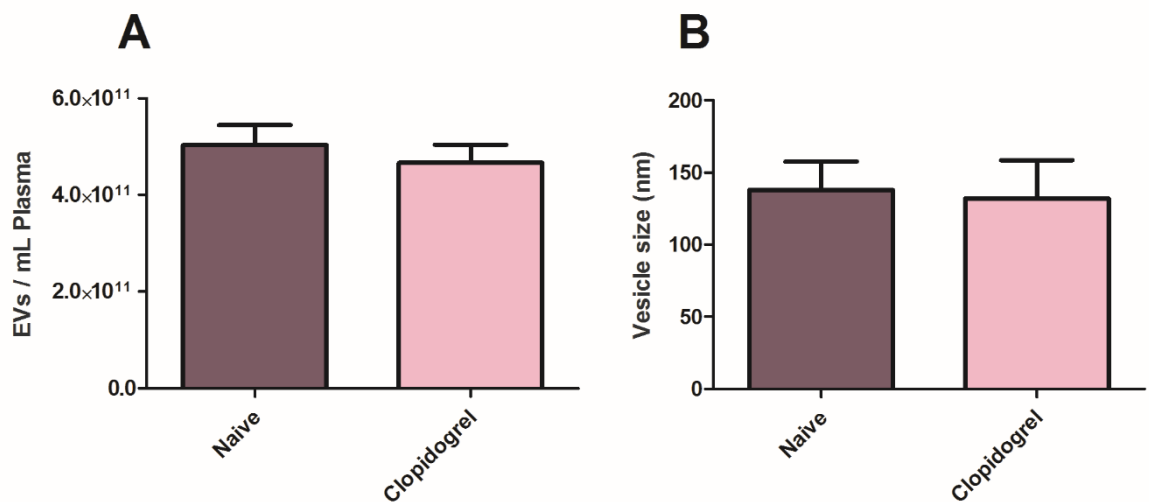


Figure 6.6 Baseline circulating plasma EV measures. (A) Baseline EV concentration per mL of plasma in the naïve and clopidogrel group. (B) Mean EV size within the naïve and clopidogrel group at baseline. Baseline refers to an average value for each patient obtained from both visits prior to ingestion of either the NO_3^- supplement or placebo [n=10].

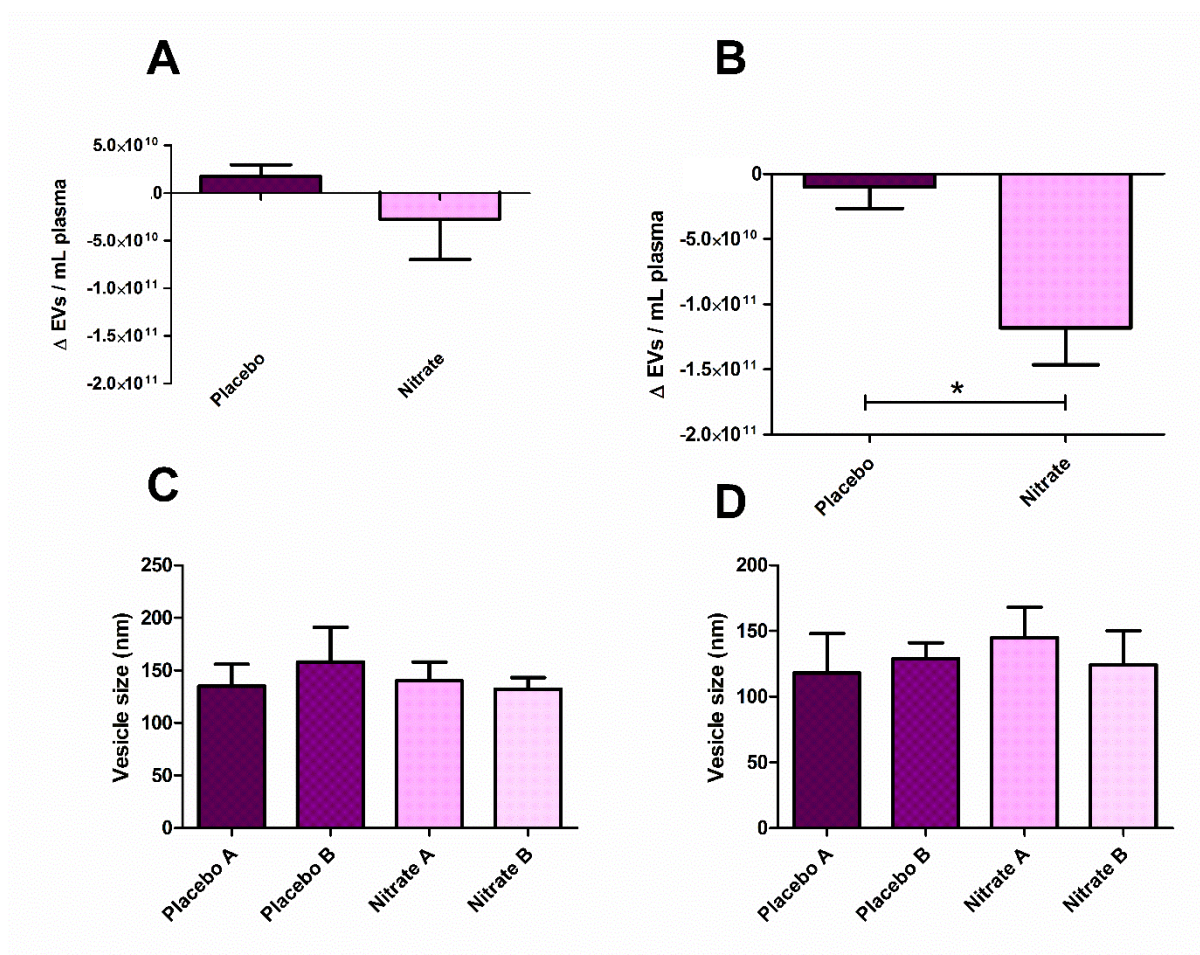


Figure 6.7 Changes in EV size and concentration following NO₃⁻ supplementation. (A) Change in EV concentration in the naïve group following both placebo and nitrate supplementation. (B) Changes in EV concentration in the clopidogrel group following both placebo and nitrate supplementation. (C) Mean EV size at all timepoints for the naïve group. (D) Mean EV size at all timepoints for the clopidogrel group. Data are expressed as mean ± SEM [n=10]. * represents p < 0.05.

6.5.5 EV size distribution profile

On assessment of the change in size distribution profile of EVs, no significant reductions were observed following NO₃⁻ supplementation within a specific size range in the naïve patient group, when compared to placebo (Figure 6.8A). NO₃⁻ supplementation within the clopidogrel group significantly reduced EVs within the size range 50-149 nm compared to placebo (50-99 nm: $-3.7 \times 10^{10} \pm 3.0 \times 10^{10}$ vs $1.0 \times 10^9 \pm 4.0 \times 10^9$; 100-149 nm: $-3.7 \times 10^{10} \pm 3.2 \times 10^{10}$ vs $2.7 \times 10^{10} \pm 8.5 \times 10^9$, $p < 0.05$ and $p < 0.001$, respectively) (Figure 6.8B). Table 6.2 outlines the changes seen within the size distribution profile of both the naïve and clopidogrel groups.

Table 6.2 Changes in the size distribution profile of EVs following placebo or NO₃⁻ supplementation

EV Size	Naïve		Clopidogrel	
	Placebo	Nitrate	Placebo	Nitrate
0-50	1.45e ⁹ ± 2.11e ⁹	-3.32e ⁹ ± 3.89e ⁹	-5.14e ⁹ ± 8.91e ⁸	-6.96e ⁹ ± 4.27e ⁹
51-100	8.31e ⁸ ± 8.93e ⁹	-3.24e ⁹ ± 1.18e ¹⁰	1.02e ⁹ ± 4.06e ⁹	-3.71e ¹⁰ ± 2.95e ¹⁰ *
101-150	3.09e ⁹ ± 6.19e ⁹	-1.30e ⁹ ± 1.26e ⁹	2.65e ⁹ ± 4.06e ⁹	-3.69e ¹⁰ ± 3.21e ¹⁰ ***
151-200	4.54e ⁹ ± 6.02e ⁹	-7.50e ⁹ ± 4.02e ⁹	-3.63e ¹⁰ ± 1.34e ¹⁰	-1.65e ¹⁰ ± 1.14e ¹⁰
201-250	2.28e ⁹ ± 4.77e ⁹	-5.10e ⁹ ± 4.02e ⁹	2.68e ⁹ ± 9.93e ⁸	-8.89e ⁹ ± 5.59e ⁹
251-300	1.39e ⁹ ± 2.35e ⁹	-3.03e ⁹ ± 2.06e ⁹	1.029e ⁹ ± 4.70e ⁸	-5.16e ⁹ ± 3.50e ⁹
301-350	1.19e ⁹ ± 1.20e ⁹	-2.60e ⁹ ± 1.21e ⁹	3.09e ⁹ ± 1.98e ⁸	-2.60e ⁹ ± 2.34e ⁹
351-400	1.35e ⁹ ± 9.61e ⁸	-1.52e ⁹ ± 6.17e ⁸	4.53e ⁷ ± 1.29e ⁸	-1.34e ⁹ ± 1.48e ⁹
401-450	1.15e ⁹ ± 9.73e ⁸	-4.15e ⁸ ± 4.10e ⁸	1.72e ⁸ ± 1.13e ⁸	-1.32e ⁹ ± 1.14e ⁹
451-500	3.86e ⁸ ± 3.15e ⁸	-3.98e ⁷ ± 1.67e ⁸	1.53e ⁷ ± 2.74e ⁷	-3.61e ⁸ ± 2.96e ⁸
501-550	3.06e ⁸ ± 1.94e ⁸	4.95e ⁷ ± 1.28e ⁸	-5.06e ⁶ ± 2.11e ⁷	-3.00e ⁸ ± 3.34e ⁸
551-600	3.15e ⁸ ± 1.62e ⁸	1.16e ⁸ ± 1.36e ⁸	-5.97e ⁶ ± 8.81e ⁶	-2.76e ⁸ ± 2.77e ⁸

NTA was used to assess the size distribution of EVs, split into 50 nm bin sizes for analysis and normalised per mL of plasma. Samples were measured in quintuplicate and the mean used in further analysis. Data are expressed as the group mean ± SEM. Results represent [n=10]. * and *** reflects p < 0.05, and 0.001 respectively, compared to the relevant placebo

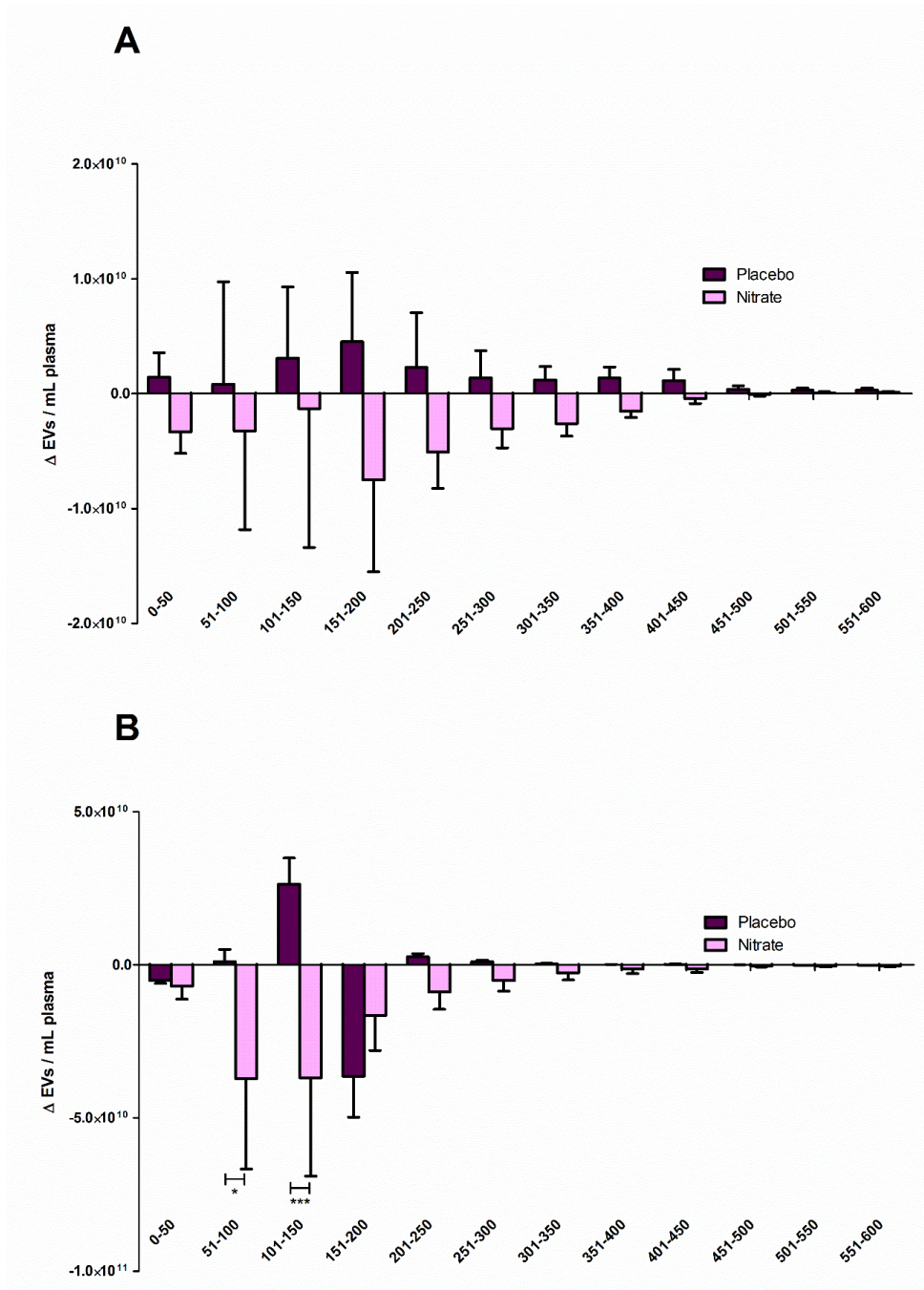


Figure 6.8 The effect of NO_3^- supplementation on size distribution profile of EVs. (A) Changes in the size distribution profile within the naïve group. (B) Changes in the size distribution profile within the clopidogrel group. Assessed in 50 nm bin sizes, results represent [n=10]. Each sample was analysed in quintuplicate and the mean was used in further analysis. Data are expressed as mean \pm SEM. * and *** reflect $p < 0.05$ and 0.001, respectively.

6.5.6 EV immunophenotyping

Comparison between the naïve and clopidogrel groups revealed that the clopidogrel group had significantly higher levels of the exosomal (CD9), platelet (CD41) and leukocyte (CD11b) marker compared to the naïve group (CD9: 32899 ± 1303 RFU vs 23812 ± 1891 RFU, $p < 0.001$. CD41: 15753 ± 1372 RFU vs 10064 ± 705 RFU, $p < 0.01$. CD11b: 14245 ± 1512 RFU vs 9578 ± 1250 RFU, $p < 0.05$). No differences were seen in baseline values for the erythrocyte (CD235a) and endothelial (CD144) markers between clopidogrel and naïve groups (CD235a: 2414 ± 379 RFU vs 1786 ± 307 RFU, $p > 0.05$. CD144: 617 ± 280 RFU vs 685 ± 247 RFU, $p > 0.05$), respectively (Figure 6.9A).

Within the naïve group, no significant differences were seen in surface protein markers for exosomes, platelets, leukocytes, erythrocytes and endothelial cells following NO_3^- supplementation compared to placebo, respectively (ΔCD9 : -471 ± 625 RFU vs 207 ± 674 RFU. ΔCD41 : -498 ± 423 RFU vs -292 ± 348 RFU. ΔCD11b : -1053 ± 934 RFU vs -1074 ± 459 RFU. ΔCD235a : -259 ± 230 RFU vs -94 ± 202 RFU. ΔCD144 : -364 ± 354 RFU vs 142 ± 635 . $p > 0.05$ for all comparisons) (Figure 6.9B).

Within the clopidogrel group, there was a significant reduction in the platelet marker CD41 following NO_3^- supplementation compared to placebo (ΔCD41 : -2120 ± 728 RFU vs 235 ± 436 RFU, $p < 0.05$), respectively. No other differences were observed between NO_3^- supplementation and placebo within the clopidogrel group (ΔCD9 : -1079 ± 744 RFU vs -172 ± 718 RFU; ΔCD11b : -877 ± 441 RFU vs -544 ± 395 RFU; CD235a: -678 ± 351 RFU vs 85 ± 422 RFU; CD144: -106 ± 336 RFU vs -185 ± 372 RFU, $p > 0.05$ for all comparisons) (Figure 6.9C).

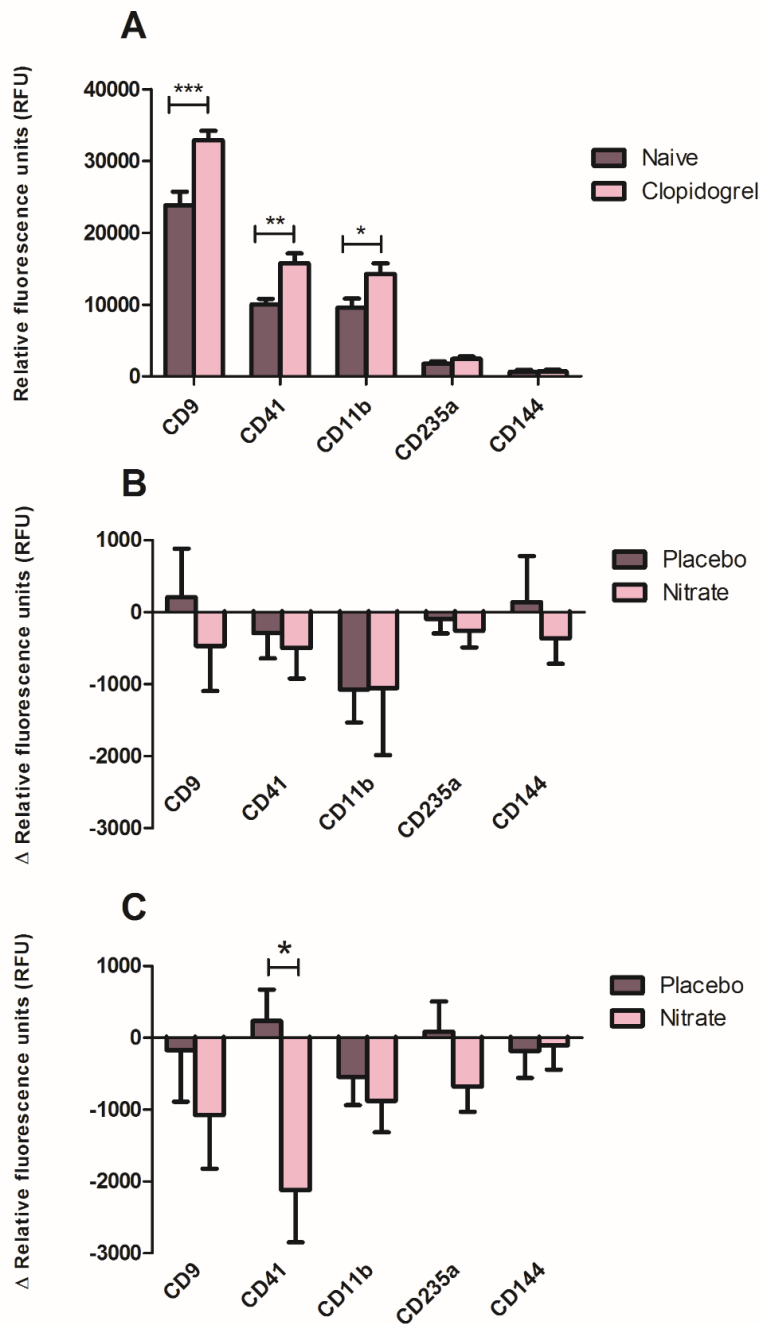


Figure 6.9 Effect of NO_3^- supplementation on EV surface proteins. (A) Difference in baseline levels of protein markers between naïve and clopidogrel groups. (B) Change in protein expression after NO_3^- supplementation/placebo in the naïve group. (C) Change in protein content after NO_3^- supplementation/placebo in the clopidogrel group. Proteins were detected using a streptavidin-europium conjugate and measured using time resolved fluorescence. Data are expressed as mean \pm SEM [n=10]. ***, ** and * reflect $p < 0.001$, $p < 0.01$ and $p < 0.05$, respectively.

6.5.7 *Ex vivo* platelet EV generation

Ex vivo experiments on platelet-rich plasma (PRP) isolated from whole blood of healthy volunteers were performed to elucidate the direct effect of NaNO₂, clopidogrel, and RSNO (GSNO and clopidogrel-SNO) (all 10 μM) on platelet-derived EV production. EV production was significantly increased following stimulation by ADP (unstimulated: $1.63e^{11} \pm 8.8e^9$ vs ADP: $3.94e^{11} \pm 1.91e^{10}$ EVs/mL, $p < 0.001$). This increase was mirrored by an increase in the platelet marker CD41 within the EV sample (unstimulated: 5826 ± 1279 RFU vs ADP: 19703 ± 1375 RFU, $p < 0.01$). The addition of clopidogrel or NaNO₂ to stimulated PRP had no effect on EV production (NaNO₂: $3.83e^{11} \pm 1.707e^{10}$ EVs/mL, clopidogrel: $3.91e^{11} \pm 1.805e^{10}$ EVs/mL, vs ADP alone $3.94e^{11} \pm 1.91e^{10}$ EVs/mL $p > 0.05$). Similarly, no change in the platelet marker CD41 was observed following NaNO₂ or clopidogrel addition (NaNO₂: 20093 ± 1244 RFU, clopidogrel: 18238 ± 2824 RFU, vs ADP control: 19703 ± 1375 RFU $p > 0.05$). The addition of clopidogrel-SNO significantly reduced the EV concentration compared to the ADP & clopidogrel ($6.209e^{10} \pm 4.074e^9$ EVs/mL vs $3.91e^{11} \pm 1.80e^{10}$ EVs/mL, $p < 0.001$). An alternative nitrosothiol, GSNO, had a similar effect to clopidogrel-SNO compared to the ADP & clopidogrel ($8.67e^{10} \pm 8.63e^9$ EVs/mL vs $3.91e^{11} \pm 1.80e^{10}$ EVs/mL, $p < 0.001$) (Figure 6.10A). These reductions were mirrored in levels of CD41 expression within the EV sample (GSNO: 9946 ± 1125 RFU, clopidogrel-SNO: 12213 ± 1924 RFU, vs ADP control: 18238 ± 2824 RFU, $p < 0.01$ and 0.05 , respectively) (Figure 6.10B).

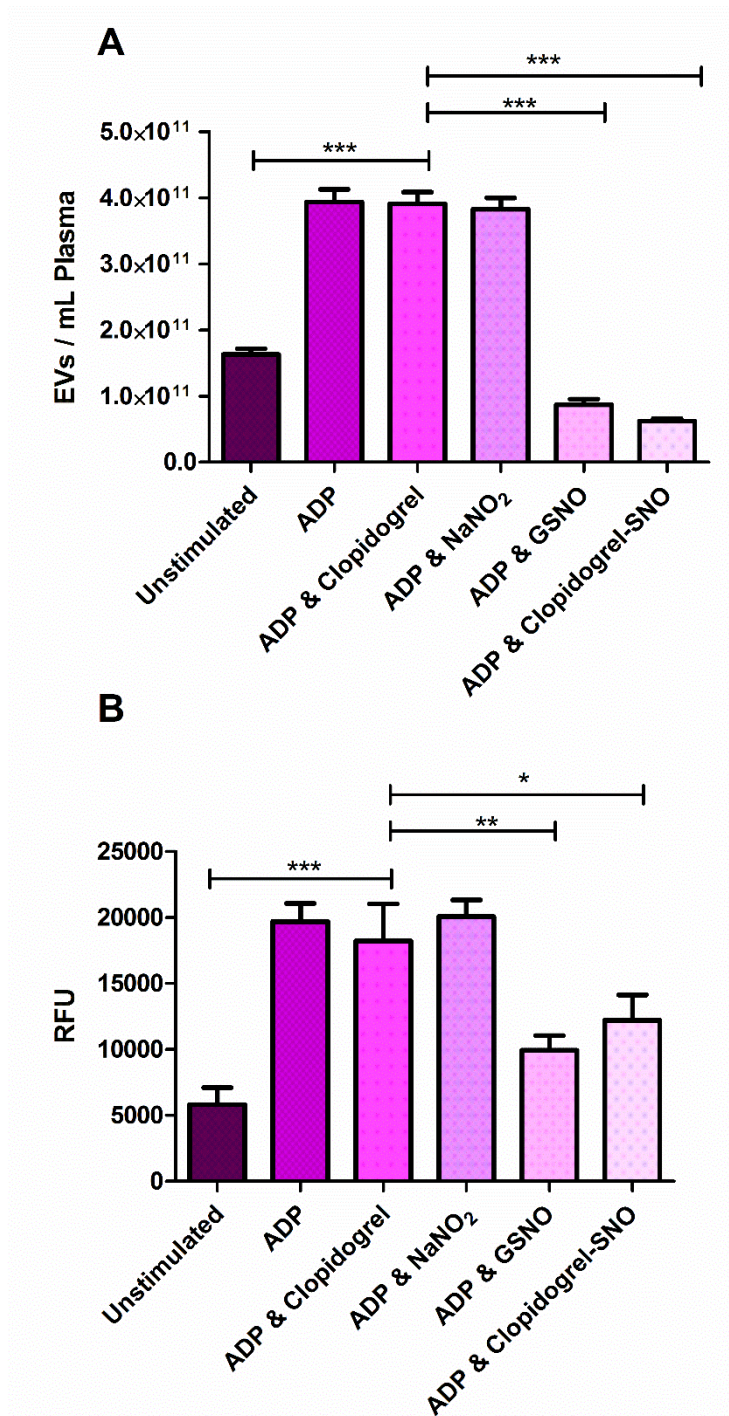


Figure 6.10 Ex vivo platelet EV production. (A) The effect of various agents on EV concentration isolated from platelet rich plasma. (B) The reduction in EV concentration was mirrored by a reduction in CD41 expression, measured by TRF. n=6, ***, ** and * reflect $p < 0.001$, $p < 0.01$ and $p < 0.05$, respectively.

6.6 Discussion

6.6.1 Key Findings

- Acute dietary NO_3^- supplementation significantly increases both plasma NO_3^- and NO_2^- levels in CAD patients (NO_3^- : $\approx 280 \mu\text{M}$; NO_2^- : $\approx 265 \text{ nM}$) irrespective of clopidogrel treatment, compared to placebo.
- NO_3^- supplementation significantly elevated RSNO levels only in patients on clopidogrel therapy.
- Platelet aggregation stimulated via the thrombin receptor was significantly reduced in the clopidogrel group following NO_3^- supplementation compared to placebo.
- NO_3^- supplementation in the clopidogrel group also significantly reduced the circulating EV concentration, compared to placebo.
- Following NO_3^- supplementation, EVs in the clopidogrel group had significantly reduced amounts of the platelet marker CD41 compared to placebo.
- *Ex vivo* studies confirmed the effect of clopidogrel-SNO on platelet-derived EV formation.

6.6.2 Main discussion

NO_3^- and NO_2^- were once thought of as inert, end products of NO metabolism. It is now widely accepted that both NO_3^- and NO_2^- represent a bioactive “storage pool” of NO; and can be metabolised in blood and tissues to be reduced back to NO and other bioactive NO metabolites. This represents an alternative to the “classical” NO formation pathway involving L-arginine and eNOS (142,593–595). NO_3^- is first reduced to NO_2^- in the body by commensal bacteria present within the oral cavity and the gastrointestinal tract, and to a far smaller degree, xanthine oxidoreductase within the liver (596). Once formed, NO_2^- is further reduced via interaction with various proteins possessing NO_2^- reductase activity (130), a reaction which is optimised in conditions of hypoxia or acidosis. The benefits of dietary NO_3^- supplementation is well documented in exercise physiology (592,597). More recently, numerous reports have shown dietary NO_3^- to have a host of beneficial effects in a CVD setting, including decreasing blood pressure (180,598), attenuating oxidative stress (551), reversing vascular dysfunction (179), and decreasing platelet aggregation (162,584).

NO bioavailability in CVD patients is known to be compromised (599), likely reflecting the endothelial dysfunction seen in these patient cohorts (123). Within this study, following NO_3^- supplementation, plasma NO_3^- and NO_2^- levels increased in both patient groups to a level similar to that which both we and others have seen previously in subjects receiving a similar dose of dietary NO_3^- (124,550,552). Interestingly, significant elevations in plasma RSNO levels following NO_3^- supplementation were only seen within the patient group receiving clopidogrel. Our group have previously shown that an acidic pH (such as that present in the stomach) can modify thienopyridines to form thienopyridine-SNO (Th-SNO) molecules *in vitro* (590). Acidification exposes the free thiol group present within this class of drugs *before* biotransformation by cytochrome P450 enzymes into active metabolites. Once the thiol group is exposed, and in the presence of NO_2^- , the drug is able to form nitrosothiol derivatives (Th-SNO). RSNO molecules possess the ability to act as NO donors (588,600), thus providing an alternative, or at least an extra step, in the nitrate-nitrite-nitric oxide pathway, and the effects seen following both NO_3^- and NO_2^- administration (173,548). *Ex vivo* investigation of platelet-derived EV generation confirmed the effect of RSNO (both GSNO and Th-SNO) on EV production. Incubation of PRP with both RSNOs significantly reduced EV production following ADP stimulation of platelets. This reduction was mirrored by a decrease in the platelet marker CD41, suggesting that the reduction was primarily due to platelet-derived EV. Consistent with these findings, our group have previously shown that clopidogrel-SNO can inhibit platelet activation in response to ADP at a level similar to that of GSNO, with similar IC_{50} values observed (clopidogrel-SNO: $10.56 \pm 1.43 \mu\text{M}$ vs GSNO: $9.80 \pm 2.28 \mu\text{M}$) (601).

Previous studies have shown that treatment with proton-pump inhibitors (PPIs), such as omeprazole, significantly attenuates clopidogrel's inhibitory effect on platelets (602). However, a systematic review concluded that platelet function did not demonstrate a clear or consistent interaction between clopidogrel and PPIs (603). Recently, Pinheiro *et al.* have shown that oral nitrite administration in rats was associated with an increase in RSNO formation, and a decrease in blood pressure. Moreover, treatment with the PPI omeprazole and the thiol-depleting agent buthionine sulfoximine attenuated the increase in plasma RSNO, and blunted the antihypertensive effects of nitrite (553). These findings, in combination with the results within this chapter, are supportive of the hypothesis that the reduction in EVs and effect on platelet reactivity may, in part, be due to the formation of circulating RSNO molecules seen only in the clopidogrel group. Patients taking PPIs were not excluded from this study, and thus the increased pH of the gastric medium may have interfered with Th-SNO formation. However, it is noteworthy that PPIs raise stomach pH from $\approx 2-3$ to $\approx 4-6$ (604–606). Our group have previously shown that RSNO formation at this pH is only marginally reduced (409).

Measurement of surface protein expression revealed that the platelet marker CD41 decreased significantly in the clopidogrel group following NO_3^- supplementation, in keeping with the hypothesis that the reduction was seen within platelet-derived EVs. Platelet activation plays a pivotal role in the development of atherosclerosis, and as a result, anti-platelet therapy is well established in the treatment of CVD (607,608). In healthy individuals, activation and adhesion of platelets to the endothelium is inhibited by endogenous production of NO, highlighted by the reduced NO bioavailability in CVD cohorts (435). Previously, NO_3^- supplementation has been shown to augment platelet inhibition *ex vivo* (584). Interestingly, prevention of the entero-salivary bioconversion of NO_3^- to NO_2^- diminished both the decrease in blood pressure and the inhibitory effects on platelet activation (609).

This study is the first of its kind to show that dietary NO_3^- supplementation can reduce circulating EV levels when administered in combination with clopidogrel. This is in agreement with a recent study by Lee *et al.*, who showed that sustained release nitrates in combination with clopidogrel significantly enhanced platelet inhibition compared to clopidogrel alone (585). The lack of RSNO produced within the naïve group in this chapter, and also the absence of a significant reduction in both platelet activation and EV production, suggests these effects are mediated, at least in part, by Th-SNO molecules produced in the stomach. This hypothesis is further strengthened by the results from *ex vivo* experiments.

Clopidogrel, once converted to its active metabolite, acts via irreversible inhibition of the P_2Y_{12} receptor, preventing the inhibition of adenylate cyclase, allowing an increase in intracellular cAMP. This, in turn, allows for cAMP-mediated phosphorylation of vasodilator-stimulated phosphoprotein (VASP-P), which modulates glycoprotein IIb/IIIa activation (610). Interestingly, activation of the P_2Y_{12} receptor has been shown to potentiate dense granule secretion in platelets (611). Granule and EV release share common cellular machinery including SNARE proteins, intracellular calcium levels and cytoskeletal reorganisation (612). It is plausible that inhibition of this pathway by clopidogrel, in combination with the inhibitory effects of NO_2^- derived NO, may be responsible for the reduction in platelet activation and EV production seen in this study. These two independent pathways could, together, have a synergistic effect, culminating in diminished platelet activation. Blockade of the P_2Y_{12} receptor has indeed been shown to greatly increase the platelet inhibitory actions of NO previously (582). However, *ex vivo* experiments suggest, at least in part, that the formation of RSNO molecules are responsible for the reduction in EV concentration. In situ, the mechanism of NO_2^- reduction to NO is likely to be multifactorial and RSNO formation may represent one of a number of pathways NO_2^- can elicit its effects.

6.6.3 Limitations

The recommendations for the isolation of EVs from plasma are continuously being updated within the EV field. Although differential ultracentrifugation remains a popular isolation technique, there are some concerns that this may also pellet some soluble material, such as albumin and lipoproteins, which may then be detected by NTA. At the time this research was performed, ultracentrifugation was the isolation technique of choice within our research team, and widely used throughout the field. Secondly, despite the robust design of a placebo-controlled, randomised, double-blind crossover study, the sample size of individual groups (n=10) is small. This size was chosen based on power calculations to detect a significant decrease in the circulating EV concentration. However, this limits the overall power of the study in terms of determining significance between other factors. For example, smaller decreases in both platelet activation and circulating EV concentration were seen in the naïve group, but were judged to be non-statistically significant. These changes may have become significant in a large sample population. Secondly, there are differences in both cardiovascular risk factors and medications between the clopidogrel and naïve groups; rendering it difficult to conclude that the difference in outcomes seen in this study are due to clopidogrel treatment, or other possible confounding factors. Many patients within both groups had been prescribed PPIs, which may have interfered with Th-SNO formation in the stomach by increasing stomach pH ($\approx 4-6$). As mentioned previously, RSNO formation is still possible at higher pH. It is possible however that if patients taking PPIs had been excluded, I may have seen a greater rise in plasma RSNO. Comparisons between naïve and clopidogrel groups showed a similar reduction in platelet aggregation, EV concentration and EV surface markers following nitrate supplementation. Thus, due to the lack of RSNO produced by the naïve group, it is unlikely that the formation of RSNO is the sole mechanism responsible for the beneficial effects of NO_3^- . Finally, this study has investigated the effect of a “one-off” acute dose of dietary NO_3^- on EV populations. Future studies should assess the effect of longer term dietary NO_3^- on RSNO formation, circulating EV levels and platelet activity in CAD patients.

6.6.4 Conclusions

In summary, this chapter has shown that dietary NO_3^- supplementation in the acute setting can reduce the total circulating plasma EVs in CAD patients on clopidogrel. This increase appears to be mediated, at least in part, by an increase in RSNO formation. The decrease in EVs was mirrored by a reduction in both platelet activation and the platelet marker CD41 within the EV sample, suggesting the decrease in EVs was predominantly platelet-derived. These results suggest that dietary NO_3^- supplementation could provide an additional adjunct to platelet inhibition with clopidogrel in CAD patients.

7 GENERAL DISCUSSION

7.1 Overview and conclusions

The primary aim of this thesis was to comprehensively assess the effect of NO metabolites (inorganic $\text{NO}_3^-/\text{NO}_2^-$) on EV production and function. Initially, the focus sought to establish the role of these metabolites within a hypoxic environment, exploring in detail the relationship between HIF, NO, and EV release. The EVs produced from endothelial cells incubated under hypoxia/normoxia with or without NaNO_2 treatment were then assessed for their pathological potential utilising a series of functional experiments. This *in vitro* work was then extended to a placebo-controlled trial in healthy volunteers, assessing their circulating EV concentrations over a 6 day dietary NO_3^- supplementation treatment plan. In addition, the effect of NO_3^- supplementation on plasma NO metabolites was measured. Finally, the effect of acute NO_3^- supplementation on EV concentration was tested in a CAD cohort, in a placebo-controlled study.

CVD remains the leading cause of mortality globally, accounting for an estimated 17.7 million deaths in 2015, 31% of all global deaths (1). Atherosclerosis, the major precursor to CVD, can be delayed via the control of modifiable risk factors and medication. The role of EVs within the progression of CVD has only emerged in the last 10-15 years (291,613). Specifically, their roles in coagulation and inflammation make them attractive targets for therapeutic modulation.

The investigation into the effect of hypoxia on EV production led to the discovery of the fascinating triad of HIF, NO and EV release. Hypoxia exposure strongly activates endothelial cells, thereby initiating a cascade of reactions. The initial event is a decrease in oxidative phosphorylation of the mitochondria, caused by the reduction in oxygen availability, leading to decreases in ATP (614). Glycolysis is activated to compensate for this decrease, which produces lactic acid and a large number of protons, decreasing the intracellular pH. The decrease in pH subsequently can stimulate the Na^+/H^+ exchanger, leading to an influx of Na^+ . The influx of extracellular Ca^{2+} could then be caused by the extrusion of Na^+ ions through the $\text{Na}^+/\text{Ca}^{2+}$ exchanger, a common pathway for intracellular Ca^{2+} increases (615). Indeed, this mechanism has been demonstrated previously in endothelial cells (428). However, results within this thesis found EV release to be HIF-1 α mediated, in agreement with other studies on breast cancer cells (430). HIF-1 α can lead to adaptations in cellular physiology necessary for EV release, such as cytoskeleton reorganisation. It is likely that hypoxia increases both $[\text{Ca}^{2+}]_i$ and HIF-1 α , which together facilitate the enhanced EV release observed. The adaptation of cellular physiology following hypoxia exposure was mirrored in the EVs released, with significant differences in the content of these EVs, including decreased thrombomodulin and TFPI levels, and increased TNF-

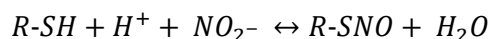
α , IL-6, and NF- κ B levels. Indeed, the transcription factor HIF can modulate expression of these genes (79,82,616), as discussed in Chapter 4. Furthermore, NO_2^- derived NO is capable of reducing $[\text{Ca}^{2+}]_i$ (617) and HIF-1 α expression (618), which evidently led to the reduction in EV production observed. NaNO_2 treatment of endothelial cells incubated in hypoxia produced EVs with reduced pro-coagulant potential, although this had no effect on their influence over leukocyte adhesion. Thus, NO_2^- not only reduces the production of EVs, but in some respects, reduces their potentially pathogenic function.

The multifaceted roles of NO within the cardiovascular system are well documented (435,619), however, work outlined in this thesis offers another potential beneficial effect of NO within the vasculature, specifically under pathological or disease settings. The nitrate-nitrite-nitric oxide pathway is a fascinating premise, which has received large amount of attention in recent years (155), with multiple research groups utilising the ability to increase NO bioavailability via a dietary supplement. It is important to note that multiple mechanisms of NO_2^- reduction to NO exist. Indeed, this reduction is greatly enhanced under hypoxic conditions, as demonstrated in Chapter 3 of this thesis, and well documented within the literature (468,620). However, due to the complexities of measuring oxygen concentration *in vivo*, it remains difficult to establish whether the hypoxia present in disease cohorts is severe enough to facilitate the reduction (468). That being said, there is evidence that NO can be produced from NO_2^- at physiological concentrations in ischaemic conditions in tissue of the cardiovascular system (621). A second possible mechanism of increasing NO bioavailability is via RSNO formation. Indeed, I observed significant increases in RSNO levels within the plasma following NO_3^- supplementation in chapter 5 and 6 of this thesis. Research from our own group (590,601) and others (553) have demonstrated the formation of RSNO when NO_2^- is exposed to an acidic environment, such as the stomach. This RSNO molecule can then diffuse into the plasma and donate both NO directly (600). Indeed, the involvement of RSNOs as active intermediates in the effects of NO_3^- and NO_2^- was demonstrated as early as 1981 by the Nobel Prize winner Louis Ignarro (622). In reality, these mechanisms are not mutually exclusive and likely exist in parallel, offering multiple methods of increasing NO bioavailability in pathological conditions.

Intriguingly, we observed large differences in NO metabolite formation between healthy volunteers (Chapter 5) and CAD patients on clopidogrel (Chapter 6). Admittedly, the source of NO_3^- between these studies differed, with BEET IT Organic beetroot juice used in chapter 5, and a Science in Sport Go⁺ Nitrate gel used in chapter 6. As a result, the total level of NO_3^- given to participants differed, with a total of 12.88 mmol given in Chapter 5 and 8.06 mmol given in Chapter 6. This is reflected in plasma NO_3^- levels 2 hours post-supplement, where, despite similar baseline NO_3^- levels ($\approx 20\text{-}30\ \mu\text{M}$), peaks of

≈500 μM were observed following the higher dose in healthy volunteers, whereas peaks of ≈250 μM were recorded in CAD patients administered 8.064 mmol of NO₃⁻. Similarly, plasma NO₂⁻ levels reached ≈500 nM 2 hours post-supplementation in healthy volunteers, in comparison to peaks of only ≈250 nM seen in CAD patients. These differences in plasma NO metabolites following varying doses of NO₃⁻ are to be expected, and are in agreement with numerous other studies using similar dosing, which have been extensively reviewed previously (124).

There is significantly less research investigating the effect of dietary NO₃⁻ supplementation on plasma RSNO formation. Within Chapters 5 and 6, baseline levels were similar between both cohorts (≈15 nM). However, plasma RSNO levels reached approximately 140 nM in healthy volunteers, with only a modest increase to around 20 nM observed in CAD patients. Whilst it is possible that this is simply due to the level of NO₃⁻ participants received, there are also several other potential reasons for this difference. Firstly, the cohorts themselves are entirely dissimilar; one group were healthy, recreationally active males, with an average age of 33. The other group were significantly older (average age of 63) males with established CAD. It is already known that CAD patients exhibit reduced NO bioavailability (9,581). It is plausible that these subjects may also exhibit reduced capability of RSNO formation. In order for RSNO to be formed, three things are required: an abundance of NO₂⁻, a protein with a free thiol (R-SH) group, and an acidic environment (an abundance of H⁺ ions). This is summarised in the equation below.



Healthy volunteers were instructed to fast at least 3 hours prior to the study commencing, in comparison to an overnight 12 hour fast that was employed in CAD patients. Thus, this may have influenced the amount of protein, and thus free thiol availability within the stomach. Furthermore, participant recruitment for Chapter 5 was performed in Norway, where a major constituent of their diet is meat and fish (623). It is possible that these high protein food groups may have facilitated the large amount of RSNO produced in comparison to the CAD patient cohort. Subjects were instructed to avoid foods high in NO₃⁻ content for the duration of the study, so it is unlikely that unconscious NO₃⁻ dosing was a factor. Another potential influence of the discrepancy is that a proportion of CAD patients were also taking PPIs, increasing the pH of the stomach. Despite evidence suggesting RSNO formation is still possible at higher pH levels (601), it is conceivable that this may have attenuated the rise in plasma RSNO observed in the CAD cohort.

This thesis is in agreement with the wealth of literature that suggests circulating EVs are elevated in CVD compared to healthy individuals (624). CAD patients had approximately 66% more circulating EVs

in comparison to the healthy volunteers in chapter 5 (5×10^{11} EVs/mL plasma vs 3×10^{11} EVs/mL plasma). In CAD patients on clopidogrel, following NO_3^- supplementation circulating EV levels were reduced to a similar level seen in healthy volunteers (3.5×10^{11} EVs/mL plasma). However, NO_3^- supplementation had no effect on EV levels in healthy volunteers. Thus, this may represent a healthy “baseline” level of EVs in individuals, with NO_3^- only taking effect when a pathological increase in EVs is present, following stimulation of cells leading to their activation, as seen in chapter 6 of this thesis.

The pleiotropic effects of thienopyridines, including clopidogrel, have been the subject of intense study within our research group. Indeed, the thesis of my colleague Dr Lawrence Thornhill extensively investigated the ability of these drugs to form RSNO compounds (625). The results within chapter 6 of this thesis compliment this work, offering a potential additional benefit of thienopyridine treatment, increasing NO bioavailability in CAD patients. The reduction in NO bioavailability is a hallmark of endothelial dysfunction, which precedes the development of CVD. Thus, the ability of a treatment to increase NO bioavailability is highly favourable. The beneficial effects of NO within the vasculature are well-known, including vasodilation, platelet inhibition, inhibition of leukocyte adhesion, and inhibition of smooth muscle cell proliferation to name but a few. This thesis offers insight into another potential beneficial effect of NO within the vasculature, demonstrating its capability to reduce circulating pro-coagulant EVs.

Investigation into the effects of boosting NO bioavailability via dietary NO_3^- supplementation has grown in the last decade. Indeed, reductions in blood pressure (162,548), platelet reactivity (162,166) and improvements in vascular function (167,626) have all already been shown. Again, this thesis offers another benefit to this list: a reduction in circulating EVs in CVD patients. In combination with the other beneficial effects reported, dietary NO_3^- supplementation represents an exciting possible therapeutic adjunct for the treatment of CVD patients.

A potential concern with sustained nitrate therapy is the development of tolerance. Primarily associated with organic nitrate (eg glyceryl trinitrate (GTN)) administration, the exact mechanism is not fully understood, but there is evidence to suggest that the mitochondrial aldehyde dehydrogenase-2 (ALDH-2) plays a role (625). It is thought that ALDH-2 is required for the activation of GTN, and the subsequent production of ROS leads to oxidation of thiol groups within the active sites of the enzyme, leading to irreversible inhibition and decreased bioactivation of GTN (627,628). Inorganic NO_3^- administration does not appear to lead to tolerance (629). Despite this, one study recently demonstrated prolonged inorganic NO_3^- supplementation in mice led to initial increases in

plasma NO_3^- and NO_2^- (2 weeks), followed by decreases over time (6, 10 and 14 weeks), suggesting either reduced NO_2^- formation, or enhanced $\text{NO}_3^-/\text{NO}_2^-$ clearance (630).

7.2 Future directions

Future research should aim to build on the themes presented in this thesis, and further explore the relationship between inorganic NO_3^- supplementation and EV production. Despite the function of endothelial-derived EVs being reviewed extensively within this thesis, platelet-derived EVs represent the greatest proportion of circulating plasma EVs (631). In addition, platelet-derived EVs are thought to be integral mediators of coagulation. Thus, the impact of NO_3^- supplementation on platelet EV production and/or function should be assessed. Ongoing work within our research group is currently optimising a method of selecting specific EV populations within a plasma-derived EV sample, utilising a magnetic-bead based assay and specific EV markers (CD41). This method would facilitate the isolation of EVs derived from a specific cell-type, such as platelets, which would further assist in the understanding of the roles different subsets of EVs play *in vivo*.

An interesting future study, potentially utilising this method, would be to assess the function of CAD patient-derived EVs following inorganic NO_3^- supplementation. This would reveal whether increasing NO bioavailability can alter the function of EVs produced *in vivo*, as demonstrated *in vitro* in Chapter 4. This thesis has already established that NO_3^- supplementation can lower the circulating concentration of EVs in CAD patients. NO_3^- supplementation has been demonstrated to alter cellular function, in both endothelial cells and platelets (162,632). The next stage in this research would be to investigate if these cellular adaptations are mirrored in the EVs they produce in an *in vivo* scenario.

Although the EV research field is rapidly accelerating, there remains discrepancies within isolation and measurement procedures within research groups, which must be addressed in order to provide clinically approved, standardised protocols that can facilitate their potential as therapeutic targets of disease. This has been recently addressed, in part, by ISEV and the establishment of standard procedures and characteristic markers (251).

Additionally, the effect of a long-term NO_3^- supplementation intervention should be assessed in a CVD patient cohort. In this thesis, a “one-off” dose of NO_3^- was given. Future studies should investigate whether the effects observed following this are sustainable when given NO_3^- treatment daily over a longer period of time. Indeed, patient recruitment is currently ongoing for a clinical trial investigating the effect of 6 months of daily dietary NO_3^- on vascular function, platelet reactivity and restenosis in patients with stable angina due to have elective PCI (633). It would be interesting to measure circulating EV levels within a similar cohort, and investigate whether EV levels correspond with patient outcomes, which has been previously reported (385).

Finally, the focus on this thesis has been modulating EVs within CVD. However, EVs are elevated in a number of disease states, including cancer. Research is ongoing in this field as to how to possibly target aspects of EV biogenesis, which may prevent tumour progression (634). Indeed, hypoxia is an integral feature of the tumour microenvironment. This thesis has demonstrated that NO_2^- derived NO is capable of modulating hypoxia-mediated EV release *in vitro*. Thus, NO_3^- supplementation may be able to offer a novel dietary intervention capable of modulating the release of these EVs.

REFERENCES

1. WHO | Cardiovascular diseases (CVDs). WHO World Health Organization; 2016; .
2. WHO | Global atlas on cardiovascular disease prevention and control. WHO World Health Organization; 2015; .
3. Mathers CD, Loncar D, Boreham J, et al. Projections of Global Mortality and Burden of Disease from 2002 to 2030. Samet J, editor. PLoS Med World Bank; 2006; 3: e442.
4. British Heart Foundation. Cardiovascular Disease Statistics 2015 - BHF [Internet]. [cited 2017 May 8].
5. British Heart Foundation. Heart statistics - cardiovascular disease in the UK - BHF [Internet]. [cited 2017 May 8].
6. Makridakis S, DiNicolantonio JJ. Hypertension: empirical evidence and implications in 2014. Open Hear Archives of Disease in childhood; 2014; 1: e000048.
7. Ferini-Strambi L, Walters AS, Sica D. The relationship among restless legs syndrome (Willis–Ekbom Disease), hypertension, cardiovascular disease, and cerebrovascular disease. J Neurol Springer Berlin Heidelberg; 2014; 261: 1051–68.
8. Ambrose JA, Barua RS. The pathophysiology of cigarette smoking and cardiovascular disease: An update. J Am Coll Cardiol 2004; 43: 1731–7.
9. Hadi HAR, Carr CS, Al Suwaidi J. Endothelial dysfunction: cardiovascular risk factors, therapy, and outcome. Vasc Health Risk Manag Dove Press; 2005; 1: 183–98.
10. Myers J. Exercise and Cardiovascular Health. Circulation 2003; 107: .
11. Poirier P, Giles TD, Bray GA, et al. Obesity and Cardiovascular Disease: Pathophysiology, Evaluation, and Effect of Weight Loss. Circulation 2006; 113: .
12. Florey. The endothelial cell. Br Med J 1966; 2: 487–90.
13. Inagami T, Naruse M, Hoover R. Endothelium as an Endocrine Organ. Annu Rev Physiol 1995; 57: 171–89.
14. Bazzoni G, Dejana E. Endothelial Cell-to-Cell Junctions: Molecular Organization and Role in Vascular Homeostasis. Physiol Rev 2004; 84: 869–901.
15. Tennant M, McGeachie JK. Blood vessel structure and function: a brief update on recent advances. Aust N Z J Surg 1990; 60: 747–53.
16. Pugsley MK, Tabrizchi R. The vascular system. An overview of structure and function. J Pharmacol Toxicol Methods 44: 333–40.
17. Williams JK, Heistad DD. Structure and function of vasa vasorum. Trends Cardiovasc Med 1996; 6: 53–7.
18. Leloup AJA, Van Hove CE, Heykers A, et al. Elastic and Muscular Arteries Differ in Structure, Basal NO Production and Voltage-Gated Ca(2+)-Channels. Front Physiol Frontiers Media SA; 2015; 6: 375.
19. Furchgott RF, Zawadzki J V. The obligatory role of endothelial cells in the relaxation of arterial smooth muscle by acetylcholine. Nature 1980; 288: 373–6.

20. Ignarro LJ, Buga GM, Wood KS, et al. Endothelium-derived relaxing factor produced and released from artery and vein is nitric oxide. *Proc Natl Acad Sci U S A* 1987; 84: 9265–9.
21. Palmer RMJ, Ferrige AG, Moncada S. Nitric oxide release accounts for the biological activity of endothelium-derived relaxing factor. *Nature* Nature Publishing Group; 1987; 327: 524–6.
22. Moncada S, Palmer RM, Higgs EA. Nitric oxide: physiology, pathophysiology, and pharmacology. *Pharmacol Rev* 1991; 43: 109–42.
23. Moncada S, Gryglewski R, Bunting S, et al. An enzyme isolated from arteries transforms prostaglandin endoperoxides to an unstable substance that inhibits platelet aggregation. *Nature* 1976; 263: 663–5.
24. Balsinde J, Winstead M V, Dennis EA. Phospholipase A₂ regulation of arachidonic acid mobilization. *FEBS Lett* 2002; 531: 2–6.
25. Iñiguez MA, Cacheiro-Llaguno C, Cuesta N, et al. Prostanoid function and cardiovascular disease. *Arch Physiol Biochem* 2008; 114: 201–9.
26. Szerafin T, Erdei N, Fülöp T, et al. Increased Cyclooxygenase-2 Expression and Prostaglandin-Mediated Dilation in Coronary Arterioles of Patients With Diabetes Mellitus. *Circ Res* 2006; 99: e12-317.
27. Féléto M. Endothelium-Dependent Hyperpolarizations: The Classical ‘EDHF’ Pathway. Morgan & Claypool Life Sciences Publisher; 2011; .
28. Busse R, Edwards G, Féléto M, et al. EDHF: bringing the concepts together. *Trends Pharmacol Sci* 2002; 23: 374–80.
29. Coleman HA, Tare M, Parkington HC. Endothelial potassium channels, endothelium-dependent hyperpolarization and the regulation of vascular tone in health and disease. *Clin Exp Pharmacol Physiol* 2004; 31: 641–9.
30. Chaytor AT, Evans WH, Griffith TM. Central role of heterocellular gap junctional communication in endothelium-dependent relaxations of rabbit arteries. *J Physiol* 1998; 561–73.
31. Agapitov A V, Haynes WG. Role of endothelin in cardiovascular disease. *J Renin-Angiotensin-Aldosterone Syst* SAGE PublicationsSage UK: London, England; 2002; 3: 1–15.
32. Schneider MP, Boesen EI, Pollock DM. Contrasting actions of endothelin ET(A) and ET(B) receptors in cardiovascular disease. *Annu Rev Pharmacol Toxicol* NIH Public Access; 2007; 47: 731–59.
33. Griesmacher A, Weigel G, Schreiner W, et al. Thromboxane A₂ generation by human umbilical endothelial cells. *Thromb Res* 1989; 56: 611–23.
34. Bustos M, Coffman TM, Saadi S, et al. Modulation of eicosanoid metabolism in endothelial cells in a xenograft model. Role of cyclooxygenase-2. *J Clin Invest* American Society for Clinical Investigation; 1997; 100: 1150–8.
35. Huang J-S, Ramamurthy SK, Lin X, et al. Cell signalling through thromboxane A₂ receptors. *Cell Signal* 2004; 16: 521–33.
36. Smyth EM. Thromboxane and the thromboxane receptor in cardiovascular disease. *Clin Lipidol* NIH Public Access; 2010; 5: 209–19.
37. van Hinsbergh VWM. The endothelium: vascular control of haemostasis. *Eur J Obstet Gynecol Reprod Biol* 2001; 95: 198–201.

38. Aird WC. Endothelium and haemostasis. *Hamostaseologie* Schattauer Publishers; 2015; 35: 11–6.
39. Verhamme P, Hoylaerts MF. THE PIVOTAL ROLE OF THE ENDOTHELIUM IN HAEMOSTASIS AND THROMBOSIS. *Acta Clin Belg* Taylor & Francis; 2006; 61: 213–9.
40. Ruggeri ZM. Von Willebrand factor, platelets and endothelial cell interactions. *J Thromb Haemost* Blackwell Science Inc; 2003; 1: 1335–42.
41. Yau JW, Teoh H, Verma S, et al. Endothelial cell control of thrombosis. *BMC Cardiovasc Disord* BioMed Central; 2015; 15: 130.
42. Osborn L. Leukocyte adhesion to endothelium in inflammation. *Cell* 1990; 62: 3–6.
43. Ley K, Laudanna C, Cybulsky MI, et al. Getting to the site of inflammation: the leukocyte adhesion cascade updated. *Nat Rev Immunol* Nature Publishing Group; 2007; 7: 678–89.
44. Ley K. The role of selectins in inflammation and disease.
45. Frank PG, Lisanti MP. ICAM-1: role in inflammation and in the regulation of vascular permeability. *Am J Physiol Heart Circ Physiol* American Physiological Society; 2008; 295: H926–7.
46. Granger DN, Senchenkova E. *Leukocyte–Endothelial Cell Adhesion*. Morgan & Claypool Life Sciences; 2010; .
47. Gahmberg CG, Valmu L, Fagerholm S, et al. Leukocyte integrins and inflammation. *Cell Mol Life Sci* 1998; 54: 549–55.
48. Piro M, Giubilato G, Pinnelli M, et al. Endothelium and inflammation. *Panminerva Med* 2005; 47: 75–80.
49. Woodfin A, Voisin M-B, Nourshargh S. PECAM-1: A Multi-Functional Molecule in Inflammation and Vascular Biology. *Arterioscler Thromb Vasc Biol* 2007; 27: 2514–23.
50. Hanna S, Etzioni A, Hvid M, et al. Leukocyte adhesion deficiencies. *Ann N Y Acad Sci* BioMed Central; 2012; 1250: 50–5.
51. Insull W, Berge KG, Wenger NK, et al. *The Pathology of Atherosclerosis: Plaque Development and Plaque Responses to Medical Treatment*. Am J Med Parthenon Publishing Group, New York; 2009; 122: S3–14.
52. Ross R, Glomset JA. *The Pathogenesis of Atherosclerosis*. N Engl J Med Massachusetts Medical Society ; 1976; 295: 420–5.
53. Deanfield JE, Halcox JP, Rabelink TJ. *Endothelial Function and Dysfunction*. *Circulation* 2007; 115: .
54. Hansson GK. *Inflammation, Atherosclerosis, and Coronary Artery Disease*. *N Engl J Med* 2005; 352: 1685–95.
55. Münzel T, Sinning C, Post F, et al. Pathophysiology, diagnosis and prognostic implications of endothelial dysfunction. *Ann Med* Taylor & Francis; 2008; 40: 180–96.
56. Stary HC, Chandler AB, Glagov S, et al. A definition of initial, fatty streak, and intermediate lesions of atherosclerosis. A report from the Committee on Vascular Lesions of the Council on Arteriosclerosis, American Heart Association. *Circulation* 1994; 89: .
57. Rensen SSM, Doevendans PAFM, van Eys GJJM. Regulation and characteristics of vascular smooth muscle cell phenotypic diversity. *Neth Heart J* Springer; 2007; 15: 100–8.

58. Jeremy J, P.H. R, E. R, et al. Nitric oxide and the proliferation of vascular smooth muscle cells. *Cardiovasc Res Oxford University Press*; 1999; 43: 580–94.
59. Badimon L, Vilahur G. Thrombosis formation on atherosclerotic lesions and plaque rupture. *J Intern Med* 2014; 276: 618–32.
60. Hansson GK. Inflammation, Atherosclerosis, and Coronary Artery Disease. *N Engl J Med Massachusetts Medical Society* ; 2005; 352: 1685–95.
61. Dyson A, Stidwill R, Taylor V, et al. Tissue oxygen monitoring in rodent models of shock. *AJP Hear Circ Physiol* 2007; 293: H526–33.
62. Carreau A, El Hafny-Rahbi B, Matejuk A, et al. Why is the partial oxygen pressure of human tissues a crucial parameter? Small molecules and hypoxia. *J Cell Mol Med Wiley-Blackwell*; 2011; 15: 1239–53.
63. Sullivan M, Galea P, Latif S. What is the appropriate oxygen tension for in vitro culture? *Mol Hum Reprod Oxford University Press*; 2006; 12: 653–653.
64. Brahimi-Horn MC, Pouyssegur J. Oxygen, a source of life and stress. *FEBS Lett* 2007; 581: 3582–91.
65. Boag JW. Cell respiration as a function of oxygen tension. *Int J Radiat Biol Relat Stud Phys Chem Med* 1970; 18: 475–8.
66. Ebbesen P, Eckardt K-U, Ciampor F, et al. Linking Measured Intercellular Oxygen Concentration to Human Cell Functions. *Acta Oncol (Madr)* 2004; 43: 598–600.
67. Semenza GL. Oxygen sensing, hypoxia-inducible factors, and disease pathophysiology. *Annu Rev Pathol Annual Reviews*; 2014; 9: 47–71.
68. Bracken CP, Fedele AO, Linke S, et al. Cell-specific Regulation of Hypoxia-inducible Factor (HIF)-1 α and HIF-2 α Stabilization and Transactivation in a Graded Oxygen Environment *. *in Press*; 2006; .
69. Hoshino Y, Morrison KJ, Vanhoutte PM. Mechanisms of hypoxic vasoconstriction in the canine isolated pulmonary artery: role of endothelium and sodium pump. *Am J Physiol* 1994; 267: L120-7.
70. Lumb AB, Slinger P. Hypoxic Pulmonary Vasoconstriction. *Anesthesiology Aspen, Karger*,; 2015; 122: 932–46.
71. Post JM, Hume JR, Archer SL, et al. Direct role for potassium channel inhibition in hypoxic pulmonary vasoconstriction. *Am J Physiol* 1992; 262: C882-90.
72. Aaronson PI, Robertson TP, Knock GA, et al. Hypoxic pulmonary vasoconstriction: mechanisms and controversies. *J Physiol Wiley-Blackwell*; 2006; 570: 53–8.
73. Michiels C. Physiological and pathological responses to hypoxia. *Am J Pathol American Society for Investigative Pathology*; 2004; 164: 1875–82.
74. Kulandavelu S, Balkan W, Hare JM. Regulation of oxygen delivery to the body via hypoxic vasodilation. *Proc Natl Acad Sci U S A National Academy of Sciences*; 2015; 112: 6254.
75. Shreeniwas R, Koga S, Karakurum M, et al. Hypoxia-mediated induction of endothelial cell interleukin-1 alpha. An autocrine mechanism promoting expression of leukocyte adhesion molecules on the vessel surface. *J Clin Invest* 1992; 90: 2333–9.
76. Michiels C, Arnould T, Remacle J. Endothelial cell responses to hypoxia: initiation of a cascade of cellular interactions. *Biochim Biophys Acta* 2000; 1497: 1–10.

77. Eltzschig HK, Carmeliet P. Hypoxia and inflammation. *N Engl J Med NIH Public Access*; 2011; 364: 656–65.
78. Dufourcq P, Seigneur M, Pruvost A, et al. Membrane thrombomodulin levels are decreased during hypoxia and restored by cAMP and IBMX. *Thromb Res* 1995; 77: 305–10.
79. Cui XY, Tinholt M, Stavik B, et al. Effect of hypoxia on tissue factor pathway inhibitor expression in breast cancer. *J Thromb Haemost* 2016; 14: 387–96.
80. Monteiro RQ, Lima LG, Gonçalves NP, et al. Hypoxia regulates the expression of tissue factor pathway signaling elements in a rat glioma model. *Oncol Lett Spandidos Publications*; 2016; 12: 315–22.
81. Görlach A, Berchner-Pfannschmidt U, Wotzlaw C, et al. Reactive oxygen species modulate HIF-1 mediated PAI-1 expression: involvement of the GTPase Rac1. *Thromb Haemost* 2003; 89: 926–35.
82. Sabit R, Thomas P, Shale DJ, et al. The Effects of Hypoxia on Markers of Coagulation and Systemic Inflammation in Patients With COPD. *Chest* 2010; 138: 47–51.
83. Goyal P, Weissmann N, Grimminger F, et al. Upregulation of NAD(P)H oxidase 1 in hypoxia activates hypoxia-inducible factor 1 via increase in reactive oxygen species. *Free Radic Biol Med* 2004; 36: 1279–88.
84. Murphy MP. How mitochondria produce reactive oxygen species. *Biochem J Portland Press Ltd*; 2009; 417: 1–13.
85. Jankov RP, Kantores C, Pan J, et al. Contribution of xanthine oxidase-derived superoxide to chronic hypoxic pulmonary hypertension in neonatal rats. *Am J Physiol - Lung Cell Mol Physiol* 2008; 294: .
86. ZANGAR R, Davydov DR, Verma S. Mechanisms that regulate production of reactive oxygen species by cytochrome P450. *Toxicol Appl Pharmacol* 2004; 199: 316–31.
87. Xia Y, Tsai AL, Berka V, et al. Superoxide generation from endothelial nitric-oxide synthase. A Ca²⁺/calmodulin-dependent and tetrahydrobiopterin regulatory process. *J Biol Chem* 1998; 273: 25804–8.
88. Takemoto M, Sun J, Hiroki J, et al. Rho-kinase mediates hypoxia-induced downregulation of endothelial nitric oxide synthase. *Circulation* 2002; 106: 57–62.
89. Prieto C, Krause B, Quezada C, et al. Hypoxia-reduced nitric oxide synthase activity is partially explained by higher arginase-2 activity and cellular redistribution in human umbilical vein endothelium. *Placenta* 2011; 32: 932–40.
90. Shi Y, Baker JE, Zhang C, et al. Chronic Hypoxia Increases Endothelial Nitric Oxide Synthase Generation of Nitric Oxide by Increasing Heat Shock Protein 90 Association and Serine Phosphorylation. *Circ Res* 2002; 91: .
91. Förstermann U, Sessa WC. Nitric oxide synthases: regulation and function. *Eur Heart J Oxford University Press*; 2012; 33: 829–37, 837a–837d.
92. Rafikov R, Fonseca F V, Kumar S, et al. eNOS activation and NO function: structural motifs responsible for the posttranslational control of endothelial nitric oxide synthase activity. *J Endocrinol NIH Public Access*; 2011; 210: 271–84.
93. Alderton WK, Cooper CE, Knowles RG. Nitric oxide synthases : structure, function and inhibition. *Biochem J* 2001; 357: 593–615.
94. Jufri NF, Mohamedali A, Avolio A, et al. Mechanical stretch: physiological and pathological

- implications for human vascular endothelial cells. *Vasc Cell BioMed Central*; 2015; 7: 8.
95. Gambaryan S, Geiger J, Schwarz UR, et al. Potent inhibition of human platelets by cGMP analogs independent of cGMP-dependent protein kinase. *Blood American Society of Hematology*; 2004; 103: 2593–600.
 96. Wang G-R, Zhu Y, Halushka P V, et al. Mechanism of platelet inhibition by nitric oxide: In vivo phosphorylation of thromboxane receptor by cyclic GMP-dependent protein kinase. *Biochemistry* 1998; 95: 4888–93.
 97. Kubes P, Suzuki M, Granger DN. Nitric oxide: An endogenous modulator of leukocyte adhesion. 1991; 88: 4651–5.
 98. Kempe S, Kestler H, Lasar A, et al. NF- κ B controls the global pro-inflammatory response in endothelial cells: evidence for the regulation of a pro-atherogenic program.
 99. Matthews JR, Botting CH, Panico M, et al. Inhibition of NF- κ B DNA binding by nitric oxide. *Nucleic Acids Res Oxford University Press*; 1996; 24: 2236–42.
 100. Peng HB, Libby P, Liao JK. Induction and stabilization of I kappa B alpha by nitric oxide mediates inhibition of NF- κ B. *J Biol Chem* 1995; 270: 14214–9.
 101. Nilsson J, Sjölund M, Palmberg L, et al. The calcium antagonist nifedipine inhibits arterial smooth muscle cell proliferation. *Atherosclerosis* 1985; 58: 109–22.
 102. Cornwell TL, Arnold E, Boerth NJ, et al. Inhibition of smooth muscle cell growth by nitric oxide and activation of cAMP-dependent protein kinase by cGMP. *Am J Physiol* 1994; 267: C1405-13.
 103. Ignarro LJ, Buga GM, Wei LH, et al. Role of the arginine-nitric oxide pathway in the regulation of vascular smooth muscle cell proliferation. *Proc Natl Acad Sci U S A National Academy of Sciences*; 2001; 98: 4202–8.
 104. Garthwaite J. *The Physiological Roles of Nitric Oxide in the Central Nervous System*. Springer Berlin Heidelberg; 2000 [cited 2017 May 18]. p. 259–75.
 105. Calabrese V, Mancuso C, Calvani M, et al. Nitric oxide in the central nervous system: neuroprotection versus neurotoxicity. *Nat Rev Neurosci* 2007; 8: 766–75.
 106. Arias-Salvatierra D, Silbergeld EK, Acosta-Saavedra LC, et al. Role of nitric oxide produced by iNOS through NF- κ B pathway in migration of cerebellar granule neurons induced by Lipopolysaccharide. *Cell Signal* 2011; 23: 425–35.
 107. Salvemini D, Billiar TR, Vodovotz Y. *Nitric Oxide and Inflammation* [Internet]. Birkhäuser Basel; 2001 [cited 2017 May 18].
 108. Ford PC, Wink DA, Stanbury DM. Autoxidation kinetics of aqueous nitric oxide. *FEBS Lett* 1993; 326: 1–3.
 109. Kelm M. Nitric oxide metabolism and breakdown. *Biochim Biophys Acta - Bioenerg* 1999; 1411: 273–89.
 110. Smith BC, Marletta MA. Mechanisms of S-nitrosothiol formation and selectivity in nitric oxide signaling. *Curr Opin Chem Biol NIH Public Access*; 2012; 16: 498–506.
 111. Carver J, Doctor A, Zaman K, et al. S-Nitrosothiol Formation. *Methods Enzymol* 2005 [cited 2017 May 19]. p. 95–105.
 112. Kissner R, Nauser T, Kurz C, et al. Peroxynitrous acid--where is the hydroxyl radical? *IUBMB Life* 55: 567–72.

113. Birben E, Sahiner UM, Sackesen C, et al. Oxidative stress and antioxidant defense. *World Allergy Organ J World Allergy Organization*; 2012; 5: 9–19.
114. Donohue JF. Ageing, smoking and oxidative stress. *Thorax BMJ Publishing Group*; 2006; 61: 461–2.
115. Krötz F, Sohn H-Y, Pohl U. Reactive Oxygen Species. *Arterioscler Thromb Vasc Biol* 2004; 24: .
116. HULTQUIST DE, PASSON PG. Catalysis of Methaemoglobin Reduction by Erythrocyte Cytochrome b₅ and Cytochrome b₅ Reductase. *Nature, Publ online* 24 Febr 1971; | doi101038/101038/newbio229252a0 *Nature Publishing Group*; 1971; 229: 252.
117. Wennmalm A, Benthin G, Edlund A, et al. Nitric oxide synthesis and metabolism in man. *Ann N Y Acad Sci* 1994; 714: 158–64.
118. Gladwin MT, Ognibene FP, Pannell LK, et al. Relative role of heme nitrosylation and beta-cysteine 93 nitrosation in the transport and metabolism of nitric oxide by hemoglobin in the human circulation. *Proc Natl Acad Sci U S A National Academy of Sciences*; 2000; 97: 9943–8.
119. Allen BW, Piantadosi CA. How do red blood cells cause hypoxic vasodilation? The SNO-hemoglobin paradigm. *Am J Physiol - Hear Circ Physiol* 2006; 291: .
120. Kleinbongard P, Dejam A, Lauer T, et al. Plasma nitrite reflects constitutive nitric oxide synthase activity in mammals. *Free Radic Biol Med* 2003; 35: 790–6.
121. Jungersten L, Ambring A, Wall B, et al. Both physical fitness and acute exercise regulate nitric oxide formation in healthy humans. *J Appl Physiol* 1997; 82: 760–4.
122. Wagner DA, Schultz DS, Deen WM, et al. Metabolic fate of an oral dose of 15N-labeled nitrate in humans: effect of diet supplementation with ascorbic acid. *Cancer Res* 1983; 43: 1921–5.
123. Kleinbongard P, Dejam A, Lauer T, et al. Plasma nitrite concentrations reflect the degree of endothelial dysfunction in humans. *Free Radic Biol Med* 2006; 40: 295–302.
124. James PE, Willis GR, Allen JD, et al. Nitrate pharmacokinetics: Taking note of the difference. *Nitric Oxide* 2015; 48: 44–50.
125. Lidder S, Webb AJ. Vascular effects of dietary nitrate (as found in green leafy vegetables & beetroot) via the Nitrate-Nitrite-Nitric Oxide pathway. *Br J Clin Pharmacol* 2012; 75: n/a-n/a.
126. Shimazu T, Kuriyama S, Hozawa A, et al. Dietary patterns and cardiovascular disease mortality in Japan: a prospective cohort study. *Int J Epidemiol* 2007; 36: 600–9.
127. Tada N, Maruyama C, Koba S, et al. Japanese dietary lifestyle and cardiovascular disease. *J Atheroscler Thromb* 2011; 18: 723–34.
128. Dontas AS, Zerefos NS, Panagiotakos DB, et al. Mediterranean diet and prevention of coronary heart disease in the elderly. *Clin Interv Aging* Dove Press; 2007; 2: 109.
129. Estruch R, Ros E, Salas-Salvadó J, et al. Primary Prevention of Cardiovascular Disease with a Mediterranean Diet. *N Engl J Med Massachusetts Medical Society*; 2013; 368: 1279–90.
130. Lundberg JO, Weitzberg E, Gladwin MT. The nitrate–nitrite–nitric oxide pathway in physiology and therapeutics. *Nat Rev Drug Discov* 2008; 7: 156–67.
131. Lundberg JO, Govoni M. Inorganic nitrate is a possible source for systemic generation of

- nitric oxide. *Free Radic Biol Med* 2004; 37: 395–400.
132. Doel JJ, Benjamin N, Hector MP, et al. Evaluation of bacterial nitrate reduction in the human oral cavity. *Eur J Oral Sci* 2005; 113: 14–9.
 133. Hyde ER, Andrade F, Vaksman Z, et al. Metagenomic analysis of nitrate-reducing bacteria in the oral cavity: implications for nitric oxide homeostasis. *PLoS One Public Library of Science*; 2014; 9: e88645.
 134. Duncan C, Dougall H, Johnston P, et al. Chemical generation of nitric oxide in the mouth from the enterosalivary circulation of dietary nitrate. *Nat Med* 1995; 1: 546–51.
 135. Govoni M, Jansson EÅ, Weitzberg E, et al. The increase in plasma nitrite after a dietary nitrate load is markedly attenuated by an antibacterial mouthwash. *Nitric Oxide* 2008; 19: 333–7.
 136. Broniowska KA, Hogg N. The Chemical Biology of S-Nitrosothiols. *Antioxid Redox Signal* 2012; 17: 969–80.
 137. Björne H, Govoni M, Törnberg DC, et al. Intra-gastric nitric oxide is abolished in intubated patients and restored by nitrite. *Crit Care Med* 2005; 33: 1722–7.
 138. Fang FC. Antimicrobial reactive oxygen and nitrogen species: concepts and controversies. *Nat Rev Microbiol* 2004; 2: 820–32.
 139. Dykhuizen RS, Frazer R, Duncan C, et al. Antimicrobial effect of acidified nitrite on gut pathogens: importance of dietary nitrate in host defense. *Antimicrob Agents Chemother American Society for Microbiology (ASM)*; 1996; 40: 1422–5.
 140. Lundberg JO, Govoni M. Inorganic nitrate is a possible source for systemic generation of nitric oxide. *Free Radic Biol Med* 2004; 37: 395–400.
 141. Lundberg JO, Gladwin MT, Ahluwalia A, et al. Nitrate and nitrite in biology, nutrition and therapeutics. *Nat Chem Biol* 2009; 5: 865–9.
 142. Lundberg JO, Weitzberg E, Gladwin MT. The nitrate-nitrite-nitric oxide pathway in physiology and therapeutics. *Nat Rev Drug Discov Nature Publishing Group*; 2008; 7: 156–67.
 143. KIMSHAPIRO D, GLADWIN M, PATEL R, et al. The reaction between nitrite and hemoglobin: the role of nitrite in hemoglobin-mediated hypoxic vasodilation. *J Inorg Biochem* 2005; 99: 237–46.
 144. Cosby K, Partovi KS, Crawford JH, et al. Nitrite reduction to nitric oxide by deoxyhemoglobin vasodilates the human circulation. *Nat Med* 2003; 9: 1498–505.
 145. Rassaf T, Flogel U, Drexhage C, et al. Nitrite Reductase Function of Deoxymyoglobin: Oxygen Sensor and Regulator of Cardiac Energetics and Function. *Circ Res* 2007; 100: 1749–54.
 146. Li H, Kundu TK, Zweier JL. Characterization of the Magnitude and Mechanism of Aldehyde Oxidase-mediated Nitric Oxide Production from Nitrite Running Title: Aldehyde oxidase mediated NO generation.
 147. Castello PR, David PS, McClure T, et al. Mitochondrial cytochrome oxidase produces nitric oxide under hypoxic conditions: implications for oxygen sensing and hypoxic signaling in eukaryotes. *Cell Metab* 2006; 3: 277–87.
 148. Gautier C, van Faassen E, Mikula I, et al. Endothelial nitric oxide synthase reduces nitrite anions to NO under anoxia. *Biochem Biophys Res Commun* 2006; 341: 816–21.

149. Katsuki S, Arnold W, Mittal C, et al. Stimulation of guanylate cyclase by sodium nitroprusside, nitroglycerin and nitric oxide in various tissue preparations and comparison to the effects of sodium azide and hydroxylamine. *J Cyclic Nucleotide Res* 1977; 3: 23–35.
150. Torfgård KE, Ahlner J. Mechanisms of action of nitrates. *Cardiovasc drugs Ther* 1994; 8: 701–17.
151. Abrams J. Beneficial actions of nitrates in cardiovascular disease. *Am J Cardiol* 1996; 77: C31–7.
152. Daiber A, Mü T. Organic Nitrate Therapy, Nitrate Tolerance, and Nitrate-Induced Endothelial Dysfunction: Emphasis on Redox Biology and Oxidative Stress.
153. Maher AR, Milsom AB, Gunaruwan P, et al. Hypoxic modulation of exogenous nitrite-induced vasodilation in humans. *Circulation* 2008; 117: 670–7.
154. Ingram TE, Fraser AG, Bleasdale RA, et al. Low-dose sodium nitrite attenuates myocardial ischemia and vascular ischemia-reperfusion injury in human models. *J Am Coll Cardiol* 2013; 61: 2534–41.
155. Weitzberg E, Hezel M, Lundberg JO. Nitrate-Nitrite-Nitric Oxide Pathway. *Anesthesiology* 2010; 113: 1460–75.
156. Webb A, Bond R, McLean P, et al. Reduction of nitrite to nitric oxide during ischemia protects against myocardial ischemia-reperfusion damage. *Proc Natl Acad Sci* 2004; 101: 13683–8.
157. Joshipura KJ, Hu FB, Manson JE, et al. The Effect of Fruit and Vegetable Intake on Risk for Coronary Heart Disease. *Ann Intern Med American College of Physicians*; 2001; 134: 1106.
158. Estruch R, Ros E, Salas-Salvadó J, et al. Primary Prevention of Cardiovascular Disease with a Mediterranean Diet. *N Engl J Med Massachusetts Medical Society*; 2013; 368: 1279–90.
159. Joshipura KJ. Fruit and Vegetable Intake in Relation to Risk of Ischemic Stroke. *JAMA* 1999; 282: 1233.
160. Liese AD, Nichols M, Sun X, et al. Adherence to the DASH Diet Is Inversely Associated With Incidence of Type 2 Diabetes: The Insulin Resistance Atherosclerosis Study. *Diabetes Care* 2009; 32: 1434–6.
161. Larsen FJ, Ekblom B, Sahlin K, et al. Effects of Dietary Nitrate on Blood Pressure in Healthy Volunteers. *N Engl J Med* 2006; 355: 2792–3.
162. Webb AJ, Patel N, Loukogeorgakis S, et al. Acute blood pressure lowering, vasoprotective, and antiplatelet properties of dietary nitrate via bioconversion to nitrite. *Hypertension* 2008; 51: 784–90.
163. Kapil V, Khambata RS, Robertson A, et al. Dietary Nitrate Provides Sustained Blood Pressure Lowering in Hypertensive Patients Novelty and Significance. *Hypertension* 2015; 65: .
164. Carlström M, Persson AEG, Larsson E, et al. Dietary nitrate attenuates oxidative stress, prevents cardiac and renal injuries, and reduces blood pressure in salt-induced hypertension. *Cardiovasc Res Oxford University Press*; 2011; 89: 574–85.
165. Srihirun S, Sriwantana T, Unchern S, et al. Platelet Inhibition by Nitrite Is Dependent on Erythrocytes and Deoxygenation. Tjwa M, editor. *PLoS One* 2012; 7: e30380.
166. Velmurugan S, Kapil V, Ghosh SM, et al. Antiplatelet effects of dietary nitrate in healthy volunteers: involvement of cGMP and influence of sex. *Free Radic Biol Med Elsevier*; 2013;

65: 1521–32.

167. Velmurugan S, Gan JM, Rathod KS, et al. Dietary nitrate improves vascular function in patients with hypercholesterolemia: a randomized, double-blind, placebo-controlled study. *Am J Clin Nutr* 2016; 103: 25–38.
168. Bondonno CP, Yang X, Croft KD, et al. Flavonoid-rich apples and nitrate-rich spinach augment nitric oxide status and improve endothelial function in healthy men and women: a randomized controlled trial. *Free Radic Biol Med* 2012; 52: 95–102.
169. Liu AH, Bondonno CP, Croft KD, et al. Effects of a nitrate-rich meal on arterial stiffness and blood pressure in healthy volunteers. *Nitric Oxide* 2013; 35: 123–30.
170. Jovanovski E, Bosco L, Khan K, et al. Effect of Spinach, a High Dietary Nitrate Source, on Arterial Stiffness and Related Hemodynamic Measures: A Randomized, Controlled Trial in Healthy Adults. *Clin Nutr Res* 2015; 4: 160–7.
171. Murray CJ, Lopez AD. Alternative projections of mortality and disability by cause 1990–2020: Global Burden of Disease Study. *Lancet* 1997; 349: 1498–504.
172. Jeddi S, Khalifi S, Ghanbari M, et al. Effects of Nitrate Intake on Myocardial Ischemia-Reperfusion Injury in Diabetic Rats. *Arq Bras Cardiol Arquivos Brasileiros de Cardiologia*; 2016; 107: 339–47.
173. Ingram TE, Pinder AG, Bailey DM, et al. Low-dose sodium nitrite vasodilates hypoxic human pulmonary vasculature by a means that is not dependent on a simultaneous elevation in plasma nitrite. *Am J Physiol Heart Circ Physiol* 2010; 298: H331-9.
174. Bailey SJ, Winyard P, Vanhatalo A, et al. Dietary nitrate supplementation reduces the O₂ cost of low-intensity exercise and enhances tolerance to high-intensity exercise in humans. *J Appl Physiol* 2009; 107: 1144–55.
175. LANSLEY KE, Winyard PG, Bailey SJ, et al. Acute Dietary Nitrate Supplementation Improves Cycling Time Trial Performance. 2011; 43: 1125–31.
176. Lansley KE, Winyard PG, Fulford J, et al. Dietary nitrate supplementation reduces the O₂ cost of walking and running: a placebo-controlled study. *J Appl Physiol* 2011; 110: 591–600.
177. Velmurugan S, Gan JM, Rathod KS, et al. Dietary nitrate improves vascular function in patients with hypercholesterolemia: a randomized, double-blind, placebo-controlled study. *Am J Clin Nutr American Society for Nutrition*; 2016; 103: 25–38.
178. Jovanovski E, Bosco L, Khan K, et al. Effect of Spinach, a High Dietary Nitrate Source, on Arterial Stiffness and Related Hemodynamic Measures: A Randomized, Controlled Trial in Healthy Adults. *Clin Nutr Res Korean Society of Clinical Nutrition*; 2015; 4: 160–7.
179. Rammos C, Hendgen-Cotta UB, Sobierajski J, et al. Dietary Nitrate Reverses Vascular Dysfunction in Older Adults With Moderately Increased Cardiovascular Risk. *J Am Coll Cardiol* 2014; 63: 1584–5.
180. Kapil V, Khambata RS, Robertson A, et al. Dietary nitrate provides sustained blood pressure lowering in hypertensive patients: a randomized, phase 2, double-blind, placebo-controlled study. *Hypertension* 2015; 65: 320–7.
181. Kenjale AA, Ham KL, Stabler T, et al. Dietary nitrate supplementation enhances exercise performance in peripheral arterial disease. *J Appl Physiol* 2011; 110: .
182. Larsen FJ, Weitzberg E, Lundberg JO, et al. Effects of dietary nitrate on oxygen cost during exercise. *Acta Physiol Blackwell Publishing Ltd*; 2007; 191: 59–66.

183. Gangolli SD, van den Brandt PA, Feron VJ, et al. Nitrate, nitrite and N-nitroso compounds. *Eur J Pharmacol Environ Toxicol Pharmacol* 1994; 292: 1–38.
184. Spiegelhalter B, Eisenbrand G, Preussmann R. Influence of dietary nitrate on nitrite content of human saliva: possible relevance to in vivo formation of N-nitroso compounds. *Food Cosmet Toxicol* 1976; 14: 545–8.
185. Tannenbaum SR. Preventive action of vitamin C on nitrosamine formation. *Int J Vitam Nutr Res Suppl* 1989; 30: 109–13.
186. Song P, Wu L, Guan W. Dietary Nitrates, Nitrites, and Nitrosamines Intake and the Risk of Gastric Cancer: A Meta-Analysis. *Nutrients Multidisciplinary Digital Publishing Institute (MDPI)*; 2015; 7: 9872–95.
187. Aschebrook-Kilfoy B, Ward MH, Gierach GL, et al. Epithelial ovarian cancer and exposure to dietary nitrate and nitrite in the NIH-AARP Diet and Health Study. *Eur J Cancer Prev* 2012; 21: 65–72.
188. Ward MH, Kilfoy BA, Weyer PJ, et al. Nitrate intake and the risk of thyroid cancer and thyroid disease. *Epidemiology NIH Public Access*; 2010; 21: 389–95.
189. Santamaria P. Nitrate in vegetables: toxicity, content, intake and EC regulation. *J Sci Food Agric* 2006; 86: 10–7.
190. COMLY HH. CYANOSIS IN INFANTS CAUSED BY NITRATES IN WELL WATER. *J Am Med Assoc American Medical Association*; 1945; 129: 112.
191. Avery AA. Infantile Methemoglobinemia: Reexamining the Role of Drinking Water Nitrates. *Environ Health Perspect* 1999; 107: 583.
192. Manassaram DM, Backer LC, Moll DM. A review of nitrates in drinking water: maternal exposure and adverse reproductive and developmental outcomes. *Environ Health Perspect National Institute of Environmental Health Science*; 2006; 114: 320–7.
193. STEINMETZ KA, POTTER JD. Vegetables, Fruit, and Cancer Prevention. *J Am Diet Assoc* 1996; 96: 1027–39.
194. CHARGAFF E, WEST R. The biological significance of the thromboplastic protein of blood. *J Biol Chem* 1946; 166: 189–97.
195. Wolf P. The Nature and Significance of Platelet Products in Human Plasma. *Br J Haematol Blackwell Publishing Ltd*; 1967; 13: 269–88.
196. Webber AJ, Johnson SA. Platelet participation in blood coagulation aspects of hemostasis. *Am J Pathol American Society for Investigative Pathology*; 1970; 60: 19–42.
197. de Duve C, Wattiaux R. Functions of Lysosomes. *Annu Rev Physiol Annual Reviews* 4139 El Camino Way, P.O. Box 10139, Palo Alto, CA 94303-0139, USA ; 1966; 28: 435–92.
198. Palade G. Intracellular aspects of the process of protein synthesis. *Science* 1975; 189: 347–58.
199. Fries E, Rothman JE. Transport of vesicular stomatitis virus glycoprotein in a cell-free extract. *Proc Natl Acad Sci U S A* 1980; 77: 3870–4.
200. Pan BT, Johnstone RM. Fate of the transferrin receptor during maturation of sheep reticulocytes in vitro: selective externalization of the receptor. *Cell* 1983; 33: 967–78.
201. Harding C, Heuser J, Stahl P. Receptor-mediated endocytosis of transferrin and recycling of the transferrin receptor in rat reticulocytes. *J Cell Biol* 1983; 97: 329–39.

202. Raposo G, Nijman HW, Stoorvogel W, et al. B lymphocytes secrete antigen-presenting vesicles. *J Exp Med* 1996; 183: 1161–72.
203. Lötvall J, Rajendran L, Gho Y-S, et al. The launch of *Journal of Extracellular Vesicles (JEV)*, the official journal of the International Society for Extracellular Vesicles - about microvesicles, exosomes, ectosomes and other extracellular vesicles. *J Extracell vesicles* Taylor & Francis; 2012; 1: .
204. Anderson HC. Vesicles associated with calcification in the matrix of epiphyseal cartilage. *J Cell Biol* 1969; 41: 59–72.
205. Karlsson M, Lundin S, Dahlgren U, et al. "Tolerosomes" are produced by intestinal epithelial cells. *Eur J Immunol* 2001; 31: 2892–900.
206. Stegmayr B, Ronquist G. Promotive effect on human sperm progressive motility by prostasomes. *Urol Res* 1982; 10: 253–7.
207. Meehan B, Rak J, Di Vizio D. Oncosomes - large and small: what are they, where they came from? *J Extracell vesicles* Taylor & Francis; 2016; 5: 33109.
208. Gould SJ, Raposo G. As we wait: coping with an imperfect nomenclature for extracellular vesicles. *J Extracell Vesicles* 2013; 2: 20389.
209. Booth AM, Fang Y, Fallon JK, et al. Exosomes and HIV Gag bud from endosome-like domains of the T cell plasma membrane. *J Cell Biol* 2006; 172: 923–35.
210. Vanlandingham PA, Ceresa BP. Rab7 Regulates Late Endocytic Trafficking Downstream of Multivesicular Body Biogenesis and Cargo Sequestration. *J Biol Chem* 2009; 284: 12110–24.
211. Théry C, Zitvogel L, Amigorena S. Exosomes: composition, biogenesis and function. *Nat Rev Immunol* Publ online 01 August 2002; | doi101038/nri855 Nature Publishing Group; 2002; 2: 569.
212. Harrison P, Gardiner C (Chris), Sargent IL. Extracellular vesicles in health and disease.
213. de Jong OG, Verhaar MC, Chen Y, et al. Cellular stress conditions are reflected in the protein and RNA content of endothelial cell-derived exosomes. *J Extracell vesicles* Taylor & Francis; 2012; 1: .
214. Henne WM, Buchkovich NJ, Emr SD. The ESCRT Pathway. *Dev Cell* 2011; 21: 77–91.
215. Hurley JH, Hanson PI. Membrane budding and scission by the ESCRT machinery: it's all in the neck. *Nat Rev Mol Cell Biol* 2010; 11: 556–66.
216. Wollert T, Wunder C, Lippincott-Schwartz J, et al. Membrane scission by the ESCRT-III complex. *Nature* 2009; 458: 172–7.
217. Colombo M, Moita C, van Niel G, et al. Analysis of ESCRT functions in exosome biogenesis, composition and secretion highlights the heterogeneity of extracellular vesicles. *J Cell Sci* 2013; 126: 5553–65.
218. Stuffers S, Sem Wegner C, Stenmark H, et al. Multivesicular Endosome Biogenesis in the Absence of ESCRTs. *Traffic* 2009; 10: 925–37.
219. Chairoungdua A, Smith DL, Pochard P, et al. Exosome release of β -catenin: a novel mechanism that antagonizes Wnt signaling. *J Cell Biol* 2010; 190: 1079–91.
220. Trajkovic K, Hsu C, Chiantia S, et al. Ceramide Triggers Budding of Exosome Vesicles into Multivesicular Endosomes. *Science* (80-) 2008; 319: 1244–7.
221. van Niel G, Charrin S, Simoes S, et al. The Tetraspanin CD63 Regulates ESCRT-Independent

- and -Dependent Endosomal Sorting during Melanogenesis. *Dev Cell* 2011; 21: 708–21.
222. Edgar JR, Eden ER, Futter CE. Hrs- and CD63-Dependent Competing Mechanisms Make Different Sized Endosomal Intraluminal Vesicles. *Traffic* 2014; 15: 197–211.
223. Perez-Hernandez D, Gutiérrez-Vázquez C, Jorge I, et al. The intracellular interactome of tetraspanin-enriched microdomains reveals their function as sorting machineries toward exosomes. *J Biol Chem American Society for Biochemistry and Molecular Biology*; 2013; 288: 11649–61.
224. Ghossoub R, Lembo F, Rubio A, et al. Syntenin-ALIX exosome biogenesis and budding into multivesicular bodies are controlled by ARF6 and PLD2. *Nat Commun* 2014; 5: 3477.
225. Savina A, Vidal M, Colombo MI. The exosome pathway in K562 cells is regulated by Rab11. *J Cell Sci* 2002; 115: 2505–15.
226. Savina A, Furlan M, Vidal M, et al. Exosome Release Is Regulated by a Calcium-dependent Mechanism in K562 Cells. *J Biol Chem* 2003; 278: 20083–90.
227. Hsu C, Morohashi Y, Yoshimura S, et al. Regulation of exosome secretion by Rab35 and its GTPase-activating proteins TBC1D10A–C. *J Cell Biol* 2010; 189: 223–32.
228. Ostrowski M, Carmo NB, Krumeich S, et al. Rab27a and Rab27b control different steps of the exosome secretion pathway. *Nat Cell Biol* 2010; 12: 19-30-13.
229. Webber JP, Spary LK, Sanders AJ, et al. Differentiation of tumour-promoting stromal myofibroblasts by cancer exosomes. *Oncogene* 2015; 34: 290–302.
230. Bobrie A, Krumeich S, Reyat F, et al. Rab27a Supports Exosome-Dependent and -Independent Mechanisms That Modify the Tumor Microenvironment and Can Promote Tumor Progression. *Cancer Res* 2012; 72: 4920–30.
231. Wang T, Gilkes DM, Takano N, et al. Hypoxia-inducible factors and RAB22A mediate formation of microvesicles that stimulate breast cancer invasion and metastasis. *Proc Natl Acad Sci U S A National Academy of Sciences*; 2014; 111: E3234-42.
232. Hyenne V, Apaydin A, Rodriguez D, et al. RAL-1 controls multivesicular body biogenesis and exosome secretion. *J Cell Biol* 2015; 211: 27–37.
233. Fader CM, Sánchez DG, Mestre MB, et al. TI-VAMP/VAMP7 and VAMP3/cellubrevin: two v-SNARE proteins involved in specific steps of the autophagy/multivesicular body pathways. *Biochim Biophys Acta - Mol Cell Res* 2009; 1793: 1901–16.
234. Colombo M, Raposo G, Théry C. Biogenesis, Secretion, and Intercellular Interactions of Exosomes and Other Extracellular Vesicles. *Annu Rev Cell Dev Biol* 2014; 30: 255–89.
235. Clark MR. Flippin' lipids. *Nat Immunol Nature Research*; 2011; 12: 373–5.
236. Hankins HM, Baldridge RD, Xu P, et al. Role of Flippases, Scramblases and Transfer Proteins in Phosphatidylserine Subcellular Distribution. *Traffic John Wiley & Sons A/S*; 2015; 16: 35–47.
237. Manno S, Takakuwa Y, Mohandas N. Identification of a functional role for lipid asymmetry in biological membranes: Phosphatidylserine-skeletal protein interactions modulate membrane stability. *Proc Natl Acad Sci* 2002; 99: 1943–8.
238. Fox JE, Austin CD, Boyles JK, et al. Role of the membrane skeleton in preventing the shedding of procoagulant-rich microvesicles from the platelet plasma membrane. *J Cell Biol* 1990; 111: 483–93.
239. Sapet C, Simoncini S, Loriod B, et al. Thrombin-induced endothelial microparticle

- generation: identification of a novel pathway involving ROCK-II activation by caspase-2. *Blood* 2006; 108: 1868–76.
240. Midura EF, Prakash PS, Johnson BL, et al. Impact of caspase-8 and PKA in regulating neutrophil-derived microparticle generation. *Biochem Biophys Res Commun* 2016; 469: 917–22.
 241. Reichstein E, Rothstein A. Effects of quinine on Ca⁺⁺-induced K⁺ efflux from human red blood cells. *J Membr Biol* 1981; 59: 57–63.
 242. Allan D, Thomas P. Ca²⁺-induced biochemical changes in human erythrocytes and their relation to microvesiculation. *Biochem J* 1981; 198: 433–40.
 243. Campbell LE, Nelson J, Gibbons E, et al. Membrane Properties Involved in Calcium-Stimulated Microparticle Release from the Plasma Membranes of S49 Lymphoma Cells. *Sci World J* 2014; 2014: 1–7.
 244. Curtis AM, Edelberg J, Jonas R, et al. Endothelial microparticles: sophisticated vesicles modulating vascular function. *Vasc Med NIH Public Access*; 2013; 18: 204–14.
 245. Wang J, Zhong Y, Ma X, et al. Analyses of Endothelial Cells and Endothelial Progenitor Cells Released Microvesicles by Using Microbead and Q-dot Based Nanoparticle Tracking Analysis. *Sci Rep Nature Publishing Group*; 2016; 6: 24679.
 246. Soriano AO, Jy W, Chirinos JA, et al. Levels of endothelial and platelet microparticles and their interactions with leukocytes negatively correlate with organ dysfunction and predict mortality in severe sepsis. *Crit Care Med* 2005; 33: 2540–6.
 247. Aatonen MT, Ohman T, Nyman TA, et al. Isolation and characterization of platelet-derived extracellular vesicles. *J Extracell vesicles Taylor & Francis*; 2014; 3: 24692.
 248. Italiano JE, Mairuhu ATA, Flaumenhaft R, et al. Clinical relevance of microparticles from platelets and megakaryocytes. *Curr Opin Hematol NIH Public Access*; 2010; 17: 578–84.
 249. El-Menshawly N, Eissa M, Farag R, et al. CD235a (Glycophorin-A) Is the Most Predictive Value Among Different Circulating Cellular Microparticles in Thrombocytopenic Human Immunodeficiency Virus Type 1. *J Clin Lab Anal* 2016; 30: 235–43.
 250. Macrì S, Pavesi E, Crescitelli R, et al. Immunophenotypic Profiling of Erythroid Progenitor-Derived Extracellular Vesicles in Diamond-Blackfan Anaemia: A New Diagnostic Strategy. Bertolini F, editor. *PLoS One Public Library of Science*; 2015; 10: e0138200.
 251. Lötvall J, Hill AF, Hochberg F, et al. Minimal experimental requirements for definition of extracellular vesicles and their functions: a position statement from the International Society for Extracellular Vesicles [Internet]. *J. Extracell. Vesicles Taylor & Francis*; Dec 22, 2014 p. 26913.
 252. Jaiswal JK, Andrews NW, Simon SM. Membrane proximal lysosomes are the major vesicles responsible for calcium-dependent exocytosis in nonsecretory cells. *J Cell Biol* 2002; 159: 625–35.
 253. Kowal J, Arras G, Colombo M, et al. Proteomic comparison defines novel markers to characterize heterogeneous populations of extracellular vesicle subtypes.
 254. Turiák L, Misják P, Szabó TG, et al. Proteomic characterization of thymocyte-derived microvesicles and apoptotic bodies in BALB/c mice. *J Proteomics* 2011; 74: 2025–33.
 255. Bobrie A, Colombo M, Krumeich S, et al. Diverse subpopulations of vesicles secreted by different intracellular mechanisms are present in exosome preparations obtained by differential ultracentrifugation [Internet]. *J. Extracell. Vesicles*. 2012 [cited 2015 Oct 6].

256. Kalra H, Simpson RJ, Ji H, et al. Vesiclepedia: A Compendium for Extracellular Vesicles with Continuous Community Annotation. *PLoS Biol Public Library of Science*; 2012; 10: e1001450.
257. Ratajczak J, Wysoczynski M, Hayek F, et al. Membrane-derived microvesicles: important and underappreciated mediators of cell-to-cell communication. *Leukemia* 2006; 20: 1487–95.
258. Valadi H, Ekström K, Bossios A, et al. Exosome-mediated transfer of mRNAs and microRNAs is a novel mechanism of genetic exchange between cells. *Nat Cell Biol* 2007; 9: 654–9.
259. Skog J, Würdinger T, van Rijn S, et al. Glioblastoma microvesicles transport RNA and proteins that promote tumour growth and provide diagnostic biomarkers. *Nat Cell Biol NIH Public Access*; 2008; 10: 1470–6.
260. Nolte-t Hoen ENM, Buermans HPJ, Waasdorp M, et al. Deep sequencing of RNA from immune cell-derived vesicles uncovers the selective incorporation of small non-coding RNA biotypes with potential regulatory functions. *Nucleic Acids Res* 2012; 40: 9272–85.
261. Subra C, Laulagnier K, Perret B, et al. Exosome lipidomics unravels lipid sorting at the level of multivesicular bodies. *Biochimie* 2007; 89: 205–12.
262. Needham D, Nunn RS. Elastic deformation and failure of lipid bilayer membranes containing cholesterol. *Biophys J* 1990; 58: 997–1009.
263. Connolly KD, Guschina IA, Yeung V, et al. Characterisation of adipocyte-derived extracellular vesicles released pre- and post-adipogenesis. *J Extracell vesicles* 2015; 4: 29159.
264. Pienimaeki-Roemer A, Kuhlmann K, Böttcher A, et al. Lipidomic and proteomic characterization of platelet extracellular vesicle subfractions from senescent platelets. *Transfusion* 2015; 55: 507–21.
265. Subra C, Grand D, Laulagnier K, et al. Exosomes account for vesicle-mediated transcellular transport of activatable phospholipases and prostaglandins. *J Lipid Res American Society for Biochemistry and Molecular Biology*; 2010; 51: 2105–20.
266. Beloribi S, Ristorcelli E, Breuzard G, et al. Exosomal Lipids Impact Notch Signaling and Induce Death of Human Pancreatic Tumoral SOJ-6 Cells. Hoheisel JD, editor. *PLoS One Public Library of Science*; 2012; 7: e47480.
267. Kim CW, Lee HM, Lee TH, et al. Extracellular membrane vesicles from tumor cells promote angiogenesis via sphingomyelin. *Cancer Res* 2002; 62: 6312–7.
268. Temchura V V., Tenbusch M, Nchinda G, et al. Enhancement of immunostimulatory properties of exosomal vaccines by incorporation of fusion-competent G protein of vesicular stomatitis virus. *Vaccine* 2008; 26: 3662–72.
269. Obregon C, Rothen-Rutishauser B, Gitahi SK, et al. Exovesicles from Human Activated Dendritic Cells Fuse with Resting Dendritic Cells, Allowing Them to Present Alloantigens. *Am J Pathol* 2006; 169: 2127–36.
270. Tian T, Zhu Y-L, Hu F-H, et al. Dynamics of exosome internalization and trafficking. *J Cell Physiol* 2013; 228: 1487–95.
271. Morelli AE, Larregina AT, Shufesky WJ, et al. Endocytosis, intracellular sorting, and processing of exosomes by dendritic cells. *Blood* 2004; 104: 3257–66.
272. N?slund TI, Paquin-Proulx D, Paredes PT, et al. Exosomes from breast milk inhibit HIV-1 infection of dendritic cells and subsequent viral transfer to CD4+ T cells. *AIDS* 2014; 28:

- 171–80.
273. Montecalvo A, Larregina AT, Shufesky WJ, et al. Mechanism of transfer of functional microRNAs between mouse dendritic cells via exosomes. *Blood* 2012; 119: 756–66.
 274. Nazarenko I, Rana S, Baumann A, et al. Cell Surface Tetraspanin Tspan8 Contributes to Molecular Pathways of Exosome-Induced Endothelial Cell Activation. *Cancer Res* 2010; 70: 1668–78.
 275. Deregibus MC, Cantaluppi V, Calogero R, et al. Endothelial progenitor cell derived microvesicles activate an angiogenic program in endothelial cells by a horizontal transfer of mRNA. *Blood* 2007; 110: 2440–8.
 276. Christianson HC, Svensson KJ, van Kuppevelt TH, et al. Cancer cell exosomes depend on cell-surface heparan sulfate proteoglycans for their internalization and functional activity. *Proc Natl Acad Sci* 2013; 110: 17380–5.
 277. Barres C, Blanc L, Bette-Bobillo P, et al. Galectin-5 is bound onto the surface of rat reticulocyte exosomes and modulates vesicle uptake by macrophages. *Blood* 2010; 115: 696–705.
 278. Mulcahy LA, Pink RC, Carter DRF. Routes and mechanisms of extracellular vesicle uptake. *J Extracell Vesicles* 2014; 3: 24641.
 279. Feng D, Zhao W-L, Ye Y-Y, et al. Cellular Internalization of Exosomes Occurs Through Phagocytosis. *Traffic* 2010; 11: 675–87.
 280. Kirchhausen T. Clathrin. *Annu Rev Biochem* 2000; 69: 699–727.
 281. Escrevente C, Keller S, Altevogt P, et al. Interaction and uptake of exosomes by ovarian cancer cells. *BMC Cancer* 2011; 11: 108.
 282. Fitzner D, Schnaars M, van Rossum D, et al. Selective transfer of exosomes from oligodendrocytes to microglia by macropinocytosis. *J Cell Sci* 2011; 124: 447–58.
 283. Nanbo A, Kawanishi E, Yoshida R, et al. Exosomes Derived from Epstein-Barr Virus-Infected Cells Are Internalized via Caveola-Dependent Endocytosis and Promote Phenotypic Modulation in Target Cells. *J Virol* 2013; 87: 10334–47.
 284. Nabi IR, Le PU. Caveolae/raft-dependent endocytosis. *J Cell Biol* 2003; 161: 673–7.
 285. Izquierdo-Useros N, Naranjo-Gomez M, Archer J, et al. Capture and transfer of HIV-1 particles by mature dendritic cells converges with the exosome-dissemination pathway. *Blood* 2009; 113: 2732–41.
 286. Rudt S, Müller RH. In vitro phagocytosis assay of nano- and microparticles by chemiluminescence. III. Uptake of differently sized surface-modified particles, and its correlation to particle properties and in vivo distribution. *Eur J Pharm Sci* 1993; 1: 31–9.
 287. Yuyama K, Sun H, Mitsutake S, et al. Sphingolipid-modulated Exosome Secretion Promotes Clearance of Amyloid- β by Microglia. *J Biol Chem* 2012; 287: 10977–89.
 288. Swanson JA. Shaping cups into phagosomes and macropinosomes. *Nat Rev Mol Cell Biol* 2008; 9: 639–49.
 289. Diehl P, Fricke A, Sander L, et al. Microparticles: major transport vehicles for distinct microRNAs in circulation. *Cardiovasc Res* 2012; 93: 633–44.
 290. Jahn R, Südhof TC. Membrane Fusion and Exocytosis. *Annu Rev Biochem* 1999; 68: 863–911.

291. Lawson C, Vicencio JM, Yellon DM, et al. Microvesicles and exosomes: new players in metabolic and cardiovascular disease. *J Endocrinol BioScientifica*; 2016; 228: R57-71.
292. Witwer KW, Buzás EI, Bemis LT, et al. Standardization of sample collection, isolation and analysis methods in extracellular vesicle research. *J Extracell vesicles Taylor & Francis*; 2013; 2: 20360.
293. Lippi G, Fontana R, Avanzini P, et al. Influence of mechanical trauma of blood and hemolysis on PFA-100 testing. *Blood Coagul Fibrinolysis* 2012; 23: 82–6.
294. Breddin HK, Harder S. Usefulness of tests to measure platelet function. *Vasa* 2003; 32: 123–9.
295. MILBURN JA, FORD I, CASSAR K, et al. Platelet activation, coagulation activation and C-reactive protein in simultaneous samples from the vascular access and peripheral veins of haemodialysis patients. *Int J Lab Hematol* 2012; 34: 52–8.
296. Lacroix R, Judicone C, Mooberry M, et al. Standardization of pre-analytical variables in plasma microparticle determination: results of the International Society on Thrombosis and Haemostasis SSC Collaborative workshop. *J Thromb Haemost* 2013; 2: 12207.
297. Jayachandran M, Miller VM, Heit JA, et al. Methodology for isolation, identification and characterization of microvesicles in peripheral blood. *J Immunol Methods* 2012; 375: 207–14.
298. Lange T, Dimitrov S, Born J. Effects of sleep and circadian rhythm on the human immune system. *Ann N Y Acad Sci* 2010; 1193: 48–59.
299. Scheer FAJL, Michelson AD, Frelinger AL, et al. The Human Endogenous Circadian System Causes Greatest Platelet Activation during the Biological Morning Independent of Behaviors. Yamazaki S, editor. *PLoS One* 2011; 6: e24549.
300. Madden LA, Vince R V., Sandström ME, et al. Microparticle-associated vascular adhesion molecule-1 and tissue factor follow a circadian rhythm in healthy human subjects. *Thromb Haemost* 2008; 99: 909–15.
301. Böing AN, van der Pol E, Grootemaat AE, et al. Single-step isolation of extracellular vesicles by size-exclusion chromatography. *J Extracell vesicles Taylor & Francis*; 2014; 3: .
302. Welton JL, Webber JP, Botos L-A, et al. Ready-made chromatography columns for extracellular vesicle isolation from plasma. *J Extracell vesicles Taylor & Francis*; 2015; 4: 27269.
303. Gyorgy B, Modos K, Pallinger E, et al. Detection and isolation of cell-derived microparticles are compromised by protein complexes resulting from shared biophysical parameters. *Blood* 2011; 117: e39–48.
304. Linares R, Tan S, Gounou C, et al. High-speed centrifugation induces aggregation of extracellular vesicles. *J Extracell vesicles Taylor & Francis*; 2015; 4: 29509.
305. van der Pol E, Böing AN, Harrison P, et al. Classification, functions, and clinical relevance of extracellular vesicles. *Pharmacol Rev* 2012; 64: 676–705.
306. Yuana Y, Levels J, Grootemaat A, et al. Co-isolation of extracellular vesicles and high-density lipoproteins using density gradient ultracentrifugation. *J Extracell Vesicles* 2014; 3: 23262.
307. Clayton A, Court J, Navabi H, et al. Analysis of antigen presenting cell derived exosomes, based on immuno-magnetic isolation and flow cytometry. *J Immunol Methods* 2001; 247: 163–74.

308. Kubota S, Chiba M, Watanabe M, et al. Secretion of small/microRNAs including miR-638 into extracellular spaces by sphingomyelin phosphodiesterase 3. *Oncol Rep Spandidos Publications*; 2015; 33: 67–73.
309. Sokolova V, Ludwig A-K, Hornung S, et al. Characterisation of exosomes derived from human cells by nanoparticle tracking analysis and scanning electron microscopy. *Colloids Surfaces B Biointerfaces* 2011; 87: 146–50.
310. Third International Meeting of ISEV 2014: Rotterdam, The Netherlands, April 30th – May 3rd, 2014. *J Extracell Vesicles Taylor & Francis*; 2014; 3: 24214.
311. Ramakrishnan DP, Hajj-Ali RA, Chen Y, et al. Extracellular vesicles activate a CD36 dependent signaling pathway to inhibit microvascular endothelial cell migration and tube formation. *Arterioscler Thromb Vasc Biol NIH Public Access*; 2016; 36: 534.
312. Kim HK, Song KS, Chung J-H, et al. Platelet microparticles induce angiogenesis in vitro. *Br J Haematol Blackwell Science Ltd*; 2004; 124: 376–84.
313. Teng X, Chen L, Chen W, et al. Mesenchymal Stem Cell-Derived Exosomes Improve the Microenvironment of Infarcted Myocardium Contributing to Angiogenesis and Anti-Inflammation. *Cell Physiol Biochem* 2015; 37: 2415–24.
314. Nolte-’t Hoen ENM, Buschow SI, Anderton SM, et al. Activated T cells recruit exosomes secreted by dendritic cells via LFA-1. *Blood* 2009; 113: 1977–81.
315. Admyre C, Bohle B, Johansson SM, et al. B cell-derived exosomes can present allergen peptides and activate allergen-specific T cells to proliferate and produce TH2-like cytokines. *J Allergy Clin Immunol* 2007; 120: 1418–24.
316. Théry C, Duban L, Segura E, et al. Indirect activation of naïve CD4+ T cells by dendritic cell-derived exosomes. *Nat Immunol* 2002; 3: 1156–62.
317. Segura E. ICAM-1 on exosomes from mature dendritic cells is critical for efficient naive T-cell priming. *Blood* 2005; 106: 216–23.
318. Bhatnagar S, Shinagawa K, Castellino FJ, et al. Exosomes released from macrophages infected with intracellular pathogens stimulate a proinflammatory response in vitro and in vivo. *Blood* 2007; 110: 3234–44.
319. MacKenzie A, Wilson HL, Kiss-Toth E, et al. Rapid secretion of interleukin-1beta by microvesicle shedding. *Immunity* 2001; 15: 825–35.
320. Kim SH, Bianco NR, Shufesky WJ, et al. MHC Class II+ Exosomes in Plasma Suppress Inflammation in an Antigen-Specific and Fas Ligand/Fas-Dependent Manner. *J Immunol* 2007; 179: .
321. Zhang B, Yin Y, Lai RC, et al. Mesenchymal Stem Cells Secrete Immunologically Active Exosomes. *Stem Cells Dev* 2014; 23: 1233–44.
322. Lo Sicco C, Reverberi D, Balbi C, et al. Mesenchymal Stem Cell-Derived Extracellular Vesicles as Mediators of Anti-Inflammatory Effects: Endorsement of Macrophage Polarization. *Stem Cells Transl Med* 2017; 6: 1018–28.
323. Gan HK, Cvrljevic AN, Johns TG. The epidermal growth factor receptor variant III (EGFRvIII): where wild things are altered. *FEBS J* 2013; 280: 5350–70.
324. Hao S, Bai O, Li F, et al. Mature dendritic cells pulsed with exosomes stimulate efficient cytotoxic T-lymphocyte responses and antitumour immunity. *Immunology* 2007; 120: 90–102.

325. Hao S, Bai O, Yuan J, et al. Dendritic cell-derived exosomes stimulate stronger CD8+ CTL responses and antitumor immunity than tumor cell-derived exosomes. *Cell Mol Immunol* 2006; 3: 205–11.
326. Dai S, Wan T, Wang B, et al. More Efficient Induction of HLA-A*0201-Restricted and Carcinoembryonic Antigen (CEA)-Specific CTL Response by Immunization with Exosomes Prepared from Heat-Stressed CEA-Positive Tumor Cells. *Clin Cancer Res* 2005; 11: 7554–63.
327. Abusamra AJ, Zhong Z, Zheng X, et al. Tumor exosomes expressing Fas ligand mediate CD8+ T-cell apoptosis. *Blood Cells, Mol Dis* 2005; 35: 169–73.
328. Kim JW, Wieckowski E, Taylor DD, et al. Fas ligand-positive membranous vesicles isolated from sera of patients with oral cancer induce apoptosis of activated T lymphocytes. *Clin Cancer Res* 2005; 11: 1010–20.
329. Andreola G, Rivoltini L, Castelli C, et al. Induction of lymphocyte apoptosis by tumor cell secretion of FasL-bearing microvesicles. *J Exp Med* 2002; 195: 1303–16.
330. Clayton A, Mitchell JP, Court J, et al. Human tumor-derived exosomes down-modulate NKG2D expression. *J Immunol* 2008; 180: 7249–58.
331. Cirri P, Chiarugi P. Cancer associated fibroblasts: the dark side of the coin. *Am J Cancer Res* 2011; 1: 482–97.
332. Owens AP, Mackman N. Microparticles in Hemostasis and Thrombosis. *Circ Res* 2011; 108: 1284–97.
333. Sinauridze EI, Kireev DA, Popenko NY, et al. Platelet microparticle membranes have 50- to 100-fold higher specific procoagulant activity than activated platelets. *Thromb Haemost* 2007; 97: 425–34.
334. Zhao L, Bi Y, Kou J, et al. Phosphatidylserine exposing-platelets and microparticles promote procoagulant activity in colon cancer patients. *J Exp Clin Cancer Res BioMed Central*; 2016; 35: 54.
335. Chen Y-W, Chen Y-C, Wang J-S. Absolute hypoxic exercise training enhances *in vitro* thrombin generation by increasing procoagulant platelet-derived microparticles under high shear stress in sedentary men. *Clin Sci* 2013; 124: 639–49.
336. Suades R, Padr? T, Vilahur G, et al. Circulating and platelet-derived microparticles in human blood enhance thrombosis on atherosclerotic plaques. *Thromb Haemost* 2012; 108: 1208–19.
337. Zubairova LD, Nabiullina RM, Nagaswami C, et al. Circulating Microparticles Alter Formation, Structure, and Properties of Fibrin Clots. *Sci Rep Nature Publishing Group*; 2015; 5: 17611.
338. Livaja Koshiar R, Somajo S, Norstr?m E, et al. Erythrocyte-Derived Microparticles Supporting Activated Protein C-Mediated Regulation of Blood Coagulation. Miyata T, editor. *PLoS One Public Library of Science*; 2014; 9: e104200.
339. Shet AS, Aras O, Gupta K, et al. Sickle blood contains tissue factor–positive microparticles derived from endothelial cells and monocytes. *Blood* 2003; 102: .
340. Markiewicz M, Richard E, Marks N, et al. Impact of endothelial microparticles on coagulation, inflammation, and angiogenesis in age-related vascular diseases. *J Aging Res Hindawi Publishing Corporation*; 2013; 2013: 734509.
341. Nieuwland R. Cellular origin of microparticles exposing tissue factor in cancer: a mixed double? *J Thromb Haemost Blackwell Publishing Ltd*; 2008; 6: 1514–6.

342. Khaspekova SG, Antonova OA, Shustova ON, et al. Activity of tissue factor in microparticles produced in vitro by endothelial cells, monocytes, granulocytes, and platelets. *Biochem Pleiades Publishing*; 2016; 81: 114–21.
343. Yáñez-Mó M, Siljander PR-M, Andreu Z, et al. Biological properties of extracellular vesicles and their physiological functions [Internet]. *J. Extracell. Vesicles*. 2015 [cited 2015 Nov 3].
344. Li M, Yu D, Williams KJ, et al. Tobacco Smoke Induces the Generation of Procoagulant Microvesicles From Human Monocytes/Macrophages. *Arterioscler Thromb Vasc Biol* 2010; 30: .
345. Midura EF, Jernigan PL, Kuethe JW, et al. Microparticles impact coagulation after traumatic brain injury. *J Surg Res* 2015; 197: 25–31.
346. Bang OY, Chung J-W, Lee MJ, et al. Cancer Cell-Derived Extracellular Vesicles Are Associated with Coagulopathy Causing Ischemic Stroke via Tissue Factor-Independent Way: The OASIS-CANCER Study. *PLoS One Public Library of Science*; 2016; 11: e0159170.
347. Leroyer AS, Isobe H, Lesèche G, et al. Cellular Origins and Thrombogenic Activity of Microparticles Isolated From Human Atherosclerotic Plaques. *J Am Coll Cardiol* 2007; 49: 772–7.
348. Huisse M-G, Lanoy E, Tcheche D, et al. Prothrombotic markers and early spontaneous recanalization in ST-segment elevation myocardial infarction. *Thromb Haemost* 2007; 98: 420–6.
349. Huisse M-G, Ajzenberg N, Feldman L, et al. Microparticle-linked tissue factor activity and increased thrombin activity play a potential role in fibrinolysis failure in ST-segment elevation myocardial infarction. *Thromb Haemost* 2009; 101: 734–40.
350. Berckmans RJ, Sturk A, Van Tienen LM, et al. Cell-derived vesicles exposing coagulant tissue factor in saliva.
351. Zwaal RFA, Comfurius P, Bevers EM. Surface exposure of phosphatidylserine in pathological cells. *C Cell Mol Life Sci* 2005; 62: 971–88.
352. Connor DE, Exner T, Ma DDF, et al. The majority of circulating platelet-derived microparticles fail to bind annexin V, lack phospholipid-dependent procoagulant activity and demonstrate greater expression of glycoprotein Ib. *Thromb Haemost* 2010; 103: 1044–52.
353. Feng B, Chen Y, Luo Y, et al. Circulating level of microparticles and their correlation with arterial elasticity and endothelium-dependent dilation in patients with type 2 diabetes mellitus. *Atherosclerosis* 2010; 208: 264–9.
354. Werner N, Wassmann S, Ahlers P, et al. Circulating CD31+/annexin V+ apoptotic microparticles correlate with coronary endothelial function in patients with coronary artery disease. *Arterioscler Thromb Vasc Biol* 2006; 26: 112–6.
355. Amabile N, Guérin AP, Leroyer A, et al. Circulating Endothelial Microparticles Are Associated with Vascular Dysfunction in Patients with End-Stage Renal Failure. *J Am Soc Nephrol* 2005; 16: 3381–8.
356. Boulanger CM, Scoazec A, Ebrahimian T, et al. Circulating microparticles from patients with myocardial infarction cause endothelial dysfunction. *Circulation* 2001; 104: 2649–52.
357. Densmore JC, Signorino PR, Ou J, et al. ENDOTHELIUM-DERIVED MICROPARTICLES INDUCE ENDOTHELIAL DYSFUNCTION AND ACUTE LUNG INJURY. *Shock* 2006; 26: 464–71.
358. Mostefai HA, Agouni A, Carusio N, et al. Phosphatidylinositol 3-kinase and xanthine oxidase

- regulate nitric oxide and reactive oxygen species productions by apoptotic lymphocyte microparticles in endothelial cells. *J Immunol* 2008; 180: 5028–35.
359. Agouni A, Mostefai HA, Porro C, et al. Sonic hedgehog carried by microparticles corrects endothelial injury through nitric oxide release. *FASEB J* 2007; 21: 2735–41.
 360. Martinez MC, Larbret F, Zobairi F, et al. Transfer of differentiation signal by membrane microvesicles harboring hedgehog morphogens. *Blood* 2006; 108: 3012–20.
 361. Kaparakis M, Turnbull L, Carneiro L, et al. Bacterial membrane vesicles deliver peptidoglycan to NOD1 in epithelial cells. *Cell Microbiol* 2010; 12: 372–85.
 362. Rautou P-E, Leroyer AS, Ramkhelawon B, et al. Microparticles From Human Atherosclerotic Plaques Promote Endothelial ICAM-1-Dependent Monocyte Adhesion and Transendothelial Migration. *Circ Res* 2011; 108: 335–43.
 363. Mesri M, Altieri DC. Endothelial cell activation by leukocyte microparticles. *J Immunol* 1998; 161: 4382–7.
 364. Mesri M, Altieri DC. Leukocyte microparticles stimulate endothelial cell cytokine release and tissue factor induction in a JNK1 signaling pathway. *J Biol Chem* 1999; 274: 23111–8.
 365. Barry OP, Pratico D, Savani RC, et al. Modulation of monocyte-endothelial cell interactions by platelet microparticles. *J Clin Invest* 1998; 102: 136–44.
 366. Barry OP, Pratico D, Lawson JA, et al. Transcellular activation of platelets and endothelial cells by bioactive lipids in platelet microparticles. *J Clin Invest* 1997; 99: 2118–27.
 367. Preston RA, Jy W, Jimenez JJ, et al. Effects of severe hypertension on endothelial and platelet microparticles. *Hypertens (Dallas, Tex 1979)* 2003; 41: 211–7.
 368. Forlow SB, McEver RP, Nollert MU. Leukocyte-leukocyte interactions mediated by platelet microparticles under flow. *Blood* 2000; 95: 1317–23.
 369. Mause SF, von Hundelshausen P, Zerneck A, et al. Platelet Microparticles: A Transcellular Delivery System for RANTES Promoting Monocyte Recruitment on Endothelium. *Arterioscler Thromb Vasc Biol* 2005; 25: 1512–8.
 370. Jansen F, Yang X, Baumann K, et al. Endothelial microparticles reduce ICAM-1 expression in a microRNA-222-dependent mechanism. *J Cell Mol Med* 2015; 19: n/a-n/a.
 371. Payne RA, Wilkinson IB, Webb DJ. Arterial Stiffness and Hypertension. *Hypertension* 2009; 55: .
 372. Luo G, Ducy P, McKee MD, et al. Spontaneous calcification of arteries and cartilage in mice lacking matrix GLA protein. *Nature* 1997; 386: 78–81.
 373. Reynolds JL, Skepper JN, McNair R, et al. Multifunctional Roles for Serum Protein Fetuin-A in Inhibition of Human Vascular Smooth Muscle Cell Calcification. *J Am Soc Nephrol* 2005; 16: 2920–30.
 374. Reynolds JL, Joannides AJ, Skepper JN, et al. Human Vascular Smooth Muscle Cells Undergo Vesicle-Mediated Calcification in Response to Changes in Extracellular Calcium and Phosphate Concentrations: A Potential Mechanism for Accelerated Vascular Calcification in ESRD. *J Am Soc Nephrol* 2004; 15: 2857–67.
 375. Kapustin A, Davies JD, Reynolds JL, et al. Calcium Regulates Key Components of Vascular Smooth Muscle Cell-Derived Matrix Vesicles to Enhance Mineralization. *Circ Res* 2011; .
 376. New SEP, Goettsch C, Aikawa M, et al. Macrophage-Derived Matrix Vesicles: An Alternative Novel Mechanism for Microcalcification in Atherosclerotic Plaques. *Circ Res* 2013; 113: 72–

7.

377. Hutcheson JD, Maldonado N, Aikawa E. Small entities with large impact: microcalcifications and atherosclerotic plaque vulnerability. *Curr Opin Lipidol Wolters Kluwer Health*; 2014; 25: 327–32.
378. Krohn JB, Hutcheson JD, Mart?nez-Mart?nez E, et al. Extracellular vesicles in cardiovascular calcification: expanding current paradigms. *J Physiol* 2016; 594: 2895–903.
379. Mizuno Y, Yagi K, Tokuzawa Y, et al. miR-125b inhibits osteoblastic differentiation by down-regulation of cell proliferation. *Biochem Biophys Res Commun* 2008; 368: 267–72.
380. Goettsch C, Rauner M, Pacyna N, et al. miR-125b Regulates Calcification of Vascular Smooth Muscle Cells. *Am J Pathol* 2011; 179: 1594–600.
381. Julich H, Willms A, Lukacs-Kornek V, et al. Extracellular Vesicle Profiling and Their Use as Potential Disease Specific Biomarker. *Front Immunol Frontiers*; 2014; 5: 413.
382. Harshman SW, Canella A, Ciarlariello PD, et al. Proteomic characterization of circulating extracellular vesicles identifies novel serum myeloma associated markers. *J Proteomics* 2016; 136: 89–98.
383. Werner N, Wassmann S, Ahlers P, et al. Circulating CD31+/Annexin V+ Apoptotic Microparticles Correlate With Coronary Endothelial Function in Patients With Coronary Artery Disease. *Arterioscler Thromb Vasc Biol* 2006; 26: 112–6.
384. Bulut D, Maier K, Bulut-Streich N, et al. Circulating Endothelial Microparticles Correlate Inversely With Endothelial Function in Patients With Ischemic Left Ventricular Dysfunction. *J Card Fail* 2008; 14: 336–40.
385. Sinning J-M, Losch J, Walenta K, et al. Circulating CD31+/Annexin V+ microparticles correlate with cardiovascular outcomes. *Eur Heart J* 2011; 32: 2034–41.
386. Raemdonck K, Braeckmans K, Demeester J, et al. Merging the best of both worlds: hybrid lipid-enveloped matrix nanocomposites in drug delivery. *Chem Soc Rev The Royal Society of Chemistry*; 2014; 43: 444–72.
387. Turturici G, Tinnirello R, Sconzo G, et al. Extracellular membrane vesicles as a mechanism of cell-to-cell communication: advantages and disadvantages. *AJP Cell Physiol* 2014; 306: C621–33.
388. Shimbo K, Miyaki S, Ishitobi H, et al. Exosome-formed synthetic microRNA-143 is transferred to osteosarcoma cells and inhibits their migration. *Biochem Biophys Res Commun* 2014; 445: 381–7.
389. Haney MJ, Klyachko NL, Zhao Y, et al. Exosomes as drug delivery vehicles for Parkinson’s disease therapy. *J Control Release* 2015; 207: 18–30.
390. György B, Hung ME, Breakefield XO, et al. Therapeutic applications of extracellular vesicles: clinical promise and open questions. *Annu Rev Pharmacol Toxicol NIH Public Access*; 2015; 55: 439–64.
391. Cheng Y, Schorey JS. Exosomes carrying mycobacterial antigens can protect mice against *Mycobacterium tuberculosis* infection. *Eur J Immunol* 2013; 43: 3279–90.
392. del Cacho E, Gallego M, Lee SH, et al. Induction of protective immunity against *Eimeria tenella* infection using antigen-loaded dendritic cells (DC) and DC-derived exosomes. *Vaccine* 2011; 29: 3818–25.
393. Beauvillain C, Juste MO, Dion S, et al. Exosomes are an effective vaccine against congenital

- toxoplasmosis in mice. *Vaccine* 2009; 27: 1750–7.
394. Escudier B, Dorval T, Chaput N, et al. Vaccination of metastatic melanoma patients with autologous dendritic cell (DC) derived-exosomes: results of the first phase I clinical trial. *J Transl Med* 2005; 3: 10.
395. Morse MA, Garst J, Osada T, et al. A phase I study of dexosome immunotherapy in patients with advanced non-small cell lung cancer. *J Transl Med* 2005; 3: 9.
396. Besse B, Charrier M, Lapierre V, et al. Dendritic cell-derived exosomes as maintenance immunotherapy after first line chemotherapy in NSCLC. *Oncoimmunology* Taylor & Francis; 2016; 5: e1071008.
397. Crampton SP, Davis J, Hughes CCW. Isolation of human umbilical vein endothelial cells (HUVEC). *J Vis Exp MyJoVE Corporation*; 2007; 183.
398. Berridge M V, Tan AS. Characterization of the cellular reduction of 3-(4,5-dimethylthiazol-2-yl)-2,5-diphenyltetrazolium bromide (MTT): subcellular localization, substrate dependence, and involvement of mitochondrial electron transport in MTT reduction. *Arch Biochem Biophys* 1993; 303: 474–82.
399. Cory AH, Owen TC, Barltrop JA, et al. Use of an aqueous soluble tetrazolium/formazan assay for cell growth assays in culture. *Cancer Commun* 1991; 3: 207–12.
400. Dragovic RA, Gardiner C, Brooks AS, et al. Sizing and phenotyping of cellular vesicles using Nanoparticle Tracking Analysis. *Nanomedicine Nanotechnology, Biol Med* 2011; 7: 780–8.
401. Carr B, Wright M. Nanoparticle Tracking Analysis: A Review of Applications and Usage in the Analysis of Exosomes and Microvesicles.
402. Filipe V, Hawe A, Jiskoot W. Critical evaluation of Nanoparticle Tracking Analysis (NTA) by NanoSight for the measurement of nanoparticles and protein aggregates. *Pharm Res* 2010; 27: 796–810.
403. Shelke GV, Lässer C, Gho YS, et al. Importance of exosome depletion protocols to eliminate functional and RNA-containing extracellular vesicles from fetal bovine serum. *J Extracell Vesicles* 2014; 3: .
404. Webber J, Clayton A. How pure are your vesicles? [Internet]. *J. Extracell. Vesicles*. 2013 [cited 2015 Sep 8].
405. Webber J, Stone TC, Katilius E, et al. Proteomics analysis of cancer exosomes using a novel modified aptamer-based array (SOMAscan™) platform. *Mol Cell Proteomics American Society for Biochemistry and Molecular Biology*; 2014; 13: 1050–64.
406. Time-resolved fluorometry | PerkinElmer [Internet]. [cited 2017 Apr 28].
407. Pinder AG, Rogers SC, Khalatbari A, et al. The measurement of nitric oxide and its metabolites in biological samples by ozone-based chemiluminescence. *Methods Mol Biol* 2008; 476: 11–28.
408. Bryan NS, Grisham MB. Methods to detect nitric oxide and its metabolites in biological samples. *Free Radic Biol Med NIH Public Access*; 2007; 43: 645–57.
409. Bundhoo SS, Anderson RA, Sagan E, et al. Direct formation of thienopyridine-derived nitrosothiols--just add nitrite! *Eur J Pharmacol* 2011; 670: 534–40.
410. Rogers SC, Gibbons LLB, Griffin S, et al. Analysis of S-nitrosothiols via copper cysteine (2C) and copper cysteine-carbon monoxide (3C) methods. - PubMed - NCBI [Internet]. *Methods*. 2013 [cited 2016 Nov 29]. p. 123–9.

411. Pettit EJ, Hallett MB. Release of 'caged' cytosolic Ca²⁺ triggers rapid spreading of human neutrophils adherent via integrin engagement. *J Cell Sci* 1998; 111: .
412. Cardinal DC, Flower RJ. The electronic aggregometer: a novel device for assessing platelet behavior in blood. *J Pharmacol Methods* 1980; 3: 135–58.
413. Tóth O, Calatzis A, Penz S, et al. Multiple electrode aggregometry: a new device to measure platelet aggregation in whole blood. *Thromb Haemost* 2006; 96: 781–8.
414. Lawrence MJ, Kumar S, Hawkins K, et al. A new structural biomarker that quantifies and predicts changes in clot strength and quality in a model of progressive haemodilution. *Thromb Res* 2014; 134: 488–94.
415. Evans PA, Hawkins K, Morris RHK, et al. Gel point and fractal microstructure of incipient blood clots are significant new markers of hemostasis for healthy and anticoagulated blood. *Blood* 2010; 116: 3341–6.
416. Muthukumar M, Winter HH. Fractal dimension of a crosslinking polymer at the gel point. *Macromolecules American Chemical Society*; 1986; 19: 1284–5.
417. Altman DG. *Practical statistics for medical research*. 1st ed. Chapman and Hall; 1991.
418. Favero G, Paganelli C, Buffoli B, et al. Endothelium and its alterations in cardiovascular diseases: life style intervention. *Biomed Res Int Hindawi Publishing Corporation*; 2014; 2014: 801896.
419. Hunt BJ, Jurd KM. Endothelial cell activation. A central pathophysiological process. *BMJ BMJ Group*; 1998; 316: 1328–9.
420. Adams DH, Shaw S. Leucocyte-endothelial interactions and regulation of leucocyte migration. *Lancet (London, England)* 1994; 343: 831–6.
421. Pober JS, Sessa WC. Evolving functions of endothelial cells in inflammation. *Nat Rev Immunol* 2007; 7: 803–15.
422. Epstein FH, Vane JR, Änggård EE, et al. Regulatory Functions of the Vascular Endothelium. *N Engl J Med* 1990; 323: 27–36.
423. Aird WC. Endothelium in health and disease. *Pharmacol Rep* 60: 139–43.
424. Pober JS, Cotran RS. Cytokines and endothelial cell biology. *Physiol Rev* 1990; 70: 427–51.
425. Aird WC. Spatial and temporal dynamics of the endothelium. *J Thromb Haemost* 2005; 3: 1392–406.
426. de Lizarrondo SM, Roncal C, Calvayrac O, et al. Synergistic Effect of Thrombin and CD40 Ligand on Endothelial Matrix Metalloproteinase-10 Expression and Microparticle Generation In Vitro and In Vivo. *Arterioscler Thromb Vasc Biol* 2012; 32: .
427. Burger D, Montezano AC, Nishigaki N, et al. Endothelial Microparticle Formation by Angiotensin II Is Mediated via Ang II Receptor Type I/NADPH Oxidase/ Rho Kinase Pathways Targeted to Lipid Rafts. *Arterioscler Thromb Vasc Biol* 2011; 31: 1898–907.
428. Berna N, Arnould T, Remacle J, et al. Hypoxia-induced increase in intracellular calcium concentration in endothelial cells: role of the Na(+)-glucose cotransporter. *J Cell Biochem* 2001; 84: 115–31.
429. Lichtenauer M, Goebel B, Fritzenwanger M, et al. Simulated temporary hypoxia triggers the release of CD31+/Annexin+ endothelial microparticles: A prospective pilot study in humans. *Clin Hemorheol Microcirc* 2014; .

430. King HW, Michael MZ, Gleadle JM. Hypoxic enhancement of exosome release by breast cancer cells. *BMC Cancer* 2012; 12: 421.
431. Semenza GL. HIF-1 mediates metabolic responses to intratumoral hypoxia and oncogenic mutations. *J Clin Invest* 2013; 123: 3664–71.
432. Lambert CM, Roy M, Robitaille GA, et al. HIF-1 inhibition decreases systemic vascular remodelling diseases by promoting apoptosis through a hexokinase 2-dependent mechanism. *Cardiovasc Res* 2010; 88: 196–204.
433. Stolze IP, Mole DR, Ratcliffe PJ. Regulation of HIF: prolyl hydroxylases. *Novartis Found Symp* 2006; 272: 15-25-36.
434. Østergaard L, Simonsen U, Eskildsen-Helmond Y, et al. Proteomics reveals lowering oxygen alters cytoskeletal and endoplasmatic stress proteins in human endothelial cells. *Proteomics WILEY-VCH Verlag*; 2009; 9: 4457–67.
435. Naseem KM. The role of nitric oxide in cardiovascular diseases. *Mol Aspects Med* 2005; 26: 33–65.
436. Hagen T, Taylor CT, Lam F, et al. Redistribution of intracellular oxygen in hypoxia by nitric oxide: effect on HIF1alpha. *Science* 2003; 302: 1975–8.
437. Agani FH, Puchowicz M, Chavez JC, et al. Role of nitric oxide in the regulation of HIF-1 α expression during hypoxia. *Am J Physiol - Cell Physiol* 2002; 283: .
438. Wang J-M, Wang Y, Huang J-Y, et al. C-Reactive protein-induced endothelial microparticle generation in HUVECs is related to BH4-dependent NO formation. *J Vasc Res* 2007; 44: 241–8.
439. Lundberg JO, Weitzberg E, Gladwin MT. The nitrate-nitrite-nitric oxide pathway in physiology and therapeutics. *Nat Rev Drug Discov Nature Publishing Group*; 2008; 7: 156–67.
440. Khambata RS, Ghosh SM, Ahluwalia A. ‘Repurposing’ of Xanthine Oxidoreductase as a Nitrite Reductase: A New Paradigm for Therapeutic Targeting in Hypertension. *Antioxid Redox Signal* 2015; 23: 340–53.
441. Li H, Samouilov A, Liu X, et al. Characterization of the magnitude and kinetics of xanthine oxidase-catalyzed nitrate reduction: evaluation of its role in nitrite and nitric oxide generation in anoxic tissues. *Biochemistry* 2003; 42: 1150–9.
442. Shiva S, Huang Z, Grubina R, et al. Deoxymyoglobin is a nitrite reductase that generates nitric oxide and regulates mitochondrial respiration. *Circ Res* 2007; 100: 654–61.
443. Basu S, Azarova NA, Font MD, et al. Nitrite reductase activity of cytochrome c. *J Biol Chem* 2008; 283: 32590–7.
444. Milosevic M, Bristow R, Chung P, et al. Prostate cancer hypoxia correlates with poor patient outcome following treatment with radiotherapy. *Int J Radiat Oncol Elsevier*; 2004; 60: S236–7.
445. Vince R V, Christmas B, Midgley AW, et al. Hypoxia mediated release of endothelial microparticles and increased association of S100A12 with circulating neutrophils. *Oxid Med Cell Longev* 2009; 2: 2–6.
446. Collins J-A, Rudenski A, Gibson J, et al. Relating oxygen partial pressure, saturation and content: the haemoglobin-oxygen dissociation curve. *Breathe (Sheffield, England)* 2015; 11: 194–201.

447. Pinder AG, James PE. When does low oxygen become hypoxia? Implications for nitrite reduction. *Circ Res* 2009; 104: e25-6.
448. Dignat-George F, Boulanger CM. The many faces of endothelial microparticles. *Arterioscler Thromb Vasc Biol* 2011; 31: 27–33.
449. Lee S-T, Chu K, Jung K-H, et al. Circulating CD62E+ microparticles and cardiovascular outcomes. *PLoS One* 2012; 7: e35713.
450. Hron G, Kollars M, Weber H, et al. Tissue factor-positive microparticles: cellular origin and association with coagulation activation in patients with colorectal cancer. *Thromb Haemost* 2007; 97: 119–23.
451. Jy W, Jimenez JJ, Mauro LM, et al. Endothelial microparticles induce formation of platelet aggregates via a von Willebrand factor/ristocetin dependent pathway, rendering them resistant to dissociation. *J Thromb Haemost* 2005; 3: 1301–8.
452. Abid Hussein MN, Böing AN, Biró E, et al. Phospholipid composition of in vitro endothelial microparticles and their in vivo thrombogenic properties. *Thromb Res* 2008; 121: 865–71.
453. Lentz BR. Exposure of platelet membrane phosphatidylserine regulates blood coagulation. *Prog Lipid Res* 2003; 42: 423–38.
454. Berra E, Roux D, Richard DE, et al. Hypoxia-inducible factor-1 alpha (HIF-1 alpha) escapes O(2)-driven proteasomal degradation irrespective of its subcellular localization: nucleus or cytoplasm. *EMBO Rep European Molecular Biology Organization*; 2001; 2: 615–20.
455. Koh MY, Powis G. Passing the baton: the HIF switch. *Trends Biochem Sci NIH Public Access*; 2012; 37: 364–72.
456. Lin Q, Cong X, Yun Z, et al. Differential hypoxic regulation of hypoxia-inducible factors 1alpha and 2alpha. *Mol Cancer Res Molecular Cancer Research*; 2011; 9: 757–65.
457. Yang S, Wu C, Xiong Z, et al. Progress on hypoxia-inducible factor-3: Its structure, gene regulation and biological function (Review). *Mol Med Rep* 2015; 12: 2411–6.
458. Zhang P, Yao Q, Lu L, et al. Hypoxia-inducible factor 3 is an oxygen-dependent transcription activator and regulates a distinct transcriptional response to hypoxia. *Cell Rep* 2014; 6: 1110–21.
459. Michiels C, Arnould T, Remacle J. Endothelial cell responses to hypoxia: initiation of a cascade of cellular interactions. *Biochim Biophys Acta - Mol Cell Res* 2000; 1497: 1–10.
460. Arnould T, Michiels C, Alexandre I, et al. Effect of hypoxia upon intracellular calcium concentration of human endothelial cells. *J Cell Physiol* 1992; 152: 215–21.
461. Comfurius P, Senden JM, Tilly RH, et al. Loss of membrane phospholipid asymmetry in platelets and red cells may be associated with calcium-induced shedding of plasma membrane and inhibition of aminophospholipid translocase. *Biochim Biophys Acta* 1990; 1026: 153–60.
462. Yano Y, Shiba E, Kambayashi J, et al. The effects of calpeptin (a calpain specific inhibitor) on agonist induced microparticle formation from the platelet plasma membrane. *Thromb Res* 1993; 71: 385–96.
463. Tyagi T, Ahmad S, Gupta N, et al. Altered expression of platelet proteins and calpain activity mediate hypoxia-induced prothrombotic phenotype. *Blood American Society of Hematology*; 2014; 123: 1250–60.
464. Pasquet J-M, Dachary-Prigent J, Nurden AT. Calcium Influx is a Determining Factor of

- Calpain Activation and Microparticle Formation in Platelets. *Eur J Biochem* 1996; 239: 647–54.
465. Allan D, Thomas P. Ca²⁺-induced biochemical changes in human erythrocytes and their relation to microvesiculation. *Biochem J* 1981; 198: 433–40.
466. Weidemann A, Breyer J, Rehm M, et al. HIF-1 α activation results in actin cytoskeleton reorganization and modulation of Rac-1 signaling in endothelial cells. *Cell Commun Signal* 2013; 11: 80.
467. Zhang Z, Naughton D, Winyard PG, et al. Generation of nitric oxide by a nitrite reductase activity of xanthine oxidase: a potential pathway for nitric oxide formation in the absence of nitric oxide synthase activity. *Biochem Biophys Res Commun* 1998; 249: 767–72.
468. Shiva S. Nitrite: A Physiological Store of Nitric Oxide and Modulator of Mitochondrial Function. *Redox Biol* 2013; 1: 40–4.
469. Kim-Shapiro DB, Gladwin MT. Mechanisms of nitrite bioactivation. *Nitric oxide Biol Chem NIH Public Access*; 2014; 38: 58–68.
470. Ingram TE, Fraser AG, Bleasdale RA, et al. Low-dose sodium nitrite attenuates myocardial ischemia and vascular ischemia-reperfusion injury in human models. *J Am Coll Cardiol* 2013; 61: 2534–41.
471. Semenza GL. Hypoxia-inducible factor 1: oxygen homeostasis and disease pathophysiology. *Trends Mol Med* 2001; 7: 345–50.
472. Huang LE, Willmore WG, Gu J, et al. Inhibition of hypoxia-inducible factor 1 activation by carbon monoxide and nitric oxide. Implications for oxygen sensing and signaling. *J Biol Chem* 1999; 274: 9038–44.
473. Sogawa K, Numayama-Tsuruta K, Ema M, et al. Inhibition of hypoxia-inducible factor 1 activity by nitric oxide donors in hypoxia. *Proc Natl Acad Sci U S A* 1998; 95: 7368–73.
474. Yin J-H, Yang D-I, Ku G, et al. iNOS Expression Inhibits Hypoxia-Inducible Factor-1 Activity. *Biochem Biophys Res Commun* 2000; 279: 30–4.
475. Mateo J, García-Lecea M, Cadenas S, et al. Regulation of hypoxia-inducible factor-1 α by nitric oxide through mitochondria-dependent and -independent pathways. *Biochem J* 2003; 376: 537–44.
476. Metzzen E, Zhou J, Jelkmann W, et al. Nitric oxide impairs normoxic degradation of HIF-1 α by inhibition of prolyl hydroxylases. *Mol Biol Cell* 2003; 14: 3470–81.
477. Sandau KB, Fandrey J, Brüne B. Accumulation of HIF-1 α under the influence of nitric oxide. *Blood* 2001; 97: 1009–15.
478. Natarajan R, Fisher BJ, Fowler AA. Regulation of hypoxia inducible factor-1 by nitric oxide in contrast to hypoxia in microvascular endothelium. *FEBS Lett* 2003; 549: 99–104.
479. Sumbayev V V, Budde A, Zhou J, et al. HIF-1 α protein as a target for S-nitrosation. *FEBS Lett* 2003; 535: 106–12.
480. Chandel NS, McClintock DS, Feliciano CE, et al. Reactive Oxygen Species Generated at Mitochondrial Complex III Stabilize Hypoxia-inducible Factor-1 during Hypoxia: A MECHANISM OF O₂ SENSING. *J Biol Chem* 2000; 275: 25130–8.
481. Zhang W, Zhou X, Yao Q, et al. HIF-1-mediated production of exosomes during hypoxia is protective in renal tubular cells. *Am J Physiol - Ren Physiol* 2017; .
482. Burnley-Hall N, Willis G, Davis J, et al. Nitrite-derived nitric oxide reduces hypoxia-inducible

- factor 1 α -mediated extracellular vesicle production by endothelial cells. *Nitric Oxide* 2017; 63: 1–12.
483. Göhner C, Schlembach D, Schleussner E, et al. PP009. Hypoxia alters syncytiotrophoblastic microparticles (STBM)-related coagulation capacities. *Pregnancy Hypertens An Int J Women's Cardiovasc Heal* 2013; 3: 70.
484. Yokota N, Koizume S, Miyagi E, et al. Self-production of tissue factor-coagulation factor VII complex by ovarian cancer cells. *Br J Cancer Nature Publishing Group*; 2009; 101: 2023–9.
485. Tadokoro H, Umezu T, Ohyashiki K, et al. Exosomes Derived from Hypoxic Leukemia Cells Enhance Tube Formation in Endothelial Cells. *J Biol Chem* 2013; 288: 34343–51.
486. Tual-Chalot S, Guibert C, Muller B, et al. Circulating Microparticles from Pulmonary Hypertensive Rats Induce Endothelial Dysfunction. *Am J Respir Crit Care Med American Thoracic Society*; 2010; 182: 261–8.
487. Zuckerbraun BS, Shiva S, Ifedigbo E, et al. Nitrite Potently Inhibits Hypoxic and Inflammatory Pulmonary Arterial Hypertension and Smooth Muscle Proliferation via Xanthine Oxidoreductase-Dependent Nitric Oxide Generation. *Circulation* 2010; 121: 98–109.
488. Webb A, Bond R, McLean P, et al. Reduction of nitrite to nitric oxide during ischemia protects against myocardial ischemia-reperfusion damage. *Proc Natl Acad Sci* 2004; 101: 13683–8.
489. Pera J, Undas A, Topor-Madry R, et al. Fibrin Clot Properties in Acute Stroke: What Differs Cerebral Hemorrhage From Cerebral Ischemia? *Stroke* 2012; 43: 1412–4.
490. Weisel JW. BIOPHYSICS: Enigmas of Blood Clot Elasticity. *Science (80-)* 2008; 320: 456–7.
491. Undas A, Ariens RAS. Fibrin Clot Structure and Function: A Role in the Pathophysiology of Arterial and Venous Thromboembolic Diseases. *Arterioscler Thromb Vasc Biol* 2011; 31: e88–99.
492. Undas A, Zawilska K, Ciesla-Dul M, et al. Altered fibrin clot structure/function in patients with idiopathic venous thromboembolism and in their relatives. *Blood* 2009; 114: 4272–8.
493. Undas A, Podolec P, Zawilska K, et al. Altered Fibrin Clot Structure/Function in Patients With Cryptogenic Ischemic Stroke. *Stroke* 2009; 40: 1499–501.
494. Palka I, Nessler J, Nessler B, et al. Altered fibrin clot properties in patients with chronic heart failure and sinus rhythm: a novel prothrombotic mechanism. *Heart* 2010; 96: 1114–8.
495. Neergaard-Petersen S, Hvas A-M, Kristensen SD, et al. The influence of type 2 diabetes on fibrin clot properties in patients with coronary artery disease. *Thromb Haemost* 2014; 112: 1142–50.
496. Ahmed Sabra,^{1,2,3} Matthew James Lawrence,^{1,2} Robert Aubrey 1, Daniel Obaid 4, Alexander Chase 4, et al. Characterisation of clot microstructure properties in stable coronary artery disease. *BMJ openheart* 2017; 4: .
497. Colle JP, Mishal Z, Lesty C, et al. Abnormal fibrin clot architecture in nephrotic patients is related to hypofibrinolysis: influence of plasma biochemical modifications: a possible mechanism for the high thrombotic tendency? *Thromb Haemost* 1999; 82: 1482–9.
498. Silveira A, Hamsten A. Fibrin Gel Architecture Influences Endogenous Fibrinolysis and May Promote Coronary Artery Disease. *Arterioscler Thromb Vasc Biol* 2006; 26: 2419–20.

499. Cui XY, Tinholt M, Stavik B, et al. Effect of hypoxia on tissue factor pathway inhibitor expression in breast cancer. *J Thromb Haemost* 2016; 14: 387–96.
500. Stavik B, Espada S, Cui XY, et al. EPAS1/HIF-2 alpha-mediated downregulation of tissue factor pathway inhibitor leads to a pro-thrombotic potential in endothelial cells. *Biochim Biophys Acta - Mol Basis Dis* 2016; 1862: 670–8.
501. Monteiro RQ, Lima LG, Gonçalves NP, et al. Hypoxia regulates the expression of tissue factor pathway signaling elements in a rat glioma model. *Oncol Lett Spandidos Publications*; 2016; 12: 315–22.
502. Yan SF, Zou YS, Gao Y, et al. Tissue factor transcription driven by Egr-1 is a critical mechanism of murine pulmonary fibrin deposition in hypoxia. *Proc Natl Acad Sci U S A* 1998; 95: 8298–303.
503. Yang Y, Loscalzo J. Regulation of Tissue Factor Expression in Human Microvascular Endothelial Cells by Nitric Oxide. *Circulation* 2000; 101: .
504. Loscalzo J, Welch G. Nitric oxide and its role in the cardiovascular system. *Prog Cardiovasc Dis* 38: 87–104.
505. Park JW, Piknova B, Nghiem K, et al. Inhibitory effect of nitrite on coagulation processes demonstrated by thrombelastography. *Nitric oxide Biol Chem NIH Public Access*; 2014; 40: 45–51.
506. Trepels T, Zeiher AM, Fichtlscherer S. The endothelium and inflammation. *Endothelium* 13: 423–9.
507. Lee HM, Choi E-J, Kim JH, et al. A membranous form of ICAM-1 on exosomes efficiently blocks leukocyte adhesion to activated endothelial cells [Internet]. *Biochem. Biophys. Res. Commun.* 2010.
508. Hartupee J, Li X, Hamilton T. Interleukin 1 α -induced NF κ B Activation and Chemokine mRNA Stabilization Diverge at IRAK1. *J Biol Chem* 2008; 283: 15689–93.
509. Wang L, Walia B, Evans J, et al. IL-6 induces NF-kappa B activation in the intestinal epithelia. *J Immunol* 2003; 171: 3194–201.
510. Xia P, Gamble JR, Rye K-A, et al. Tumor necrosis factor- α induces adhesion molecule expression through the sphingosine kinase pathway. *Cell Biol* 1998; 95: 14196–201.
511. Ledebur HC, Parks TP. Transcriptional regulation of the intercellular adhesion molecule-1 gene by inflammatory cytokines in human endothelial cells. Essential roles of a variant NF-kappa B site and p65 homodimers. *J Biol Chem* 1995; 270: 933–43.
512. Neish AS, Williams AJ, Palmer HJ, et al. Functional analysis of the human vascular cell adhesion molecule 1 promoter. *J Exp Med* 1992; 176: 1583–93.
513. Schindler U, Baichwal VR. Three NF-kappa B binding sites in the human E-selectin gene required for maximal tumor necrosis factor alpha-induced expression. *Mol Cell Biol* 1994; 14: 5820–31.
514. Pan J, McEver RP. Regulation of the human P-selectin promoter by Bcl-3 and specific homodimeric members of the NF-kappa B/Rel family. *J Biol Chem* 1995; 270: 23077–83.
515. Jy W, Minagar A, Jimenez JJ, et al. Endothelial microparticles (EMP) bind and activate monocytes: elevated EMP-monocyte conjugates in multiple sclerosis. *Front Biosci* 2004; 9: 3137–44.
516. Carreau A, Kieda C, Grillon C. Nitric oxide modulates the expression of endothelial cell

- adhesion molecules involved in angiogenesis and leukocyte recruitment. *Exp Cell Res* 2011; 317: 29–41.
517. Zampolli A, Basta G, Lazzerini G, et al. Inhibition of endothelial cell activation by nitric oxide donors. *J Pharmacol Exp Ther* 2000; 295: 818–23.
 518. Greijer AE, van der Wall E. The role of hypoxia inducible factor 1 (HIF-1) in hypoxia induced apoptosis. *J Clin Pathol* BMJ Publishing Group; 2004; 57: 1009–14.
 519. Arnould T, Michiels C, Alexandre I, et al. Effect of hypoxia upon intracellular calcium concentration of human endothelial cells. *J Cell Physiol* Wiley Subscription Services, Inc., A Wiley Company; 1992; 152: 215–21.
 520. BretVerhoven B, Schlegel RA, Williamson P. Mechanisms of Phosphatidylserine Exposure, A Phagocyte Recognition Signal, on Apoptotic T Lymphocytes.
 521. Aharon A, Tamari T, Brenner B. Microparticles Induce Procoagulant and Apoptotic Effects on Endothelial Cells. *Blood* 2015; 108: .
 522. Mezentsev A, Merks RMH, O’Riordan E, et al. Endothelial microparticles affect angiogenesis in vitro: role of oxidative stress. *Am J Physiol - Hear Circ Physiol* 2005; 289: .
 523. Brodsky S V., Zhang F, Nasjletti A, et al. Endothelium-derived microparticles impair endothelial function in vitro. *Am J Physiol - Hear Circ Physiol* 2004; 286: .
 524. Zhang Q, Shang M, Zhang M, et al. Microvesicles derived from hypoxia/reoxygenation-treated human umbilical vein endothelial cells promote apoptosis and oxidative stress in H9c2 cardiomyocytes. *BMC Cell Biol BioMed Central*; 2016; 17: 25.
 525. Willis GR. Characterisation of microparticles and nitro-oxidative stress in cardiometabolic disease. 2015.
 526. Nozaki T, Sugiyama S, Koga H, et al. Significance of a Multiple Biomarkers Strategy Including Endothelial Dysfunction to Improve Risk Stratification for Cardiovascular Events in Patients at High Risk for Coronary Heart Disease. *J Am Coll Cardiol* 2009; 54: 601–8.
 527. Greening DW, Xu R, Gopal SK, et al. Proteomic insights into extracellular vesicle biology – defining exosomes and shed microvesicles. *Expert Rev Proteomics* Taylor & Francis; 2017; 14: 69–95.
 528. Tkach M, Théry C. Communication by Extracellular Vesicles: Where We Are and Where We Need to Go. *Cell* 2016; 164: 1226–32.
 529. Tramontano AF, O’Leary J, Black AD, et al. Statin decreases endothelial microparticle release from human coronary artery endothelial cells: implication for the Rho-kinase pathway. *Biochem Biophys Res Commun* 2004; 320: 34–8.
 530. Amano M, Nakayama M, Kaibuchi K. Rho-kinase/ROCK: A key regulator of the cytoskeleton and cell polarity. *Cytoskeleton* 2010; 67: 545–54.
 531. Kato M, Blanton R, Wang G-R, et al. Direct binding and regulation of RhoA protein by cyclic GMP-dependent protein kinase α . *J Biol Chem* American Society for Biochemistry and Molecular Biology; 2012; 287: 41342–51.
 532. Camargo LM, França CN, Izar MC, et al. Effects of simvastatin/ezetimibe on microparticles, endothelial progenitor cells and platelet aggregation in subjects with coronary heart disease under antiplatelet therapy. *Brazilian J Med Biol Res = Rev Bras Pesqui medicas e Biol Associação Brasileira de Divulgação Científica*; 2014; 47: 432–7.
 533. Horn P, Amabile N, Angeli FS, et al. Dietary flavanol intervention lowers the levels of

- endothelial microparticles in coronary artery disease patients. *Br J Nutr* 2013; 111: 1245–52.
534. Duarte J, Francisco V, Perez-Vizcaino F. Modulation of nitric oxide by flavonoids. *Food Funct* 2014; 5: 1653–68.
535. Benito S, Lopez D, Sáiz MP, et al. A flavonoid-rich diet increases nitric oxide production in rat aorta. *Br J Pharmacol Blackwell Publishing Ltd*; 2002; 135: 910–6.
536. Machha A, Achike FI, Mustafa AM, et al. Quercetin, a flavonoid antioxidant, modulates endothelium-derived nitric oxide bioavailability in diabetic rat aortas. *Nitric Oxide* 2007; 16: 442–7.
537. Babbitt DM, Diaz KM, Fearheller DL, et al. Endothelial Activation Microparticles and Inflammation Status Improve with Exercise Training in African Americans. *Int J Hypertens* 2013; 2013: 1–8.
538. Green DJ, Dawson EA, Groenewoud HMM, et al. Is Flow-Mediated Dilation Nitric Oxide Mediated?: A Meta-Analysis. *Hypertension* 2014; 63: 376–82.
539. Gilligan DM, Panza JA, Kilcoyne CM, et al. Contribution of endothelium-derived nitric oxide to exercise-induced vasodilation. *Circulation* 1994; 90: .
540. Green DJ, Maiorana A, O'Driscoll G, et al. Effect of exercise training on endothelium-derived nitric oxide function in humans. *J Physiol Blackwell Science Ltd*; 2004; 561: 1–25.
541. Lemaster K, DeVallance E, Branyan K, et al. Aerobic Exercise Improves Nitric Oxide Bioavailability and Endothelium-Dependent Vasorelaxation in Aortic Rings of Obese Zucker Rats. *FASEB J Federation of American Societies for Experimental Biology*; 2016; 30: 1240.28-1240.28.
542. Braga VAVN, Couto GK, Lazzarin MC, et al. Aerobic Exercise Training Prevents the Onset of Endothelial Dysfunction via Increased Nitric Oxide Bioavailability and Reduced Reactive Oxygen Species in an Experimental Model of Menopause. *Torrens C, editor. PLoS One Public Library of Science*; 2015; 10: e0125388.
543. Marin C, Ramirez R, Delgado-Lista J, et al. Mediterranean diet reduces endothelial damage and improves the regenerative capacity of endothelium. *Am J Clin Nutr* 2011; 93: 267–74.
544. Clifford T, Howatson G, West DJ, et al. The potential benefits of red beetroot supplementation in health and disease. *Nutrients* 2015; 7: 2801–22.
545. Richardson G, Hicks SL, O'Byrne S, et al. The ingestion of inorganic nitrate increases gastric S-nitrosothiol levels and inhibits platelet function in humans. *Nitric Oxide* 2002; 7: 24–9.
546. Hendgen-Cotta UB, Luedike P, Totzeck M, et al. Dietary nitrate supplementation improves revascularization in chronic ischemia. *Circulation* 2012; 126: 1983–92.
547. Vivekananthan DP, Penn MS, Sapp SK, et al. Use of antioxidant vitamins for the prevention of cardiovascular disease: meta-analysis of randomised trials. *Lancet* 2003; 361: 2017–23.
548. Kapil V, Milsom AB, Okorie M, et al. Inorganic nitrate supplementation lowers blood pressure in humans: role for nitrite-derived NO. *Hypertension* 2010; 56: 274–81.
549. Hendgen-Cotta UB, Luedike P, Totzeck M, et al. Dietary nitrate supplementation improves revascularization in chronic ischemia. *Circulation* 2012; 126: 1983–92.
550. Muggeridge DJ, Howe CCF, Spendiff O, et al. The Effects of a Single Dose of Concentrated Beetroot Juice on Performance in Trained Flatwater Kayakers. *Int J Sport Nutr Exerc Metab* 2013; 23: 498–506.

551. Carlström M, Persson AEG, Larsson E, et al. Dietary nitrate attenuates oxidative stress, prevents cardiac and renal injuries, and reduces blood pressure in salt-induced hypertension. *Cardiovasc Res* 2011; 89: 574–85.
552. Wylie LJ, Kelly J, Bailey SJ, et al. Beetroot juice and exercise: pharmacodynamic and dose-response relationships. *J Appl Physiol* 2013; 115: .
553. Pinheiro LC, Amaral JH, Ferreira GC, et al. Gastric S-nitrosothiol formation drives the antihypertensive effects of oral sodium nitrite and nitrate in a rat model of renovascular hypertension. *Free Radic Biol Med* 2015; 87: 252–62.
554. Montenegro MF, Sundqvist ML, Nihlén C, et al. Profound differences between humans and rodents in the ability to concentrate salivary nitrate: Implications for translational research. *Redox Biol* 2016; 10: 206–10.
555. Megson IL, Sogo N, Mazzei FA, et al. Inhibition of human platelet aggregation by a novel S-nitrosothiol is abolished by haemoglobin and red blood cells in vitro: implications for anti-thrombotic therapy. *Br J Pharmacol* 2000; 131: 1391–8.
556. Vilahur G, Baldellou MI, Segalés E, et al. Inhibition of thrombosis by a novel platelet selective S-nitrosothiol compound without hemodynamic side effects. *Cardiovasc Res Oxford University Press*; 2004; 61: 806–16.
557. de Belder AJ, MacAllister R, Radomski MW, et al. Effects of S-nitroso-glutathione in the human forearm circulation: evidence for selective inhibition of platelet activation. *Cardiovasc Res* 1994; 28: 691–4.
558. Arnelle DRR, Stamler JSS. NO⁺, NO, and NO⁻ donation by S-nitrosothiols: implications for regulation of physiological functions by S-nitrosylation and acceleration of disulfide formation. *Arch Biochem Biophys* 1995; 318: 279–85.
559. Gordge MP, Hothersall JS, Noronha-Dutra AA. Evidence for a cyclic GMP-independent mechanism in the anti-platelet action of S-nitrosoglutathione. *Br J Pharmacol Blackwell Publishing Ltd*; 1998; 124: 141–8.
560. Connolly KD, Willis GR, Datta DBN, et al. Lipoprotein-apheresis reduces circulating microparticles in individuals with familial hypercholesterolemia. *J Lipid Res* 2014; 55: 2064–72.
561. Knijff-Dutmer EAJ, Koerts J, Nieuwland R, et al. Elevated levels of platelet microparticles are associated with disease activity in rheumatoid arthritis. *Arthritis Rheum* 2002; 46: 1498–503.
562. Lin Z-B, Ci H-B, Li Y, et al. Endothelial microparticles are increased in congenital heart diseases and contribute to endothelial dysfunction. *J Transl Med* 2017; 15: 4.
563. Trappenburg MC, van Schilfgaarde M, Marchetti M, et al. Elevated procoagulant microparticles expressing endothelial and platelet markers in essential thrombocythemia. *Haematologica Ferrata Storti Foundation*; 2009; 94: 911–8.
564. Kim H., Song K., Park Y., et al. Elevated levels of circulating platelet microparticles, VEGF, IL-6 and RANTES in patients with gastric cancer: possible role of a metastasis predictor. *Eur J Cancer* 2003; 39: 184–91.
565. Abstracts from the Third International Meeting of ISEV 2014 Rotterdam, The Netherlands, April 30(th) - May 3(rd), 2014. *J Extracell vesicles Taylor & Francis*; 2014; 3: 24214.
566. Puddu P, Puddu GM, Cravero E, et al. The involvement of circulating microparticles in inflammation, coagulation and cardiovascular diseases. *Can J Cardiol* 2010; 26: 140–5.

567. Ardoin SP, Shanahan JC, Pisetsky DS. The Role of Microparticles in Inflammation and Thrombosis. *Scand J Immunol* 2007; 66: 159–65.
568. Kurachi M, Mikuni M, Ishizaki Y. Extracellular Vesicles from Vascular Endothelial Cells Promote Survival, Proliferation and Motility of Oligodendrocyte Precursor Cells. *PLoS One Public Library of Science*; 2016; 11: e0159158.
569. Mallat Z, Benamer H, Hugel B, et al. Elevated Levels of Shed Membrane Microparticles With Procoagulant Potential in the Peripheral Circulating Blood of Patients With Acute Coronary Syndromes. *Circulation* 2000; 101: 841–3.
570. Cherian P, Hankey GJ, Eikelboom JW, et al. Endothelial and platelet activation in acute ischemic stroke and its etiological subtypes. *Stroke* 2003; 34: 2132–7.
571. Boilard E, Nigrovic PA, Larabee K, et al. Platelets amplify inflammation in arthritis via collagen-dependent microparticle production. *Science NIH Public Access*; 2010; 327: 580–3.
572. Ando M, Iwata A, Ozeki Y, et al. Circulating platelet-derived microparticles with procoagulant activity may be a potential cause of thrombosis in uremic patients. *Kidney Int* 2002; 62: 1757–63.
573. Tomer A, Harker LA, Kasey S, et al. Thrombogenesis in sickle cell disease. *J Lab Clin Med* 2001; 137: 398–407.
574. Galli M, Grassi A, Barbui T. Platelet-derived microvesicles in thrombotic thrombocytopenic purpura and hemolytic uremic syndrome. *Thromb Haemost* 1996; 75: 427–31.
575. Tan KT, Lip GYH. The potential role of platelet microparticles in atherosclerosis. *Thromb Haemost* 2005; 94: 488–92.
576. Adamski P, Koziński M, Ostrowska M, et al. Overview of pleiotropic effects of platelet P2Y12 receptor inhibitors. *Thromb Haemost* 2014; 112: 224–42.
577. Warnholtz A, Ostad MA, Velich N, et al. A single loading dose of clopidogrel causes dose-dependent improvement of endothelial dysfunction in patients with stable coronary artery disease: results of a double-blind, randomized study. *Atherosclerosis* 2008; 196: 689–95.
578. Heitzer T, Rudolph V, Schwedhelm E, et al. Clopidogrel improves systemic endothelial nitric oxide bioavailability in patients with coronary artery disease: evidence for antioxidant and antiinflammatory effects. *Arterioscler Thromb Vasc Biol* 2006; 26: 1648–52.
579. Patel SH, Rachchh MA, Jadav PD. Evaluation of anti-inflammatory effect of anti-platelet agent-clopidogrel in experimentally induced inflammatory bowel disease. *Indian J Pharmacol* 2012; 44: 744–8.
580. Behan MWH, Fox SC, Heptinstall S, et al. Inhibitory effects of P2Y12 receptor antagonists on TRAP-induced platelet aggregation, procoagulant activity, microparticle formation and intracellular calcium responses in patients with acute coronary syndromes. *Platelets* 2005; 16: 73–80.
581. Anderson TJ. Nitric oxide, atherosclerosis and the clinical relevance of endothelial dysfunction. *Heart Fail Rev* 2003; 8: 71–86.
582. Kirkby NS, Lundberg MH, Chan M V, et al. Blockade of the purinergic P2Y12 receptor greatly increases the platelet inhibitory actions of nitric oxide. *Proc Natl Acad Sci U S A* 2013; 110: 15782–7.
583. Gkaliagkousi E, Ritter J, Ferro A. Platelet-derived nitric oxide signaling and regulation. *Circ Res* 2007; 101: 654–62.

584. Velmurugan S, Kapil V, Ghosh SM, et al. Antiplatelet effects of dietary nitrate in healthy volunteers: involvement of cGMP and influence of sex. *Free Radic Biol Med* 2013; 65: 1521–32.
585. Lee DH, Kim MH, Guo LZ, et al. Concomitant nitrates enhance clopidogrel response during dual anti-platelet therapy. *Int J Cardiol* 2016; 203: 877–81.
586. Maron BA, Tang S-S, Loscalzo J. S-nitrosothiols and the S-nitrosoproteome of the cardiovascular system. *Antioxid Redox Signal Mary Ann Liebert, Inc.*; 2013; 18: 270–87.
587. Lee S-J, Kim K-M, Namkoong S, et al. Nitric Oxide Inhibition of Homocysteine-induced Human Endothelial Cell Apoptosis by Down-regulation of p53-dependent Noxa Expression through the Formation of S-Nitrosohomocysteine. *J Biol Chem* 2005; 280: 5781–8.
588. Arnelle DR, Stamler JS. NO⁺, NO, and NO⁻ donation by S-nitrosothiols: implications for regulation of physiological functions by S-nitrosylation and acceleration of disulfide formation. *Arch Biochem Biophys* 1995; 318: 279–85.
589. Al-Sa'doni H, Ferro A. S-Nitrosothiols: a class of nitric oxide-donor drugs. *Clin Sci (Lond)* 2000; 98: 507–20.
590. Anderson RA, Bundhoo S, James PE. A new mechanism of action of thienopyridine antiplatelet drugs - a role for gastric nitrosthil metabolism? *Atherosclerosis* 2014; 237: 369–73.
591. Daymond S. Does acute dietary nitrate supplementation enhance well-trained hockey players' performance in game specific intermittent exercise? Cardiff Metropolitan University; 2015; .
592. Curtis KJ, O'Brien KA, Tanner RJ, et al. Acute Dietary Nitrate Supplementation and Exercise Performance in COPD: A Double-Blind, Placebo-Controlled, Randomised Controlled Pilot Study. Schooling CM, editor. *PLoS One Public Library of Science*; 2015; 10: e0144504.
593. Gladwin MT, Schechter AN, Kim-Shapiro DB, et al. The emerging biology of the nitrite anion. *Nat Chem Biol* 2005; 1: 308–14.
594. Reutov VP, Sorokina EG. NO-synthase and nitrite-reductase components of nitric oxide cycle. *Biochem Biokhimiia* 1998; 63: 874–84.
595. van Faassen EE, Bahrami S, Feelisch M, et al. Nitrite as regulator of hypoxic signaling in mammalian physiology. *Med Res Rev* 2009; 29: 683–741.
596. Jansson EA, Huang L, Malkey R, et al. A mammalian functional nitrate reductase that regulates nitrite and nitric oxide homeostasis. *Nat Chem Biol Nature Publishing Group*; 2008; 4: 411–7.
597. Jones AM. Dietary nitrate supplementation and exercise performance. *Sports Med* 2014; 44 Suppl 1: S35-45.
598. Bond V, Curry BH, Adams RG, et al. Effects of Nitrate Supplementation on Cardiovascular and Autonomic Reactivity in African-American Females. *ISRN Physiol* 2014; 2014: .
599. Lundberg JO, Gladwin MT, Weitzberg E. Strategies to increase nitric oxide signalling in cardiovascular disease. *Nat Rev Drug Discov Nature Research*; 2015; 14: 623–41.
600. Singh RJ, Hogg N, Joseph J, et al. Mechanism of Nitric Oxide Release from S-Nitrosothiols. *J Biol Chem American Society for Biochemistry and Molecular Biology*; 1996; 271: 18596–603.
601. Bundhoo SS, Anderson RA, Sagan E, et al. Direct formation of thienopyridine-derived

- nitrosothiols — Just add nitrite! *Eur J Pharmacol* 2011; 670: 534–40.
602. Gilard M, Arnaud B, Cornily J-C, et al. Influence of Omeprazole on the Antiplatelet Action of Clopidogrel Associated With Aspirin: The Randomized, Double-Blind OCLA (Omeprazole Clopidogrel Aspirin) Study. *J Am Coll Cardiol* 2008; 51: 256–60.
603. Kwok CS, Loke YK. Effects of proton pump inhibitors on platelet function in patients receiving clopidogrel: a systematic review. *Drug Saf* 2012; 35: 127–39.
604. Tutuian R, Katz PO, Bochenek W, et al. Dose-dependent control of intragastric pH by pantoprazole, 10, 20 or 40 mg, in healthy volunteers. *Aliment Pharmacol Ther* 2002; 16: 829–36.
605. Shin JS, Lee JY, Cho KH, et al. The pharmacokinetics, pharmacodynamics and safety of oral doses of ilaprazole 10, 20 and 40 mg and esomeprazole 40 mg in healthy subjects: a randomised, open-label crossover study. *Aliment Pharmacol Ther* 2014; 40: 548–61.
606. Gan KH, Geus WP, Lamers CB, et al. Effect of omeprazole 40 mg once daily on intraduodenal and intragastric pH in *H. pylori*-negative healthy subjects. *Dig Dis Sci* 1997; 42: 2304–9.
607. Davì G, Patrono C. Platelet activation and atherothrombosis. *N Engl J Med* 2007; 357: 2482–94.
608. Michelson AD. Antiplatelet therapies for the treatment of cardiovascular disease. *Nat Rev Drug Discov* 2010; 9: 154–69.
609. Kapil V, Haydar SMA, Pearl V, et al. Physiological role for nitrate-reducing oral bacteria in blood pressure control. *Free Radic Biol Med Elsevier*; 2013; 55: 93–100.
610. Angiolillo DJ, Luis Ferreiro J. Platelet Adenosine Diphosphate P2Y₁₂ Receptor Antagonism: Benefits and Limitations of Current Treatment Strategies and Future Directions. *Rev Española Cardiol (English Ed Elsevier)*; 2010; 63: 60–76.
611. Dangelmaier C, Jin J, Smith JB, et al. Potentiation of thromboxane A₂-induced platelet secretion by Gi signaling through the phosphoinositide-3 kinase pathway. *Thromb Haemost* 2001; 85: 341–8.
612. Flaumenhaft R. Molecular basis of platelet granule secretion. *Arterioscler Thromb Vasc Biol* 2003; 23: 1152–60.
613. Jansen F, Nickenig G, Werner N. Extracellular Vesicles in Cardiovascular Disease: Potential Applications in Diagnosis, Prognosis, and Epidemiology. *Circ Res* 2017; 120: 1649–57.
614. Janssens D, Michiels C, Delaive E, et al. Protection of hypoxia-induced ATP decrease in endothelial cells by ginkgo biloba extract and bilobalide. *Biochem Pharmacol* 1995; 50: 991–9.
615. Anderson SE, Murphy E, Steenbergen C, et al. Na-H exchange in myocardium: effects of hypoxia and acidification on Na and Ca. *Am J Physiol* 1990; 259: C940–8.
616. Dufourcq P, Seigneur M, Pruvost A, et al. Membrane thrombomodulin levels are decreased during hypoxia and restored by cAMP and IBMX. *Thromb Res* 1995; 77: 305–10.
617. Takeuchi K, Watanabe H, Tran Q-K, et al. Nitric oxide: inhibitory effects on endothelial cell calcium signaling, prostaglandin I₂ production and nitric oxide synthase expression. *Cardiovasc Res* 2004; 62: 194–201.
618. Berchner-Pfannschmidt U, Yamac H, Trinidad B, et al. Nitric oxide modulates oxygen sensing by hypoxia-inducible factor 1-dependent induction of prolyl hydroxylase 2. *J Biol*

Chem 2007; 282: 1788–96.

619. Strijdom H, Chamane N, Lochner A. Nitric oxide in the cardiovascular system: a simple molecule with complex actions. *Cardiovasc J Afr Clinics Cardive Publishing (Pty) Ltd.*; 2009; 20: 303.
620. Webb AJ, Milsom AB, Rathod KS, et al. Mechanisms underlying erythrocyte and endothelial nitrite reduction to nitric oxide in hypoxia: role for xanthine oxidoreductase and endothelial nitric oxide synthase. *Circ Res* 2008; 103: 957–64.
621. Zweier JL, Wang P, Samouilov A, et al. Enzyme-independent formation of nitric oxide in biological tissues. *Nat Med* 1995; 1: 804–9.
622. Ignarro LJ, Lipton H, Edwards JC, et al. Mechanism of vascular smooth muscle relaxation by organic nitrates, nitrites, nitroprusside and nitric oxide: evidence for the involvement of S-nitrosothiols as active intermediates. *J Pharmacol Exp Ther* 1981; 218: 739–49.
623. Engeset D, Alsaker E, Ciampi A, et al. Dietary patterns and lifestyle factors in the Norwegian EPIC cohort: The Norwegian Women and Cancer (NOWAC) study. *Eur J Clin Nutr Nature Publishing Group*; 2005; 59: 675–84.
624. Boulanger CM, Loyer X, Rautou P-E, et al. Extracellular vesicles in coronary artery disease. *Nat Rev Cardiol* 2017; 14: 259–72.
625. Thornhill L. The Effect of Thienopyridines and Non-Thienopyridines on Nitric Oxide Metabolism in Patients with Stable Angina. *Cardiff University*; 2016.
626. d’El-Rei J, Cunha AR, Trindade M, et al. Beneficial Effects of Dietary Nitrate on Endothelial Function and Blood Pressure Levels. *Int J Hypertens Hindawi Publishing Corporation*; 2016; 2016: 1–6.
627. Münzel T, Daiber A, Mülsch A. Explaining the Phenomenon of Nitrate Tolerance. *Circ Res* 2005; 97: .
628. Omar SA, Artime E, Webb AJ. A comparison of organic and inorganic nitrates/nitrites. *Nitric Oxide* 2012; 26: 229–40.
629. Dejam A, Hunter CJ, Tremonti C, et al. Nitrite Infusion in Humans and Nonhuman Primates: Endocrine Effects, Pharmacokinetics, and Tolerance Formation. *Circulation* 2007; 116: 1821–31.
630. Marsch E, Theelen TL, Janssen BJA, et al. The effect of prolonged dietary nitrate supplementation on atherosclerosis development. *Atherosclerosis* 2016; 245: 212–21.
631. Antwi-Baffour S, Adjei J, Aryeh C, et al. Understanding the biosynthesis of platelets-derived extracellular vesicles. *Immunity, Inflamm Dis Wiley-Blackwell*; 2015; 3: 133–40.
632. Bakker E, Engan H, Patrician A, et al. Acute dietary nitrate supplementation improves arterial endothelial function at high altitude: A double-blinded randomized controlled cross over study. *Nitric Oxide* 2015; 50: 58–64.
633. Rathod KS, Jones DA, Van-Eijl TJA, et al. Randomised, double-blind, placebo-controlled study investigating the effects of inorganic nitrate on vascular function, platelet reactivity and restenosis in stable angina: protocol of the NITRATE-OCT study. *BMJ Open BMJ Publishing Group*; 2016; 6: e012728.
634. Vader P, Breakefield XO, Wood MJA. Extracellular vesicles: emerging targets for cancer therapy. *Trends Mol Med NIH Public Access*; 2014; 20: 385–93.

APPENDICES

Appendix 1.1

Appendix 1.1A Levels of coagulation proteins in EVs.

Marker	21% O ₂ EVs	21% O ₂ & NaNO ₂ EVs	1% O ₂ EVs	1% O ₂ & NaNO ₂ EVs
vWF	11389 ± 1765	12534 ± 3688	12385 ± 2186	10111 ± 1103
Tissue factor	5958 ± 1644	4239 ± 605	7666 ± 1698	9505 ± 1260
Thrombomodulin	17230 ± 2319	15967 ± 1559	9465 ± 819*	9522 ± 909*
TFPI	19723 ± 2698	19323 ± 2053	9799 ± 2353*	8524 ± 1084* †

Values are relative fluorescence units (RFU). * reflects $p < 0.05$ compared to 21% O₂ EVs. † reflects $p < 0.05$ compared to 21% O₂ & NaNO₂ EVs. Results represent [n=5].

Appendix 1.1B Levels of pro-inflammatory cytokines and transcription factors in EVs.

Marker	21% O ₂ EVs	21% O ₂ & NaNO ₂ EVs	1% O ₂ EVs	1% O ₂ & NaNO ₂ EVs
TNF-α	11073 ± 452**	9816 ± 552***	16476 ± 882	11240 ± 785**
IL-1α	7063 ± 315	7349 ± 629	7306 ± 1533	10545 ± 2005
IL-6	9800 ± 384***††	8461 ± 967***†††	20916 ± 659	17763 ± 1574
IL-8	12327 ± 983	16194 ± 600	14148 ± 371	12160 ± 1229
NF-κB	6547 ± 553***††	4273 ± 543***†††	13647 ± 475	14518 ± 1976

Values are relative fluorescence units (RFU). ** and *** reflect $p < 0.01$ and $p < 0.001$ respectively, compared to 1% O₂ EVs. †† and ††† reflect $p < 0.01$ and $p < 0.001$ respectively, compared to 1% O₂ & NaNO₂ EVs. Results represent [n=5].

Appendix 1.1C Levels of adhesion molecules in EVs

Marker	21% O ₂ EVs	21% O ₂ & NaNO ₂ EVs	1% O ₂ EVs	1% O ₂ & NaNO ₂ EVs
VCAM-1	18295 ± 373	16148 ± 682	21247 ± 1306	16383 ± 3415
ICAM-1	17968 ± 795	13403 ± 1208	19764 ± 3790	12739 ± 2414
PECAM-1	16029 ± 2260	13092 ± 2306	15286 ± 2795	12891 ± 3815
P-Selectin	17263 ± 1643	11072 ± 1211	17058 ± 1098	17587 ± 1291
E-Selectin	15592 ± 1324	13208 ± 1551	19711 ± 1968	16086 ± 2333

Values are relative fluorescence units. Results represent [n=5].

Appendix 1.1D Levels of exosomal, endothelial and hypoxia markers in EVs.

Marker	21% O ₂ EVs	21% O ₂ & NaNO ₂ EVs	1% O ₂ EVs	1% O ₂ & NaNO ₂ EVs
CD9	42044 ± 2450	45510 ± 1540	45091 ± 514	43424 ± 2946
ALIX	16228 ± 1965	16369 ± 1913	18151 ± 834	17410 ± 954
TSG101	23584 ± 2251	18002 ± 1273	23338 ± 2040	18317 ± 1885
HIF-1α	367 ± 367***+++	610 ± 610***+++	13618 ± 1642	16648 ± 1339
CD144	20315 ± 1172	20244 ± 1317	21965 ± 485	22835 ± 1547

Values are relative fluorescence units. *** reflects $p < 0.001$ compared to 1% O₂ EVs. +++ reflects $p < 0.001$ compared to 1% O₂ & NaNO₂ EVs. Results represent [n=5].

Appendix 1.2

Appendix 1.2A Acute change (Day 1) in the size distribution profile of EVs following BR juice or placebo.

EV Size	Placebo	BR Juice
0-50	$2.00e^8 \pm 1.50e^8$	$-2.54e^7 \pm 1.80e^8$
51-100	$-8.28e^9 \pm 2.4e^{10}$	$-1.04e^9 \pm 9.36e^9$
101-150	$-3.12e^{10} \pm 1.80e^{10}$	$4.06e^{10} \pm 2.56e^{10}$
151-200	$7.18e^9 \pm 7.985e^9$	$1.92e^{10} \pm 1.58e^{10}$
201-250	$7.99e^9 \pm 1.03e^{10}$	$1.38e^{10} \pm 8.17e^9$
251-300	$1.51e^{10} \pm 1.02e^{10}$	$8.93e^9 \pm 6.13e^9$
301-350	$9.70e^9 \pm 6.20e^9$	$1.46e^9 \pm 8.40e^8$
351-400	$3.87e^9 \pm 2.62e^9$	$4.69e^8 \pm 1.91e^8$
401-450	$9.01e^8 \pm 7.63e^8$	$2.38e^8 \pm 2.13e^8$
451-500	$1.72e^8 \pm 1.20e^8$	$2.01e^8 \pm 1.06e^8$
501-550	$1.49e^8 \pm 1.06e^8$	$1.50e^8 \pm 8.77e^7$
551-600	0 ± 0	0 ± 0

NTA was used to assess changes in the size distribution of EVs, split into 50 nm bin sizes for analysis and normalised per mL of plasma. Samples were measured in quintuplicate and the mean used in further analysis. Results represent [n=8]. Data are expressed mean \pm SEM.

Appendix 1.2B Chronic change (Day 1-6) in the size distribution profile of EVs following BR juice or placebo.

EV Size	Placebo	BR Juice
0-50	$1.84e^8 \pm 9.89e^7$	$7.15e^8 \pm 7.15e^7$
51-100	$-8.32e^8 \pm 2.26e^{10}$	$-3.6e^{10} \pm 2.23e^{10}$
101-150	$-2.77e^{10} \pm 1.91e^{10}$	$-1.30e^{10} \pm 1.70e^{10}$
151-200	$2.18e^{10} \pm 2.57e^{10}$	$9.22e^9 \pm 8.952e^9$
201-250	$1.09e^{10} \pm 1.25e^{10}$	$1.10e^{10} \pm 6.83e^9$
251-300	$6.32e^9 \pm 4.85e^9$	$4.04e^9 \pm 3.73e^9$
301-350	$1.77e^9 \pm 3.97e^8$	$2.20e^9 \pm 1.42e^9$
351-400	$2.44e^8 \pm 1.36e^8$	$9.78e^8 \pm 4.64e^8$
401-450	$2.44e^8 \pm 1.58e^8$	$4.46e^8 \pm 3.10e^8$
451-500	$-3.99e^6 \pm 4.20e^6$	$2.32e^8 \pm 1.19e^8$
501-550	0 ± 0	$2.53e^7 \pm 9.97e^6$
551-600	0 ± 0	0 ± 0

NTA was used to assess changes in the size distribution of EVs, split into 50 nm bin sizes for analysis and normalised per mL of plasma. Samples were measured in quintuplicate and the mean used in further analysis. Results represent [n=8]. Data are expressed mean \pm SEM.

Appendix 1.2C Acute change (Day 6) in the size distribution profile of EVs following BR juice or placebo.

EV Size	Placebo	BR Juice
0-50	$3.80e^8 \pm 1.63e^8$	$1.83e^8 \pm 1.63e^8$
51-100	$2.02e^9 \pm 1.33e^{10}$	$5.86^9 \pm 5.85e^9$
101-150	$1.48e^{10} \pm 1.92e^{10}$	$3.24e^{10} \pm 8.44e^9$
151-200	$1.77e^9 \pm 1.24e^{10}$	$-1.18e^{10} \pm 7.36e^9$
201-250	$-1.68e^{10} \pm 1.22e^{10}$	$-4.36e^9 \pm 6.53e^9$
251-300	$-7.45e^9 \pm 4.39e^9$	$-2.87e^9 \pm 4.00e^9$
301-350	$-1.88e^9 \pm 4.34e^8$	$-8.22e^8 \pm 1.60e^9$
351-400	$-2.53e^8 \pm 1.38e^8$	$-5.12e^8 \pm 5.00e^8$
401-450	$-2.27e^8 \pm 1.48e^8$	$-2.34e^8 \pm 3.52e^8$
451-500	$-3.21e^6 \pm 2.10e^6$	$-1.92e^8 \pm 1.20e^8$
501-550	0 ± 0	$2.14e^7 \pm 4.71e^7$
551-600	0 ± 0	0 ± 0

NTA was used to assess changes in the size distribution of EVs, split into 50 nm bin sizes for analysis and normalised per mL of plasma. Samples were measured in quintuplicate and the mean used in further analysis. Results represent [n=8]. Data are expressed mean \pm SEM.

Appendix 1.3

Appendix 1.3 Effect of BR juice on EV surface protein.

Marker	Day 1: Pre-treatment		Day 1: Post-treatment		Day 6: Pre-treatment		Day 6: Post-treatment	
	BR Juice	Placebo	BR Juice	Placebo	BR Juice	Placebo	BR Juice	Placebo
CD9	54761 ± 2810	56521 ± 2831	53528 ± 2438	54803 ± 1661	53308 ± 2495	55338 ± 2042	48175 ± 3517	51443 ± 3263
CD41	20835 ± 1381	20008 ± 1179	18698 ± 864	17316 ± 989	18563 ± 1467	18639 ± 839	18754 ± 1372	18360 ± 1235
CD11b	25663 ± 1939	21920 ± 1022	26992 ± 3038	23852 ± 1710	26522 ± 2104	24096 ± 1775	26381 ± 2322	22542 ± 847
CD235a	7505 ± 612	7304 ± 460	7593 ± 730	7386 ± 495	6637 ± 534	6446 ± 783	6469 ± 807	6264 ± 564
CD144	3455 ± 403	3893 ± 197	3166 ± 428	3768 ± 282	2945 ± 470	4085 ± 224	2894 ± 562	3607 ± 386

Fluorescence values for both BR Juice and placebo at all time points for the exosome marker (CD9), platelet marker (CD41), leukocyte marker (CD11b), erythrocyte marker (CD235a) and endothelial marker (CD144). Data represent mean ± SEM [n=8].